Advancing Forward Osmosis for Energy-efficient Wastewater Treatment towards Enhanced Water Reuse and Resource Recovery

Shiqiang Zou

Dissertation Submitted to the Faculty of Virginia Polytechnic Institute and State University

In Partial Fulfillment of the Requirements for the Degree of

Doctor of Philosophy in Civil Engineering

Zhen (Jason) He, Chair

Andrea M. Dietrich

Zhiwu (Drew) Wang

Rui Qiao

April 16th, 2019

Blacksburg, VA

Keywords: Forward Osmosis, Wastewater Treatment, Water Reuse, Resource Recovery, Energy Analysis, Reverse Solute Flux

Advancing Forward Osmosis for Energy-efficient Wastewater Treatment towards Enhanced Water Reuse and Resource Recovery

Shiqiang Zou

Abstract (academic)

Current treatment of wastewater can effectively remove the contaminants; however, the effluent is still not widely reused because of some undesired substances like pathogens and trace organic chemicals. To promote water reuse, membrane-based technologies have emerged as a robust and more efficient alternative to current treatment practice. Among these membrane processes, forward osmosis (FO) utilizes an osmotic pressure gradient across a semi-permeable membrane to reclaim high-quality water. Still, several key challenges remain to be addressed towards broader FO application, including energy-intensive draw regeneration to yield product water and salinity buildup in the feed solution. To bypass energy-intensive draw regeneration, commercial solid fertilizers was utilized as a regeneration-free draw solute (DS), harvesting fresh water towards direct agricultural irrigation. However, using nutrient-rich fertilizers as DS resulted in an elevated reverse solute flux (RSF). This RSF, known as the cross-membrane diffusion of DS to the feed solution, led to deteriorated solute buildup on the feed side, reduced osmotic driving force, increased fouling propensity, and higher operation cost. To effectively mitigate solute buildup while achieving energy-efficient water reclamation, a parallel electrodialysis (ED) device was integrated to FO for DS recovery in the feed solution. The salinity in the feed solution was consistently controlled below 1 mS cm^{-1} via the hybrid FO-ED system. Considering solute buildup is merely a consequence of RSF, direct control of RSF was further investigated via operational strategy (i.e., an electrolysis-assisted FO) and membrane modification (i.e., surface coating of zwitterion-functionalized carbon nanotubes). Significantly reduced RSF (> 50% reduction) was obtained in both approaches with minor energy/material investment. With two major bottlenecks being properly addressed for energy-efficient water reclamation, FO was further integrated with a microbial electrolysis cell (MEC) to achieve integrated nutrient-energy-water recovery from high-strength wastewater (i.e., the digestor centrate). The abovementioned research projects are among the earliest efforts to address multiple key challenges of FO during practical application, serving as a cornerstone to facilitate the transformation of current water/wastewater treatment plant to resource recovery hub in order to ensure global food-energy-water security.

Advancing Forward Osmosis for Energy-efficient Wastewater Treatment towards Enhanced Water Reuse and Resource Recovery

Shiqiang Zou

Abstract (general audience)

Exploring alternative water supply, for instance via reusing wastewater, will be essential to deal with the global water crisis. Current wastewater treatment can effectively remove the contaminants; however, the treated wastewater is still not widely reused due to the possible presence of residual contaminants. In recent years, membrane-based technologies have emerged as a promising treatment process to produce clean water. Among all available membrane technologies, forward osmosis (FO) takes advantage of the osmotic pressure difference across a special membrane to extract fresh water from a low-salinity FEED solution (for example, wastewater) to a high-salinity DRAW solution. The reclaimed fresh water can be reused for other applications. Still, the FO process is facing several critical challenges for broader applications. The first challenge is that additional energy is required to separate clean water from the diluted DRAW solution, leading to notably increased energy consumption for the FO process. To bypass this energy-intensive separation, commercial solid fertilizers was utilized as a separation-free DRAW solution for FO process. Once the clean water is extracted to the DRAW solution (fertilizer), the diluted fertilizer solution together with the fresh water can be directly used for agricultural irrigation. The second challenge is that, when fertilizer is applied as the DRAW solution, nutrient-rich fertilizers can penetrate the FO membrane and escape to the FEED solution (wastewater). This phenomenon is known as the reverse solute flux (RSF). RSF can result in many adverse effects, such as wastewater contamination and increased operational cost. To prevent this, we used an additional device named electrodialysis to effectively recapture the “escaped” fertilizers in the FEED solution. Besides this indirect approach to recover escaped fertilizers, we also investigated direct approaches to control RSF, including operational strategy and membrane modification. With two major challenges being properly addressed for energy-efficient water reclamation, FO was further combined with a microbial electrolysis cell (MEC) to achieve multiple resource recovery from wastewater, including water, nutrient, and energy components. The abovementioned research projects are among the earliest efforts to address multiple key challenges of FO during water and resource recovery from wastewater to ensure global food-energy-water security.

Acknowledgments

Looking back at my entire Ph.D. journey, I feel fortunate to know some many genuine people and continuously follow my heart to tap my potential in wastewater treatment and resource recovery. Blacksburg really treats me well through these four years, and I'm proud to say it gradually becomes a second home to me. All my laughter, struggle, tears, and my endless effort at Virginia Tech will become a lifetime memory.

I can still remember receiving my offer to be admitted to the Ph.D. program at Virginia Tech four years ago. It feels like yesterday. Thirteen hours of flight from Beijing to Washington D.C made me think about my four years ahead. When the excitement wore off, I was a little bit concerned about getting a Ph.D. diploma in a U.S. university. However, my first meeting with my Ph.D. advisor, Dr. Zhen (Jason) He, gave me lots of hope. Along the four years, Dr. He has helped me not only in my academic career but also in my personal life. His guidance has walked me through all the struggles and bitterness to what I've become today. All my committee members, including Dr. Andrea M. Dietrich, Dr. Zhiwu (Drew) Wang, and Dr. Rui Qiao, have also offered me constructive suggestions and comments to my research projects and scientific papers. Other faculty members coming from several departments and even other universities, including Dr. Zhiting Tian, Dr. Stephen M. Martin, Dr. Thomas Diller, Dr. Amanda Morris, Dr. David Kuhn, and Dr. Shihong Lin, offered me valuable collaborating opportunities to dive into interdisciplinary research. Thank you for making this difficult journey much easier for me!

I'm fortunate to have full family support to set aside four years and dive into a research field. My parents not only provide me additional financial support to my current Ph.D. assistantship so that I can have a decent and comfortable life in Blacksburg, but also love me throughout my whole life unconditionally. When I felt down or depressed about my research projects, my parents always gave me a video call and cheered me up. Both of them do not have a college degree, but they could offer lots of useful advice from their life experience and asked me to look at the bright side of a problem/challenge. I would also like to thank my girlfriend, Lili Li, for her company during my Ph.D. study. As Ph.D. students, we understand all the struggles during this journey and share so many common languages. We also had lots of wonderful memories of traveling and exploring around the world during vacations. I sincerely wish her to graduate on time as she has spent so much time and effort in her research project.

All these four years, I felt being loved by all my friends at VT. As an old Chinese proverb said, you can count on your parents when you are at home, but you have to rely on your friends when traveling around the world. I would first like to thank my best friend and former roommate, Kaisen Lin, for putting up with me through the past four years. He helped me a lot in moving house, purchasing my vehicle, and other daily stuff. I cannot ask for a better friend to go through graduate school than him. Second, I want to thank Syeed Iskander for being such a great lab mate, and we have overcome so many challenges together in these four years. I have truly learned quite a lot from this guy. All the EBBLers, including Zheng Ge, Qingyun Ping, Jian Li, Shuai Luo, Xiaojin Li, Xiaoxue Xiang, Xuhui Zeng, Akshay Jain, Xingjian Liu, Nicholas Benn, Yuan Pan, Wei Wang, Bing Xu, and Zixuan Wang, are a big and warm family to me. We had so many joy and laughter, especially all the sweet get-together during the holidays. Within EBBL, we have supported each other when facing all kinds of difficulties. EBBL rocks and I love all of you guys!

Money cannot buy you anything, but without money, you cannot conduct any research. Hence, I should give a significant part of the credit to my funding organizations and agencies, including National Science Foundation, Institute for Critical Technology and Applied Science, Water INTERface IGEP program, and the Via Teaching Scholar Program at Department of Civil and Environmental Engineering. With all the financial support, I have survived graduate school and published all the quality research work.

I would also very much like to thank all the staff members in our department and other departments, especially Aili Wang, Steve McCartney, Julie Petruska, Elizabeth “Jody” Smiley, Aaron “AJ” Prussin, Beth Lucas, Sarah Martin, and Lindy Cranwell. All these staff members helped me a lot in learning instruments, administrative paperwork, reimbursement, and class registration. Many thanks to all the staff members at the Christiansburg Wastewater Treatment Plant, including John, Helen, Josh, etc. I really appreciate your help in collecting anaerobic sludge from the digestor and secondary effluent and aerobic sludge from the aerobic basin.

All my accomplishment today should be attributed to the love and strong support from my advisor, my family members, my dear friends, and the Virginia Tech community. I hope I make all of you proud during and after these four years.

Thank you, Virginia Tech! Once a Hokie, always a Hokie.

Publication List (Virginia Tech)

First-author Journal Publication (* stands for co-first author)

1. **Zou, S.**,* Smith, E.,* Martin, S., & He, Z. (2019) Mitigation of Bidirectional Solute Flux in Forward Osmosis via Membrane Surface Coating of Zwitterion Functionalized Carbon Nanotubes. *Under Review*.

2. **Zou, S.**, Qin, M., & He, Z. (2019) Tackle reverse solute flux in forward osmosis towards sustainable water recovery: reduction and perspectives. *Water Research* 49, 362-374.

3. **Zou, S.**,* Guan, L.,* Taylor, D.P., Kuhn, D., & He, Z. (2018) Nitrogen removal from water of a recirculating aquaculture system by a bioelectrochemical system. *Aquaculture* 497, 74-81.

4. **Zou, S.** & He, Z. (2018) Efficiently "pumping out" value-added resources from wastewater by bioelectrochemical systems: a review from energy perspectives. *Water Research* 131, 62-73.

5. Zhang, B.,* **Zou, S.**,* Cai, R., Li, M., & He, Z. (2018) High-efficient photocatalytic disinfection of Escherichia coli under visible light using carbon supported Vanadium Tetrasulfide nanocomposites. *Applied Catalysis B: Environmental* 224, 383-393.

6. **Zou, S.**,* Kanimba, E.,* Diller, T.E., Tian, Z., & He, Z. (2018) Modelling assisted evaluation of direct electricity generation from waste heat of wastewater via a thermoelectric generator. *Science of the Total Environment* 635, 1215-1224.

7. **Zou, S.** & He, Z. (2017) Electrodialysis recovery of reverse-fluxed fertilizer draw solute during forward osmosis water treatment. *Chemical Engineering Journal* 330, 550-558.

8. **Zou, S.**, Qin, M., Moreau, Y., & He, Z. (2017) Nutrient-energy-water recovery from synthetic sidestream centrate using a microbial electrolysis cell - forward osmosis hybrid system. *Journal of Cleaner Production* 154, 16-25.

9. **Zou, S.** & He, Z. (2017) Electrolysis-assisted mitigation of reverse solute flux in a three-chamber forward osmosis system. *Water Research* 115, 111-119.

10. **Zou, S.**, Yuan, H., Childress, A., & He, Z. (2016) Energy consumption by recirculation: a missing parameter when evaluating forward osmosis. *Environmental Science & Technology* 50, 6827-6829.

11. **Zou, S.** & He, Z. (2016) Enhancing wastewater reuse by forward osmosis with self-diluted commercial fertilizers as draw solutes. *Water Research* 99 (1), 235-243.

Coauthored Journal Publication

1. Wu, S., **Zou, S.**, Yang, Y., Qian, G., & He, Z. (2018) Enhancing the performance of an osmotic microbial fuel cell through self-buffering with reverse-fluxed sodium bicarbonate. *Chemical Engineering Journal* 349, 241-248.

3. Cecconet, D., **Zou, S.**, Capodaglio, A.G., & He, Z. (2018) Evaluation of energy consumption of treating nitrate-contaminated groundwater by bioelectrochemical systems. *Science of the Total Environment* 636, 881-890.

4. Wu, Z., **Zou, S.**, Zhang, B., Wang, L., & He, Z. (2018) Forward osmosis promoted in-situ formation of struvite with simultaneous water recovery from digested swine wastewater. *Chemical Engineering Journal* 342, 274-280.

5. Qin, M., White, C., **Zou, S.**, & He, Z. (2018) Passive separation of recovered ammonia from catholyte for reduced energy consumption in microbial electrolysis cell. *Chemical Engineering Journal* 334, 2303-2307.

6. Wu, S., **Zou, S.**, Liang, G., Qian, G., & He, Z. (2018) Enhancing recovery of magnesium as struvite from landfill leachate by treatment of calcium with simultaneous reduction of liquid volume via forward osmosis. *Science of the Total Environment* 610-611, 137-146.

7. Yang, Y., Chen, M., **Zou, S.**, Long, T., Yang, X., & He, Z. (2017) Efficient recovery of polyelectrolyte draw solutes in forward osmosis towards sustainable water treatment. *Desalination* 422, 134-141.

8. Iskander, S., **Zou, S.**, Brazil, B., Novak, J., & He, Z. (2017) Energy consumption by forward osmosis treatment of landfill leachate for water recovery. *Waste Management* 63, 284-291.

9. Xiang, X., **Zou, S.**, & He, Z. (2017) Energy consumption of water recovery from wastewater in a submerged forward osmosis system with commercial liquid fertilizers as draw solutes. *Separation and Purification Technology* 174, 432-438.

Table of Contents

List of Figures

List of Tables

1 Introduction

(The content of this chapter comes from three published papers, including "Zou, S., Qin, M., and He, Z. (2019) Tackle reverse solute flux in forward osmosis towards sustainable water recovery: reduction and perspectives. *Water Research*, 49, 362-374", "Zou, S., Yuan, H., Childress, A., and He, Z. (2016) Energy consumption by recirculation: a missing parameter when evaluating forward osmosis. *Environmental Science & Technology*, 50(13), 6827-6829", and "Zou, S. and He, Z. Efficiently "pumping out" value-added resources from wastewater by bioelectrochemical systems: a review from energy perspectives. *Water Research*, 131, 62-73".)

1.1 Background

Rapid population growth and urbanization have created a "Perfect Storm" with water scarcity, increasing nutrient demand for food production, and energy shortage (McCarty et al. 2011). It has been estimated that by the year 2030, the world will need 30% more water, 50% more energy, and 50% more food (estimated by International Energy Agency, Food and Agriculture Organization, and International Food Policy Research Institute). The food-energy-water issue is further complicated by their interdependency: (1) Energy is constantly required to produce clean water and nutrient, for instance conventional wastewater treatment and ammonia synthesis consumes 3% of the US electricity (Water 2006) and 2% of the global electricity (Kermeli et al. 2017), respectively; (2) Water drives both the energy and food production, as thermoelectric power plants and agriculture irrigation being the top 2 categories (41% and 37%) of US water withdrawals (Maupin 2018); (3) Food security serves as the cornerstone of our social-economic development, and over fertilization and agriculture wastes not only lead to severe eutrophication on US east coast but also cost Americans $157 billion per year in damages to human health and the environment (Sobota et al. 2015). To effectively tackle this "Perfect Storm," the current paradigm to separately manage nutrient/food, energy, and water should be evolved via a "Nexus Thinking." Especially, the "Nexus Thinking" should be extended to wastewater management as wastewater fits in the center of the food-energy-water hub (Mo and Zhang 2013), considering wastewater could potentially serve as an emerging source to produce valuable nutrients (e.g., N and P), environmental-friendly bioenergy, and fresh water towards water reuse (Tong and Elimelech 2016).

Focusing on the water part of this "Perfect Storm," the imbalance between limited fresh water supply and mounting water demand hinders the rapid development of our society (Hoekstra and Wiedmann 2014). Alternative water sources, for instance via wastewater reuse and seawater desalination, must be explored to address the food-water-energy nexus (Oh et al. 2014). To achieve this goal, membrane-based water treatment, e.g., microfiltration (MF), ultrafiltration (UF), and membrane bioreactors (MBR), have been widely applied in past decades for water purification and desalination (Shannon et al. 2008). However, the reuse of filtrate or permeate is affected by the potential presence of pathogens (e.g., *Legionella* and *E. coli*) (EPA 2012) and trace chemicals (e.g., endocrine-disrupting compounds and heavy metals) (Wang et al. 2016). To minimize human health risk and avoid ingestion of xenobiotics, reverse osmosis (RO) as an advanced and robust technology has been implemented for water purification at the expense of high energy investment (1.5-4.0 kWh m^{-3}) (Yangali-Quintanilla et al. 2011). Hence, the most challenging technical barrier that sits between wastewater and reusable fresh water (and eventually between a wastewater treatment plant and an integrated nutrient-energy-water (NEW) recovery hub) is lacking a resilient, scalable, energy-efficient, and cost-effective water or resource reclamation technology tailored to wastewater.

1.2 Forward Osmosis

In recent years, osmotic driven membrane process (OMDP), especially forward osmosis (FO) or FO-based systems, have emerged as a potentially energy-efficient alternative for versatile applications, such as seawater desalination (Linares et al. 2014, McCutcheon et al. 2006), wastewater treatment (Holloway et al. 2007, Iskander et al. 2017, Zou et al. 2017), brine concentration (McGinnis et al. 2013, Tang and Ng 2008), food processing (Garcia-Castello et al. 2009, Sant'Anna et al. 2012), bioenergy production (Ge et al. 2013, Qin and He 2017), and power generation (Logan and Elimelech 2012, Yip et al. 2011). FO harnesses osmotic pressure gradient across a semi-permeable membrane to reclaim high-quality water, offering major merits include reduced operating pressure, high rejection of undesired compounds (comparable to RO), reversible membrane fouling, and less energy demand if energy-intensive draw regeneration can be appropriately solved (Liu et al. 2011, Su et al. 2012). The primary application of the FO process lies in two realms. The first pertains to systems where FO essentially serve as high-quality

pretreatment for a downstream desalination process (e.g., RO or distillation process), which reconcentrates the draw solution and provides high-quality product water. The second realm pertains to systems that do not require a reconcentration process, including the osmotic concentration of complex feed solutions for volume reduction (e.g., domestic and industrial wastewater) and osmotic dilution of application-specific draw solutes (e.g., fertilizers).

Though natural osmosis phenomenon has long been observed, the term "forward osmosis" first appeared in 1956 (Kamiya and Tazawa 1956). Over the following 60 years, the development of FO has gone through four stages, with substantial process advancement in each stage (Fig. 1.1). Before the middle 1970s, the initial effort was dedicated to proposing a general framework, including design parameters, osmosis kinetics, and the feasibility of extracting potable water from various feed sources in FO systems (Kessler and Moody 1976, Moody and Kessler 1976, Votta 1974).

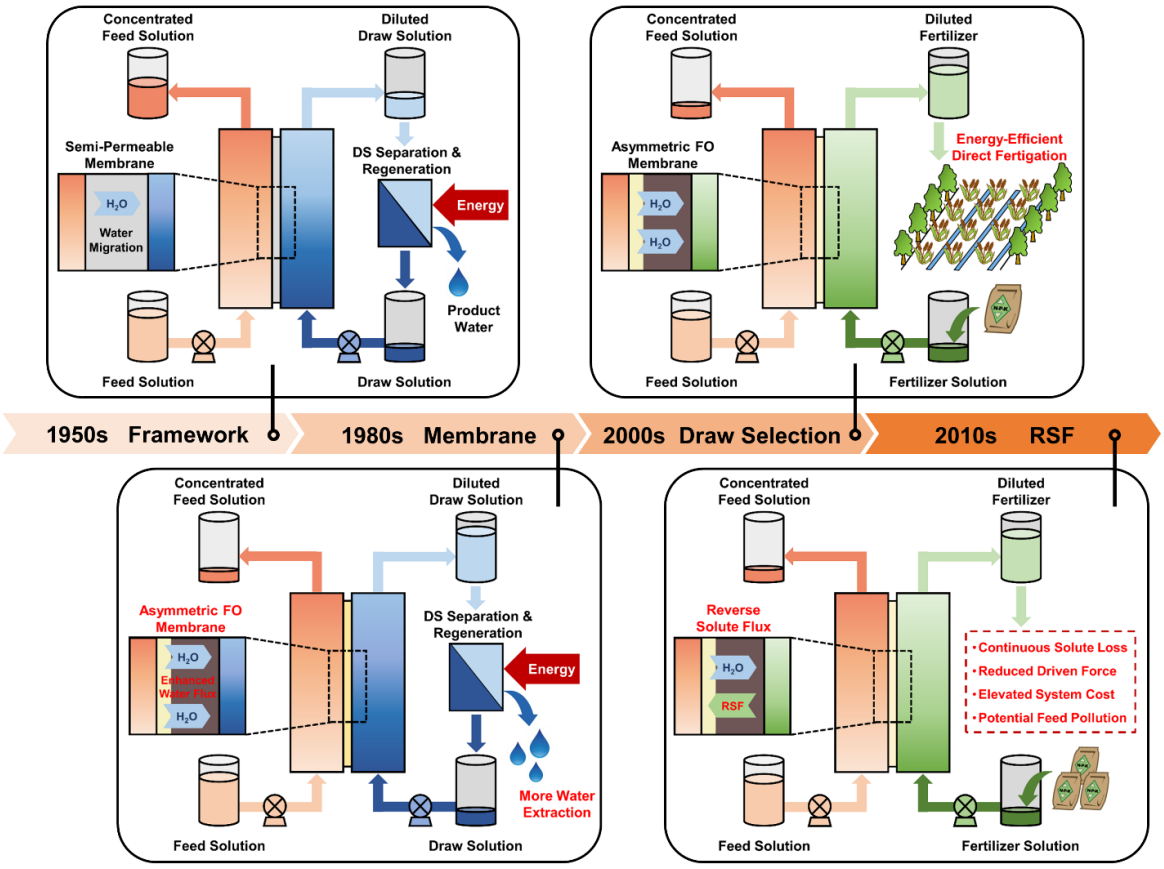

Figure 1.1 Roadmap of the four-stage FO development. The cross-flow FO module design is revised from a previous study with permission (Shaffer et al. 2015).

As a result, the trinity FO setup was proposed, including the low osmotic pressure feed solution, the high osmotic draw solution, and the middle semi-permeable membrane. From the middle 1970s to 1990s, the FO research started to focus more on fabricating a special "FO membrane" towards a more efficient water recovery performance, instead of using general semi-permeable materials (e.g., animal bladders and rubber) (Anderson 1977) and RO membranes (Kravath and Davis 1975). These efforts led to the development of asymmetric FO membrane made of a non-porous active layer and a porous support layer (Zhao et al. 2012). Unlike a pressure-driven RO process that generated fresh water directly, the "energy-efficient" FO process can only yield diluted draw solution, requiring energy- and cost-intensive downstream separation to regenerate draw solutes (DS) (Zou et al. 2017). The third stage of FO development aimed at smart selection of easily-recoverable DS, ranging from economically viable and non-toxic inorganic DS (Achilli et al. 2010), to phase-separation DS (Cai and Hu 2016), such as magnetic nanoparticles (Alejo et al. 2017), thermolytic ammonium bicarbonate (Qin and He 2014), and organic polymers (Yang et al. 2017, Zhang et al. 2015). However, these DS suffer from high cost due to complicated preparation (Minami et al. 2010), large solute loss (Zou et al. 2017), or weakened separation after regeneration (Ling et al. 2010). Hence, finding an ideal DS is extremely important for an energy-efficient and stable FO process.

Another critical challenge and also a key impediment remained to be solved in the fourth (current) stage is the salinity buildup on the feed side, resulted from both reverse solute flux (RSF, a major contributor) and concentrating effect by FO membrane rejection (Hancock and Cath 2009). RSF is defined as the cross-membrane diffusion of DS to the feed side driven by solute concentration difference (Phillip et al. 2010). The detrimental effects of RSF include gradual loss of DS, reduced osmotic driving force (i.e., lower water flux), increased fouling propensity, and elevated operation cost due to periodical replenishment of draw solutes (Akther et al. 2015). Accumulation of the reverse-fluxed DS, such as ammonium and phosphorus, will require further treatment of the feed stream (Phillip et al. 2010). To understand the solute permeation principle, lab-scale experiments integrated with mathematical modeling have been conducted to explore concentration polarization (both external and internal polarizations) (Phillip et al. 2010, Yaroshchuk 2010), solute-solvent interaction (Su and Chung 2011, Yong et al. 2012a), solute-solute interaction (Irvine et al. 2013, Lu et al. 2014), and chemical equilibrium (Yong et al. 2012b). The reverse permeation of solute ions is strongly linked to both intrinsic membrane parameters

(affected by thickness, tortuosity, and porosity) (McCutcheon and Elimelech 2006) and solute characteristics (e.g., hydrated ion radius, aqueous diffusivity, solution viscosity, and ion charges) (Zhao and Zou 2011). For example, smaller hydrated ions have an elevated tendency to penetrate the FO active layer (Wang et al. 2010). Meanwhile, ion charge plays a pivotal role in the magnitude of RSF. Because most FO membranes, made of either cellulose triacetate (CTA) or polyamide thin film composite (TFC), are negatively charged, resulting in easier cross-membrane penetration for DS cations than anions via Donnan dialysis and facilitated transport (Sarkar et al. 2010). To maintain solution electroneutrality, DS anions either permeate FO membrane together with cations or exchange with anions from the feed solution (Irvine et al. 2013). It is worth noting that some neutral DS, e.g., urea and ethylene glycol, have demonstrated significantly higher RSF compared to charged ions in FO process (Yong et al. 2012a, Zou and He 2016). To sum up, much effort is still required to achieve effective RSF control and enhance the competitiveness of the FO process.

1.3 Energy Consumption in Forward Osmosis

FO has been widely referred to as an "energy-efficient" process or an energy-efficient pretreatment process for a subsequent desalination process (e.g., RO); however, energy consumption data has rarely been reported in the literature (Shaffer et al. 2015). The possible energy consumers in an FO include: pretreatment of the feed and draw solutions (e.g., filtration), recirculation pump(s), draw solution reconcentration, fouling control, and post-treatment of the concentrated feed solution. In most cases, physical backwashing can be used to achieve at least 90% performance recovery from fouling, and the associated energy consumption is expected to be low (though lacking quantitative data in literature). Hence, it is expected that 71-98% of the total energy input, quantified as the specific energy consumption (SEC, kWh per m^3 reclaimed water), goes to the solute regeneration process. An early study of a hybrid FO-RO system provided an estimated SEC of 25 kWh m^{-3}, with 76% (19 kWh m^{-3}) being consumed by solute reconcentration (i.e., RO) (Cath et al. 2005). In another study, the energy-intensive RO process was eliminated by using a thermolytic NH_3-CO_2 draw solution that could be thermally reconcentrated using waste heat. This resulted in a significant reduction of the SEC for the whole system (0.84 kWh m^{-3}) with 71% (0.60 kWh m^{-3}) attributed to energy requirements for reconcentration (McGinnis and Elimelech 2007). In this case, 29% (0.24 kWh m^{-3}) was required for recirculation pumps; from this study, a threshold

value of 0.25 kWh m^{-3} was later used by many studies addressing energy-related issues in FO systems excluding solute reconcentration. Given that FO systems are typically operated using flow rates ranging from 400 to 1000 mL min^{-1} (8.5-21.3 cm s^{-1} in a 1.0-cm pipe) in bench-scale studies with an even higher recirculation implemented for pilot-scale application, the cost of recirculation can become a decisive factor in FO competitiveness.

As an essential part of an FO system, the recirculation pumps not only serve to transfer well-mixed solutions to the membrane; they also provide hydraulic shear forces to minimize potential fouling. However, very few studies (less than five publications from 2005 to 2016) have reported energy consumption of recirculation pumps, and the majority of those have not shown clear calculations. In a recent study that has quantified the SEC associated with recirculation pumps, a submerged FO system with treated wastewater as the feed and commercial fertilizer as the draw solution was evaluated (Zou and He 2016). In this scenario, the reconcentration process is eliminated through direct use of the diluted fertilizer, and thus, the recirculation pump was considered to be the major energy consumer. Power requirement by a recirculation pump is determined by the flow rate and hydraulic head loss (which is related to the diameter of the tubing) (Kim et al. 2011). Under a flow rate of 10 mL min^{-1} (0.85 cm s^{-1}, 0.5 cm tubing), the FO system reclaimed 155 mL water in 24 h, rendering an SEC of 0.02 ± 0.01 kWh m^{-3} (Fig.1.2). The estimated SEC was higher (11.93 ± 3.08 kWh m^{-3}) for a flow rate of 250 mL min^{-1} (21.25 cm s^{-1}). A higher flow rate is expected to promote mass transfer between the bulk solution and the membrane boundary layer, leading to reduced external concentration polarization (ECP) together with enhanced driving force (i.e., osmotic gradient). However, this enhancement was rather limited (water recovery of 182 mL at 250 mL min^{-1}) due to the negligible ECP at relatively low water fluxes. It was estimated that a minimum SEC of 1.86 ± 0.47 and 11.93 ± 3.08 kWh m^{-3} would be required in a regeneration-free FO system for flow velocities of 8.50 and 21.25 cm s^{-1} (which are typical values reported in the FO studies), respectively. The SEC estimate is largely affected by hydraulic head loss and the diameter of the tubing associated with the recirculation pumps, and thus the data presented here are only an example and may not represent energy consumption by FO systems with different configuration/operation. However, it does indicate that the high flow rates used in many laboratory-scale studies may need to be reconsidered in light of the energy required for recirculation. Although water flux may be enhanced with a higher recirculation rate in some FO systems and/or under different operating conditions, the increased energy demand

must be considered. Furthermore, to truly realize the energy efficiency of FO, lower flow rates may be favored. This has significant implication for the design of next-generation FO membranes; current research emphasizes the design of membranes with high water permeability to achieve high fluxes. Perhaps additional research is needed to prioritize high selectivity (low salt permeability) over productivity in order to improve not only energy efficiency but overall process efficiency. For sure, improved reporting of energy consumption for bench-, pilot-, and demonstration-scale studies would enable a better understanding of the competing challenges towards achieving high efficiencies and advancing FO commercialization.

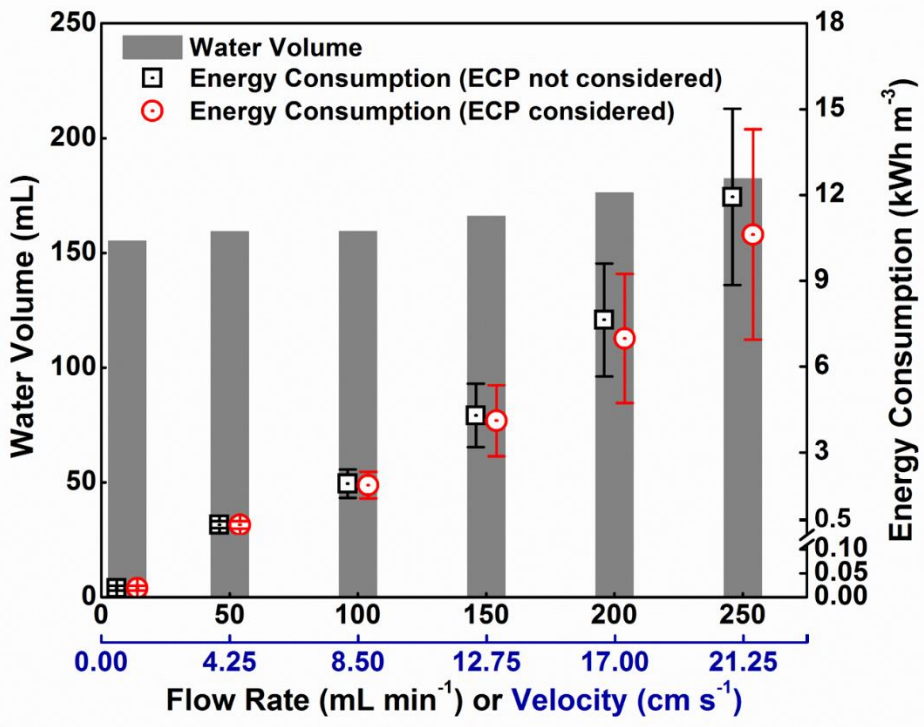

Figure 1.2 SEC and recovered water volume under different flow rates or velocities in a submerged FO operated for 24 h using the treated wastewater as the feed and 1-M commercial fertilizer solution as the draw. The data at the recirculation flow rate of 0-100 mL min^{-1} were obtained from a previous study with permission (Zou and He 2016).

1.4 Bioelectrochemical Systems

Though FO can offer energy-efficient recovery of fresh water, wastewater still contains a large amount of other valuable resources, including nutrients (e.g., nitrogen and phosphorus) and

bioenergy derived from organic wastes (Tong and Elimelech 2016). To achieve integrated NEW recovery, FO needs be synergistically coupled with other treatment processes to transform the current wastewater treatment plant into a sustainable NEW resource recovery hub. Among the newly developed treatment concepts, bioelectrochemical systems (BES) have demonstrated a promising potential with versatile applications to achieve specific resource recovery goals and broader flexibility in treating various types of wastewater (Logan and Rabaey 2012).

A typical BES employs exoelectrogens (electrochemically-active microorganisms donating electrons to the electrode) as anodic bio-catalysts to anaerobically oxidize the organics in wastewater (Logan 2009), or electrotrophs (electrochemically-active microorganisms receiving electrons from electrode) as cathodic bio-catalysts to achieve CO_2/HCO_3^- reduction (Lovley 2011). The released electrons from anode are transferred through an external circuit to a terminal electron acceptor in its cathode, thereby generating electric current. BES can be generally categorized into several groups based on their functions: (1) microbial fuel cells (MFC) focus on direct electricity generation with oxygen as a representative terminal electron acceptor; (2) microbial electrolysis cells (MEC) are able to accomplish hydrogen gas production and/or nutrient enrichment with externally applied voltage; (3) microbial electrosynthesis cell (MES), operated similarly to MECs, can reduce carbon dioxide to various organics with microbial catalysts in a cathode; and (4) microbial desalination cells (MDC) can produce fresh water from seawater or brackish water driven by the self-produced electric field or assisted by external power supply (Fig. 1.3) (Wang and Ren 2013). Among all four groups, MEC has been deemed as a perfect supplement to FO in order to recovery nutrient and energy from wastewater towards integrated NEW recovery.

To realize conversion of chemical energy from organics in wastewater to that stored in hydrogen gas, MEC requires a small voltage being exerted between anode and cathode. The exerted voltage (>0.2 V, serving as the bias between electrodes) is significantly lower than the theoretical value for water splitting (>1.23 V) (Bockris et al. 1985). Nutrient recovery is deemed as another unique advantage of MEC comparing to other biological nutrient removal or membrane treatment processes (Colombo et al. 2017, Qin and He 2017). As the dominant form of nitrogen, ammonium can reach several hundreds to thousands microgram per liter in high-strength wastewater. Conventional biological nutrient removal (e.g., nitrification/denitrification and Anammox) focuses on eliminating ammonium from wastewater with consumption of a large

amount of energy and chemicals and generation of excess biosolids. Recovery of ammonia from wastewater, instead of removal, has the potential to reduce the energy consumption of the treatment processes and supply valuable nitrogen elements for agricultural or other practices (Kuntke et al. 2012). Two major mechanisms has been revealed during ammonia separation in BES (Kim et al. 2008, Sleutels et al. 2009), including diffusion driven by concentration gradient across CEM and migration induced by an electric field (serving as proton shuttle) (Cord-Ruwisch et al. 2011). Both mechanisms are associated with current generation that creates an pH gradient. To efficiently separate ammonia out of the catholyte, a coupled stripping process is required via the use of the produced hydrogen gas or external aeration (at the cost of additional energy consumption).

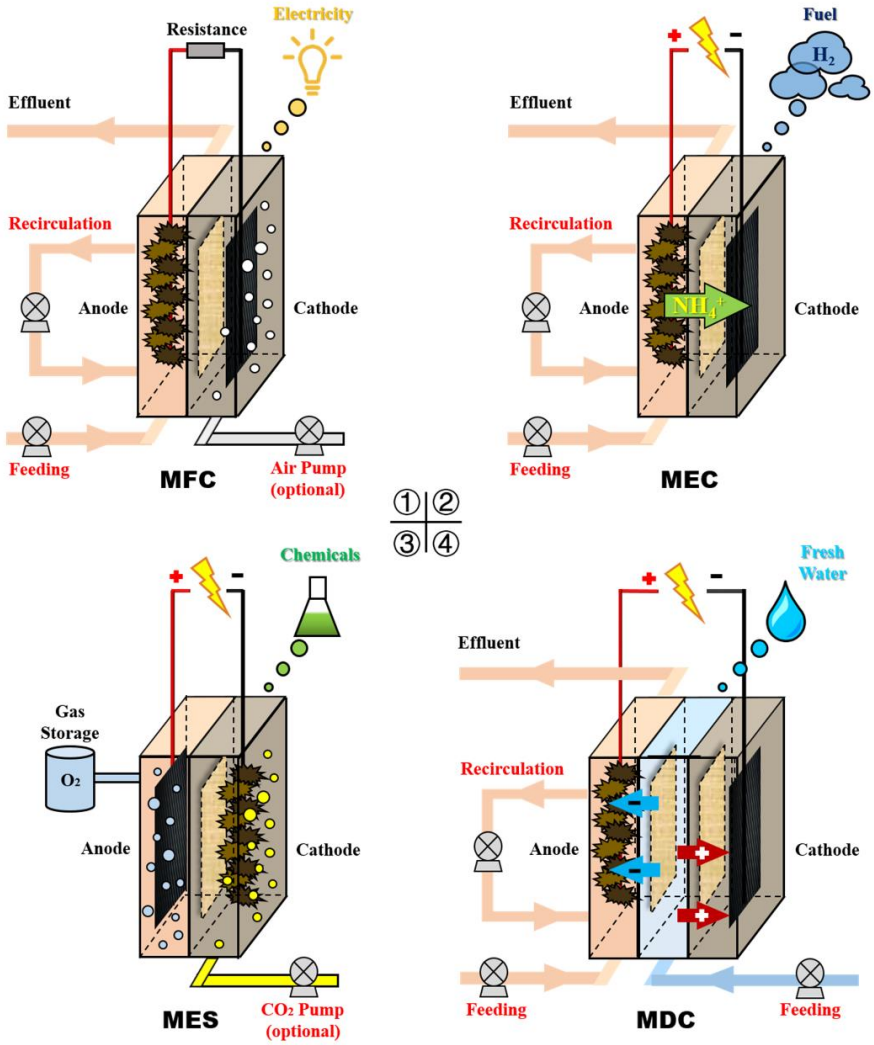

Figure 1.3 Schematics of typical microbial fuel cell (MFC), microbial electrolysis cell (MEC), microbial electrosynthesis system (MES), and microbial desalination cell (MDC).

1.5 Outline

This dissertation has in total eight (8) chapters. The overarching goal of all the studies is to address the current challenges facing by FO in order to enhance its competitiveness against other membrane processes and to promote its broader application in water reuse and resource recovery.

The first specific aim (**SA1**) of this dissertation is to propose and evaluate cost-effective DS to bypass DS regeneration/separation in order to achieve energy-efficient water recovery. The previous FO study tends to use inorganic DS for water reclamation, leading to additional energy investment and an energy-intensive FO process. Using fertilizers as draw solutes in forward osmosis (FO) can accomplish direct water reuse with elimination of recycling DS towards a true "energy-efficient" process. In this study, three commercial fast-release all-purpose solid fertilizers were examined as draw solutes in a submerged FO system for water extraction from either deionized (DI) water or the treated wastewater. This is the first FO study using solid commercial fertilizers with comprehensive assessment.

The second specific aim (**SA2**) of this dissertation is to propose and investigate operational strategy to recover reverse-fluxed DS in the feed solution in order to mitigate salinity buildup issue. When nutrient-rich DS (such as the fertilizers in **SA1**) is applied in the FO system, we find that some parts of the DS (especially the inorganic nitrogen in the form of ammonium, nitrate, and nitrite) can migrate through the FO membrane and get into the feed solution, leading to potential pollution to the original feed (e.g., the wastewater) and elevated operation cost if further treatment is required before discharge. One potential strategy to address this issue is to recapture these escaped DS from the feed solution. To achieve this, an electrodialysis (ED) has been utilized as an effective approach to separate these "escaped" DS from the feed solution. In this study, a forward osmosis - electrodialysis (FO-ED) hybrid system has been constructed by using diammonium phosphate (DAP, $(NH_4)_2HPO_4$), a common fertilizer, as a non-regeneration draw solute to achieve water reclamation and mitigation of salinity buildup. This is also the first study to integrate ED device with FO for DS separation in the feed solution towards DS reuse.

The third specific aim (**SA3**) is to explore and optimize operational strategy to inhibit RSF in order to achieve *in-situ* RSF reduction. RSF can cause loss of draw solutes, salinity build-up and undesired contamination at the feed side. Previous study (i.e., **SA2**) can achieve successful control of salinity buildup by utilization of ED device, but salinity or solute buildup is just a

consequence of RSF. Effective strategy must be proposed to address RSF directly to control this DS leaking phenomenon. Considering inorganic DS contains positively and negatively charged ions, we hypothesize that ion transport pattern can be manipulated by exerting an electric field. In this study, *in-situ* electrolysis was employed to mitigate RSF in a three-chamber FO system ("e-FO") with Na_2SO_4 as a draw solute and deionized (DI) water as a feed. This is the first study to exploit weak electrolysis with minimal energy input to achieve *in-situ* RSF mitigation.

The fourth specific aim (**SA4**) is to effectively control RSF through membrane modification. We have utilized several "external" strategies to mitigate RSF or RSF consequences (i.e., salinity buildup). The ultimate cause of RSF is the FO membrane itself failing to be a perfect barrier, and hence we need to focus on the membrane itself in order to eliminate RSF. Manufacturing a completely new and perfect FO membrane could take a very long time with comprehensive evaluation and optimization. Alternatively, membrane modification on existing commercial membrane can serve as a more viable and convenient approach at this stage. In this study, mitigation and control of bidirectional solute flux in FO process has been comprehensively investigated via surface coating of zwitterion-functionalized carbon nanotubes (Z-CNT). Specific RSF and FSF with a unit of gram diffused solute per liter recovered water were selected to enable better comparison with previous studies. This research is among the first few studies to utilize Z-CNT towards a reduce bidirectional flux in the FO system.

The fifth specific aim (**SA5**) is to conduct a comprehensive review of all available techniques to mitigate RSF. Prior to this study, there is no universal parameters have been developed to compare RSF control performance among various studies, making it difficult to position us in this "battle" against RSF. From our perspectives, we have observed the adverse effect of RSF (**SA1**) and have made tremendous effort (from **SA2** to **SA4**) to control and mitigate RSF in the FO system, yet it is of equal importance to know the current research status in this field as well as challenges faced when addressing RSF issues. In this study, we have conducted a review of existing RSF reduction approaches, including operational strategies (e.g., pressure-, electricity-, and ultrasound-assisted osmosis) and advanced membrane development (e.g., new membrane fabrication and existing membrane modification). We have also analyzed the literature data to reveal the current status of RSF reduction. A new parameter, mitigation ratio (MR), was proposed and used together with specific RSF (SRSF) to evaluate RSF reduction performance. Potential

research directions have been discussed to help with future RSF control. This review intends to shed more light on how to effectively tackle solute leakage towards a more cost-effective and environmental-friendly FO treatment process.

The last specific aim (**SA6**) is to synergistically integrated FO and MEC to achieve nutrient-energy-water recovery from wastewater. FO, as a standalone process, can only recover the freshwater part from the wastewater. However, there are lots of other resources within the wastewater, including nutrients and organics. Integrated recovery of nutrients, water, and energy from wastewater (e.g., high-strength sidestream centrate) offers benefits such as reusable resource, minimized discharge and cost-savings in mainstream treatment. Herein, we have comprehensively evaluated the feasibility of the aforementioned NEW recovery from synthetic centrate by using this hybrid MEC-FO system (linked to a struvite precipitation process). A detailed mass balance has been constructed under a closed-loop operation to access MEC-FO overall performance on the system level. This study is also one of the first endeavors to tackle integrated NEW recovery from wastewater by using an energy-efficient process. The results can serve as a cornerstone to upgrade current wastewater treatment plants to a sustainable NEW resource recovery hub, addressing mounting resource needs while ensuring food-energy-water security on a global scale.

1.6 Attribution

Each coauthor is duly credited for his or her contribution to this work, both in their sharing of ideas and technical expertise.

Zhen He, Ph.D., Professor of Civil and Environmental Engineering (Principal Investigator)

Department of Civil and Environmental Engineering, Virginia Polytechnic Institute and State University, Blacksburg, VA 24061

Coauthor of Chapter 1, 2, 3, 4, 5, 6, and 7

Amy Childress, Ph.D., Professor of Civil and Environmental Engineering

Department of Civil and Environmental Engineering, University of Southern California, Los Angeles, CA 90089

Coauthor of Chapter 1

Heyang Yuan, Ph.D.

Department of Civil and Environmental Engineering, University of Illinois at Urbana-Champaign, IL 61801

Coauthor of Chapter 1

Ethan D. Smith

Department of Chemical Engineering, Virginia Polytechnic Institute and State University, Blacksburg, VA 24061

Coauthor of Chapter 5

Stephen M. Martin, Ph.D., Associate Professor of Chemical Engineering

Department of Chemical Engineering, Virginia Polytechnic Institute and State University, Blacksburg, VA 24061

Coauthor of Chapter 5

Mohan Qin, Ph.D.

Department of Chemical and Environmental Engineering, Yale University, New Haven, CT 06520

Coauthor of Chapter 6 and 7

Yann Moreau, Ph.D.

Veolia Research & Innovation North American, Chicago, IL 60601

Coauthor of Chapter 7

References

Achilli, A., Cath, T.Y. and Childress, A.E. (2010) Selection of inorganic-based draw solutions for forward osmosis applications. Journal of Membrane Science 364(1), 233-241.

Akther, N., Sodiq, A., Giwa, A., Daer, S., Arafat, H.A. and Hasan, S.W. (2015) Recent advancements in forward osmosis desalination: A review. Chemical Engineering Journal 281, 502-522.

Alejo, T., Arruebo, M., Carcelen, V., Monsalvo, V.M. and Sebastian, V. (2017) Advances in draw solutes for forward osmosis: Hybrid organic-inorganic nanoparticles and conventional solutes. Chemical Engineering Journal 309, 738-752.

Anderson, D.K. (1977) Concentration of dilute industrial wastes by Direct osmosis.

Bockris, J.O.M., Dandapani, B., Cocke, D. and Ghoroghchian, J. (1985) On the splitting of water. International Journal of Hydrogen Energy 10(3), 179-201.

Cai, Y. and Hu, X.M. (2016) A critical review on draw solutes development for forward osmosis. Desalination 391, 16-29.

Cath, T.Y., Gormly, S., Beaudry, E.G., Flynn, M.T., Adams, V.D. and Childress, A.E. (2005) Membrane contactor processes for wastewater reclamation in space: Part I. Direct osmotic concentration as pretreatment for reverse osmosis. Journal of Membrane Science 257(1), 85-98.

Cord-Ruwisch, R., Law, Y. and Cheng, K.Y. (2011) Ammonium as a sustainable proton shuttle in bioelectrochemical systems. Bioresource Technology 102(20), 9691-9696.

EPA, U.S. (2006) Wastewater Management Fact Sheet, Energy Conservation, EPA 832-F-06-024. Washington, D.C.

EPA, U.S. (2012) Guidelines for water reuse. Washington, D.C.

Garcia-Castello, E.M., McCutcheon, J.R. and Elimelech, M. (2009) Performance evaluation of sucrose concentration using forward osmosis. Journal of Membrane Science 338(1-2), 61-66.

Ge, Z., Ping, Q., Xiao, L. and He, Z. (2013) Reducing effluent discharge and recovering bioenergy in an osmotic microbial fuel cell treating domestic wastewater. Desalination 312, 52-59.

Hancock, N.T. and Cath, T.Y. (2009) Solute coupled diffusion in osmotically driven membrane processes. Environmental Science & Technology 43(17), 6769-6775.

Hoekstra, A.Y. and Wiedmann, T.O. (2014) Humanity's unsustainable environmental footprint. Science 344(6188), 1114-1117.

Holloway, R.W., Childress, A.E., Dennett, K.E. and Cath, T.Y. (2007) Forward osmosis for concentration of anaerobic digester centrate. Water Research 41(17), 4005-4014.

Irvine, G.J., Rajesh, S., Georgiadis, M. and Phillip, W.A. (2013) Ion selective permeation through cellulose acetate membranes in forward osmosis. Environmental Science & Technology 47(23), 13745-13753.

Iskander, S.M., Zou, S., Brazil, B., Novak, J.T. and He, Z. (2017) Energy consumption by forward osmosis treatment of landfill leachate for water recovery. Waste Management 63, 284-291.

Kamiya, N. and Tazawa, M. (1956) Studies on water permeability of a single plant cell by means of transcellular osmosis. Protoplasma 46(1-4), 394-422.

Kermeli, A., Worrell, E., Graus, W. and Corsten, M. (2017) Energy Efficiency and Cost Saving Opportunities for Ammonia and Nitrogenous Fertilizer Production-An ENERGY STAR® Guide for Energy and Plant Managers, EPA-United States Environmental Protection Agency.

Kessler, J. and Moody, C. (1976) Drinking water from sea water by forward osmosis. Desalination 18(3), 297-306.

Kim, J., Kim, K., Ye, H., Lee, E., Shin, C., McCarty, P.L. and Bae, J. (2011) Anaerobic Fluidized Bed Membrane Bioreactor for Wastewater Treatment. Environmental Science & Technology 45(2), 576-581.

Kim, J.R., Zuo, Y., Regan, J.M. and Logan, B.E. (2008) Analysis of ammonia loss mechanisms in microbial fuel cells treating animal wastewater. Biotechnology and Bioengineering 99(5), 1120-1127.

Kravath, R.E. and Davis, J.A. (1975) Desalination of sea water by direct osmosis. Desalination 16(2), 151-155.
Linares, R.V., Li, Z., Sarp, S., Bucs, S.S., Amy, G. and Vrouwenvelder, J.S. (2014) Forward osmosis niches in seawater desalination and wastewater reuse. Water Research 66, 122-139.
Ling, M.M., Wang, K.Y. and Chung, T.-S. (2010) Highly water-soluble magnetic nanoparticles as novel draw solutes in forward osmosis for water reuse. Industrial & Engineering Chemistry Research 49(12), 5869-5876.
Liu, Z., Bai, H., Lee, J. and Sun, D.D. (2011) A low-energy forward osmosis process to produce drinking water. Energy & Environmental Science 4(7), 2582-2585.
Logan, B.E. (2009) Exoelectrogenic bacteria that power microbial fuel cells. Nature Reviews Microbiology 7(5), 375-381.
Logan, B.E. and Elimelech, M. (2012) Membrane-based processes for sustainable power generation using water. Nature 488(7411), 313.
Logan, B.E. and Rabaey, K. (2012) Conversion of wastes into bioelectricity and chemicals by using microbial electrochemical technologies. Science 337(6095), 686-690.
Lovley, D.R. (2011) Powering microbes with electricity: direct electron transfer from electrodes to microbes. Environmental Microbiology Reports 3(1), 27-35.
Lu, X., Boo, C., Ma, J. and Elimelech, M. (2014) Bidirectional Diffusion of Ammonium and Sodium Cations in Forward Osmosis: Role of Membrane Active Layer Surface Chemistry and Charge. Environmental Science & Technology 48(24), 14369-14376.
Maupin, M.A. (2018) Summary of estimated water use in the United States in 2015, US Geological Survey.
McCarty, P.L., Bae, J. and Kim, J. (2011) Domestic wastewater treatment as a net energy producer–can this be achieved? Environmental Science & Technology 45(17), 7100-7106.
McCutcheon, J.R. and Elimelech, M. (2006) Influence of concentrative and dilutive internal concentration polarization on flux behavior in forward osmosis. Journal of Membrane Science 284(1), 237-247.
McCutcheon, J.R., McGinnis, R.L. and Elimelech, M. (2006) Desalination by ammonia–carbon dioxide forward osmosis: influence of draw and feed solution concentrations on process performance. Journal of Membrane Science 278(1), 114-123.
McGinnis, R.L. and Elimelech, M. (2007) Energy requirements of ammonia–carbon dioxide forward osmosis desalination. Desalination 207(1), 370-382.
McGinnis, R.L., Hancock, N.T., Nowosielski-Slepowron, M.S. and McGurgan, G.D. (2013) Pilot demonstration of the NH3/CO2 forward osmosis desalination process on high salinity brines. Desalination 312, 67-74.
Minami, H., Kimura, A., Kinoshita, K. and Okubo, M. (2010) Preparation of Poly(acrylic acid) Particles by Dispersion Polymerization In an Ionic Liquid. Langmuir 26(9), 6303-6307.
Mo, W. and Zhang, Q. (2013) Energy–nutrients–water nexus: integrated resource recovery in municipal wastewater treatment plants. Journal of Environmental Management 127, 255-267.
Moody, C. and Kessler, J. (1976) Forward osmosis extractors. Desalination 18(3), 283-295.
Oh, Y., Lee, S., Elimelech, M., Lee, S. and Hong, S. (2014) Effect of hydraulic pressure and membrane orientation on water flux and reverse solute flux in pressure assisted osmosis. Journal of Membrane Science 465, 159-166.
Phillip, W.A., Yong, J.S. and Elimelech, M. (2010) Reverse draw solute permeation in forward osmosis: modeling and experiments. Environmental Science & Technology 44(13), 5170-5176.
Qin, M. and He, Z. (2014) Self-Supplied Ammonium Bicarbonate Draw Solute for Achieving Wastewater Treatment and Recovery in a Microbial Electrolysis Cell-Forward Osmosis-Coupled System. Environmental Science & Technology Letters 1(10), 437-441.
Qin, M. and He, Z. (2017) Resource recovery by osmotic bioelectrochemical systems towards sustainable wastewater treatment. Environmental Science: Water Research & Technology 3(4), 583-592.
Sant'Anna, V., Marczak, L.D.F. and Tessaro, I.C. (2012) Membrane concentration of liquid foods by forward osmosis: Process and quality view. Journal of Food Engineering 111(3), 483-489.

Sarkar, S., SenGupta, A.K. and Prakash, P. (2010) The Donnan membrane principle: opportunities for sustainable engineered processes and materials, Environemental Science & Technology 44(4), 1161-1166.
Shaffer, D.L., Werber, J.R., Jaramillo, H., Lin, S. and Elimelech, M. (2015) Forward osmosis: Where are we now? Desalination 356, 271.
Shannon, M.A., Bohn, P.W., Elimelech, M., Georgiadis, J.G., Marinas, B.J. and Mayes, A.M. (2008) Science and technology for water purification in the coming decades. Nature 452(7185), 301-311.
Sleutels, T.H.J.A., Lodder, R., Hamelers, H.V.M. and Buisman, C.J.N. (2009) Improved performance of porous bio-anodes in microbial electrolysis cells by enhancing mass and charge transport. International Journal of Hydrogen Energy 34(24), 9655-9661.
Sobota, D.J., Compton, J.E., McCrackin, M.L. and Singh, S. (2015) Cost of reactive nitrogen release from human activities to the environment in the United States. Environmental Research Letters 10(2), 025006.
Su, J. and Chung, T.-S. (2011) Sublayer structure and reflection coefficient and their effects on concentration polarization and membrane performance in FO processes. Journal of Membrane Science 376(1-2), 214-224.
Su, J., Zhang, S., Ling, M.M. and Chung, T.-S. (2012) Forward osmosis: an emerging technology for sustainable supply of clean water. Clean Technologies and Environmental Policy, 1-5.
Tang, W. and Ng, H.Y. (2008) Concentration of brine by forward osmosis: performance and influence of membrane structure. Desalination 224(1-3), 143-153.
Tong, T. and Elimelech, M. (2016) The Global Rise of Zero Liquid Discharge for Wastewater Management: Drivers, Technologies, and Future Directions. Environmental Science & Technology 50(13), 6846-6855.
Votta, F. (1974) Concentration of Industial Waste by Direct Osmosis.
Wang, H. and Ren, Z.J. (2013) A comprehensive review of microbial electrochemical systems as a platform technology. Biotechnology Advances 31(8), 1796-1807.
Wang, R., Shi, L., Tang, C.Y., Chou, S., Qiu, C. and Fane, A.G. (2010) Characterization of novel forward osmosis hollow fiber membranes. Journal of Membrane Science 355(1), 158-167.
Wang, X., Chang, V.W.C. and Tang, C.Y. (2016) Osmotic membrane bioreactor (OMBR) technology for wastewater treatment and reclamation: Advances, challenges, and prospects for the future. Journal of Membrane Science 504, 113-132.
Yang, Y., Chen, M., Zou, S., Yang, X., Long, T.E. and He, Z. (2017) Efficient recovery of polyelectrolyte draw solutes in forward osmosis towards sustainable water treatment. Desalination 422, 134-141.
Yangali-Quintanilla, V., Li, Z., Valladares, R., Li, Q. and Amy, G. (2011) Indirect desalination of Red Sea water with forward osmosis and low pressure reverse osmosis for water reuse. Desalination 280(1), 160-166.
Yaroshchuk, A. (2010) Influence of osmosis on the diffusion from concentrated solutions through composite/asymmetric membranes: Theoretical analysis. Journal of Membrane Science 355(1-2), 98-103.
Yip, N.Y., Tiraferri, A., Phillip, W.A., Schiffman, J.D., Hoover, L.A., Kim, Y.C. and Elimelech, M. (2011) Thin-film composite pressure retarded osmosis membranes for sustainable power generation from salinity gradients. Environmental Science & Technology 45(10), 4360-4369.
Yong, J.S., Phillip, W.A. and Elimelech, M. (2012a) Coupled reverse draw solute permeation and water flux in forward osmosis with neutral draw solutes. Journal of Membrane Science 392–393, 9-17.
Yong, J.S., Phillip, W.A. and Elimelech, M. (2012b) Reverse permeation of weak electrolyte draw solutes in forward osmosis. Industrial & Engineering Chemistry Research 51(41), 13463-13472.
Zhang, H.M., Li, J.J., Cui, H.T., Li, H.J. and Yang, F.L. (2015) Forward osmosis using electric-responsive polymer hydrogels as draw agents: Influence of freezing-thawing cycles, voltage, feed solutions on process performance. Chemical Engineering Journal 259, 814-819.
Zhao, S. and Zou, L. (2011) Relating solution physicochemical properties to internal concentration polarization in forward osmosis. Journal of Membrane Science 379(1), 459-467.

Zhao, S., Zou, L., Tang, C.Y. and Mulcahy, D. (2012) Recent developments in forward osmosis: opportunities and challenges. Journal of Membrane Science 396, 1-21.
Zou, S. and He, Z. (2016) Enhancing wastewater reuse by forward osmosis with self-diluted commercial fertilizers as draw solutes. Water Research 99, 235-243.
Zou, S., Qin, M., Moreau, Y. and He, Z. (2017) Nutrient-energy-water recovery from synthetic sidestream centrate using a microbial electrolysis cell - forward osmosis hybrid system. Journal of Cleaner Production 154, 16-25.

2 Enhancing Wastewater Reuse by Forward Osmosis with Self-Diluted Commercial Fertilizers as Draw Solutes

(This chapter has been published as "Zou, S. and He, Z. (2016) Enhancing wastewater reuse by forward osmosis with self-diluted commercial fertilizers as draw solutes. *Water Research*, 99, 234-243")

2.1 Abstract

Using fertilizers as draw solutes in forward osmosis (FO) can accomplish wastewater reuse with elimination of recycling draw solute. In this study, three commercial fast-release all-purpose solid fertilizers (F1, F2 and F3) were examined as draw solutes in a submerged FO system for water extraction from either deionized (DI) water or the treated wastewater. Systematic optimizations were conducted to enhance water extraction performance, including operation modes, initial draw concentrations and *in-situ* chemical fouling control. Under the active layer facing the feed (AL-F or FO) mode, a maximum of 324 mL water was harvested using 1-M F1, which provided 41% of the water need for fertilizer dilution for irrigation. Among the three fertilizers, F1 containing less urea content was the most favored because of a higher water extraction and a lower reverse solute flux (RSF) of major nutrients. Using the treated wastewater as a feed solution resulted in a comparable water extraction performance (317 mL) to that of DI water in 72 h and a maximum water flux of 4.2 LMH. Solute build-up on the feed side was mainly attributed to the concentrating effect for phosphorous (81%) and RSF for total nitrogen (98%) and potassium (75%). Reducing recirculation intensity from 100 to 10 mL min^{-1} did not obviously decrease water flux but significantly reduced the energy consumption from 1.86 to 0.02 kWh m^{-3}. These results have demonstrated the feasibility of using commercial solid fertilizers as draw solutes for extracting reusable water from wastewater and challenges such as reverse solute flux will need to be further addressed.

2.2 Graphical Abstract

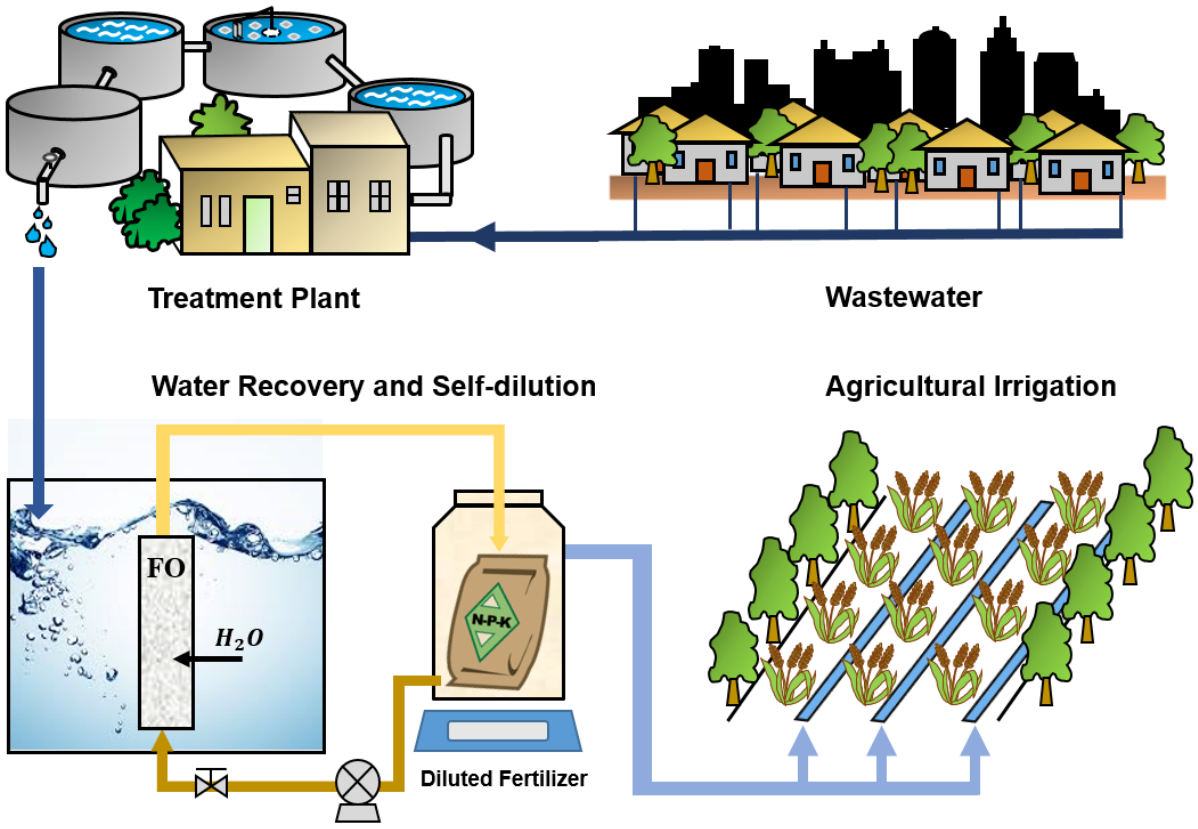

2.3 Keywords

Forward osmosis; Commercial fertilizers; Reverse solute flux; Wastewater reuse; Energy

2.4 Introduction

Agricultural irrigation is considered as a water-intensive process and consumes 72% of global freshwater withdrawal (Cai and Rosegrant 2003). Exploring alternative water supply for irrigation, for instance via reusing wastewater, will be of great importance (Xie et al. 2015). One of the key challenges to accomplish sustainable water recovery in FO is the separation and recovery of draw solutes, which accounts for most of the energy consumption (Achilli et al. 2010, McGinnis and Elimelech 2007). Novel draw solutes including the self-separated ionic solution (Bowden et al. 2012, Cai et al. 2015) and thermolytic ammonium bicarbonate (NH_3-CO_2) (McCutcheon et al. 2005) were proposed for easy regeneration while maintaining high osmotic pressure and desirable water flux. However, regeneration of those draw solutes still bears problems. For example, recovery of NH_3-CO_2 requires relatively high decomposition temperature (at least 60 °C), leading to additional energy input, and the thermal-responsive ionic solution may result in potential environmental concerns and health risks due to leakage of ionic solutes.

Fertilizers were proposed and investigated as draw solutes to eliminate the need for regeneration (Table 2.1). The self-diluted fertilizers can be directly used for agricultural irrigation, providing an alternative to bypass the energy-intensive draw solute recovery process (Hoover et al. 2011). Phuntsho et al. (2011) proposed nine inorganic chemicals as hypothetical fertilizers and evaluated their osmotic dilution performance in a cross-flow FO system by using DI water as feed (Phuntsho et al. 2011). Subsequent laboratory studies verified the feasibility of continuous water recovery from synthetic brackish groundwater and seawater (Lotfi et al. 2015, Majeed et al. 2015, Phuntsho et al. 2013, Phuntsho et al. 2014, Phuntsho et al. 2012a, Phuntsho et al. 2012b, Sahebi et al. 2015). A pilot-scale fertilizer drawn forward osmosis and nanofiltration (FDFO-NF) was recently established and had been successfully operated for six months (Phuntsho et al. 2016). Although the prior studies have investigated both single chemical reagent such as NH_4NO_3 and KCl, and blended draw solutes containing defined chemicals, all-purpose commercial fertilizers with a full-spectrum supplement of nutrients that are designed for practical applications have not been well examined in FO. A recent study demonstrated the osmotic dilution of the commercial all-purpose liquid fertilizers (Xie et al. 2015); however, liquid fertilizers are less favored than solid fertilizers because of the problems associated with storage and transportation. Therefore, there is a need to study water recovery by using commercially available solid fertilizers.

In this study, three commercial fast-release and all-purpose solid fertilizers were examined as draw solutes in a submerged FO system for water extraction from either DI water or the treated wastewater. The submerged FO configuration was employed because it has less energy consumption, rendering a small footprint, more operation flexibility, and easily scalable features (van Haandel and van der Lubbe 2012), compared to cross-flow FO systems. Water flux and recovery as a percentage of required water for fertilizer dilution were evaluated with different fertilizers or concentrations. The detailed nutrient distribution (N/P/K) in both draw and feed, as well as nutrient loss, were investigated. Operation modes and energy consumption of the FO system were studied and analyzed.

2.5 Materials and Methods

2.5.1 Characteristics of fertilizers and preparation of draw solution

The commercial all-purpose solid fertilizers were obtained from retailers with detailed information in Table 2.2. All three fertilizers (noted as "F1", "F2", and "F3") are widely used on farms and gardens for high yields. Due to the complexity of fertilizer composition, the fertilizer concentration was quantified by total nitrogen concentration, which was calculated based on the information from the manufacturer. For example, 1 M fertilizer in this study means its theoretical total nitrogen concentration is 1 mol L^{-1}. To prepare draw solutions, fertilizer was first dissolved in 100 mL DI water with pH adjustment (0.2 mol L^{-1} NaOH, dropwise) to around 7.0 and then centrifuged at 5000 rpm for 10 min to remove undissolved particles/precipitants. Of this 100-mL solution, 10 mL was used to analyze the nutrient concentrations, and 85 mL was applied as the draw solution. The remaining solids were preserved in the fridge and could be added to final diluted fertilizers to avoid possible loss of trace elements (not studied here).

2.5.2 Setup and operation of a submerged FO system

The flat-plate FO cell contained two pieces of cellulose triacetate (CTA) membranes with a total surface area (S) of 0.0025 m^2 (Hydration Technologies Inc., Albany, OR, USA) and is installed on both sides of the FO cell, creating a middle chamber of 13 mL for draw solution. The CTA membrane had a guaranteed pH tolerance of 2-12 suggested by its manufacturer (Alsvik and Hägg 2013). Plastic mesh was applied outside the FO membranes to prevent potential swelling. The FO

cell was submerged in the feed solution in a 1-L plastic beaker (Fig. 2.1), and the feed solution was either DI water or the treated wastewater (Peppers Ferry Wastewater Treatment Plant, Radford, VA, USA). The feed solution was supplemented periodically to maintain a constant liquid volume of 500 mL. The characteristics of the treated wastewater are shown in Table 2.3. The FO system was operated under a batch mode with different fertilizers and/or various initial concentrations. For each batch test, 85 mL fertilizer solution was recirculated in the middle chamber of the FO cell at 100 mL min^{-1} (6.7 cm s^{-1}) unless stated elsewhere. Water samples were taken every 24 h for water quality analysis. The whole experiment was operated in a temperature-controlled lab (20 ± 2 °C) with a centralized air conditioning system.

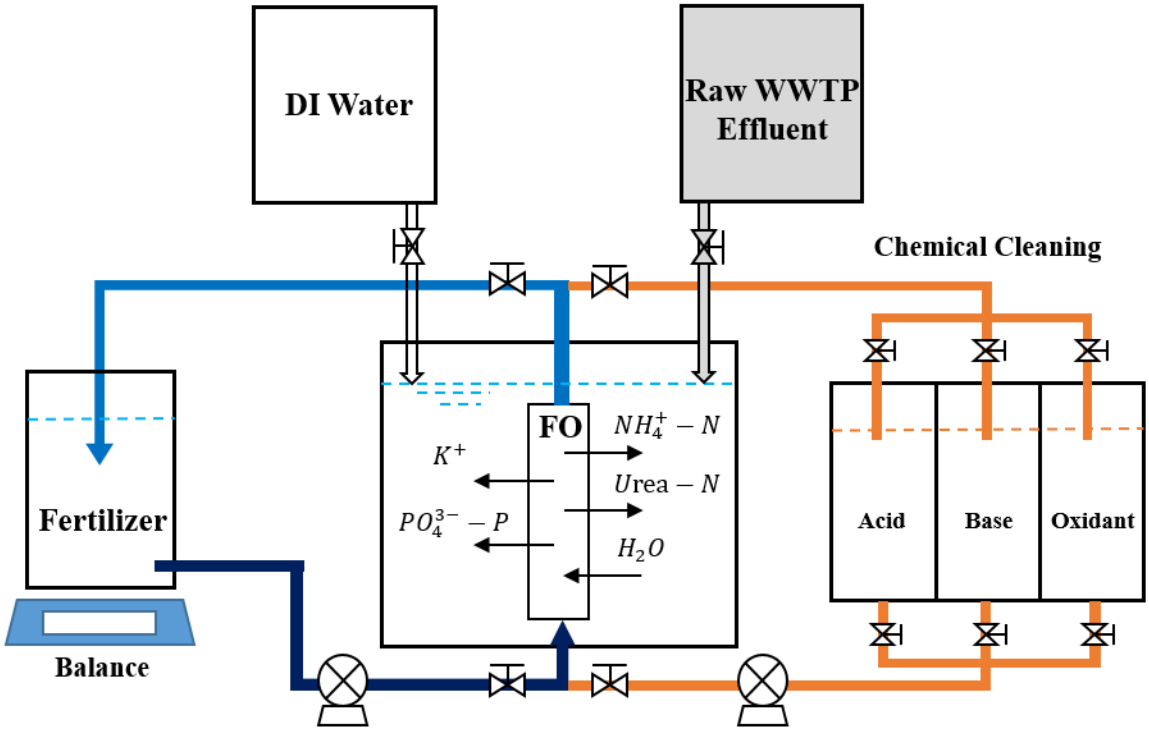

Figure 2.1 Schematic of submerged forward osmosis with in-situ chemical cleaning system.

2.5.3 Experimental procedure

A series of system optimization experiments were performed with DI water as the feed, including operation mode (i.e., membrane orientation), fouling control, reverse solute flux (RSF), fertilizer (draw) concentration. The active layer of the CTA membrane faced either the draw (AL-D, PRO mode) or the feed (AL-F, FO mode) to examine the effect of different operating modes using 1-M F1 as the draw. The F1 concentration was varied at 1M, 2M, and 3M for studying water extraction

and dilution rate. Comparison of three fertilizers (F 1-3) was conducted by operating the FO system with each fertilizer at a concentration of 1 M and under the FO mode. The optimized operation conditions (above-mentioned) were applied for examining water recovery from the treated wastewater by using the treated wastewater as the feed and 1-M F1 as the draw. Different recirculation rates, i.e., 10 mL min^{-1}, 50 mL min^{-1} and 100 mL min^{-1}, were successively investigated towards minimized energy consumption by the FO system. A batch test was terminated if the specific water flux (J_{sp}) at the last hour of each 24-hour cycle was less than 1.0 LMH, according to a previous study (Qin and He 2014).

The fouling of the FO membrane was studied with or without *in situ* fouling control under an FO mode. The pristine membrane was operated under the FO mode for water extraction (first test), and without any chemical cleaning, it was directly applied in the second test for determination of fouling situation; *in situ* chemical cleaning was then performed prior to the third test to investigate the fouling control performance. Due to the complex characteristics of fertilizer solution, fouling should be expected on the porous supportive layer (draw chamber), including the irreversible clogging by sparingly dissolved $FePO_4$, $Cu_3(PO_4)_2$ and $Zn_3(PO_4)_2$. Effective removal of resistant foulants could be achieved by three-stage chemical washing at the end of each batch test: acid (HCl, pH=3), base (NaOH, pH=11), and oxidant (NaClO, 10% v/v), and each stage lasted for 30 min, followed by 30 min rinse with DI water. The chemical cleaning was applied only to the draw side, where severe fouling was expected. Although using wastewater as a draw could cause fouling on the feed side of the FO membrane, the treated wastewater contained very low concentrations of organic and inorganic contaminants and the resulted fouling could be removed by backwash and/or flushing. All the cleaning solutions were reused over the 4-month operation, thereby lowering the related cost and limiting their environmental effects under proper control.

2.5.4 Measurement and analysis

The concentrations of ammonium (NH_4^+-N), nitrite (NO_2^--N), nitrate (NO_3^--N), total nitrogen (TN), and total phosphorus were determined by using a spectrophotometer according to the manufacturer instruction (DR 890, HACH Company, USA). The concentration of potassium (K^+) was quantified by ion chromatography (Dionex LC20 ion chromatograph, Sunnnyvale, USA) together with an ED40 electrochemical detector. Conductivity was measured with a benchtop conductivity meter

with a temperature sensor (Mettler-Toledo, Columbus, OH, USA). Water flux of the FO system was determined by the change of weight recorded on an electronic balance (Scort Pro, Ohous, Columbia, MD, USA) according to the previous studies (Lu and He 2015, Yuan et al. 2016). Because urea (CH_4ON_2) is the dominant organic component in all fertilizers, the concentration of urea-nitrogen (Urea-N) is indirectly estimated by TOC (TOC-Vcsn, Shimadzu, Japan) and calculated with the following equation:

$$C_{Urea-N} = \frac{C_{org.C}}{12} \times 2 \quad \text{(Eq. 2.1)}$$

where the unit of $C_{org.C}$ and C_{urea-N} is mg L^{-1} and mmol L^{-1}, respectively.

In the FO process, water extraction is mainly driven by the difference of osmotic pressure between the draw solution and the feed solution. Hence, the theoretical water flux (J_w, L m^{-2} h^{-1}, LMH) is described by Eq. 2.2.

$$Jw = A(\pi_D - \pi_F) \quad \text{(Eq. 2.2)}$$

where A (L m^{-2} h^{-1} bar^{-1}) is the pure water permeability coefficient of a specific membrane; π_D and π_F are osmotic pressure at the draw side and the feed side, respectively. The water permeability coefficient (A), ranging from 0.6-1.0 L m^{-2} h^{-1} bar^{-1}, has been extensively studied for CTA membrane (Cath et al. 2013, Phuntsho et al. 2012b, Xie et al. 2015). The osmotic pressure (π, bar) of a solution is determined by the solute concentration (Eq. 2.3).

$$\pi = \frac{nRT}{V} \quad \text{(Eq. 2.3)}$$

where n (mol) is the mole of the solute, R is the ideal gas constant (0.083 L bar $K^{-1}mol^{-1}$), T (K) is absolute temperature, and V (L) is solution volume. DI water has zero osmotic pressure.

The average water flux (J_a) and specific water flux (J_{sp}) are calculated by Eq. 2.4 and 2.5, respectively. J_a is defined as the unit permeate water volume (at the draw side) over a certain period of time to demonstrate total tendency, while J_{sp} is defined as the unit permeate water volume in one specific hour to track down subtle performance changes. $m_{t,D}$ and $m_{t-1,D}$ represent the mass of draw solution at a specific time t and t-1 (h), respectively. It is assumed that the mass change of

draw solution is mainly attributed to permeate water, and hence water density (ρ) is chosen for volume conversion.

$$J_a = \frac{m_{t+\Delta t,D} - m_{t,D}}{\rho \cdot S \cdot \Delta \mathrm{t}} \quad \text{(Eq. 2.4)}$$

$$J_{sp} = \frac{m_{t,D} - m_{t-1,D}}{\rho \cdot S} \quad \text{(Eq. 2.5)}$$

The solute build-up (SBU) at feed side and nutrient loss rate (NLR) at draw side are quantified by Eq. 2.6 and Eq. 2.7, respectively. SBU and NLR are presented in mmol m^{-2} h^{-1}.

$$SBU = \frac{n_{f,F} - n_{i,F}}{S \cdot t} = \frac{V_F \cdot (C_{f,F} - C_{i,F})}{S \cdot t} \quad \text{(Eq. 2.6)}$$

$$NLR = \frac{n_{i,D} - n_{f,D}}{S \cdot t} = \frac{V_{i,D} \cdot C_{i,D} - (V_{i,D} + V_{recovered}) \cdot C_{f,D}}{S \cdot t} \quad \text{(Eq. 2.7)}$$

where $n_{i,F}$ and $n_{f,F}$ are initial and final mole of target solute in the feed, respectively. $C_{i,F}$ and $C_{f,F}$ are initial and final mole concentration in the feed, respectively. V_F is feed volume (500 mL constant). Likewise, $n_{i,D}$ and $n_{f,D}$ are initial and final mole in the draw (fertilizer) solution. $C_{i,D}$ and $C_{f,D}$ are initial and final mole concentration in the draw, respectively. The final volume of draw should be the sum of initial volume ($V_{i,D)}$ and recovered water volume ($V_{recovered}$, L). t stands for operating time (h).

For a specific solute, SBU is typically resulted from the concentrating effect in feed (due to membrane rejection of feed solute) and reverse solute flux (RSF) from draw solution. The RSF (mmol m^{-2} h^{-1}) and concentrating effect (mmol m^{-2} h^{-1}) are calculated as Eq. 2.8 and 2.9.

$$RSF = \frac{V_F \cdot C_{f,F} - (V_F + V_{recovered}) \cdot C_{i,F}}{S \cdot t} \quad \text{(Eq. 2.8)}$$

$$Concentrating\ Effect = \frac{V_{recovered} \cdot C_{i,F}}{S \cdot t} \quad \text{(Eq. 2.9)}$$

When DI water is used as feed, $C_{i,F}$=0 and hence no concentrating effect is observed. Under such case, RSF=SBU.

Dilution rate (DR, %) is calculated as the volumetric ratio between the recovered water ($V_{recovered}$, L) and the required water ($V_{required}$, L) for making applicable (diluted) fertilizer according to Eq. 2.10. Due to possible nutrition loss via reverse salt flux and/or ammonia volatilization (Overrein and Moe 1967), the required water is less than theoretical water volume suggested by the fertilizer manufacturer (Table 2.2).

$$DR = \frac{V_{recovered}}{V_{required}} = \frac{V_{recovered}}{V_{theoretical} \cdot NLR} \times 100\% \quad \text{(Eq. 2.10)}$$

The specific energy consumption (SEC, (Shaffer et al. 2012)) for unit recovered water (E, kWh m^{-3}) is estimated as Eq. 2.11:

$$E = \frac{P_{system}}{Q} \approx \frac{P_{pump}}{Q} = \frac{P_{pump} \cdot \rho}{m_{t,D} - m_{t-1,D}} \quad \text{(Eq. 2.11)}$$

where P_{system} and P_{pump} (kW) are the energy consumption of the FO system and recirculation pump, and Q (m^3 h^{-1}) is recovered water flow rate. It is assumed that the power consumption of the FO system is mainly attributed to the recirculation pump. However, it should be noted that additional energy would be required for centrifuge, chemical cleaning (pumping and chemical production) and mitigation of salinity build-up on the feed side, and this energy is difficult to quantify.

2.6 Results and Discussion

2.6.1 Optimization of self-dilution performance

To establish the feasibility of using commercial fertilizer to recover water and identify the optimal operating conditions such as membrane orientation, fouling control, initial draw concentration, a series of experiments were conducted using F1 as the draw solute and DI water as feed.

2.6.1.1 Operation mode

Two operation modes, AL-F (FO mode) and AL-D (PRO mode), were examined in the FO system to maximize water extraction (Fig. 2.2). The AL-F mode harvested 324 mL of water, 48% more than that of the AL-D mode (219 mL) within 72 h (Fig. 2.2A). The difference in water extraction should be attributed to internal concentration polarization (ICP) inside the asymmetric

FO membrane (McCutcheon and Elimelech 2006). When the porous supportive layer is installed at the feed side (AL-D), the diffused draw solutes (i.e. RSF) will gradually accumulate in the thick support layer, caused by relatively static environment at the supportive layer and a high rejection rate of attached active layer, forming a concentrative ICP and lowering the effective osmotic gap ($\Delta\pi$eff) (Wang et al. 2016). A dilutive ICP, on the other hand, is usually formed under the AL-F with even lower $\Delta\pi$eff and lower theoretical water flux (Cath et al. 2006). However, the observed maximum water flux (Fig. 2.2B and 2.2D) for the AL-F (5.8 LMH) outcompeted that of the AL-D (3.6 LMH), which was attributed to the intensified fouling induced by concentrative ICP in the porous supportive layer under AL-D, hindering efficient water permeation.

The conductivity profiles of two operation modes were rather similar (Fig. 2.2C). The slightly lower conductivity of the draw solution in the AL-F mode could be caused by dilution with more permeated water. On the feed side, the higher conductivity in the AL-F mode could result from enhanced RSF induced by higher water flux. This observation is in agreement with a previous finding that the ratio between water flux and RSF was subjected to Eq. 2.12 (Phillip et al. 2010):

$$\frac{Water\ Flux}{RSF} = \frac{A}{B} nRT \qquad \text{(Eq. 2.12)}$$

where B is the salt permeability coefficient. Similar to A (Eq. 2.12), B is recognized as another intrinsic membrane parameter. Hence, for a specific membrane, the fixed ratio renders a positive correlation between water flux and RSF. Because the RSF is comparable between both operation modes, the AL-F mode would be more favored due to improved water extraction.

2.6.1.2 Fouling and *in-situ* control

Membrane fouling is a vital issue that should be addressed when utilizing commercial solid fertilizer as draw solutes. Fouling, caused by inorganic scaling/precipitation, organic deposition or attached microorganisms (biofouling), will reduce permeate water flux and aggravate membrane maintenance expenses (Le-Clech et al. 2006, Meng et al. 2009). To alleviate membrane fouling, physical backwashing as well as chemical cleaning are usually integrated for ideal fouling control (Le-Clech et al. 2005). In the current study, draw solution made from fertilizer can bear moderate

fouling propensity, due to some sparingly soluble contents generated from elements such as Cu, Fe, P, and S.

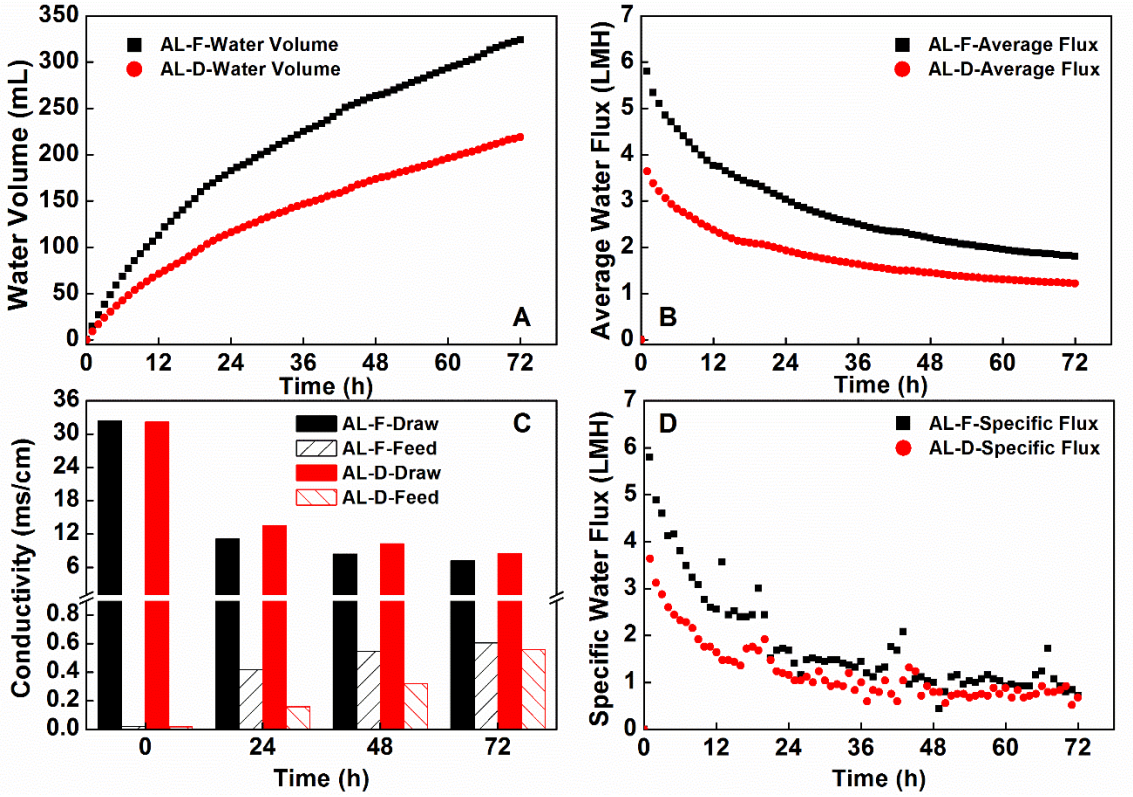

Figure 2.2 The performance of the FO system affected by membrane orientations, activated layer facing draw (AL-D, PRO mode) and activated layer facing feed (AL-F, FO mode): (A) accumulated water volume; (B) average water flux, (C) solution conductivity; and (D) specific water flux.

Membrane fouling was evaluated by using 1 M F1 as the draw solution (Fig. 2.3). Although the AL-D mode exhibited a lower fouling level (Fig. 2.4), the AL-F mode outcompeted the AL-D mode for water extraction and flux. Thus, the AL-F mode was chosen for this test. In the AL-F mode, the permeate water volume reduced from 152 mL to 129 mL in the 18 h (Fig. 2.3A), with a decrease in the maximum water flux from 5.8 LMH to 2.8 LMH (Fig. 2.3B). Due to the submerged configuration and complexity of the foulants (maybe highly resistant), in-situ chemical cleaning instead of physical backwashing was employed for fouling control. In the absence of biological processes, it is assumed that fouling should be mostly attributed to inorganic scaling (potentially

irreversible). Successive chemical washing consisting of acid, base, and oxidants was proved to be effective in water flux recovery, followed by sufficient DI rinse to eliminate the dissolved foulants from the FO system. After cleaning, permeated water volume and maximum water flux was 98% and 93% recovered, respectively. Same in-situ chemical cleaning was applied for the rest of the study to prolong membrane lifespan. All the chemical solutions were reused to minimize environmental impact.

While the aforementioned fouling was effectively controlled with in-situ chemical cleaning, using uncentrifuged fertilizer solution may clog the membrane and pose permanent damage to the FO membrane. The measured maximum water flux was 0.95 LMH even after in-situ chemical cleaning, representing only 18% of that with the pristine FO membrane. The water extraction was reduced to 25% of that harvested by pristine FO membrane in 18 h. Therefore, appropriate pretreatment would be required to isolate the undissolved particles (e.g., through filtration) to prevent irreversible fouling of the FO membrane.

2.6.1.3 Nutrient distribution and loss

The distribution of critical nutrient elements in the fertilizer, i.e., N, P, and K, were examined at the system level (combining that in both the draw and the feed solutions). Fig. 2.5 shows the concentration and distribution of TN, NH_4^+-N, and Urea-N within a 72-h operation of the FO system. The total amount of TN in the FO system was reduced from 91 to 81 mmol in 72 h (Fig. 2.5A). Significant RSF occurred within the first 24 h, decreasing the TN in the draw to 44 mmol and increasing its presence in the feed to 47 mmol (Fig. 2.5B and C). Given relatively stable TN amount in the draw but a slight decrease in the feed after 24 h, the 11% of the TN loss was possibly related to volatilization of urea on the feed side. Urea is a widely utilized fertilizer, due to its relatively high N content (45%), and in this study, Urea-N made up of more than 85% initial TN in F1. The loss of TN usually goes through urea hydrolysis and ammonia volatilization (Overrein and Moe 1967). Through hydrolysis, Urea-N will be converted to NH_4^+-N, which is in consistent with the increase of total NH_4^+-N in the FO system (Fig. 2.5A). Since the feed solution had a larger volume and was not completed sealed, the loss of TN from the feed solution could be more intensive than that of draw solution (Fig. 2.5B). It was observed that 9% of the total loss of potassium (Fig. 2.6A) and 8% of phosphorus (Fig. 2.6B) was lost in the FO system, likely related to precipitation and/or salting-out effect on beaker wall induced by long-term operation.

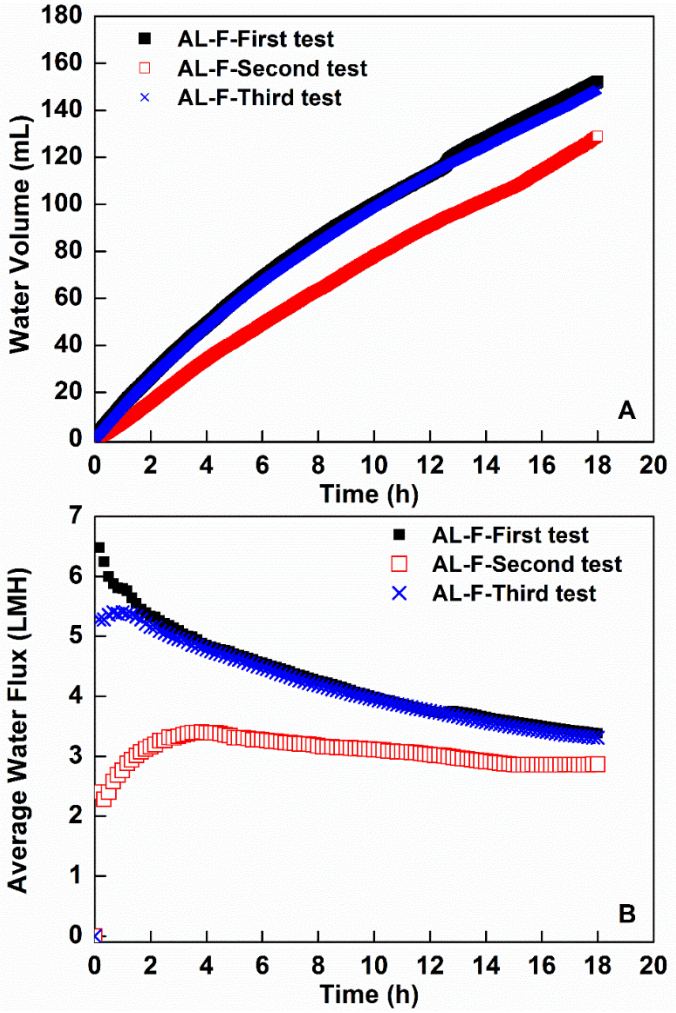

Figure 2.3 Comparison of (A) accumulated water volume and (B) average water flux with or without in-situ chemical cleaning under AL-F mode (FO mode). In the first test, a pristine FO membrane was used and, without any chemical cleaning, it was then applied in the second test to determine the fouling situation. A third test was performed after the membrane (second test) was in-situ chemically cleaned. During each test, 1-M F1 and DI water were applied as draw and feed, respectively.

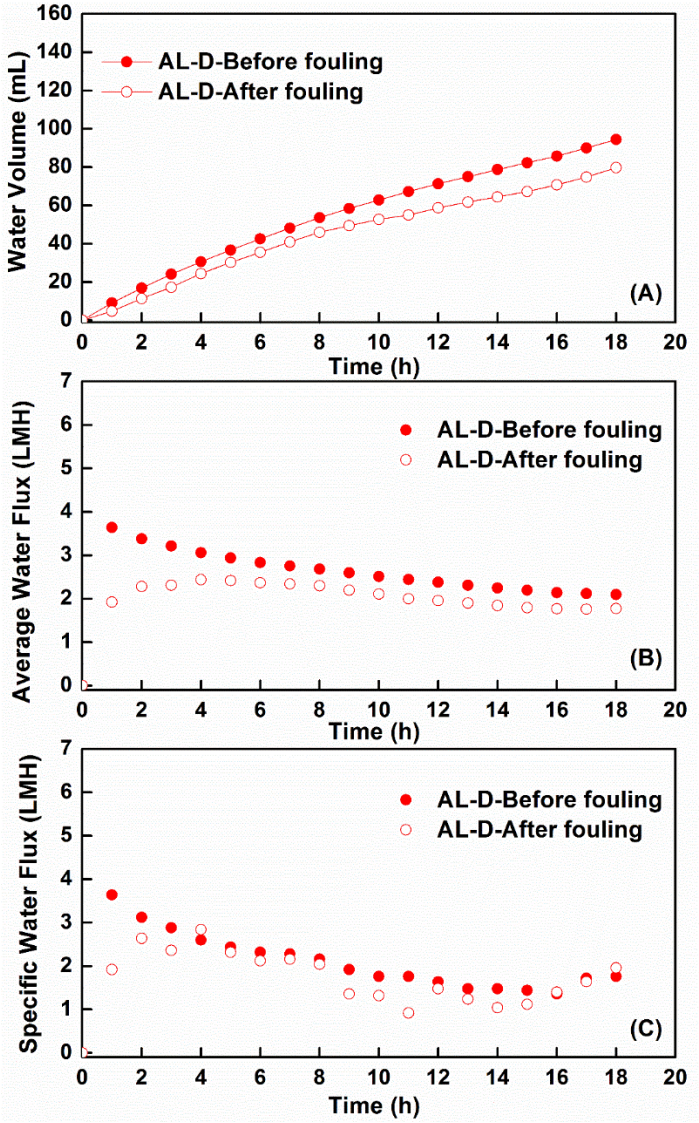

Figure 2.4 Comparison of (A) accumulated water volume and (B) average water flux and (C) specific water flux before and after fouling under AL-D mode (active layer facing the draw).

Nutrients will inevitably diffuse to the feed side because of the limitation of the FO membrane (Hancock and Cath 2009). In this study, RSF resulted in about 50% of TN diffusion to the feed side within 24 h (Fig. 2.5B) with an RSF of 193.95 mmol m^{-2} h^{-1} (Table 2.4). This RSF rate is consistent with the findings of other studies (Majeed et al. 2015, Phuntsho et al. 2013, Phuntsho et al. 2012a, Phuntsho et al. 2012b). The high mobility of urea across the FO membrane can be explained by its small molecular weight and uncharged status in solution, which increases its diffusion tendency (Hancock and Cath 2009). The RSF of NH_4^+-N and K were 17.06 and 5.67

mmol m^{-2} h^{-1} (Table 2.4), respectively. In accordance with the prior studies (Achilli et al. 2010, Phuntsho et al. 2011), multivalent ions with larger hydrated radii (Nightingale Jr 1959), such as P (as in PO_4^{3-}), exhibited the lowest RSF (0.47 mmol m^{-2} h^{-1}) compared to the monovalent ions (Table 2.4). The loss of the key fertilizer components from the draw side would increase the operational cost and also cause the disposal problems of the feed solution due to the accumulation of those compounds. Although a lower RSF may be achieved through the development of advanced membrane materials with higher values of A/B (Tang et al. 2010), complete elimination of RSF is unattainable at the current stage.

2.6.1.4 Effects of initial fertilizer concentration

Three initial draw concentrations (1M, 2M, and 3M) were investigated for water extraction, and as expected, the highest draw concentration of 3 M led to the highest water flux of 12.7 LMH (Fig. 2.7A). The enhanced osmotic gap (driving force) was formed at a higher draw concentration, resulting in a larger water extraction capability in the FO system (Eq. 2.2 and 2.3). According to the water flux baseline of 1 LMH, the operation length varied from 72 h with 1M or 2M to 96 h with 3M. The final amount of TN in the draw exhibited a linear correlation with the initial draw amount (inset, Fig. 2.7A), and the similar linear tendency was obtained for both K and P (R^2>0.99, Table 2.2).

The FO system did not achieve full dilution of the fertilizer to reach its application concentration. For example, 85 mL of the 1-M F1 solution would need 800 mL water (Table 2.2, nutrient loss rate considered) for its dilution, and the FO recovered 324 mL water (using DI water as a feed); therefore, the FO provided 40.5% of the water need (dilution rate). Although a higher initial draw concentration resulted in more water extraction, the relevant dilution rate actually decreased, because of a higher demand for dilution water. The dilution rate decreased from 40.5 to 23.2 % when the initial draw solution increased from 1 to 3 M (Fig. 2.7B). Meanwhile, the higher RSF occurred at a higher draw concentration could accelerate solute accumulation on the feed side. Therefore, a relatively low-concentration fertilizer solution may be more advantageous to achieve diluted fertilizer by the FO system.

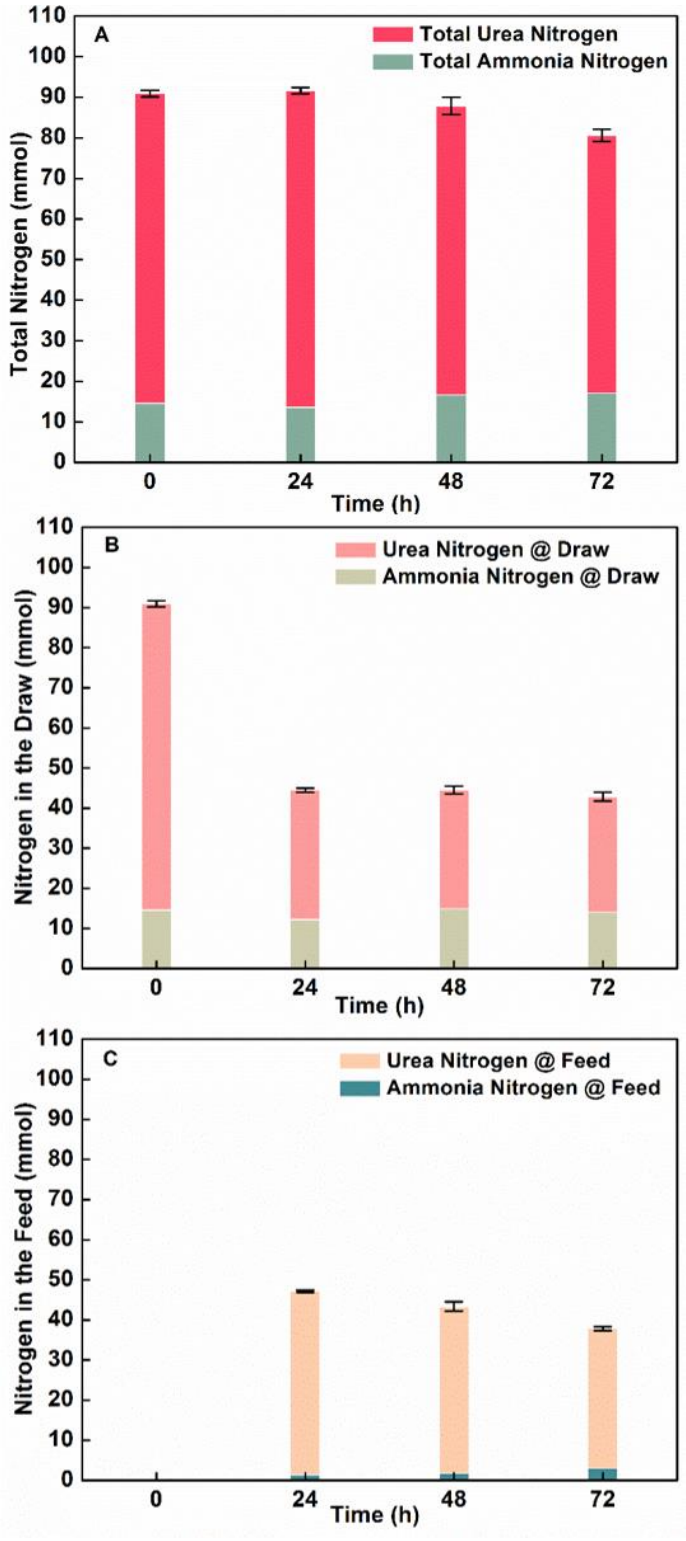

Figure 2.5 Distribution of nitrogen within the 72-h operation under the AL-F mode (FO mode): the mole profiles of total nitrogen (both urea and ammonia nitrogen) in (A) the whole FO system; (B) the draw solution; and (C) the feed solution.

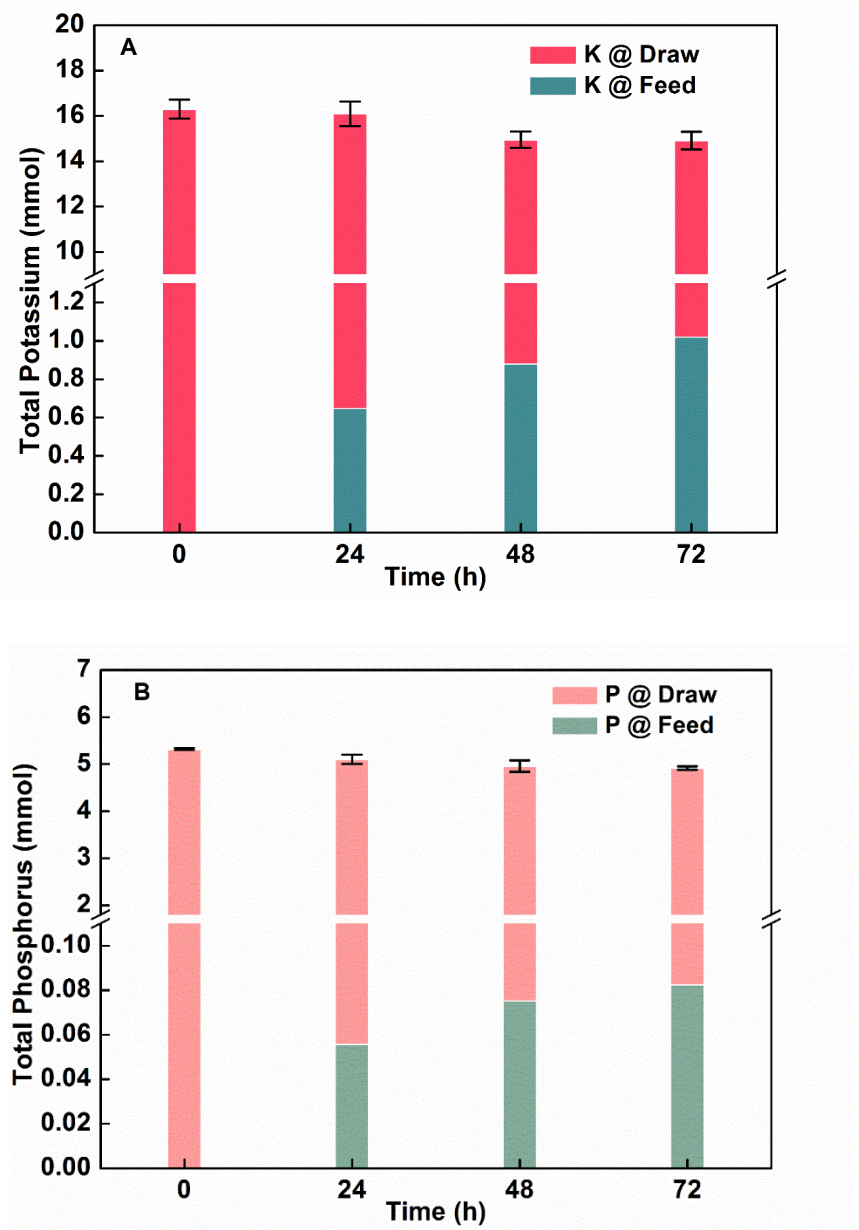

Figure 2.6 Distribution of (A) potassium and (B) phosphorus within the 72-h operation under AL-F mode. The mole profiles were presented with 1-M F1 as draw solutes.

2.6.2 Performance with different fertilizers

Another two commercially available solid fertilizers (F2 and F3) were also examined for water extraction at a 1-M concentration, and the comparison of the three fertilizers is shown in Fig. 2.8. The ratio of Urea-N in TN was different among these three fertilizers with the following order:

F2>F1>F3. As expected, the maximum water flux was in contrast to Urea-N content: F3>F1>F2 (Fig. 2.8A). The F2 had the lowest water flux of 4.32 LMH and its extraction only lasted for 48 h when reaching the specific water flux < 1 LMH, resulting in water extraction of only 177.4 mL.

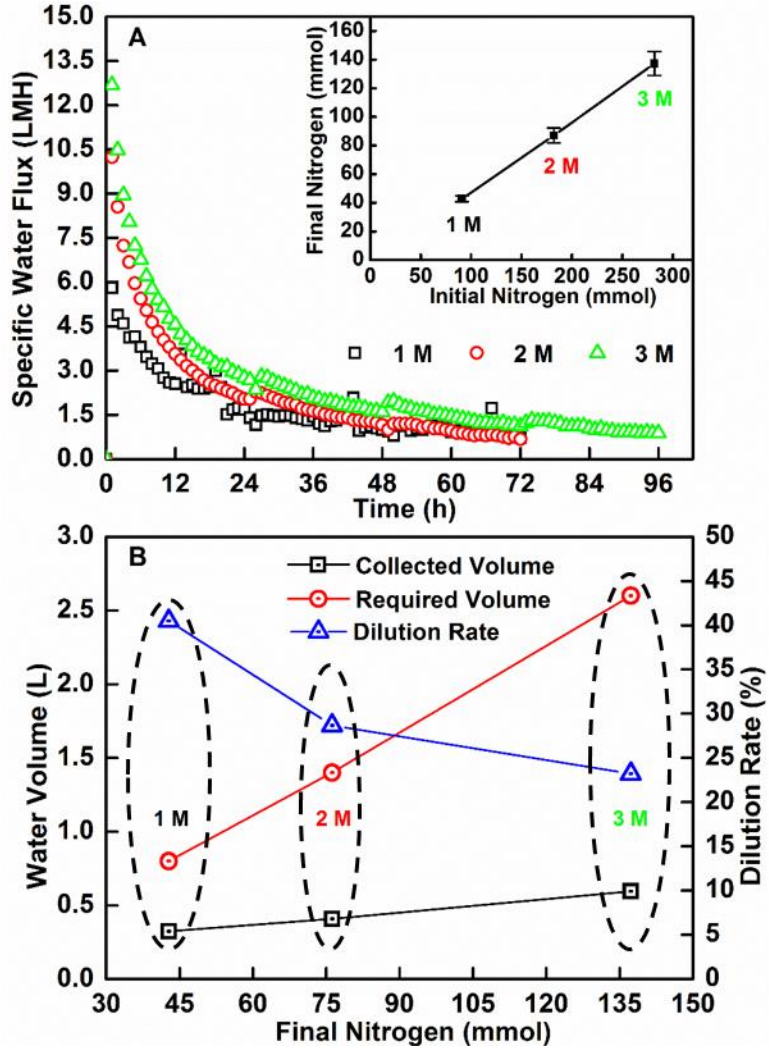

Figure 2.7 The performance of the FO system affected by the concentration of the F1: (A) specific water flux and total nitrogen amount; and (B) the collected/required water volume and corresponding dilution rates. The fertilizer concentration is quantified by mole concentration of total nitrogen (1M, 2M and 3M).

The operating period with the F3 doubled that of the F2 for 96 h, likely benefited from its higher ratio of NH_4^+-N; the volume of the recovered water tripled to 545.6 mL. However, the F2 achieved a much higher dilution rate of 55.0% than that of the F1 (40.5%) or the F3 (36.5%),

because of its lower requirement of the dilution water volume (0.39 L, Table 2.2). The F3 had the highest required water volume for dilution (1.51 L). Regarding the RSF, the F1 has the lowest value except for Urea-N (Fig. 2.8B). The comparison suggests that those three commercial solid fertilizers can act as draw solutes with different levels of water extraction, and the fertilizer with a lower urea content could be favored because of higher water extraction and lower RSF. Because the 1-M F1 had low RSF and relatively high water extraction and dilution rate, it was used for examining water recovery from the treated wastewater effluent.

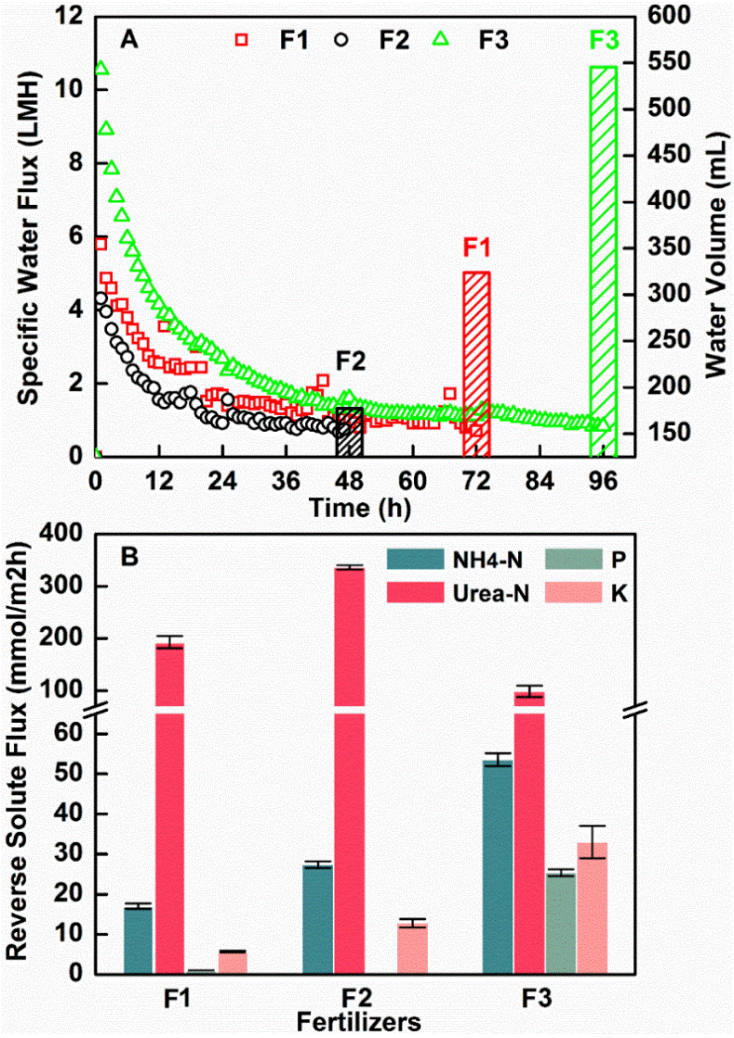

Figure 2.8 The performance of the FO system with three different fertilizers (F1, F2, and F3) at a concentration of 1 M: (A) the accumulated water volume and specific water flux; and (B) reverse solute flux of main nutrient elements.

2.6.3 Water recovery from the treated wastewater

The wastewater effluent was collected from a local municipal wastewater treatment plant and tested with 1-M F1 as the draw. The FO system recovered 317 mL of water within 72 h, which was comparable to that from the DI water (324 mL, Fig. 2.9A). A notable lag in specific water flux was observed with the treated wastewater at the beginning, resulting in a reduced maximum water flux of 4.20 LMH (Fig. 2.9B) affected by the higher conductivity (thus lower osmotic gap) of the treated wastewater in the presence of various compounds (Table 2.3), such as inorganic ions (NH_4^+-N, K^+, PO_4^{3-}-P) and soluble microbial products (SMP). The RSF of the major ions were similar under both operation conditions (DI vs. the treated effluent, data not shown). The dilution rate with the treated wastewater was 38.2%, slightly lower than that of the DI water. Organic fouling of the FO membrane on the feed side (active layer) due to the wastewater would take a long time to appear, because of extremely low COD and TOC concentration in the treated wastewater (Table 2.3). Thus, the proposed *in-situ* chemical cleaning at draw side was sufficient for fouling control (wastewater as feed). It is worth noting that the elevated nutrient concentration was detected in the final concentrated feed: the NH_4^+-N concentration increased from 2 mg L^{-1} to 40 mg L^{-1}, K^+ increased from 10.5 mg L^{-1} to 69.5 mg L^{-1}, while PO_4^{3-}-P increased from 2.5 mg L^{-1} to 5 mg L^{-1}. As Fig. 2.9C indicates, the solute build-up in the final feed solution was mainly attributed to reverse solute flux (RSF) for NH_4^+-N (92%), TN (98%) and K (75%). However, the concentrated P mostly came from treated wastewater by the salt rejection of FO membrane (concentrating effect, 81%). The increased nutrient concentrations in the treated wastewater must be addressed, and additional treatment such as nitrogen removal (e.g., anammox) may be needed (Li et al. 2015).

2.6.4 Energy consumption of the FO system

Although the FO process has been widely studied as an energy efficient process, the performance and data of energy consumption were rarely reported in the literature. In the present FO system, the pump for recirculation of the draw solution was the major energy consumer for water recovery, and its energy consumption was expressed in kWh m^{-3}. Three recirculation rates, 10 mL min^{-1}, 50 mL min^{-1} and 100 mL min^{-1}, were examined. As shown in Fig. 2.10A, the amount of the recovered water within 24-h operation was similar among the three recirculating conditions with comparable

specific water flux. It is expected that increasing recirculation rate can reduce the external concentration polarization (ECP), resulting in a higher and more stable $\Delta\pi_{eff}$. However, a relatively

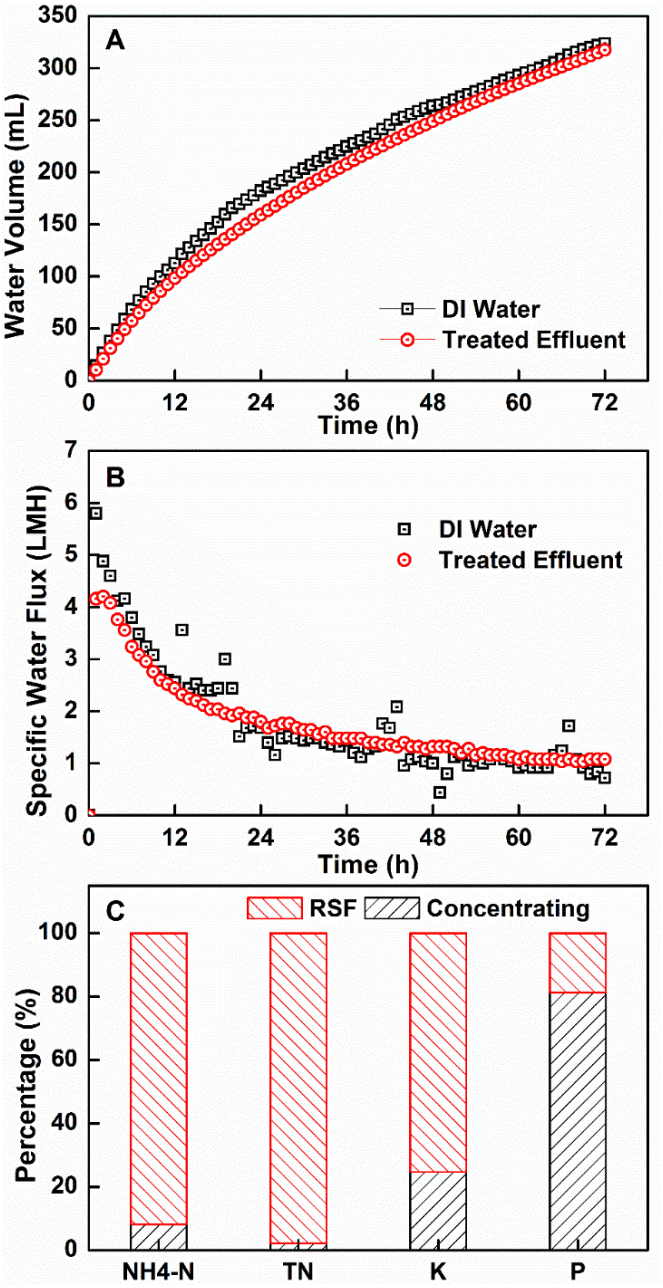

Figure 2.9 The FO performance with the treated wastewater using 1-M F1 as a draw solution: (A) recovered water volume; (B) specific water flux; and (C) percentage of solute build-up at feed side. Both A and B provide a direct comparison of FO performance by using either DI water or treated wastewater as a feed solution. Fig. 2.9 (C) represents the solute build-up by applying treated wastewater as feed.

lower water flux generated by the present FO renders a negligible ECP, and hence limited improvement in water recovery capacity was obtained at higher recirculation rates. In addition, the relatively short testing time (24 hours) would not allow the development of a cake layer under low recirculation rates, which could cause water flux to decrease in long-term operation. The energy consumption profile at different recirculation rates was presented in Fig. 2.10B. The highest recirculation rate of 100 mL min^{-1} required 1.86 ± 0.47 kWh m^{-3}, which was reduced to 0.47 ± 0.13 kWh m^{-3} at 50 mL min^{-1}. Further reduction of the recirculation rate to 10 mL min^{-1} exhibited the lowest energy consumption of 0.02 ± 0.01 kWh m^{-3}, which was about 1.1% and 4.3% of energy consumption with 100 mL min^{-1} and 50 mL min^{-1}, respectively. The energy consumption of the present FO system (at 10 mL min^{-1}) for water recovery was significantly lower than other water recovery approaches such as reverse osmosis (as low as 2 kWh m^{-3}) (Shannon et al. 2008), mechanical vapor compression (down to 20 kWh m^{-3}) (Elimelech and Phillip 2011, Thiel et al. 2015), and even self-supplied FO with thermolytic ammonium bicarbonate (0.1 kWh m^{-3}) (Qin and He 2014).

2.7 Conclusion

The results of this study have demonstrated the feasibility of water recovery using commercial solid fertilizers, though some challenges remain to be addressed including alleviating reverse salt flux, examining its long-term performance and fouling on the feed side of the FO membrane with using treated wastewater as a feed.

- Under the AL-F mode, the recovered water could provide up to 41% of the required water for diluting fertilizer by using 1-M F1, and a higher initial fertilizer concentration (3-M F1) resulted in a lower dilution rate (23.2%) because of its higher demand for dilution water.
- The water extraction capacity of the FO was affected by different fertilizers with a negative correlation to the corresponding urea content. The rate of RSF of the individual components followed the trend: Urea-N > NH_4-N > K > P.
- Solute build-up on the feed side was observed and mainly attributed to the concentrating effect for phosphorous (81%) and RSF for total nitrogen (98%) and potassium (75%).

- Membrane fouling was effectively controlled during the entire experiment with in-situ and reusable chemical cleaning, with 98% and 93% of recovery for permeated water volume and maximum water flux, respectively.
- Reducing recirculation intensity from 100 to 10 mL min^{-1} did not obviously decrease water flux but significantly reduced the energy consumption from 1.86 to 0.02 kWh m^{-3}.

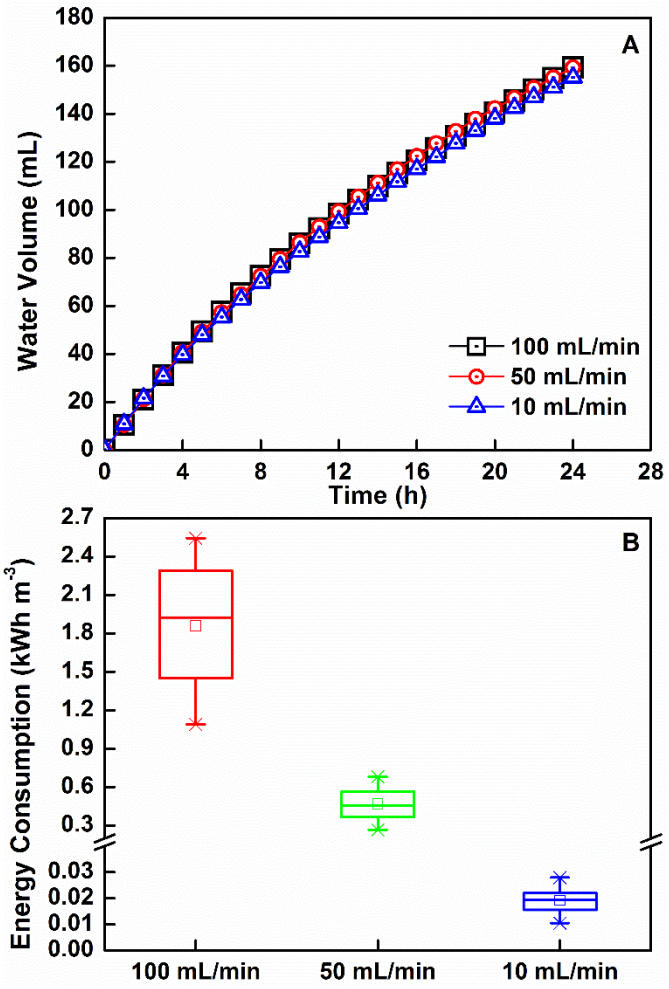

Figure 2.10 Water recovery (A) and energy consumption (B) of the FO system with three different recirculation rates (100, 50, 10 mL min^{-1}) by using the treated wastewater as feed and 1-M F1 as the draw.

References

Achilli, A., Cath, T.Y. and Childress, A.E. (2010) Selection of inorganic-based draw solutions for forward osmosis applications. Journal of Membrane Science 364(1), 233-241.

Alsvik, I.L. and Hägg, M.-B. (2013) Pressure retarded osmosis and forward osmosis membranes: materials and methods. Polymers 5(1), 303-327.

Bowden, K.S., Achilli, A. and Childress, A.E. (2012) Organic ionic salt draw solutions for osmotic membrane bioreactors. Bioresource Technology 122, 207-216.

Cai, X. and Rosegrant, M.W. (2003) World Water Productivity: Current Situation and Future Options, CAB International.

Cai, Y.F., Wang, R., Krantz, W.B., Fane, A.G. and Hu, X. (2015) Exploration of using thermally responsive polyionic liquid hydrogels as draw agents in forward osmosis. RSC Advances 5(118), 97143-97150.

Cath, T.Y., Elimelech, M., McCutcheon, J.R., McGinnis, R.L., Achilli, A., Anastasio, D., Brady, A.R., Childress, A.E., Farr, I.V. and Hancock, N.T. (2013) Standard methodology for evaluating membrane performance in osmotically driven membrane processes. Desalination 312, 31-38.

Elimelech, M. and Phillip, W.A. (2011) The future of seawater desalination: energy, technology, and the environment. Science 333(6043), 712-717.

Hancock, N.T. and Cath, T.Y. (2009) Solute coupled diffusion in osmotically driven membrane processes. Environmental Science & Technology 43(17), 6769-6775.

Hoover, L.A., Phillip, W.A., Tiraferri, A., Yip, N.Y. and Elimelech, M. (2011) Forward with Osmosis: Emerging Applications for Greater Sustainability. Environmental Science & Technology 45(23), 9824-9830.

Li, X., Lu, Y. and He, Z. (2015) Removal of reverse-fluxed ammonium by anammox in a forward osmosis system using ammonium bicarbonate as a draw solute. Journal of Membrane Science 495, 424-430.

Lotfi, F., Phuntsho, S., Majeed, T., Kim, K., Han, D.S., Abdel-Wahab, A. and Shon, H.K. (2015) Thin film composite hollow fibre forward osmosis membrane module for the desalination of brackish groundwater for fertigation. Desalination 364, 108-118.

Lu, Y. and He, Z. (2015) Mitigation of Salinity Buildup and Recovery of Wasted Salts in a Hybrid Osmotic Membrane Bioreactor–Electrodialysis System. Environmental Science & Technology 49(17), 10529-10535.

Majeed, T., Sahebi, S., Lotfi, F., Kim, J.E., Phuntsho, S., Tijing, L.D. and Shon, H.K. (2015) Fertilizer-drawn forward osmosis for irrigation of tomatoes. Desalination and Water Treatment 53(10), 2746-2759.

McCutcheon, J.R., McGinnis, R.L. and Elimelech, M. (2005) A novel ammonia-carbon dioxide forward (direct) osmosis desalination process. Desalination 174(1), 1-11.

McGinnis, R.L. and Elimelech, M. (2007) Energy requirements of ammonia-carbon dioxide forward osmosis desalination. Desalination 207(1-3), 370-382.

Nightingale Jr, E. (1959) Phenomenological theory of ion solvation. Effective radii of hydrated ions. The Journal of Physical Chemistry 63(9), 1381-1387.

Overrein, L. and Moe, P. (1967) Factors affecting urea hydrolysis and ammonia volatilization in soil. Soil Science Society of America Journal 31(1), 57-61.

Phuntsho, S., Hong, S., Elimelech, M. and Shon, H.K. (2013) Forward osmosis desalination of brackish groundwater: Meeting water quality requirements for fertigation by integrating nanofiltration. Journal of Membrane Science 436, 1-15.

Phuntsho, S., Kim, J.E., Johir, M.A., Hong, S., Li, Z., Ghaffour, N., Leiknes, T. and Shon, H.K. (2016) Fertilizer drawn forward osmosis process: Pilot-scale desalination of mine impaired water for fertigation. Journal of Membrane Science 508, 22-31.

Phuntsho, S., Lotfi, F., Hong, S., Shaffer, D.L., Elimelech, M. and Shon, H.K. (2014) Membrane scaling and flux decline during fertiliser-drawn forward osmosis desalination of brackish groundwater. Water Research 57, 172-182.

Phuntsho, S., Shon, H.K., Hong, S., Lee, S. and Vigneswaran, S. (2011) A novel low energy fertilizer driven forward osmosis desalination for direct fertigation: Evaluating the performance of fertilizer draw solutions. Journal of Membrane Science 375(1–2), 172-181.

Phuntsho, S., Shon, H.K., Hong, S., Lee, S., Vigneswaran, S. and Kandasamy, J. (2012a) Fertiliser drawn forward osmosis desalination: the concept, performance and limitations for fertigation. Reviews in Environmental Science and Bio-Technology 11(2), 147-168.

Phuntsho, S., Shon, H.K., Majeed, T., El Saliby, I., Vigneswaran, S., Kandasamy, J., Hong, S. and Lee, S. (2012b) Blended Fertilizers as Draw Solutions for Fertilizer-Drawn Forward Osmosis Desalination. Environmental Science & Technology 46(8), 4567-4575.

Qin, M. and He, Z. (2014) Self-Supplied Ammonium Bicarbonate Draw Solute for Achieving Wastewater Treatment and Recovery in a Microbial Electrolysis Cell-Forward Osmosis-Coupled System. Environmental Science & Technology Letters 1(10), 437-441.

Sahebi, S., Phuntsho, S., Eun Kim, J., Hong, S. and Kyong Shon, H. (2015) Pressure assisted fertiliser drawn osmosis process to enhance final dilution of the fertiliser draw solution beyond osmotic equilibrium. Journal of Membrane Science 481, 63-72.

Shaffer, D.L., Yip, N.Y., Gilron, J. and Elimelech, M. (2012) Seawater desalination for agriculture by integrated forward and reverse osmosis: Improved product water quality for potentially less energy. Journal of Membrane Science 415–416, 1-8.

Shannon, M.A., Bohn, P.W., Elimelech, M., Georgiadis, J.G., Marinas, B.J. and Mayes, A.M. (2008) Science and technology for water purification in the coming decades. Nature 452(7185), 301-311.

Tang, C.Y., She, Q., Lay, W.C., Wang, R. and Fane, A.G. (2010) Coupled effects of internal concentration polarization and fouling on flux behavior of forward osmosis membranes during humic acid filtration. Journal of Membrane Science 354(1), 123-133.

Thiel, G.P., Tow, E.W., Banchik, L.D., Chung, H.W. and Lienhard, J.H. (2015) Energy consumption in desalinating produced water from shale oil and gas extraction. Desalination 366, 94-112.

van Haandel, A.C. and van der Lubbe, J.G. (2012) Handbook of biological wastewater treatment: design and optimisation of activated sludge systems. Water Intelligence Online 11, 9781780400808.

Xie, M., Zheng, M., Cooper, P., Price, W.E., Nghiem, L.D. and Elimelech, M. (2015) Osmotic dilution for sustainable greenwall irrigation by liquid fertilizer: Performance and implications. Journal of Membrane Science 494, 32-38.

Yuan, H., Abu-Reesh, I.M. and He, Z. (2016) Mathematical modeling assisted investigation of forward osmosis as pretreatment for microbial desalination cells to achieve continuous water desalination and wastewater treatment. Journal of Membrane Science 502, 116-123.

Table 2.1 The studies about fertilizer-driven forward osmosis with different feed solutions.

No.	Draw	Draw Conc.	Feed	Configuration	Ref.
1	Inorganic chemicals	0.3 to 3.0 mol L^{-1}	DI water	Cross-flow FO	(Phuntsho et al. 2011)
2	Inorganic chemicals and urea	1.0 mol L^{-1}	DI water and synthetic brackish ground water	Cross-flow FO	(Phuntsho et al. 2012b)
3	Inorganic chemicals and urea	1.0 mol L^{-1}	Synthetic brackish water	Cross-flow FO NF-FO and FO-NF	(Phuntsho et al. 2013)
4	Inorganic chemicals	1.0 mol L^{-1}	Synthetic brackish water	Cross-flow FO	(Phuntsho et al. 2014)
5	Inorganic chemicals and urea	1.0 mol L^{-1}	Synthetic sea water	Cross-flow FO	(Majeed et al. 2015)
6	Inorganic chemicals	1.0, 2.0 mol L^{-1}	Synthetic brackish water	Hollow fiber FO	(Lotfi et al. 2015)
7	Liquid fertilizer	100%, 50%, 25% fertilizer	Raw Sewage	Cross-flow FO	(Xie et al. 2015)
8	Inorganic chemicals	0.1, 3.0 mol L^{-1}	Synthetic brackish water	Pressure-assisted FO	(Sahebi et al. 2015)
9	Inorganic chemicals	0.5, 0.95, 1.89, 2.84 mol L^{-1}	Mine-impaired saline water	Pilot-scale FO-NF	(Phuntsho et al. 2016)
10	Commercial solid fertilizers	1.0, 2.0, 3.0 mol L^{-1}	DI water and treated wastewater effluent	Submerged FO	This Study

Table 2.2 Characteristics of different commercial fertilizers in self-diluted FO system

Draw	N-P-K value [a]	Conc. (M)	Mass (g)	Initial pH	Adjust pH	$V_{theoretical}$ (L) [b]	Cond. (ms/cm)	Initial Nutrient Amount (mmol) [c]					Final Nutrient Amount (mmol) [c]				
								Total N	NH_4-N	Urea-N	P	K	Total N	NH_4-N	Urea-N	P	K
F1	24-8-16	1[d]	5.85	3.6	7.00 ±0.05	1.87 (0.80)	32.2	90.9	14.9	76.4	5.3	16.3	42.8	12.2	28.8	4.8	13.9
		1[e]	5.85			1.87 (0.80)	34.8	93	15.4	77.6	6.4	18.3	42.6	12.0	30.6	5.9	16.5
		2[c]	11.70			3.74 (1.43)	61.1	183.9	30.7	153.2	11.2	30.8	76.2	20.9	53.4	8.0	20.7
		3[c]	17.55			5.61 (2.57)	82.0	281.7	49.8	231.9	17.8	44.9	137.3	28.5	108.8	11.3	29.1
F2	36-0-6	1[c]	3.89	6.3		1.24 (0.39)	19.8	88.7	10.3	78.4	-[e]	6.4	31.7	5.7	26.1	-[f]	3.3
F3	15-30-15	1[c]	9.33	3.7		2.98 (1.51)	63.8	101.0	38.7	62.3	36.2	25.5	50.1	22.0	28.1	26.6	15.6

a The N-P-K value is a vital parameter for fertilizers provided by the manufacturer, indicating the wt% of N, P_2O_5 and K_2O.

b The value in brackets are $V_{required}$.

c The values are total nutrient amounts in draw solution.

d The values were obtained when DI water was applied as feed.

e The values were obtained when raw effluent from local wastewater treatment plant was applied as feed.

f Fertilizer 2 does not contain any phosphorus.

Table 2.3 Characteristics of treated wastewater

Parameters	Average value
COD (mg/L)	0[a]
TOC (mg/L)	5.40 ± 0.53
pH	7.37 ± 0.61
Conductivity (μS/cm)	506.3 ± 19.9
NH_4-N (mg/L)	2.0 ± 2.2
TN (mg/L)	16.3 ± 0.9
Total Phosphorus (mg/L)	2.6 ± 0.5
K^+ (mg/L)	10.5 ± 1.2
Mg^{2+} (mg/L)	3.2 ± 0.6
Ca^{2+} (mg/L)	19.3 ± 1.3

a No COD was detected in the treated wastewater.

Table 2.4 Reverse solute flux of different fertilizers under various scenarios

Fertilizers	Conc. (mol/L)	Reverse Solute Flux (mmol m^{-2} h^{-1})			
		NH_4-N	Urea-N	K	P
F1	1[a]	17.06	193.05	5.67	0.47
	1[b]	8.04	225.5	4.50	0.34
	2	41.94	346.94	32.76	0.40
	3	52.08	348.89	44.37	8.96
F2	1	27.38	336.16	12.75	-[c]
F3	1	53.57	98.23	33.00	25.34

a The values were obtained when DI water was applied as feed.

b The values were obtained when raw effluent from local wastewater treatment plant was applied as feed.

c Fertilizer 2 does not contain any phosphorus content.

3 Electrodialysis Recovery of Reverse-fluxed Fertilizer Draw Solute during Forward Osmosis Water Treatment

(This chapter has been published as "Zou, S. and He, Z. (2017) Electrodialysis recovery of reverse-fluxed fertilizer draw solute during forward osmosis water treatment. *Chemical Engineering Journal*, 330, 550-558")

3.1 Abstract

Wastewater reuse is important to address the challenge of water shortage but direct reuse could still introduce undesired contaminants to final products, e.g., via agricultural irrigation. Advanced membrane treatment such as forward osmosis can further purify the treated wastewater with recovery of high quality water. Herein, a forward osmosis - electrodialysis (FO-ED) hybrid system has been investigated by using diammonium phosphate (DAP), a common fertilizer, as a non-regeneration draw solute to achieve water reclamation and mitigation of salinity buildup. The system achieved consistent water recovery in the FO with low specific reverse solute flux for both NH_4^+-N (0.063 g L^{-1}) and PO_4^{3-}-P (0.083 g L^{-1}). Intensified fouling condition was observed when actual treated wastewater was applied as the feed, requiring periodical membrane cleaning. There were only Na^+, Cl^- and small amounts of organics being presented in the recovered water (diluted draw solution of FO) at an acceptable level towards water reuse for agricultural irrigation. The ED accomplished successful recovery of 96.6 ± 3.0 % reverse-fluxed DAP under 3.0 V 1-hour daily operation, which could be reused in the FO. The energy consumption of the hybrid system was as low as 0.72 kWh m^{-3} or 0.45 kWh kg^{-1}. These results have demonstrated a synergy between FO and ED for creating an energy-efficient solution to enhance wastewater reuse.

3.2 Graphical Abstract

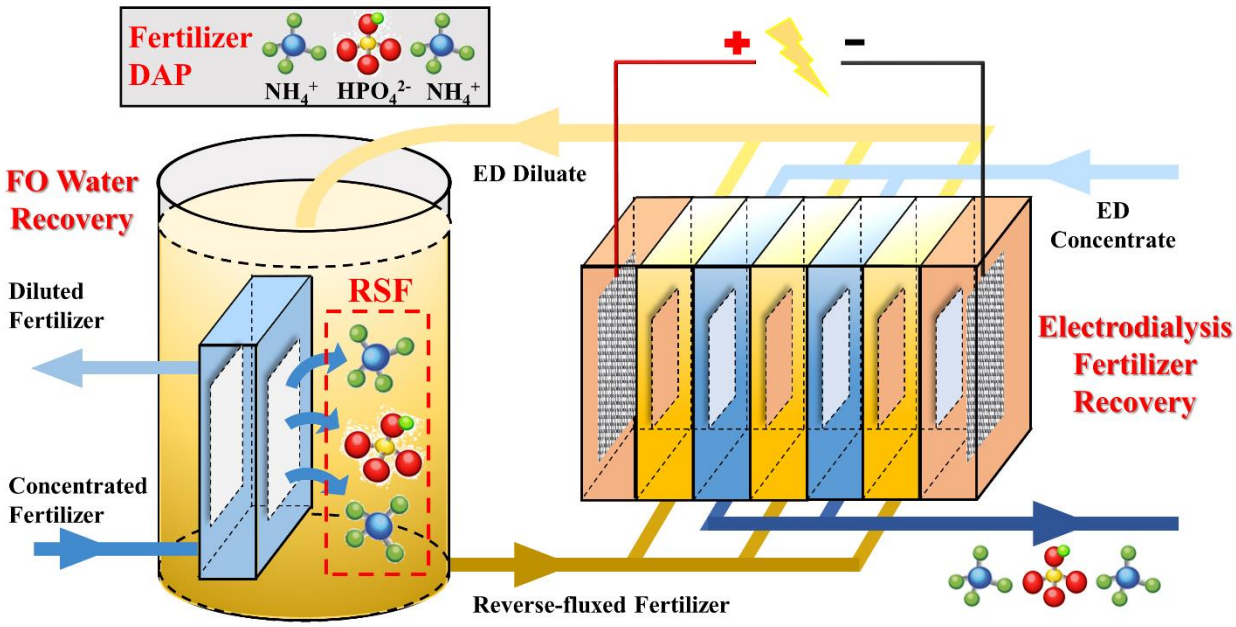

3.3 Keywords

Forward osmosis; Electrodialysis; Salinity buildup; Wastewater reuse; Energy

3.4 Introduction

Using reclaimed wastewater for agricultural irrigation has become an attractive solution to address mounting fresh water shortage and ever-increasing food demand (Paltiel et al. 2016). Although most contaminants are effectively removed via conventional wastewater treatment processes, reclaimed wastewater still contains undesirable substances like pathogens (e.g., *Legionella* and *E. coli*) (EPA 2012) and trace organic chemicals (e.g., endocrine-disrupting chemicals) (Weber et al. 2006), thereby raising potential health concerns when consuming wastewater-irrigated products in terms of microbiological safety and ingestion of xenobiotics (e.g. pharmaceutical compounds) (Malchi et al. 2014, Wu et al. 2014). To reduce human exposure risk and enhance wastewater reuse, advanced water recovery/purification technologies would be needed. A growing interest is focused on the robust membrane separation processes capable of recovering high-quality water with reduced cost and minimized environmental impact (Shannon et al. 2008). Among the emerging membrane technologies, FO can contribute to efficient fresh water recovery by utilizing osmotic pressure gradient across a semi-permeable membrane (Phuntsho et al. 2013, Zou et al. 2016). It has great merits of high contaminant rejection rates and lower fouling propensity when compared to pressure-driven processes such as RO (Holloway et al. 2007).

Unlike pressure-driven RO processes that can generate fresh water directly, water molecules migrate across the FO membrane to the high-concentration draw solution side, forming a homogeneous diluted draw solution. Hence, to yield the final product water, extra energy and cost are required for separating draw solutes from the aqueous phase, either through downstream separation process or via adopting self-separated draw solutes. This will also recover or regenerate draw solutes for reuse. The downstream separation process, such as pressure- (e.g., RO), thermal- (e.g., membrane distillation), or electricity-driven (e.g., electrodialysis) processes, requires a large amount of energy investment, increasing the operating expense (Zou et al. 2017). The innovative self-separated draw solutes rely on induced phase separation by using magnetic nanoparticles (Alejo et al. 2017), thermolytic ammonium bicarbonate (NH_3-CO_2) (Qin and He 2014), and electricity-responsive organic polymers (Zhang et al. 2015). However, these magnetic-, thermal-, and pH-responsive draw solutes suffer from high cost due to complicated preparation (Minami et al. 2010), large reverse solute loss (Zou et al. 2017), and/or weakened self-separation property after regeneration (Ling et al. 2010). Alternatively, draw solutes that do not require

separation/regeneration and can be applied directly after FO dilution would potentially address energy and cost issues (Zhao et al. 2012). For example, concentrated fruit juice or sugar can be used as a draw solution to recover clean water for direct drinking purpose or emergency relief (Butler et al. 2013, Sant'Anna et al. 2012). The regeneration-free fertilizer-driven FO (FDFO) process (Phuntsho et al. 2012) uses the self-diluted fertilizers as draw solutes, which can be directly used for agricultural irrigation without energy-intensive solute regeneration (Hoover et al. 2011). Commercial all-purpose liquid and solid fertilizers have been studied for osmotic dilution (Xiang et al. 2017, Zou and He 2016). A pilot-scale fertilizer drawn forward osmosis and nanofiltration (FDFO-NF) was recently established and had been successfully operated for six months (Phuntsho et al. 2016).

Despite great promise and advantages of FDFO, a key challenge and also impediment remained unsolved is the salinity buildup on the feed side, resulting from both reverse solute flux (RSF) and concentration effect by FO membrane rejection (Hancock and Cath 2009). RSF is defined as the cross-membrane diffusion of draw solutes to the feed, and can result in severe loss of draw solutes, rendering reduced osmotic driving force (lower water flux), increased fouling propensity, and elevated operation cost due to periodical replenishment of draw solutes (Akther et al. 2015). Accumulation of the reverse-fluxed draw solutes, such as nutrients originated from fertilizers, will require further treatment of the feed stream (Phillip et al. 2010). Thus, mitigation of solute accumulation on the feed side is important, and several approaches have been proposed and studied. For example, continuous desalination of the concentrated feed through integrated electrodialysis (ED) and filtration (e.g., microfiltration) deliver more stable performance in salinity control on the feed side (Lu and He 2015, Luo et al. 2015). A previous study reported the use of ED to remove and recover NaCl draw solute from the feed side of an osmotic membrane bioreactor (OMBR) treating primary effluent, and demonstrated effective recovery with potentially low energy input (Lu and He 2015).

Herein, a regeneration-free fertilizer draw solute, diammonium phosphate ($(NH_4)_2HPO_4$, DAP), was examined in an FO treating synthetic and actual reclaimed wastewater, and ED was employed to remove and recover reverse-fluxed draw solute from the feed side. DAP was chosen due to its low specific RSF, direct application for fertigation, moderate pH (~8.0) and low cost (Phuntsho et al. 2011). The specific objectives of this study were to (1) examine water recovery

and RSF in the FO affected by operation parameters, i.e., initial draw solution concentration; (2) investigate draw solute removal and recovery by the ED under various exerted voltages; and (3) evaluate specific energy consumption of the hybrid system for minimized energy investment.

3.5 Materials and Methods

3.5.1 FO-ED hybrid system and experiments

The FO-ED hybrid system consisted of a submerged FO module and an ED module, and was operated in a semi-continuous mode in a temperature-controlled lab (20 ± 2 °C) with a centralized air conditioning system (Fig. 3.1). Both modules were hydraulically connected via recirculation of the feed solution between the feed tank of the FO and the desalination chambers of the ED. In the FO module, a constant feed volume (~500 mL) was maintained via periodical supplement of either DI water or treated wastewater (Christiansburg Wastewater Treatment Plant, Christiansburg, VA, USA). The first stage of the experiment focused on FO water recovery by using DI water as the feed. Three different initial draw concentrations (0.5, 1.0, and 2.0 mol L^{-1} DAP) were studied, with the ED module not turning on at this stage to solely investigate the magnitude of salinity buildup (i.e., RSF, no concentrating effect due to DI water as the feed). Diluted DAP was replaced for every 24 hours. The second stage of the experiment targeted at mitigation of salinity buildup via the ED module by using 1-M DAP as the draw. Because the theoretical thermodynamic voltage of water decomposition is 1.23 V, a minimum voltage of 2.0 V was selected considering the overpotential effect (Wang et al. 2014b). The ED module was only turned on for a certain period (23h at 2.0V, 7h at 2.5V, 1h at 3.0V under each 24-h semi-continuous cycle) for control of feed conductivity to ~1.0 mS cm^{-1}. No fouling control was implemented in the first two stages of experiments (system optimization). Specific energy consumption (SEC) of the FO-ED system was quantified under 2.5V and 3.0V (DI as the feed), and the applied voltage with a stable salinity mitigation and lowest SEC (3.0V) was then selected for the third stage of experiment in which the treated wastewater was applied as a feed to investigate the system performance (e.g. water recovery, salinity buildup, and fouling situation) and overall energy consumption. The FO feed (DI water or wastewater), ED concentrate, and ED electrolyte were not replaced in the second stage and third stage of the experiment.

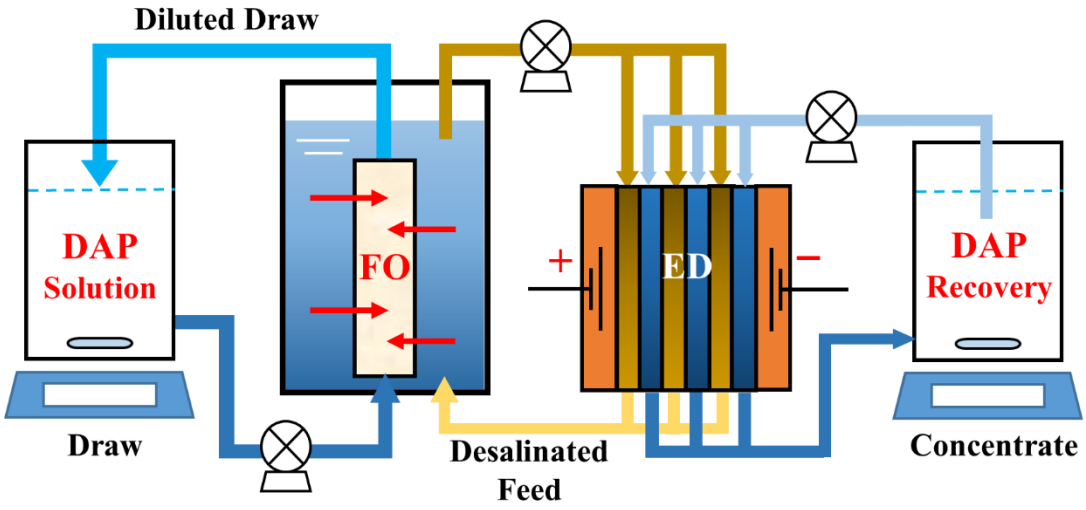

Figure 3.1 Schematic of the FO-ED hybrid system.

3.5.2 FO setup

A flat-plate FO cell (11×10 cm) contained two pieces of cellulose triacetate membranes (CTA, 6×5 cm effective area each) with a total surface area (S) of 0.006 m^2 (Hydration Technologies Inc., Albany, OR, USA) and being installed on both sides of the FO cell with the active layer facing the feed (FO mode), creating a middle chamber of 30 mL for draw solution. The FO cell was submerged in the feed solution in a 1-L plastic beaker. To replace the draw solution, the diluted DAP solution was fully drained from the FO module, and 200 mL fresh DAP solution (pH not adjusted, pH=8.4-8.6) was recirculated in the submerged FO cell at 30 mL min^{-1} (2.55 cm s^{-1}). Considering a minor effect of external concentration polarization in FO mode (active layer facing feed), no recirculation was implemented on the feed side to reduce energy investment (McCutcheon and Elimelech 2006, Zou and He 2016). Water samples (both feed and draw solutions) were taken before the replacement of fresh draw solution on a 24-h interval for water quality analysis.

3.5.3 ED setup

A bench scale ED module (64002, PCCell GmbH, Heusweiler, Germany) was set up with 5 cell pairs, with each cell pair assembled with one desalination chamber and one concentrate chamber separated by alternating cation exchange membrane (CEM, 8×8 cm effective area) and anion exchange membrane (AEM, 8×8 cm effective area). Each desalination or concentrate chamber had

a thickness of 0.5 mm (secured by a patented mesh spacer), and the total volume of five desalination or five concentrate chambers was 30 mL, respectively. The Titane electrodes (7×7 cm effective area) were placed in the bilateral anode and cathode chambers (identical volume of 30 mL), and then connected to an external power supply. The concentrate (200-mL 0.005-M DAP, 1.0 mS cm^{-1}) and electrolyte (200-mL 0.1-M DAP, 14.3 mS cm^{-1}) were recirculated separately between the ED module and external reservoirs. The concentrate volume was documented daily to quantify potential electro-osmosis.

3.5.4 Analytical methods

The ED voltage was monitored (2-min interval) over an external resistor of 1 Ω. The concentrations of ammonium nitrogen (NH_4^+-N) and phosphorus (PO_4^{3-}-P) were determined by using a spectrophotometer according to the manufacturer instruction (DR 890, HACH Company, USA). The concentration of other ions (e.g., Cl^-, NO_3^-, K^+, Ca^{2+}, and Mg^{2+}) was quantified by ion chromatography (Dionex LC20 ion chromatograph, Sunnyvale, USA) together with an ED40 electrochemical detector. Conductivity was measured with a benchtop conductivity meter (Mettler-Toledo, Columbus, OH, USA) with a temperature sensor. Water flux was determined by measuring the change of water weight on an electronic balance (Scort Pro, Ohous, Columbia, MD, USA) at a 30-s interval. In the FO, quantification of water flux (e.g. average water flux, J_a) and solute buildup at the feed side (mmol m^{-2} h^{-1}) were based on a previous study (Zou and He 2016). Specific RSF (g L^{-1}, Eq. 3.1) was also calculated as the ratio of RSF (J_s, g m^{-2} h^{-1}, gMH) and maximum water flux (J_w, L $m^{-2}h^{-1}$, LMH).

$$Specific\ RSF = \frac{J_s}{J_w} \qquad \text{(Eq. 3.1)}$$

The energy consumption was evaluated on the whole system level (FO-ED), and the consumption rate was normalized by unit treated wastewater (kWh m^{-3}) or unit recovered solute (kWh kg^{-1} solute). In the FO-ED system, the major energy consumers were one recirculation pump in FO module (for draw solution) and external power supply with three recirculation pumps in ED module (for diluate or feed solution, concentrate, and electrolyte). Calculation of power consumption by pump head was based on Eq. 3.2:

$$P_{pump} = \frac{Q_{pump} \times (H_{hydraulic} + H_{dynamic})}{\eta} = \frac{v\pi d^2 / 4 \times (\rho g h + \rho v^2 / 2)}{\eta} \quad \text{(Eq. 3.2)}$$

where $H_{hydraulic}$ (Pa) and $H_{dynamic}$ (Pa) are the hydraulic and dynamic head provided by pump, Q_{pump} (m^3 s^{-1}) is the recirculation rate, η (%) is the efficiency of this pump, h (m) is the difference of water height before and after the pump, d (m) is the diameter of the tube, v (m s^{-1}) is the water velocity. For the external power supply, the consumed power was calculated as Eq. 3.3:

$$P_{electricity} = IU \quad \text{(Eq. 3.3)}$$

where I (A) is the current detected across the external resistance (1 Ω), U (V) is the applied voltage. The total energy consumption (W_{total}, kWh) was quantified via Eqs. 3.4-3.6:

$$W_{FO} = P_{FO,pump} \times t_1 \quad \text{(Eq. 3.4)}$$

$$W_{ED} = (P_{ED,pump} + P_{ED,electricity}) \times t_2 \quad \text{(Eq. 3.5)}$$

$$W_{total} = W_{FO} + W_{ED} \quad \text{(Eq. 3.6)}$$

where W_{pump} (kWh) and $W_{electricity}$ (kWh) are the energy consumption of the recirculation pump and external voltage supply. Note that, unlike the FO module pumps, the recirculation pumps in ED module were turned on only for a specific period of time every day ($t_2 < t_1 = 24$ h). Hence, SEC for unit recovered water (E_w, kWh m^{-3}) and unit recovered solute (E_s, kWh kg^{-1} solute) were estimated as Eq. 3.7:

$$E_w = \frac{W_{total}}{V} \text{ or } E_s = \frac{W_{total}}{m} \quad \text{(Eq. 3.7)}$$

where V (m^3) and m (kg) are recovered water volume and desalinated salt within 24 hours (one semi-continuous cycle), respectively.

3.6 Results and Discussion

3.6.1 Water recovery in FO

Three initial draw concentrations, i.e., 0.5, 1.0 and 2.0 mol L^{-1} DAP, were examined in the FO module for water recovery (while the ED module was not turned on in this test, Fig. 3.2). A total

of 271.6 mL water was recovered by using 0.5 mol L^{-1} DAP as the draw in 24 hours, with a maximum J_w of 2.5 LMH (Fig. 3.2A). When 200-mL 1 mol L^{-1} DAP was applied in the FO, 32.5% more water (360.0 mL) was recovered within the same operation period together with an elevated maximum J_w (3.6 LMH). The elevated water recovery performance should be attributed to the enhanced osmotic gap (driving force) at a higher draw concentration. Further increase of initial draw concentration to 2.0 mol L^{-1} rendered a slightly larger water recovery volume (375.5 mL). It should be noted that a lag was observed at the beginning of the experiment when using 2.0 mol L^{-1} DAP as the draw, indicating a potential membrane fouling condition (Fig. 3.2A). The limited enhancement of water recovery between 1.0 and 2.0 mol L^{-1} DAP should be related to non-linear correlation between osmotic pressure (i.e., driven force) and draw solute concentration at a higher concentration (Cath et al. 2006) as well as inefficient water permeation and mass transfer induced by internal concentration polarization (ICP) within FO membrane (Wang et al. 2014a).

Enhanced water recovery under a higher initial draw concentration could lead to more severe salinity buildup on the feed side, due to a positive relation between water flux (J_w) and RSF (J_s) (Phillip et al. 2010). The final feed conductivity increased from 0.67 mS cm^{-1} at 0.5 mol L^{-1} to 0.82 mS cm^{-1} at 1.0 mol L^{-1}, and eventually reached 0.98 mS cm^{-1} at 2.0 mol L^{-1}. A similar increasing trend was observed for both NH_4^+-N and PO_4^{3-}-P concentrations and the magnitude of RSF in the final feed solution (Fig. 3.2B and 3.2C). The NH_4^+-N concentration increased from 58 mg L^{-1} (0.5 mol L^{-1}) to 62 mg L^{-1} (2.0 mol L^{-1}), rendering an elevated RSF from 0.20 gMH (0.5 mol L^{-1}) to 0.22 gMH (2.0 mol L^{-1}). The PO_4^{3-}-P concentration also increased from 60 mg L^{-1} (0.5 mol L^{-1}) to 72 mg L^{-1} (2.0 mol L^{-1}), resulting in an increase of RSF from 0.25 gMH (0.5 mol L^{-1}) to 0.30 gMH (2.0 mol L^{-1}). To better evaluate the magnitude of RSF under different initial draw concentrations, RSF was normalized by the maximum water flux (i.e., specific RSF) to quantify how much salt would be leaked into the feed per unit fresh water reclaimed. The lowest specific RSF for both NH_4^+-N (0.063 g L^{-1}) and PO_4^{3-}-P (0.083 g L^{-1}) was observed by using 1.0 mol L^{-1} DAP as the draw (Fig. 3.2B and 3.2C). The obtained specific RSF for DAP was comparable with that reported

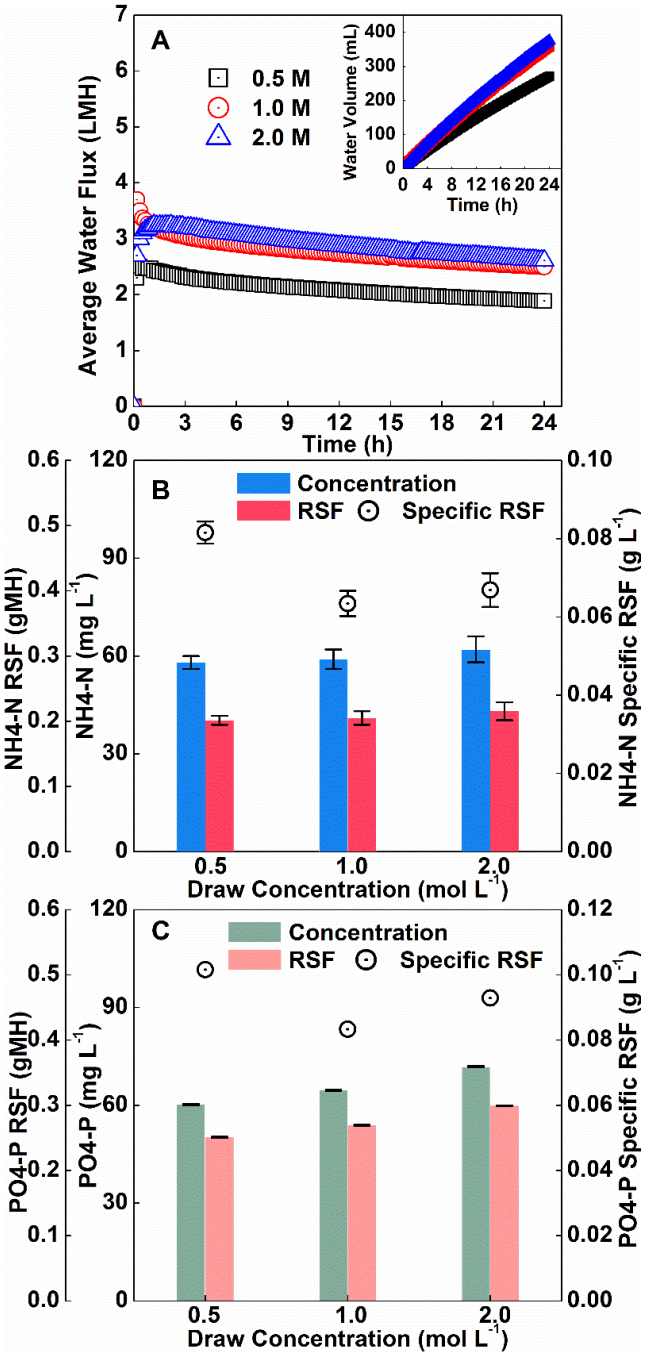

Figure 3.2 FO performance under various initial draw concentrations regarding (A) average water flux and extracted water volume (inset), (B) NH_4^+-N concentration in feed solution with corresponding RSF and specific RSF, and (C) PO_4^{3-}-P concentration in feed solution with corresponding RSF and specific RSF.

in previous literature (0.070 gMH for NH_4^+-N and 0.078 gMH for PO_4^{3-}-P), and was significantly lower than other common inorganic salts (e.g., KNO_3 and NH_4Cl) (Phuntsho et al. 2011). Although NH_4^+-N alone should have a high cross-membrane leaking potential because of its smaller hydrated ion radius, its actual net diffusion was reduced due to the much larger radius of its anion counterpart (PO_4^{3-} and HPO_4^{2-}). Hence, 1.0 mol L^{-1} DAP exhibited desirable water recovery performance together with a low specific RSF and was selected for the following experiments.

3.6.2 Draw solute recovery in ED

To effectively control salinity buildup and recover reverse-fluxed solute on the feed side, three different voltages (2.0, 2.5 and 3.0 V) were exerted on the ED module to understand their effects on the FO-ED hybrid system better. This feasibility test was conducted by operating the FO-ED for 24 hours with no ED effect (0 V) to create a benchmark salinity level in feed solution (0.83 mS cm^{-1}), following by another 24-h operation (1-M DAP solution replaced) with various applied voltages (0 V for blank control, 2.0, 2.5 or 3.0 V for experiment systems, Fig. 3.3). With an applied voltage of 2.0 V, successful but limited electrolysis was observed, accompanied with a very small amount of current generated during a 23-h operation period (3-6 mA in steady state, Fig. 3.3A). As a result, a slightly reduced salinity (1.28 mS cm^{-1}) was observed at the end of the operation period, comparing to that of the blank control on the second day (1.61 mS cm^{-1} at 0 V, Fig. 3.3B). The reduced conductivity in the feed (or ED dilutate) was due to ion migration (mainly NH_4^+-N and PO_4^{3-}-P) across the AEM and CEM driven by an electric field. With an alternative setting of AEM and CEM inside the ED module, charged ions could be successfully isolated from the feed (or ED dilutate) and reconcentrated in the adjacent concentrate stream. To enhance salinity mitigation on the feed side, a higher voltage of 2.5 V was then applied with a current of 7-14 mA at steady state (Fig. 3.3A). Elevated electrolysis led to more desirable salinity reduction to 0.94 mS cm^{-1} after 7-h ED operation. Further increase of the exerting voltage to 3.0 V resulted in a much larger current generation (27-44 mA at steady state, Fig. 3.3A) and a shortened operation length (only 1 h) to control conductivity below 1.0 mS cm^{-1} (0.89 mS cm^{-1}, Fig. 3.3B). Therefore, both 2.5 and 3.0 V demonstrated great potential for simultaneous salinity mitigation and solute recovery in the FO-ED system.

The FO-ED hybrid system was then operated under 2.0, 2.5 and 3.0 V for an extended period to investigate system stability and potential fouling issue (DI as the feed). Notable salinity

buildup (from 0 to 1.60 mS cm^{-1}) on the feed side was observed in the absence of ED operation for the first two days (Fig. 3.4A), together with a dramatic increase of both NH_4^+-N (from 0 to 158 mg L^{-1}) and PO_4^{3-}-P (from 0 to 127 mg L^{-1}, Fig. 3.4B). Starting from day 3, the ED module was operated at 2.5 V for 7 h each day, and the feed conductivity was stably controlled at 0.84-1.05 mS cm^{-1} over the following 6 days. Consistent NH_4^+-N (78-84 mg L^{-1}) and PO_4^{3-}-P (64-76 mg L^{-1}) concentrations were detected in the feed stream (Fig. 3.4B). The reverse-fluxed solute in the

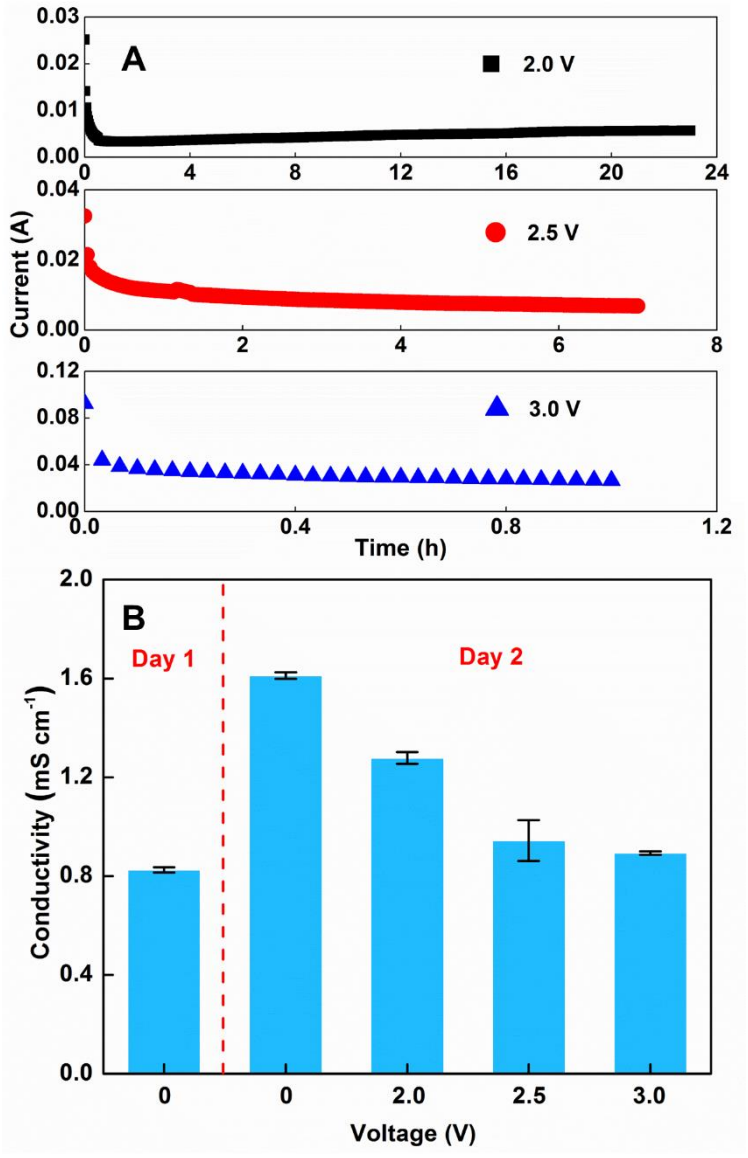

Figure 3.3 FO-ED feasibility test under various exerted voltages regarding (A) detected current, and (B) conductivity in feed solution in day 1 and day 2.

feed solution was continuously separated to the concentrated stream of ED module, leading to a gradually increased concentrate conductivity from 1.06 to 9.61 mS cm^{-1} (day 8, Fig. 3.4A). Switching to an exerted voltage of 2.0 V rendered a limited salinity mitigation performance (day 9 and 10). Elevated feed conductivity (from 0.90 to 1.61 mS cm^{-1}), increased NH_4^+-N and PO_4^{3-}-P concentrations, and invariable ED concentrate conductivity were all observed even after 23-h ED operation, which aligned well with the previous 2.0-V feasibility test. Further voltage increase to 3.0 V offered a stable system performance over the following 8 days. With only 1-hour daily ED operation, conductivity was well controlled at 0.97-1.09 mS cm^{-1} (Fig. 3.4A), so were the levels of NH_4^+-N (76-83 mg L^{-1}) and PO_4^{3-}-P (63-68 mg L^{-1}, Fig. 3.4B). The final conductivity of the ED concentrate reached 14.9 mS cm^{-1} (~0.11 mol L^{-1} DAP, recovering 96.6 ± 3.0 % reverse-fluxed DAP daily) and could be further increased under a long-term operation. Recovered DAP in the ED concentrate could either be applied for agricultural irrigation at lower concentrations or reapplied as FO draw solution at high levels.

Electro-osmosis, a liquid movement induced by an applied potential across the ion exchange membrane, was observed under both 2.5 and 3.0 V with a notable volume increment of the ED concentrate (Fig. 3.4C). The concentrate volume increased from 200 to 247 mL under 2.5 V over the 6-day operation, rendering an average daily increment of 7.8 mL and water flux of 0.002 LMH within the 7-h daily operation. A negligible volume increase was observed (from 247 to 250 mL) in the following two days under 2.0 V applied voltage. A gradual increase of concentrate volume (from 250 to 289 mL) was resumed under a voltage of 3.0 V, resulting in an average daily increment of 4.9 mL and water flux of 0.008 LMH within the 1-h daily operation. Thus, the higher voltage applied, the larger electro-osmosis water flux could be obtained, serving as an additional source for freshwater recovery. It is worth noting that stable water recovery performance was observed due to negligible membrane fouling and well-controlled salinity buildup on the feed side. For example, a consistent daily water recovery volume of ~ 350 mL was determined with a maximum water flux of 2.8-3.2 LMH over the 9-day operation (Fig. 3.5A). The comparable daily water extraction capability also led to consistent conductivity (38.0-38.5 mS cm^{-1}) and pH (8.10-8.18) in the final diluted draw solution (Fig. 3.5B). Considering no fouling control strategy was adopted, the FO-ED system exhibited great water recovery performance and system stability owing to synergistic cooperation between these two modules.

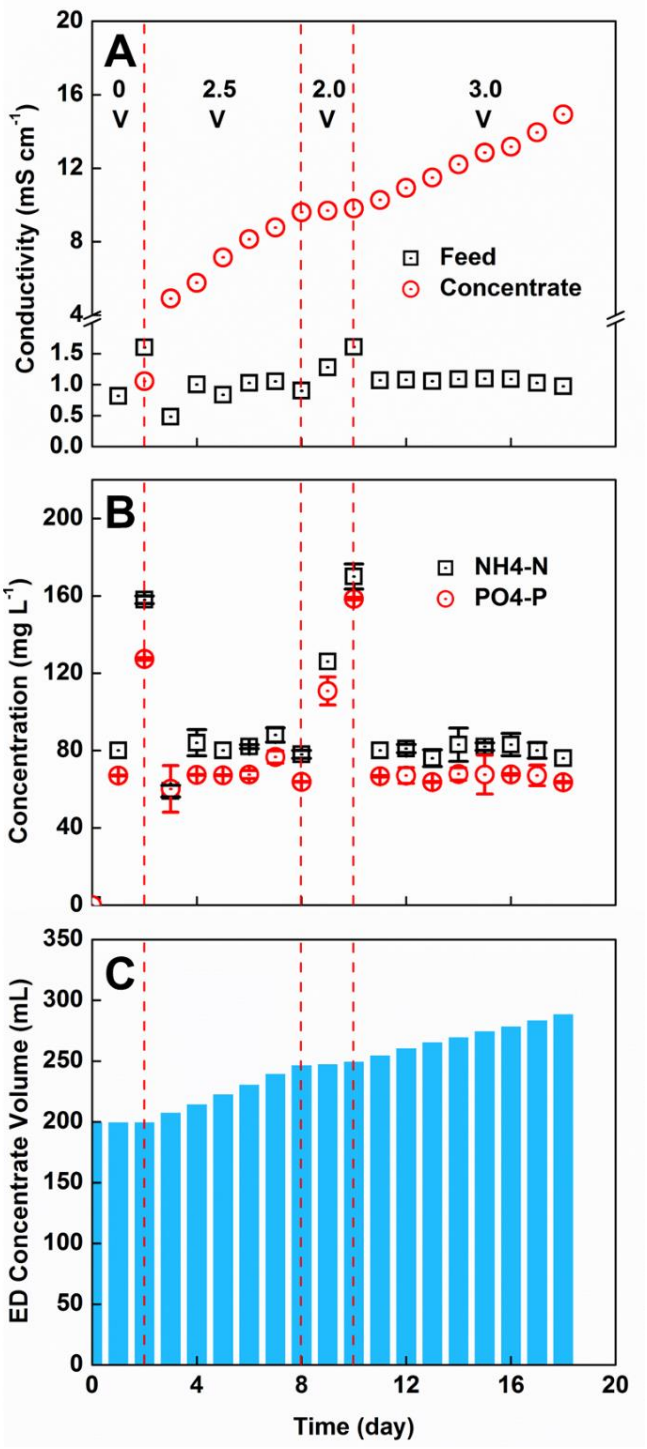

Figure 3.4 FO-ED performance under an extended operation period regarding (A) conductivity in the feed solution (FO module) and the concentrate solution (ED module), (B) NH_4^+-N and PO_4^{3-}-P concentration in the feed solution, and (C) volume increase of ED concentrate due to electro-osmosis.

3.6.3 Energy Consumption

Considering both 2.5 and 3.0 V exhibited stable water recovery, consistent draw solute isolation, and effective salinity mitigation, selection of an exerted voltage was based on the comparison of energy consumption on the whole FO-ED system level (DI as the feed). In the current FO-ED system, energy was mainly consumed by one recirculation pump in the FO module (30 mL min^{-1}, for draw solution) and external power supply with three recirculation pumps in the ED module (30 mL min^{-1}, for diluate (feed solution), concentrate, and electrolyte). With an applied voltage of 2.5 V under 7-h ED operation, 0.97 kJ energy was required by the FO-ED every day, with 9.1% by

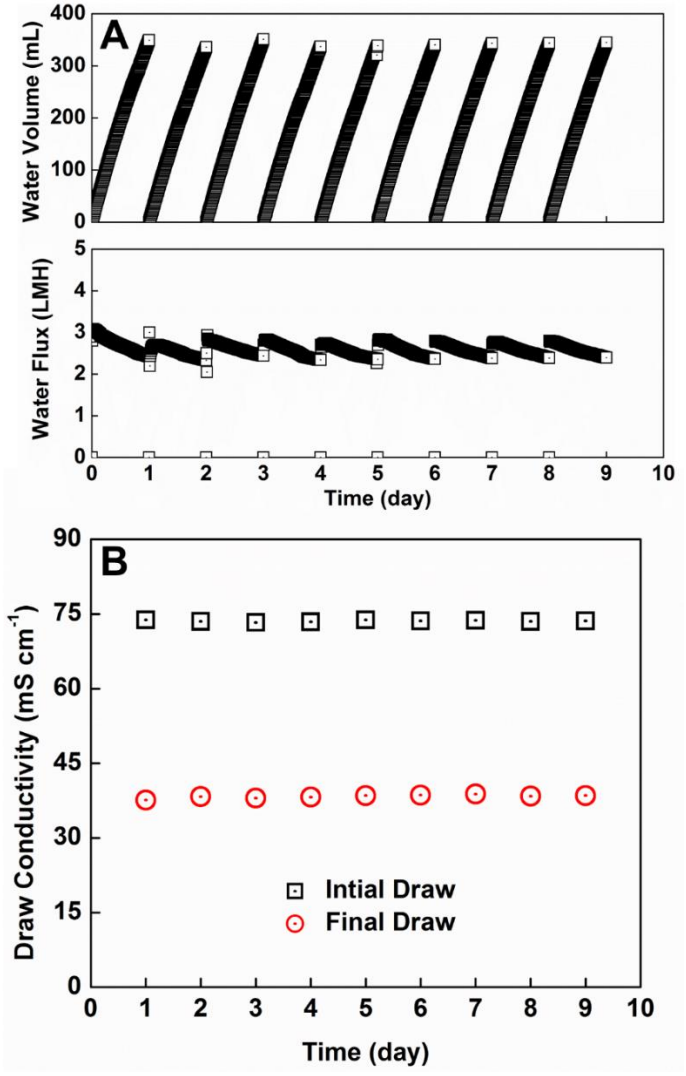

Figure 3.5 FO-ED performance under an extended operation period regarding (A) extracted water volume and average water flux, and (B) initial and final draw conductivity.

the FO module and the rest 90.9% supporting ED module (Fig. 3.6A). Within the ED module alone, external power supply required a majority of 0.81 kJ (91.2%). Increasing the exerted voltage to 3.0 V for 1-h ED operation led to a 55.2% reduction of overall energy consumption (0.44 kJ), with 20.4% went to FO module and the rest 79.6% powering ED module (Fig. 3.6B). External power

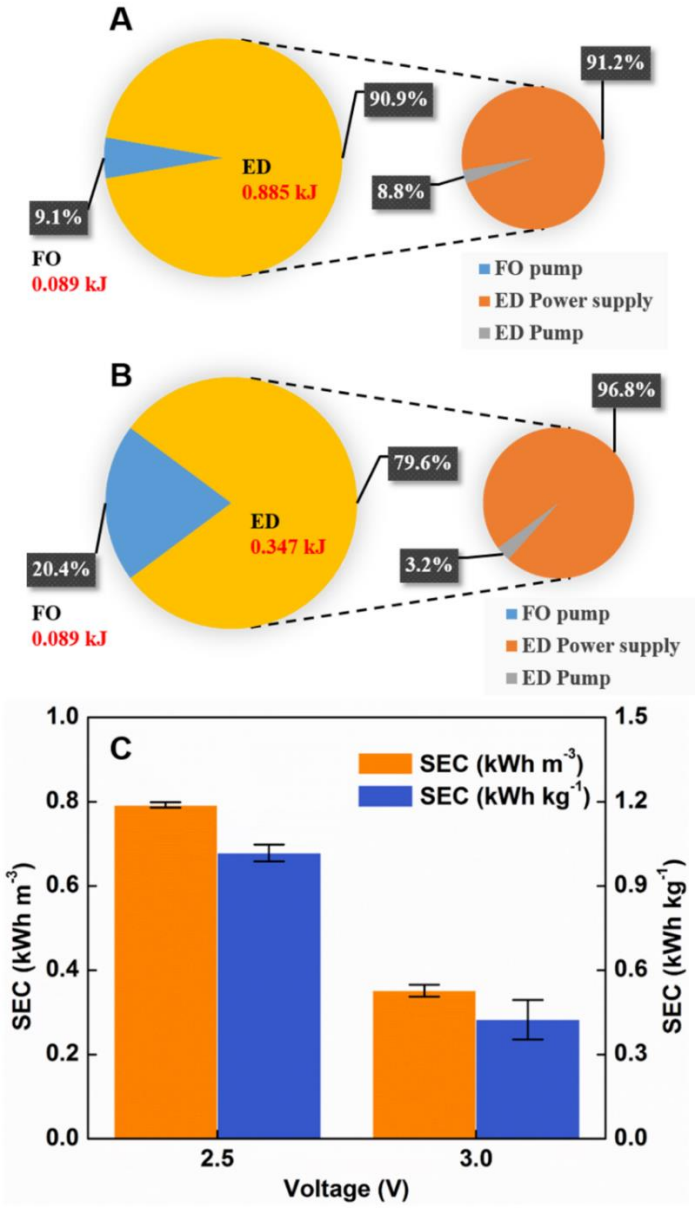

Figure 3.6 Energy profiles of the FO-ED system with DI water as the feed: (A) composition of energy consumption under 2.5 V; (B) composition of energy consumption under 3 V; and (C) specific energy consumption (SEC) under 2.5 V and 3 V when normalized by unit recovered water and unit desalinated salt, respectively.

supply still was the primary energy consumer (96.8%) within the ED module alone. Further energy analysis focused on the system-level SEC, which is a widely applied energy parameter in the water/wastewater field via normalizing energy consumption to unit recovered water or unit desalinated salt (Fig. 3.6C). The SEC under an applied voltage of 2.5 V was 0.79 kWh m^{-3} water or 1.02 kWh kg^{-1} solute, which was greatly reduced to 0.35 kWh m^{-3} water (55.7% reduction) or 0.42 kWh kg^{-1} solute (58.8% reduction) under an applied voltage of 3.0V. The result demonstrated that 3.0 V outcompeted 2.5 V due to a notable lower SEC, rendering a more energy-efficient and cost-effective system. It should be noted that all the above analysis was based on DI water as the feed, and a higher SEC should be expected when wastewater was applied as the feed in practical applications, due to less water recovery volume (reduced osmotic gap) and more considerable energy investment (e.g., prolonged ED operation time and potential fouling control).

3.6.4 System performance with actual treated wastewater

The stable water recovery performance and effective salinity mitigation by using DI water as the feed warranted further investigation of treating actual wastewater. Considering both fouling development and concentrating effect were in positive correlation with recovered water amount, a lower DAP concentration (0.5 mol L^{-1}, replaced daily from day 1 to day 5) was first applied in FO-ED system (3.0V exerted voltage) to evaluate system performance. During the first two days, ED was not turned on to solely investigate water recovery performance and magnitude of salinity buildup. The FO recovered 151.3 mL of water from actual wastewater on the first day, which is about 55.7% of that using DI as the feed (271.6 mL), and the recovered volume was further decreased to 132.7 mL on the second day (Fig. 3.7A). The result demonstrated that intensified fouling, possibly via deposition of trace organic compounds such as extracellular polymeric substances and other undissolved particles, could greatly hinder the physical water permeation (Ding et al. 2016, Mi and Elimelech 2008) and create a more severe internal concentration polarization (ICP), rendering a reduced osmotic pressure gradient across the active layer of FO membrane and diminished driven force (Tang et al. 2010). Meanwhile, augmented salinity buildup was observed on the first day from 0.50 to 1.26 mS cm^{-1} (0.76 mS cm^{-1} increment vs. 0.67 mS cm^{-1} increment when DI was the feed), ending up in 1.88 mS cm^{-1} on the second day. This was due to the coactions of concentrating effect and enhanced RSF resulting from fouling-induced concentration polarization (She et al. 2012). The FO membrane was cleaned at the beginning of

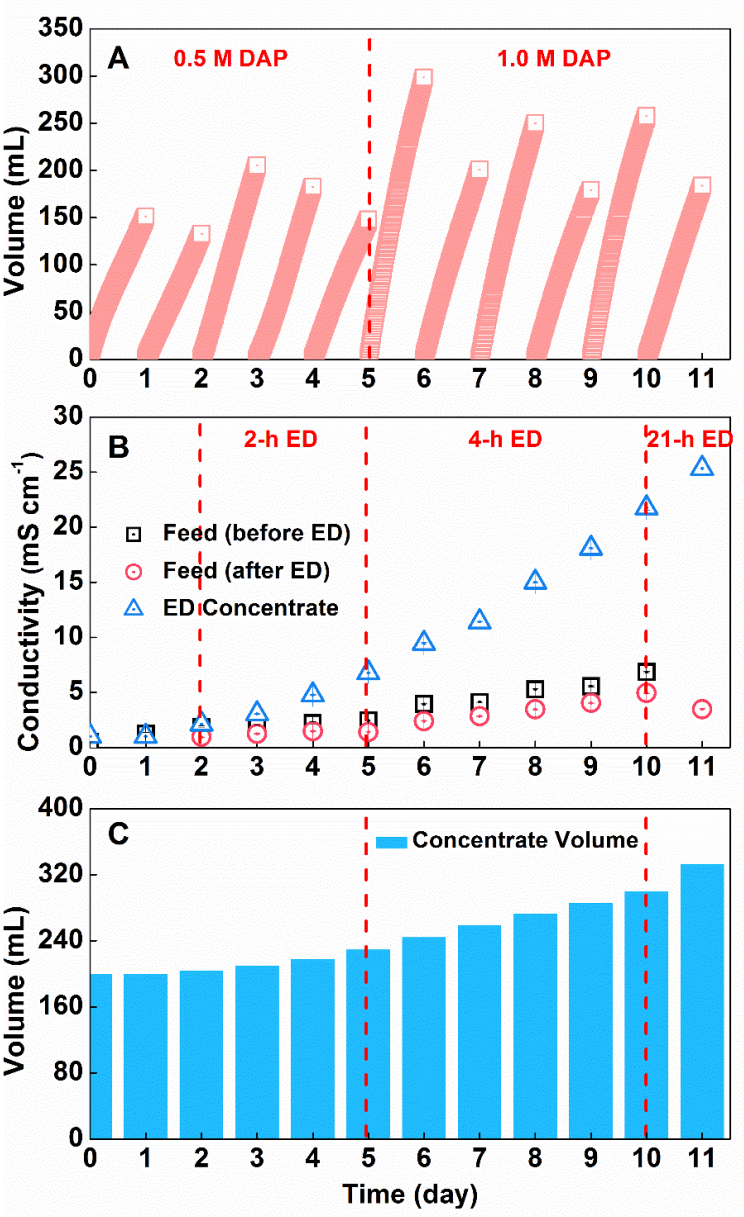

Figure 3.7 The FO-ED performance with actual treated wastewater as the feed regarding: (A) water recovery volume with 0.5 and 1.0 M DAP, respectively; (B) conductivity in the feed solution (FO module, before and after ED operation) and the concentrate solution (ED module); and (C) volume increase of ED concentrate due to electro-osmosis.

day 3, together with ED being turned on for two hours to controlling salinity buildup. As a result, the conductivity of the feed was successfully reduced from 1.88 to 0.95 mS cm^{-1} (after 2-hour ED

operation), and a higher water recovery of 205.1 mL was achieved at the end of the third day due to less fouling and partially recovered cross-membrane osmotic pressure gradient. However, low water recovery performance was still observed on day 4 (182.7 mL) and day 5 (148.1 mL). Those results indicated that using treated wastewater as the feed would require effective strategies for reducing membrane fouling such as more frequent cleansing and/or backwash.

The FO-ED operation was further conducted with 1.0 mol L^{-1} DAP solution as the draw (replaced every two days, starting from day 6). A volume of 298.5 mL fresh water was recovered within 24 hours (85.3% of water recovery amount with DI as the feed), and another 200.7 mL was extracted on the following day (Fig. 3.7A). The enlarged water recovery amount inevitably promoted salinity buildup on the feed side, resulting in 3.94 and 4.13 mS cm^{-1} in day 6 and 7, respectively. To deal with fast salinity increment, the length of the ED operation was extended to four hours, leading to a final conductivity of 2.38 and 2.82 mS cm^{-1} (day 6 and 7, respectively, Fig. 3.7B). Membrane cleaning was performed at the beginning of day 10 to remove deposited foulants, resulting in slightly increased water recovery amount of 257.6 mL. Considering that the feed conductivity reached to 6.85 mS cm^{-1} by the end of day 10, the ED module was operated for 21 hours on the day 11 to achieve a final feed conductivity of 3.46 mS cm^{-1}. It is worth noting that a more prominent electro-osmosis effect was observed in the ED due to a lower solution resistance of wastewater and hence elevated current generation under the same applied voltage (30-52 mA at steady state). An average daily increment of 8.7 and 13.8 mL was observed in ED concentrate from day 1-5 and day 6-10, with a maximum increment of 33 mL after 21-h ED operation on day 11 (Fig. 3.7C). The total ED concentrate volume increased from 200 to 333 mL in 11 days.

As no membrane being the "perfect barrier," concerns have been raised for direct application of reclaimed water due to potential contamination of inorganic ions and organics originated from wastewater (Xie et al. 2012). The concentrations of major ions were quantified in the FO feed, the FO draw, and the ED concentrate after 11-day operation (Fig. 3.8). High concentrations of NH_4^+-N (480.1 mg L^{-1}) and PO_4^{3-}-P (433.4 mg L^{-1}, Fig. 3.8A) were detected in the FO feed, due to continuous leakage of draw solute into the feed side. Other ions originated in the treated wastewater, such as K^+, Na^+, and Cl^-, could end up in the feed solution, ED concentrate, and final diluted draw (owing to forward salt flux, FSF (Zou et al. 2017)). A small amount of K^+ was detected in diluted draw solution, suggesting a lower FSF propensity comparing to Na^+ (Na^+

has smaller hydrated ion radius, Fig. 3.8B). Negligible amounts of Ca^{2+}, Mg^{2+}, and SO_4^{2-} were detected in all solution samples, resulting from the formation of sparingly soluble precipitants such as $CaSO_4$, $Ca_3(PO_4)_2$, $Mg_3(PO_4)_2$, or even $MgNH_4PO_4$ (struvite). These precipitants could lead to intensified inorganic fouling on FO membrane and potential deposition/clogging inside the ED module. The nitrate level was low in the FO feed (1.4 mg L^{-1}), the FO draw (0.3 mg L^{-1}), and the ED concentrate (not detected, Fig. 3.8C), probably due to biological degradation (i.e., denitrification and/or assimilation). In addition to DAP, only Na^+ (25.9 mg L^{-1}), Cl^- (8.5 mg L^{-1}) and some organics (23.7-25.5 mg O_2 L^{-1}) were presented at an acceptable level in the diluted draw solution (EPA 2012). Thus, the recovered water can be applied for safe and direct water reuse (e.g., agricultural irrigation). In the ED concentrate, ~0.2 mol L^{-1} DAP was recovered over the 11-day operation (5866.7 mg L^{-1} NH_4^+-N and 6213.3 mg L^{-1} PO_4^{3-}-P, Fig. 3.8C) together with the presence of other ions and organic matter (75.7 mg O_2 L^{-1}). The recovered reverse-fluxed DAP may be further used as a draw in the FO module for continuing water recovery.

Detailed energy evaluation was conducted on the system level for treating wastewater. With 0.5 mol L^{-1} DAP as the draw under 2-h ED daily operation, 0.53 kJ energy was required by the FO-ED. A total of 0.10 kJ extra energy was spent on ED pump (extended operation time) and ED power supply (higher current generation due to less solution resistance) comparing to DI water as the feed (Fig. 3.9A). When 1.0 mol L^{-1} DAP was applied as the draw under 4-h ED daily operation, a notable increase of overall energy consumption was observed (1.60 kJ), with 1.47 kJ energy (94.7%) powering ED module (Fig. 3.9A). Further SEC analysis revealed that, with 1.0 mol L^{-1} DAP as the draw, 1.49 kWh m^{-3} water or 0.73 kWh kg^{-1} solute should be required, which was greatly reduced to 0.72 kWh m^{-3} water (51.7% reduction) or 0.45 kWh kg^{-1} solute (38.3% reduction) when shifting to 0.5 mol L^{-1} DAP as the draw. This energy consumption rate was less than the high-pressure reverse osmosis (HPRO) for agricultural irrigation (>2.5 kWh m^{-3} (Shaffer et al. 2012)) and low-pressure reverse osmosis coupled with forward osmosis (LPRO-FO, ~1.5 kWh m^{-3} (Yangali-Quintanilla et al. 2011)). It should be noted that, although reversible fouling of the FO membrane could be effectively controlled, extra energy consumption and cost would be expected and need to be evaluated in scaled-up FO-ED systems.

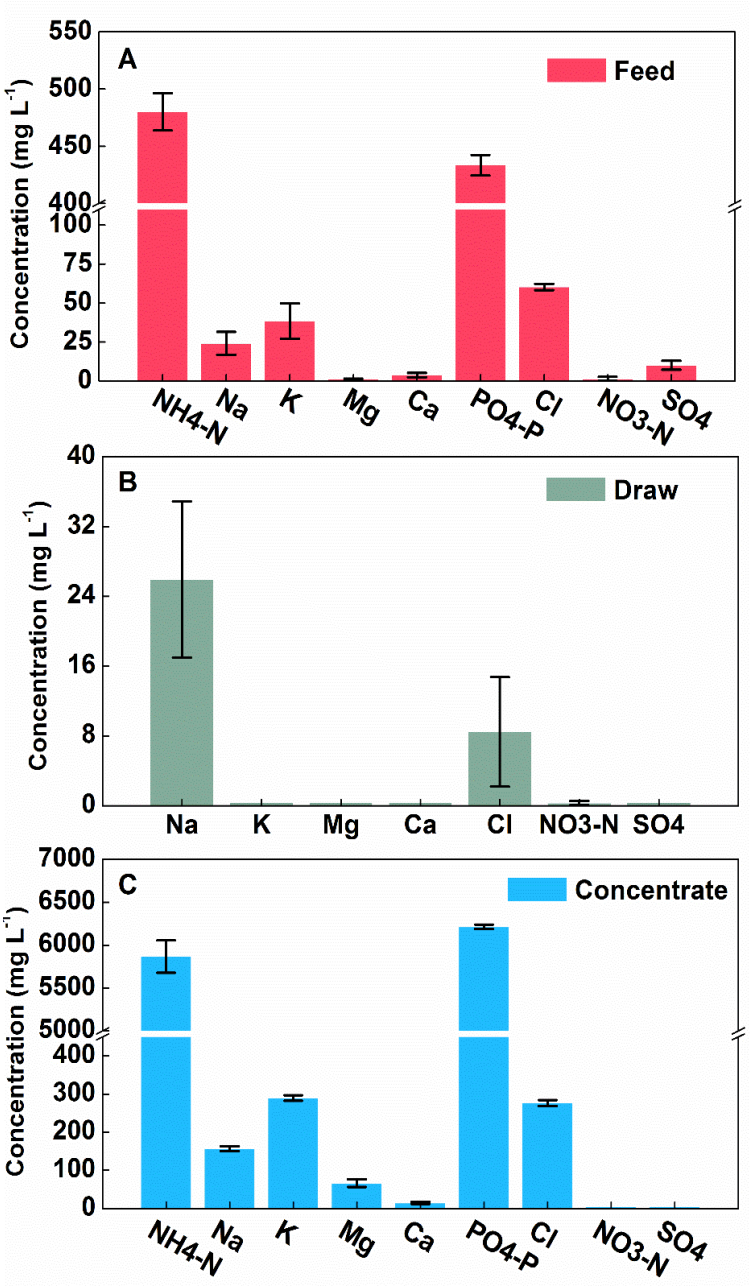

Figure 3.8 The concentrations of major ions with the treated wastewater as the feed in: (A) the FO feed solution; (B) the FO draw solution; and (C) the ED concentrate solution.

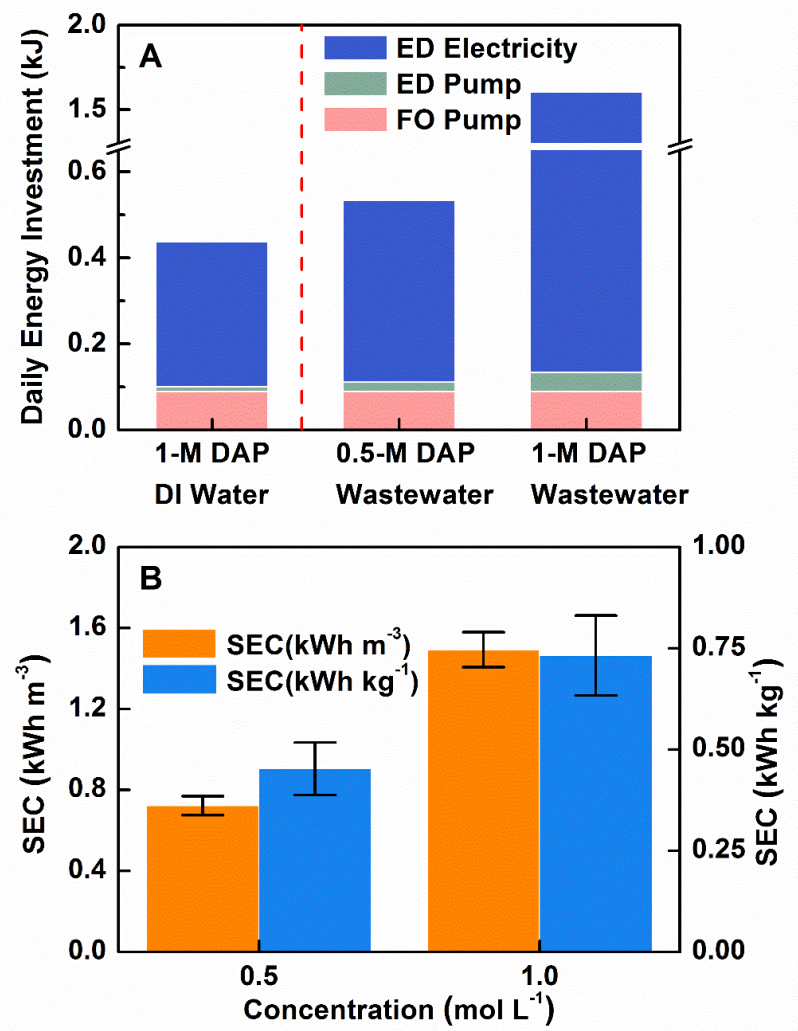

Figure 3.9 Energy profiles of FO-ED system with treated wastewater as the feed regarding (A) composition of energy consumption with 0.5 mol L^{-1} and 1.0 mol L^{-1} DAP as the draw comparing to that with DI water as the feed and 1.0 mol L^{-1} DAP as the draw, and (B) specific energy consumption (SEC) when normalized by unit recovered water and unit desalinated salt, respectively.

3.7 Conclusions

In this study, a fertilizer was studied as a non-regeneration draw solute in an FO-ED hybrid system to achieve water reclamation for direct reuse and mitigation of salinity buildup via electrodialysis recovery. While FO-ED exhibited a stable performance extracting fresh water from DI water, intensified fouling condition was observed when using actual treated wastewater as the feed,

leading to reduced water recovery amount and enhanced salinity buildup induced by coactions of concentrating effect and enhanced RSF. Periodical cleaning of foulants on the FO membrane should be preferred for better water recovery, salinity mitigation, and enhanced stability. Quantification of ion concentration and COD level showed that the quality of the recovery water could meet the requirement of direct water reuse (e.g., agricultural irrigation). The energy consumption of the FO-ED system energy consumption could be significantly lower than the existing treatment systems. These results have demonstrated that the effective synergy between FO and ED could render a reliable, energy-efficient, and cost-effective solution for enhanced water reuse, warranting further investigation in scaling-up systems.

References

Akther, N., Sodiq, A., Giwa, A., Daer, S., Arafat, H.A. and Hasan, S.W. (2015) Recent advancements in forward osmosis desalination: A review. Chemical Engineering Journal 281, 502-522.

Alejo, T., Arruebo, M., Carcelen, V., Monsalvo, V.M. and Sebastian, V. (2017) Advances in draw solutes for forward osmosis: Hybrid organic-inorganic nanoparticles and conventional solutes. Chemical Engineering Journal 309, 738-752.

Butler, E., Silva, A., Horton, K., Rom, Z., Chwatko, M., Havasov, A. and McCutcheon, J.R. (2013) Point of use water treatment with forward osmosis for emergency relief. Desalination 312, 23-30.

Cath, T.Y., Childress, A.E. and Elimelech, M. (2006) Forward osmosis: principles, applications, and recent developments. Journal of Membrane Science 281(1), 70-87.

Ding, Y., Tian, Y., Liu, J., Li, N., Zhang, J., Zuo, W. and Li, Z.P. (2016) Investigation of microbial structure and composition involved in membrane fouling in the forward osmosis membrane bioreactor treating anaerobic bioreactor effluent. Chemical Engineering Journal 286, 198-207.

EPA, U.S. (2012) Guidelines for water reuse. Washington, D.C.

Hancock, N.T. and Cath, T.Y. (2009) Solute coupled diffusion in osmotically driven membrane processes. Environmental Science & Technology 43(17), 6769-6775.

Holloway, R.W., Childress, A.E., Dennett, K.E. and Cath, T.Y. (2007) Forward osmosis for concentration of anaerobic digester centrate. Water Research 41(17), 4005-4014.

Hoover, L.A., Phillip, W.A., Tiraferri, A., Yip, N.Y. and Elimelech, M. (2011) Forward with Osmosis: Emerging Applications for Greater Sustainability. Environmental Science & Technology 45(23), 9824-9830.

Ling, M.M., Wang, K.Y. and Chung, T.-S. (2010) Highly water-soluble magnetic nanoparticles as novel draw solutes in forward osmosis for water reuse. Industrial & Engineering Chemistry Research 49(12), 5869-5876.

Lu, Y. and He, Z. (2015) Mitigation of Salinity Buildup and Recovery of Wasted Salts in a Hybrid Osmotic Membrane Bioreactor–Electrodialysis System. Environmental Science & Technology 49(17), 10529-10535.

Luo, W., Hai, F.I., Kang, J., Price, W.E., Nghiem, L.D. and Elimelech, M. (2015) The role of forward osmosis and microfiltration in an integrated osmotic-microfiltration membrane bioreactor system. Chemosphere 136, 125-132.

Malchi, T., Maor, Y., Tadmor, G., Shenker, M. and Chefetz, B. (2014) Irrigation of Root Vegetables with Treated Wastewater: Evaluating Uptake of Pharmaceuticals and the Associated Human Health Risks. Environmental Science & Technology 48(16), 9325-9333.
McCutcheon, J.R. and Elimelech, M. (2006) Influence of concentrative and dilutive internal concentration polarization on flux behavior in forward osmosis. Journal of Membrane Science 284(1), 237-247.
Mi, B. and Elimelech, M. (2008) Chemical and physical aspects of organic fouling of forward osmosis membranes. Journal of Membrane Science 320(1), 292-302.
Minami, H., Kimura, A., Kinoshita, K. and Okubo, M. (2010) Preparation of Poly(acrylic acid) Particles by Dispersion Polymerization In an Ionic Liquid. Langmuir 26(9), 6303-6307.
Paltiel, O., Fedorova, G., Tadmor, G., Kleinstern, G., Maor, Y. and Chefetz, B. (2016) Human Exposure to Wastewater-Derived Pharmaceuticals in Fresh Produce: A Randomized Controlled Trial Focusing on Carbamazepine. Environmental Science & Technology 50(8), 4476-4482.
Phillip, W.A., Yong, J.S. and Elimelech, M. (2010) Reverse draw solute permeation in forward osmosis: modeling and experiments. Environmental Science & Technology 44(13), 5170-5176.
Phuntsho, S., Kim, J.E., Johir, M.A., Hong, S., Li, Z., Ghaffour, N., Leiknes, T. and Shon, H.K. (2016) Fertilizer drawn forward osmosis process: Pilot-scale desalination of mine impaired water for fertigation. Journal of Membrane Science 508, 22-31.
Phuntsho, S., Sahebi, S., Majeed, T., Lotfi, F., Kim, J.E. and Shon, H.K. (2013) Assessing the major factors affecting the performances of forward osmosis and its implications on the desalination process. Chemical Engineering Journal 231, 484-496.
Phuntsho, S., Shon, H.K., Hong, S., Lee, S. and Vigneswaran, S. (2011) A novel low energy fertilizer driven forward osmosis desalination for direct fertigation: Evaluating the performance of fertilizer draw solutions. Journal of Membrane Science 375(1–2), 172-181.
Phuntsho, S., Shon, H.K., Majeed, T., El Saliby, I., Vigneswaran, S., Kandasamy, J., Hong, S. and Lee, S. (2012) Blended Fertilizers as Draw Solutions for Fertilizer-Drawn Forward Osmosis Desalination. Environmental Science & Technology 46(8), 4567-4575.
Qin, M. and He, Z. (2014) Self-Supplied Ammonium Bicarbonate Draw Solute for Achieving Wastewater Treatment and Recovery in a Microbial Electrolysis Cell-Forward Osmosis-Coupled System. Environmental Science & Technology Letters 1(10), 437-441.
Sant'Anna, V., Marczak, L.D.F. and Tessaro, I.C. (2012) Membrane concentration of liquid foods by forward osmosis: Process and quality view. Journal of Food Engineering 111(3), 483-489.
Shaffer, D.L., Yip, N.Y., Gilron, J. and Elimelech, M. (2012) Seawater desalination for agriculture by integrated forward and reverse osmosis: Improved product water quality for potentially less energy. Journal of Membrane Science 415-416, 1-8.
Shannon, M.A., Bohn, P.W., Elimelech, M., Georgiadis, J.G., Marinas, B.J. and Mayes, A.M. (2008) Science and technology for water purification in the coming decades. Nature 452(7185), 301-311.
She, Q., Jin, X., Li, Q. and Tang, C.Y. (2012) Relating reverse and forward solute diffusion to membrane fouling in osmotically driven membrane processes. Water Research 46(7), 2478-2486.
Tang, C.Y., She, Q., Lay, W.C., Wang, R. and Fane, A.G. (2010) Coupled effects of internal concentration polarization and fouling on flux behavior of forward osmosis membranes during humic acid filtration. Journal of Membrane Science 354(1), 123-133.
Wang, J., Dlamini, D.S., Mishra, A.K., Pendergast, M.T.M., Wong, M.C., Mamba, B.B., Freger, V., Verliefde, A.R. and Hoek, E.M. (2014a) A critical review of transport through osmotic membranes. Journal of Membrane Science 454, 516-537.
Wang, M., Wang, Z., Gong, X. and Guo, Z. (2014b) The intensification technologies to water electrolysis for hydrogen production–A review. Renewable and Sustainable Energy Reviews 29, 573-588.
Weber, S., Khan, S. and Hollender, J. (2006) Human risk assessment of organic contaminants in reclaimed wastewater used for irrigation. Desalination 187(1), 53-64.
Wu, X., Conkle, J.L., Ernst, F. and Gan, J. (2014) Treated Wastewater Irrigation: Uptake of Pharmaceutical and Personal Care Products by Common Vegetables under Field Conditions. Environmental Science & Technology 48(19), 11286-11293.

Xiang, X., Zou, S. and He, Z. (2017) Energy consumption of water recovery from wastewater in a submerged forward osmosis system using commercial liquid fertilizer as a draw solute. Separation and Purification Technology 174, 432-438.
Xie, M., Nghiem, L.D., Price, W.E. and Elimelech, M. (2012) Comparison of the removal of hydrophobic trace organic contaminants by forward osmosis and reverse osmosis. Water Research 46(8), 2683-2692.
Yangali-Quintanilla, V., Li, Z., Valladares, R., Li, Q. and Amy, G. (2011) Indirect desalination of Red Sea water with forward osmosis and low pressure reverse osmosis for water reuse. Desalination 280(1), 160-166.
Zhang, H.M., Li, J.J., Cui, H.T., Li, H.J. and Yang, F.L. (2015) Forward osmosis using electric-responsive polymer hydrogels as draw agents: Influence of freezing-thawing cycles, voltage, feed solutions on process performance. Chemical Engineering Journal 259, 814-819.
Zhao, S., Zou, L., Tang, C.Y. and Mulcahy, D. (2012) Recent developments in forward osmosis: opportunities and challenges. Journal of Membrane Science 396, 1-21.
Zou, S. and He, Z. (2016) Enhancing wastewater reuse by forward osmosis with self-diluted commercial fertilizers as draw solutes. Water Research 99, 235-243.
Zou, S., Qin, M., Moreau, Y. and He, Z. (2017) Nutrient-energy-water recovery from synthetic sidestream centrate using a microbial electrolysis cell-Forward osmosis hybrid system. Journal of Cleaner Production 154, 16-25.
Zou, S., Yuan, H., Childress, A. and He, Z. (2016) Energy Consumption by Recirculation: A Missing Parameter When Evaluating Forward Osmosis. Environmental Science & Technology 50(13), 6827-6829.

4 Electrolysis-Assisted Mitigation of Reverse Solute Flux in a Three-Chamber Forward Osmosis System

(This chapter has been published as "Zou, S. and He, Z. (2017) Electrolysis-assisted mitigation of reverse solute flux in a three-chamber forward osmosis system. *Water Research*, 115, 111-119")

4.1 Abstract

Forward osmosis (FO) has been widely studied for desalination or water recovery from wastewater, and one of its key challenges for practical applications is reverse solute flux (RSF). RSF can cause loss of draw solutes, salinity build-up and undesired contamination at the feed side. In this study, *in-situ* electrolysis was employed to mitigate RSF in a three-chamber FO system ("e-FO") with Na_2SO_4 as a draw solute and deionized (DI) water as a feed. Operation parameters including applied voltage, membrane orientation and initial draw concentrations were systematically investigated to optimize the e-FO performance and reduce RSF. Applying a voltage of 1.5 V achieved a RSF of 6.78 ± 0.55 mmol m^{-2} h^{-1} and a specific RSF of 0.138 ± 0.011 g L^{-1} in the FO mode and with 1 M Na_2SO_4 as the draw, rendering ~57% reduction of solute leakage compared to the control without the applied voltage. The reduced RSF should be attributed to constrained ion migration induced by the coactions of electric dragging force (≥ 1.5 V) and high solute rejection of the FO membrane. Reducing the intensity of the solution recirculation from 60 to 10 mL min^{-1} significantly reduced specific energy consumption of the e-FO system from 0.693 ± 0.127 to 0.022 ± 0.004 kWh m^{-3} extracted water or from 1.103 ± 0.059 to 0.044 ± 0.002 kWh kg^{-1} reduced reversed solute. These results have demonstrated that the electrolysis-assisted RSF mitigation could be an energy-efficient method for controlling RSF towards sustainable FO applications.

4.2 Graphical Abstract

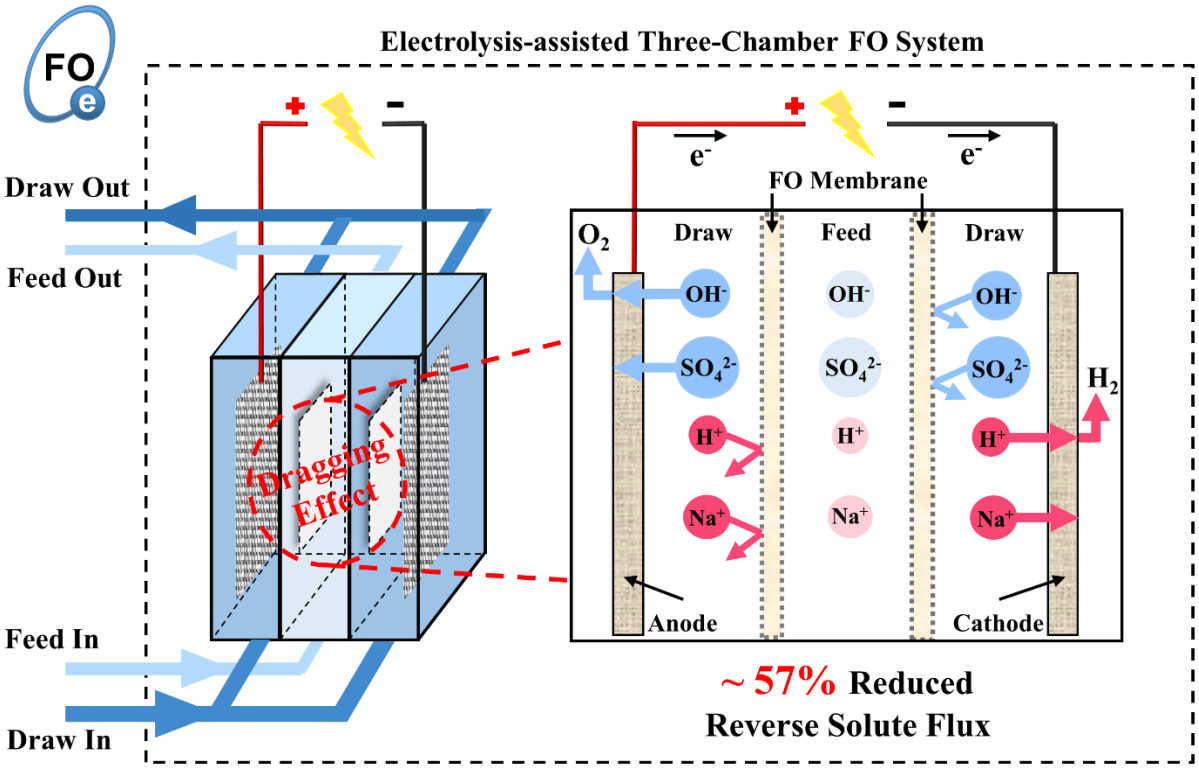

4.3 Keywords

Forward osmosis; Electrolysis; Reverse solute flux; In-situ mitigation; Energy consumption

4.4 Introduction

Osmotically driven membrane processes are being developed to address global freshwater shortage, wastewater reuse and water-energy nexus (Cath et al. 2013, Ng et al. 2006). Among those processes, FO uses osmotic pressure gradient across a semi-permeable membrane to reclaim high-quality water for versatile applications, such as irrigation, food processing and life support (Cath et al. 2006). The major advantages of FO-based water treatment systems include reduced operating pressure, high rejection of undesired compounds, low fouling intensity of FO membranes, and less energy demand if energy-intensive draw regeneration can be properly addressed (Liu et al. 2011, Su et al. 2012).

A key challenge and also impediment for FO applications is the reverse solute flux (RSF) (Achilli et al. 2009, Hancock and Cath 2009). RSF is defined as the cross-membrane diffusion of draw solutes to the diluted feed, and can result in severe loss of draw solutes and gradual salinity build-up at the feed side, leading to reduced osmotic driving force, increased fouling propensity, and elevated operation cost due to periodical replenishment of draw solutes (Achilli et al. 2010, Boo et al. 2012). Accumulation of the reversed draw solutes will require further treatment of the feed solution before it can be discharged to a natural water body (Phillip et al. 2010). Thus, mitigation of solute accumulation at the feed side is important, and several approaches have been proposed and studied, including the use of microorganisms to biologically degrade specific draw solutes, such as NH_4^+, NO_3^-, VFAs and EDTA, in the feed (e.g. anammox and osmotic membrane bioreactor, OMBR) (Holloway et al. 2015, Li et al. 2015), and continuous desalination of the concentrated feed through integrated electrodialysis (ED), filtration (e.g., microfiltration), and/or bioelectrochemical systems (BES) with recoverable draw solutes (Lu and He 2015, Luo et al. 2015, Qin and He 2014). Although these methods can effectively reduce salinity accumulation at the feed side, they cannot mitigate or reduce RSF. Alternatively, novel membrane fabrication/modification methods can render reduced RSF, such as chemically cross-linked layer-by-layer polyelectrolytes and biomimetic membrane embedded with Aquaporin Z (Qiu et al. 2011, Wang et al. 2012). However, a notable trade-off between RSF and water flux as well as unsatisfied mechanical strength were observed in these modified membranes (Chung et al. 2012a).

The researchers have also attempted to decrease RSF through the selection of appropriate draw solutes. Inorganic solutes were extensively investigated in FO systems, and the candidates

with a lower ratio of RSF to water flux (J_s/J_w) were of great interest (Table 4.1) (Achilli et al. 2010). It was reported that multivalent ions with larger hydrated radii, e.g., PO_4^{3-}, Ca^{2+}, and Mg^{2+}, could exhibit a lower cross-membrane diffusion rate and hence decrease solute leakage (Achilli et al. 2010, Nguyen et al. 2015). However, they could serve as the precursor of inorganic scaling, leading to severe membrane fouling (Phillip et al. 2010). The viability of some low J_s/J_w solutes, for instance $MgSO_4$, was hindered by their relatively high specific cost ($7.35 to make 1-L draw solution with an osmotic pressure of 2.8 MPa) (Achilli et al. 2010). Magnetic nanoparticles were also proposed as an emerging solute because they exhibited low RSF and could be separated by magnetic field and/or ultrafiltration (Ling and Chung 2011a, b) Nonetheless, agglomerated nanoparticles required further ultrasonication for performance recovery, leading to weakened magnetic properties (Chung et al. 2012b, Ling et al. 2010).

Given the importance of RSF to FO applications, there is a critical need for developing effective methods to reduce RSF (Zou and He 2016). In our previous study, a hybrid OMBR-ED system was developed for efficient draw solute recovery and mitigation of salinity build-up at the feed side (Lu and He 2015). In an ED module, migration of ions across the ion-exchange membranes is achieved under the applied electric field. Herein, we employed the concept of electrolysis to an FO system for *in-situ* reduction of RSF. This electrolysis-assisted FO (e-FO) system contained two draw chambers (hydraulically connected) and one feed chamber; such a design was to minimize the effect of pH on the electrodes. Na_2SO_4 was chosen as a draw solute due to its relatively low specific cost, desired J_s/J_w ratio (half of the commonly adopted NaCl under same osmotic pressure, Table 4.1) and stable chemical property (cannot be electrolyzed in a solution). The specific objectives of this study were to (1) demonstrate the effectiveness of applied voltage on reducing RSF; (2) examine the ion migration pattern and other key performance parameters, such as water flux, recirculation rate, and fouling intensity; and (3) analyze energy consumption by electrolysis and system operation. To the best of our knowledge, this is the first study accomplishing *in-situ* RSF reduction through operational strategies.

4.5 Materials and Methods

4.5.1 e-FO system setup and operation

The three-chamber e-FO system consisted of two bilateral draw chambers (hydraulically connected) and one middle feed chamber (Fig. 4.1). Two pieces of cellulose triacetate (CTA) membranes with a total surface area (S) of 0.0032 m^2 (Hydration Technologies Inc., Albany, OR, USA) were installed with their active layers facing the feed (FO mode), creating an identical volume of 16 mL for each chamber (4×4×1 cm). Two stainless steel meshes (4×4 cm, ~1.4 cm distance), acting as both the electrode and swelling control, were placed close to the FO membrane (~0.2 cm) in the draw chambers and connected to an external power supply (CSI3644A, Circuit Specialists, Inc., Mesa, AZ, USA).

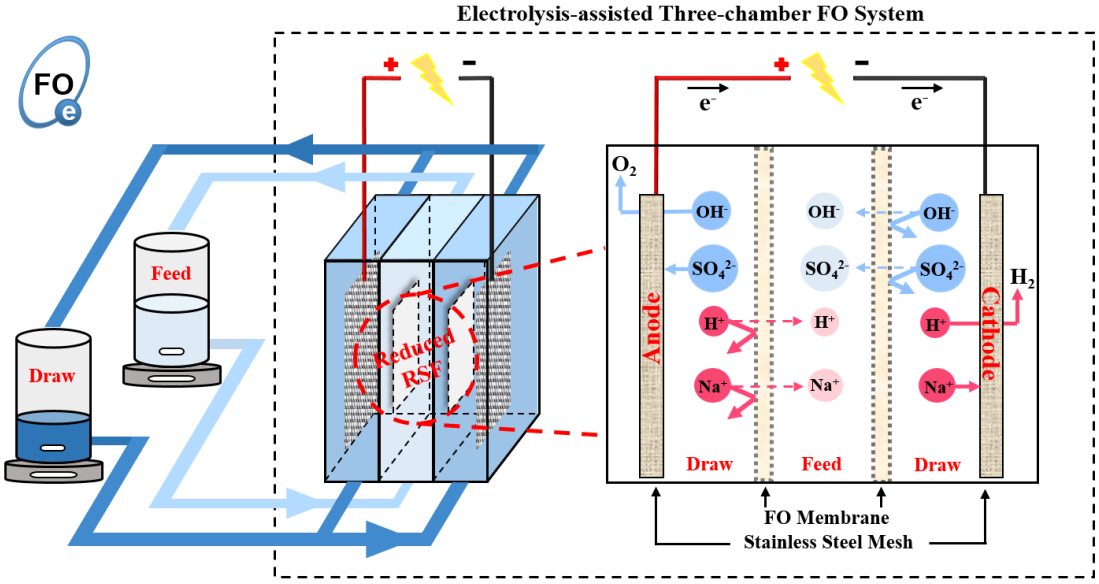

Figure 4.1 Schematic of the electrolysis-assisted three-chamber forward osmosis system.

During operation, 200 mL of 1-M Na_2SO_4 (conductivity 87.1-88.4 mS cm^{-1}) was used as a draw solution; the effluents from both draw chambers were mixed and then recirculated back to the draw chambers. Deionized (DI) water was used as the feed solution and recirculated between the feed chamber and an external storage bottle; DI water was supplemented periodically to maintain a constant liquid volume of 500 mL. For each batch test, the e-FO system was operated for 24 h with water sampled every hour for the first 6-h operation and at the end of each test. The experiment was operated without any biological activities and in a temperature-controlled lab (20 ± 2 °C).

4.5.2 Experimental procedure

The feasibility of the e-FO system was first examined with an external voltage supply of 0 V (control system) and 3 V (experiment system), respectively. No voltage was applied to both systems in the first hour. When some solute ions gradually migrated to the feed side due to RSF, the feed conductivity was expected to increase and then the external power supply was turned on (at the end of the first hour) for the experiment system. The recirculation rate was set at 60 mL min^{-1} (4 cm s^{-1}) for all the draw and feed chambers in the feasibility test (Table 4.2). A series of system optimizations were then performed for the e-FO in terms of applied voltage (1 V, 1.5 V, 2 V and 3 V), membrane orientation (active layer facing feed and draw, i.e. FO and PRO mode), and initial draw concentration (0.5 M, 1 M, and 1.5 M) (Table 4.2). Fouling situation of the FO membrane was studied through monitoring water flux performance in three successive batch tests (24 h, FO mode) with 1 M Na_2SO_4 (200 mL) as the draw and DI water as the feed (500 mL constant). Because Na_2SO_4 was the only solute involved, fouling was mainly expected on the porous supportive layer (draw chamber, FO mode). Effective removal of residual foulants was achieved by i*n-situ* osmotic backwashing: DI water (1 L) and 1 M Na_2SO_4 (200 mL) were pumped into the draw and the feed chambers, respectively, for 6 h, followed by 30 min rinse with DI water.

4.5.3 Measurement and analysis

The pH of water samples was measured by using a benchtop pH meter (Oakton Instruments, Vernon Hills, IL, USA). The concentrations of sodium (Na^+) and sulfate (SO_4^{2-}) were quantified by using ion chromatography (Dionex LC20 ion chromatograph, Sunnnyvale, USA) together with an ED40 electrochemical detector. Total dissolved iron was determined by Hach FerroVer® Method 8008 according to the instruction. Conductivity was measured with a benchtop conductivity meter with a temperature sensor (Mettler-Toledo, Columbus, OH, USA). The voltage across the external resistance (1 Ω) in the circuit was recorded every 2 min by a digital multimeter (Keithley Instruments Inc., Cleveland, OH, USA). Water flux was determined by measuring the change of water weight on an electronic balance (Scort Pro, Ohous, Columbia, MD, USA) at a 30-s interval according to a previous study (Yuan et al. 2016). The flux recovery rate in fouling test was calculated as the ratio of maximum water flux (in the first hour) between backwash and pristine membranes. The solute build-up (SBU) at the feed side was quantified by Eq. 4.1 with a unit of mmol m^{-2} h^{-1} (Zou and He 2016). SBU is typically resulted from the concentrating effect in

the feed (due to membrane rejection of the feed solute) and reverse solute flux (RSF, mmol $m^{-2} h^{-1}$) from the draw solution (Phillip et al. 2010). When DI water is used as the feed, $C_{i,F}$=0 and hence no concentrating effect is observed. Under such a case:

$$SBU = RSF = \frac{n_{f,F} - n_{i,F}}{S \times t} = \frac{V_F \times (C_{f,F} - C_{i,F})}{S \times t} \quad \text{(Eq. 4.1)}$$

where $n_{i,F}$ and $n_{f,F}$ are the initial and final mole of Na_2SO_4 in the feed, respectively. $C_{i,F}$ and $C_{f,F}$ are initial and final Na_2SO_4 concentration in the feed, respectively. V_F is feed volume (500 mL constant). t (h) stands for operating time. S (m^2) is the total surface area of the FO membrane. Specific RSF ($g L^{-1}$) was also calculated for comparison with previous studies (Phillip et al. 2010), and defined as the ratio of J_s ($g m^{-2}h^{-1}$, GMH) and J_a (LMH):

$$Specific\ RSF = \frac{J_s}{J_a} = \frac{RSF \times Mw}{Ja \times 1000} \quad \text{(Eq. 4.2)}$$

Based on water flux performance together with the reduced reverse solute, energy consumption of the e-FO system was evaluated either with a different voltage (1 V, 1.5 V, 2 V and 3 V) or a different recirculation rate (10 mL min^{-1}, 30 mL min^{-1} and 60 mL min^{-1} for all chambers). The energy consumption rate was normalized either by unit recovered water or unit reduced reverse solute. It is assumed that the power consumption of the e-FO system is mainly attributed to the recirculation pump and the power supply. The specific energy consumption (SEC) for unit recovered water (E_w, kWh m^{-3}) is estimated as (Shaffer et al. 2012):

$$E_w = \frac{P_{system}}{Q} \approx \frac{P_{pump} \times \rho}{m_{t,D} - m_{t\text{-}1,D}} \ or \ \frac{(P_{pump} + P_{electricity}) \times \rho}{m_{t,D} - m_{t\text{-}1,D}} \quad \text{(Eq. 4.3)}$$

where P_{pump} (kW) and $P_{electricity}$ (kW) are the power consumption of the recirculation pump and external voltage supply, and Q ($m^3 h^{-1}$) is recovered water flow rate. $m_{t,D}$ and $m_{t\text{-}1,D}$ represent the mass of draw solution at a specific time t and t-1 (h), respectively.

The SEC for unit reduced solute (E_s, kWh kg^{-1}) is defined as the amount of reduced reverse solute because of an external power supply and estimated as:

$$E_s = \frac{P_{electricity} \times t}{\Delta m_{solute,f}} = \frac{P_{electricity} \times t}{m_{solute,control.f} - m_{solute,experiment.f}} \quad \text{(Eq. 4.4)}$$

where $\Delta m_{solute,\ f}$ (kg) is the reduced solute mass due to applied voltage by comparing the control ($m_{solute,control.f}$) and the experiment groups ($m_{solute,experiment.f}$). The SEC for unit reduced solute based on the entire e-FO system ($E_{s,total}$, kWh kg^{-1}) is determined by:

$$E_{s,total} = \frac{(P_{pump} + P_{electricity}) \times t}{m_{solute,control.f} - m_{solute,experiment.f}} \quad \text{(Eq. 4.5)}$$

4.6 Results and discussion

4.6.1 Feasibility of the e-FO system

The feasibility of the e-FO system was investigated for its water flux performance, RSF reduction, and comparison with a two-chamber FO system that was also assisted by electrolysis. With an applied voltage of 3 V, the e-FO system generated comparable average water flux (maximum ~9.0 LMH) and the volume of the recovered water (~450 mL) within 24 h when compared to that with 0 V. However, a notable decrease in the conductivity of the final feed solution from 536 ± 12 (0 V) to 343 ± 9 μS cm^{-1} (3 V) was observed, rendering reduction of 35.9 ± 0.3 %. The reduced conductivity should be primarily attributed to less reverse-fluxed solute from the draw, resulting in a mitigated RSF of 9.53 ± 0.49 mmol m^{-2} h^{-1} with 3 V, significantly lower than 15.57 ± 0.23 mmol m^{-2} h^{-1} with 0 V. Meanwhile, a more desired specific RSF (i.e. J_s/J_a) of 0.194 ± 0.010 g L^{-1} was achieved against the control system and that reported in the literature (0.320-0.330 g L^{-1}, Table S3). For comparison, a two-chamber conventional FO was examined with or without applied voltage (Fig. 4.2). The results show that the three-chamber e-FO system had merits in terms of water extraction capability, solution pH and system stability. The three-chamber e-FO system outcompeted the conventional two-chamber FO with a notable increase in the maximum water flux (tripled, Fig. 4.2A). When electrolysis (3 V) was applied to the two-chamber FO system, unbalanced pH in both the feed (3.02 ± 0.03) and the draw (10.70 ± 0.21) solutions was detected,

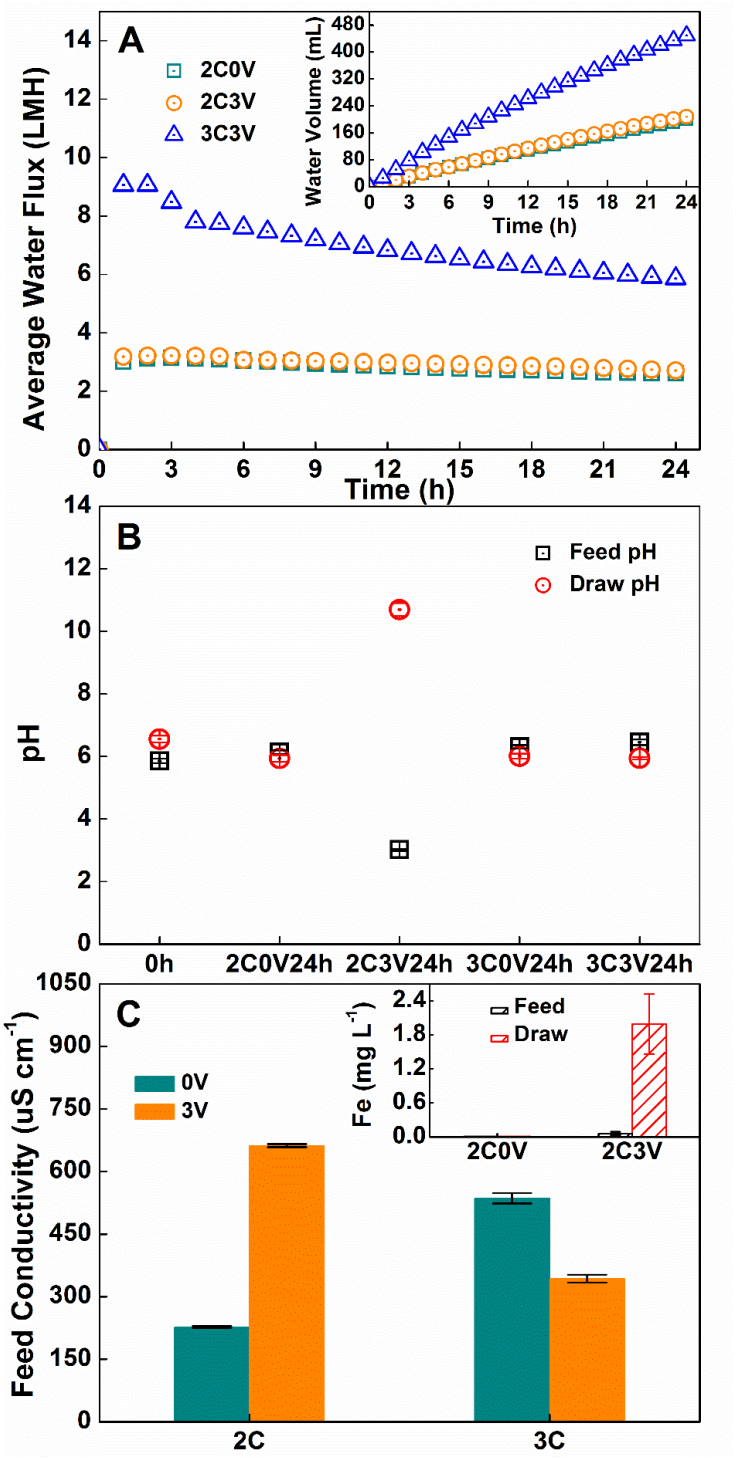

Figure 4.2 Performance profiles of different e-FO systems in terms of (A) average water flux as well as recovered water volume, (B) pH variations in both the draw and feed, and (C) final feed conductivity and Fe^{3+} level (embedded). "2C" and "3C" stand for two-chamber and three-chamber system, respectively.

which could cause the damage of electrodes and membrane in long-term operation; after 24-h operation, the elevated Fe^{3+} level (1.99 ± 0.53 mg L^{-1}) was detected in the final feed solution of the two-chamber FO system, indicating the corrosion of the anode electrode (Fig. 4.2C embedded). The three-chamber e-FO system, on the other hand, had very stable pH in both solutions (Fig. 4.2B). It was worth noting that the applied voltage induced an adverse effect in the two-chamber e-FO system with tripled feed conductivity (662 ± 4 μS cm^{-1} with 3 V vs. 227 ± 2 μS cm^{-1} with 0 V, Fig. 4.2C), indicating the increased ion concentration from elevated RSF and generated H^+/Fe^{3+} (Fig. 4.2B and 4.2C embedded). Hence, the three-chamber e-FO system offered cost-savings in long-term operation with advantages of higher water flux, less solute loss via reduced RSF, prolonged electrode lifespan and stable water quality (e.g. solution pH).

4.6.2 Effect of applied voltage

To better understand the effects of the applied voltage on electrolysis-assisted RSF mitigation, the external voltage was then successively reduced from 3 V to 2 V, 1.5 V, and 1 V. As a result, the current decreased from 2.04 ± 0.41 mA (3 V) to 0.26 ± 0.01 mA (2 V), and then 0.037 ± 0.001 mA (1.5 V) (Fig. 4.3A). Interestingly, with the decrease of the applied voltage from 3 V to 1.5 V, the electrolysis-assisted mitigation of RSF was enhanced, and the lowest conductivity of 257 ± 6 μS cm^{-1} in the final feed solution and the lowest RSF of 6.78 ± 0.55 mmol m^{-2} h^{-1} were achieved with 1.5 V (Fig. 4.3B and 4.3C). The specific RSF with 1.5 V (0.138 ± 0.011 g L^{-1}) was more than 70% lower than that of the control system (0 V) and the conventional cross-flow FO systems (Table 4.3). It should be noted that the theoretical thermodynamic voltage of water decomposition is 1.23 V, and a threshold voltage of 1.5 V should be expected for successful albeit limited electrolysis (Bockris et al. 1985), considering the overpotential effects (Wang et al. 2014b). Below the threshold voltage, an extremely low current of 0.002 ± 0.001 mA and negligible production of H_2 and O_2 with 1 V indicated a failure of water splitting, supported by the previous study that detectable electrolysis-induced gas production occurred with at least 1.5 V (Tuna et al. 2009). As a result, no inhibition of RSF was expected with 1 V, which led to similar feed conductivity (525 ± 7 μS cm^{-1}) and RSF (15.51 ± 0.15 mmol m^{-2} h^{-1}) to those in the control system (0 V). Elevated initial water flux was observed in the first hour with a peak value appeared under 1.5 V (9.84 ± 0.37 LMH) compared to that under 0 V (8.06 ± 0.25 LMH, Fig. 4.3D). The overall average water

flux and recovered volume was independent of the applied voltage with negligible water loss from the splitting reaction. No obvious temperature variations were detected in all water samples.

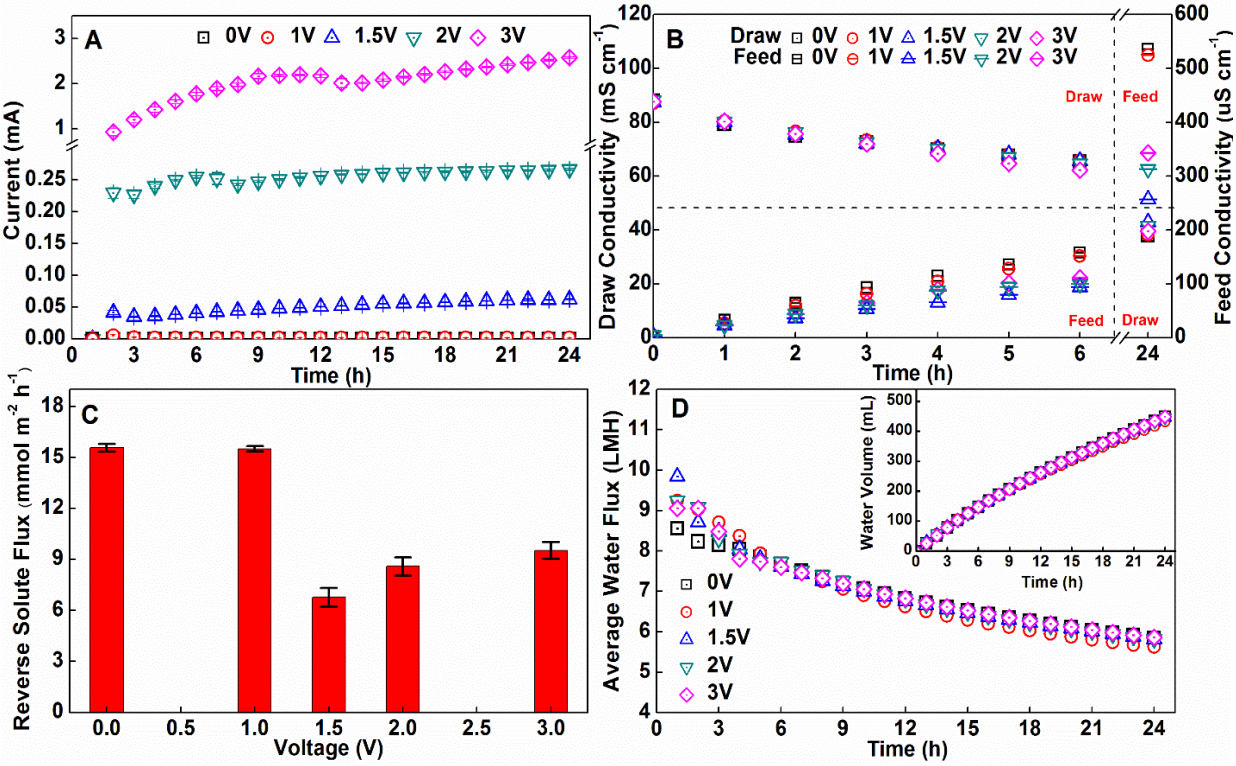

Figure 4.3 The performance of the e-FO system under different applied voltages: (A) current generation; (B) conductivity variations in the draw and the feed solution; (C) reverse solute flux; and (D) water flux and the volume of the extracted water.

The reduced RSF should be attributed to ion migration induced by the coactions of both the effective electric field (≥ 1.5V with water electrolysis) and high solute rejection of FO membrane. The e-FO system exhibited a similar process to that of ED, with H^+ reduction to H_2 at the cathode and OH^- oxidation to O_2 at the anode; meanwhile, Na^+ and SO_4^{2-} migrated from the draw solution into the feed solution driven by concentration gradients. With an applied voltage ≥ 1.5V, the potential difference between the electrodes could generate a dragging effect that is highly-effective in retaining opposite-charged ions (anions at the anode and cations at the cathode), whereas an applied voltage < 1.5 V failed to maintain an effective dragging force with the absence of water splitting. However, unlike ED that is equipped with ion exchange membrane, the e-FO

system contained FO membrane only allow the draw solute ions to diffuse through by indirect partitioning, which is partially governed by a cross-membrane concentration gradient (Phillip et al. 2010). Thus, the same-charged ions (cations at the anode and anions at the cathode) will be repelled by the electrode (i.e., repelling effect), but fail to diffuse through the FO membrane due to membrane rejection efficiently. As a result, the higher voltage applied above 1.5 V, the faster same-charged ions will be accumulated at the boundary layer, which exceeded the reduced concentration of opposite-charged ions via dragging effect, eventually creating a larger concentration gradient together with diffusion force. This explanation is in accordance with the increased RSF and the conductivity of the final feed solution from 1.5 V to 3 V (Fig. 4.3B and C). The strengthened diffusion load of ions induced by the repelling effect can also lead to detectable fouling situation. For example, ~14% reduction in both water volume and maximum flux was observed with 3 V after three-time batch tests (Fig. 4.4). This reversible fouling could be controlled by osmotic backwashing with a recovery rate of 98% (Le-Clech et al. 2005).

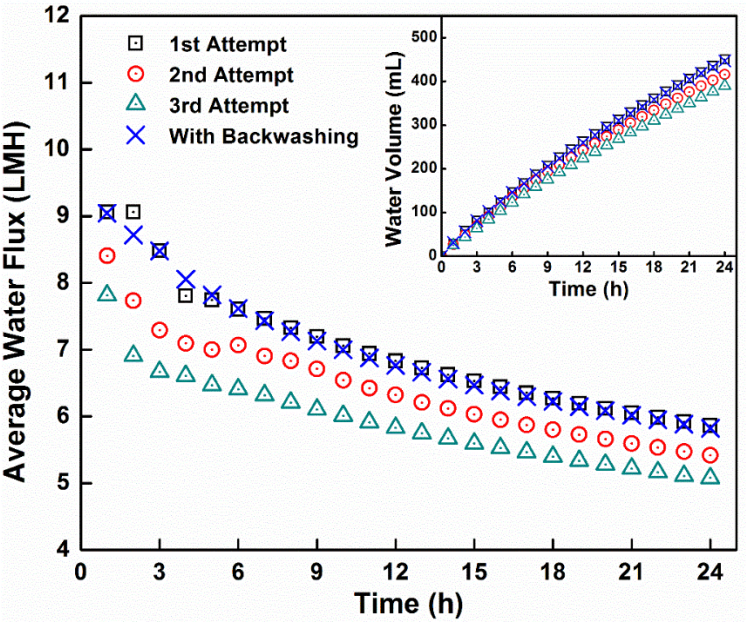

Figure 4.4 Membrane performance in terms of recovered water volume and average water flux with and without in-situ backwashing under an applied voltage of 3.0V.

Cross-membrane migration of ions (Na^+, H^+, SO_4^{2-}, and OH^-) also led to pH variation in both the draw and feed solutions, highly depending on the applied voltage (Fig. 4.5A). According

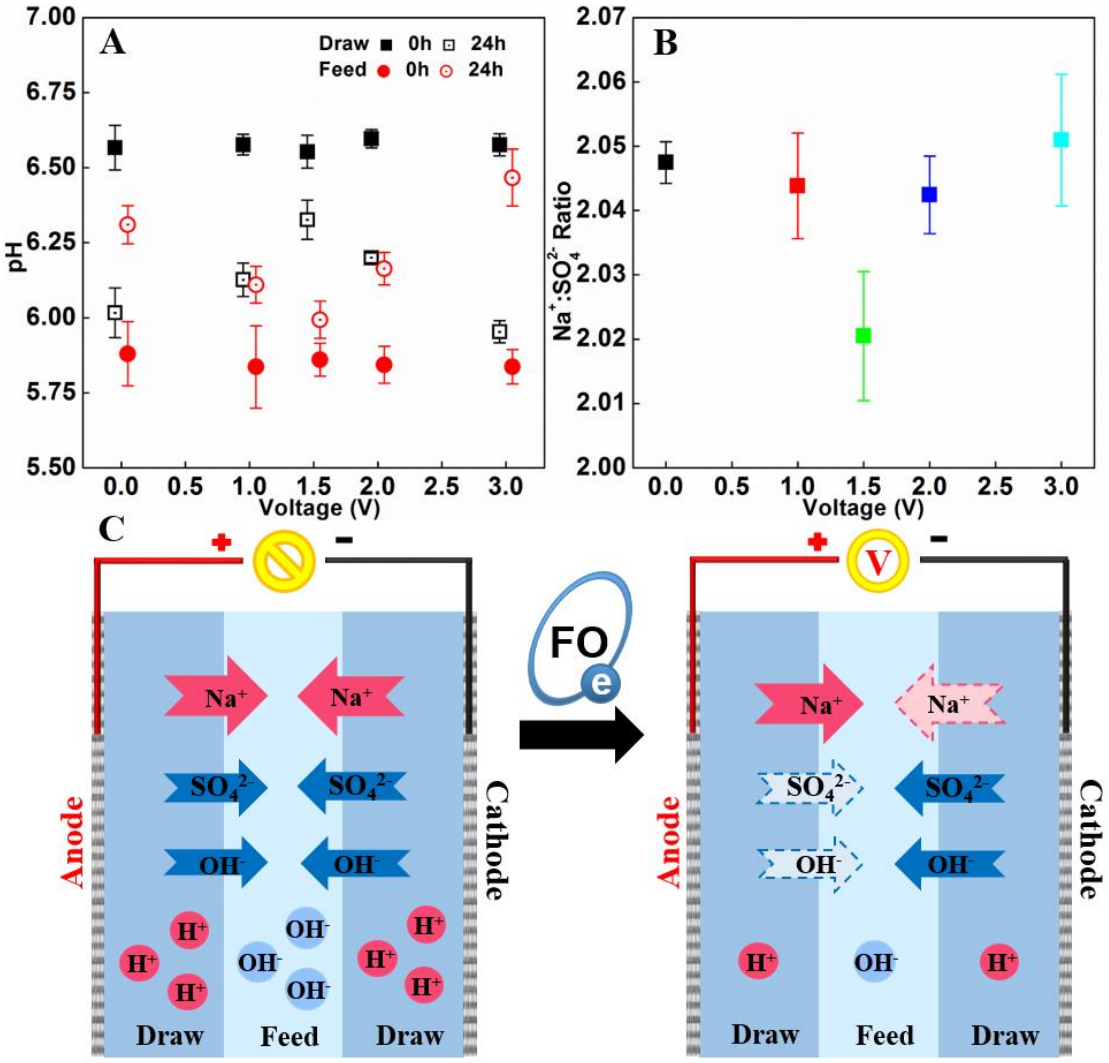

Figure 4.5 The profiles of (A) pH variations; (B) ratio of Na^+ to SO_4^{2-}; and (C) proposed ion migration pattern.

to the prior studies (Achilli et al. 2010, Phuntsho et al. 2011), multivalent ions with larger hydrated radii (Nightingale Jr 1959), such as PO_4^{3-} and SO_4^{2-}, exhibited lower diffusion rates compared to monovalent ions (e.g., K^+ and Na^+). Assuming 2 mol of Na^+ diffuse to the middle feed chamber, 1 mol of SO_4^{2-} should migrate at the same time; SO_4^{2-} may be partially substituted by OH^-, rendering a ratio of Na^+ to SO_4^{2-} larger than 2 (2.047 ± 0.003 with 0 V, Fig. 4.5B). Hence, this Na^+-governed diffusion, due to a higher cross-membrane concentration gradient of Na^+, will lead to excess diffusion of OH^- to the feed (0 V, Fig. 4.5C). This assumption was validated with slight

pH increase in the feed (from 5.88 ± 0.11 to 6.31 ± 0.06) and corresponding pH drop in the draw solution (from 6.56 ± 0.07 to 6.02 ± 0.08), respectively (0 V, Fig. 4.5A). A comparable Na^+:SO_4^{2-} ratio of 2.044 ± 0.008 was observed with 1 V. However, when 1.5V was applied to the e-FO system, the solution pH was affected to a less degree in both the feed (from 5.86 ± 0.06 to 5.99 ± 0.06) and the draw (from 6.55 ± 0.05 to 6.33 ± 0.07, Fig. 4.5A), and a Na^+:SO_4^{2-} ratio of 2.020 ± 0.010 was closer to the theoretical value (1.5 V, Fig. 4.5B), resulted from less migration of solute ions, especially Na^+ (Fig. 3C). With further increase of external voltage from 1.5 V to 3 V (accompanied by increasing current generation), the repelling effect might become dominant, leading to more Na^+ leakage (a Na^+:SO_4^{2-} ratio of 2.051 ± 0.010 at 3 V, Fig. 4.5B). This would enhance OH^- diffusion to neutralize the excess Na^+, rendering augmented pH variation with 3 V (Fig. 4.5A).

Although relatively stable solution pH was achieved by mixing the anolyte and the catholyte in the e-FO system, a high voltage (e.g., 3 V) could generate more H^+ inside the anode chamber, causing the undesired corrosion of the electrode (Fig. 4.6). Soluble iron (Fe^{3+}) was detected in the final draw solution with 3 V operation (1.50 ± 0.08 mg L^{-1}, Table S4), and this concentration could be higher with a longer term of operation. Thus, a moderate voltage of 1.5 V, though relatively low in electrolytic efficiency of water splitting, would be more favored due to reduced solute leakage by dragging effect (56.5 ± 2.3 % for RSF and 56.8 ± 2.9 % for specific RSF compared to that with 0 V, Fig. 4.3 and Table 4.3), negligible water loss due to splitting reaction (< 0.001 mL L^{-1} recovered water), alleviated repellence of same-charged ions, and prolonging electrode lifespan. To avoid electrode corrosion during the long-term operation, the non-corrosive materials such as platinum and/or iridium may also be considered as the electrodes, though at a higher expense.

4.6.3 Effect of membrane orientation

The e-FO system was further investigated for the effect of the membrane orientation (FO vs. PRO mode) with an applied voltage of 0 V or 1.5 V. It was found that the PRO mode exhibited higher water flux (12.31 ± 0.25 to 12.97 ± 0.53 LMH), because of concentrative internal concentration polarization (ICP) and a larger effective osmotic gap ($\Delta\pi_{eff}$) (McCutcheon et al. 2006), than that of the FO mode (8.06 ± 0.29 to 9.84 ± 0.17 LMH, Fig. 4.7A). However, in the PRO mode, there was negligible difference in the conductivity of the final feed solution between 0 V (749 ± 8 μS cm^{-1}) and 1.5 V (755 ± 12 μS cm^{-1}, Fig. 4.7B), while significant reduction of RSF in FO mode was

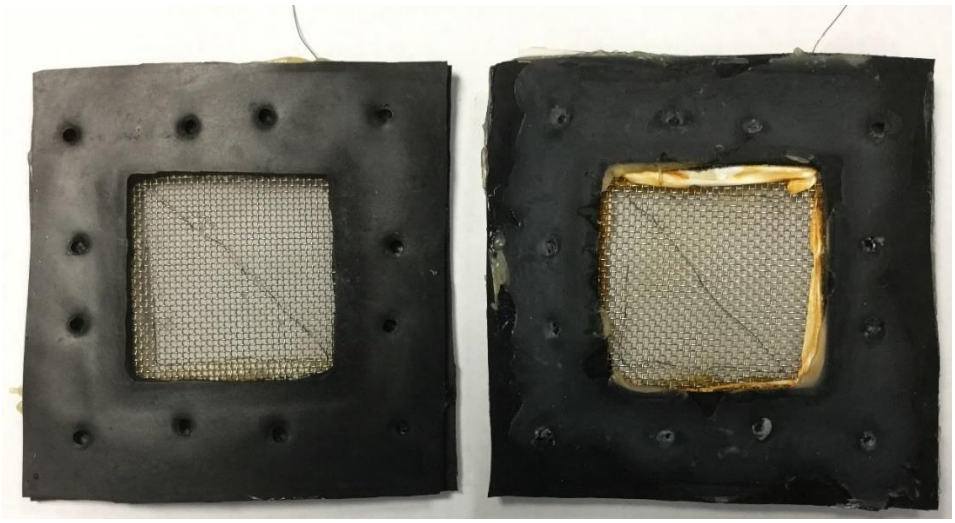

Figure 4.6 Comparison of electrode corrosion inside e-FO system under (left) 0V-2V and (right) 3V. The electrode is made from stainless steel mesh and then connected to external power supply with titanium wire.

observed with the draw conductivity decreasing from 536 ± 12 μS cm^{-1} with 0 V to 257 ± 6 μS cm^{-1} with 1.5 V. This could be explained by the voltage-affected ion diffusion pattern inside the asymmetric FO membrane (Fig. 4.7C). According to a previous study, diffusion of draw solute across the active layer (J_s^A) without an effective electric field (≥ 1.5V in the current case) can be calculated using Fick's law of diffusion (Eq. 4.6) (Phillip et al. 2010).

$$J_s^A = -D^A \frac{dC}{dt} = -\frac{D^A}{t_A}(C_a^i - C_f) = -\frac{D^A}{t_A}(C_a^i - 0) \qquad \text{(Eq. 4.6)}$$

where D^A is the diffusion coefficient of draw solute in the active layer, t_A is the thickness of the active layer, C_a^i is the concentration of draw solute on the active layer side of the supportive layer-active layer interface, and C_f is the concentration of draw solute in the feed (assuming $C_f^i \approx C_f$ in an FO system with negligible external concentration polarization, ECP) (Cath et al. 2006). Initially, C_f equaled to 0 as DI was applied as the feed. Similarly, diffusion of draw solute across the supportive layer (J_s^S) can be quantified (Eq. 4.7, applied voltage < 1.5 V).

$$J_s^S = -D^S \frac{dC}{dt} = -\frac{D^S}{t_S}(C_d^i - C_s^i) = -\frac{D^S}{t_S}(C_d - 0) \qquad \text{(Eq. 4.7)}$$

where D^S is the diffusion coefficient of draw solute in the supportive layer, t_S is the thickness of the supportive layer, C_s^i is the concentration of draw solute on the supportive layer side of the supportive layer-active layer interface (initially equals to 0), and C_d is the concentration of draw solute in the draw chamber (assuming $C_d^i \approx C_d$).

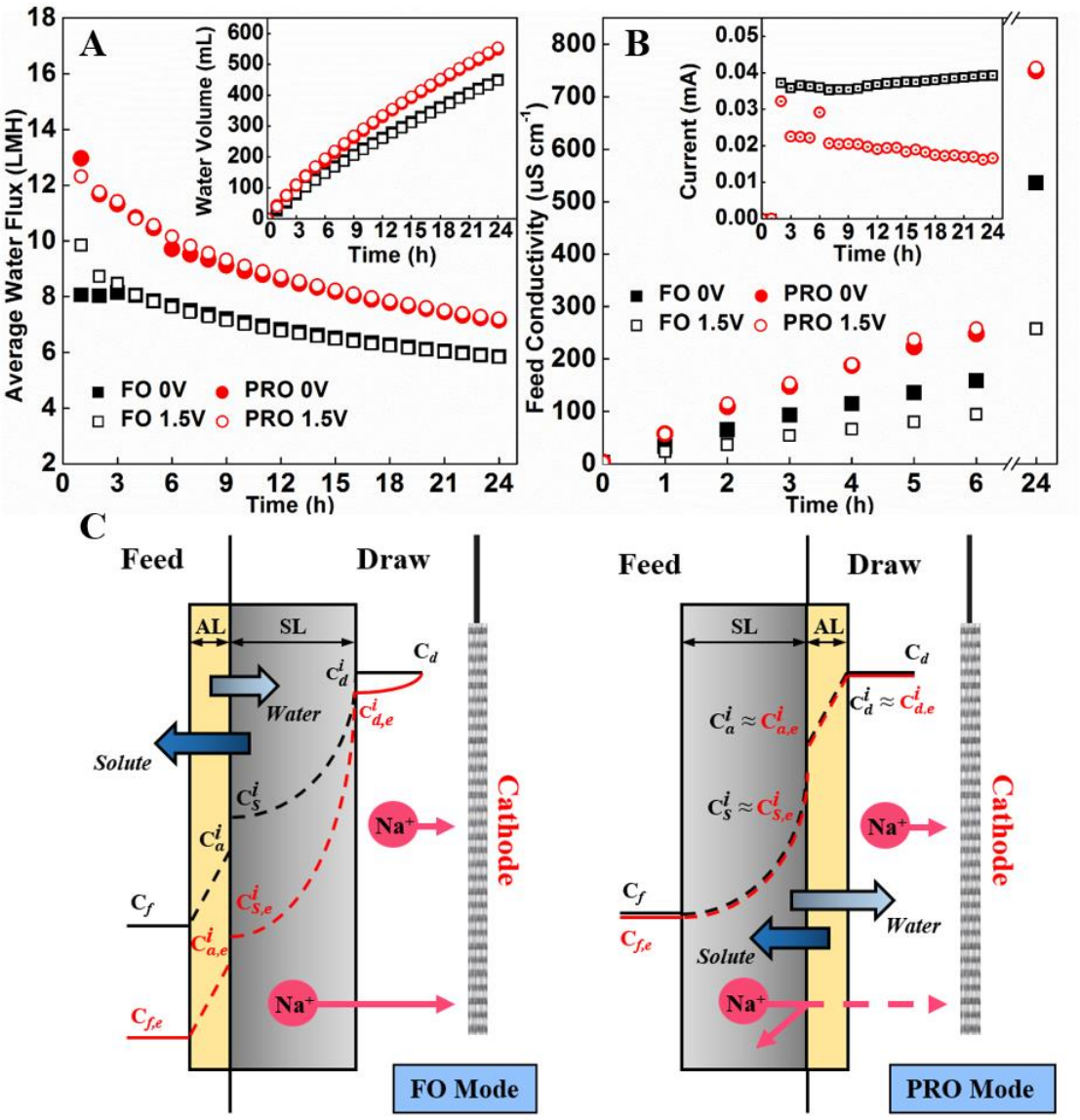

Figure 4.7 The e-FO performance under two different membrane orientations, FO mode and PRO mode: (A) water flux; (B) conductivity and current variations in feed solutions; and (C) the proposed ion diffusion pattern inside asymmetric FO membrane. In Fig. 4.7C, the black line is the ion diffusion pattern without applied voltage (0V), and the red line with a subscript "e" is the ion diffusion pattern with applied voltage (1.5V).

When an effective voltage (≥ 1.5V) was exerted on the e-FO system, ion migration induced by the electric field should be taken into account together with ion diffusion in the supportive layer. The modified ion transport ($J_{s,e}^{S}$) across the supportive layer can be calculated using Nernst-Plank equation (Eq. 4.8, initially $C_{s,e}^{i}$=0).

$$J_{s,e}^{S} = -\frac{D^{S}}{t_{S}}(C_{d,e}^{i} - C_{s,e}^{i} - \frac{FzC_{d}}{RT}E) = -\frac{D^{S}}{t_{S}}(C_{d,e}^{i} - 0 - \frac{FzC_{d}}{RT}E) \quad \text{(Eq. 4.8)}$$

Comparing Eq. 4.7 and 4.8, when 1.5 V was exerted, Na^{+} in both the draw solution and the supportive layer would migrate towards the cathode electrode, leading to a relatively lower concentration of the draw solute on the supportive layer ($C_{d,e}^{i} < C_{d} \approx C_{d}^{i}$) and hence reduced ion transport ($J_{s,e}^{S} < J_{s}^{S}$). Eventually, slower ion transport in the active layer could be achieved under an effective electric field ($J_{a,e}^{A} < J_{a}^{A}$ under FO mode, detailed explanation in Supplementary Materials), resulting in reduced ion concentration in the feed chamber compared to that with 0 V over an extended period of time ($C_{f}^{e} < C_{f}$, FO mode, Fig. 4.7C).

When the active layer facing the draw (the PRO mode), only Na^{+} in the bulk solution could be dragged towards the cathode electrode at the draw side, rendering a similar concentration on the interface ($C_{d}^{i} \approx C_{d,e}^{i}$ in the PRO mode; ECP was not considered, Fig. 4.7C). Hence, comparable solute concentrations on the supportive side of supportive-active layer interface would be expected ($C_{s,e}^{i} \approx C_{s}^{i}$, the PRO mode, Fig. 4.7C). Despite the attempt of migration towards the cathode from the feed side, Na^{+} in the supportive layer would be rejected by the active layer (the PRO mode, Fig. 4C), leading to similar ion diffusion in the active layer ($J_{s,e}^{A} \approx J_{s}^{A}$). Failure of voltage-induced ion migration in PRO mode further rendered lower average current (0.020 ± 0.004 mA, 1.5 V, Fig. 4.7B embedded) compared to that in the FO mode (0.037 ± 0.001 mA, 1.5 V).

It should be noted that, although the e-FO system achieved reduced RSF in the FO mode, no significant difference in water flux and volume was observed after 24-h operation between 0 V and 1.5 V (Fig. 4.7A). Water flux across the active layer can be quantified by Eq. 4.9.

$$Jw = A(\pi_{D} - \pi_{F}) = A(C_{a}^{i} - C_{f})RT = A(C_{a}^{i} - 0)RT \quad \text{(Eq. 4.9)}$$

In the FO mode, owing to the dragging effect, $C_{a,e}^{i}$ would be lower than C_{a}^{i}, leading to an immediate smaller $J_{w,e}$ than J_{w}. However, because of more draw solute diffusion to the feed with 0 V (larger loss), C_{a}^{i} would be expected to decrease relatively faster than $C_{a,e}^{i}$. These two contrary

effects might have compensated each other during the long-term operation, resulting in comparable water flux and volume of the extracted water. Note that electro-osmosis was not considered in water flux because its major effect was to reduce concentration polarization (negligible in an FO process) by enhancing the fluid movement and thus mass transfer in the boundary layer (Liang et al. 2016).

4.6.4 Effect of initial draw concentration

In an FO system, both water flux and RSF are governed by the solute concentration gradient across the FO membrane (Eq. 4.6 and 4.9). When the initial Na_2SO_4 concentration increased from 0.5 M to 1.0 M, water flux increased from 4.6 ± 0.6 LMH to 6.9 ± 0.7 LMH in 24 h, resulting in 150% increase in the volume of water extraction (Fig. 4.8A). However, further increasing the Na_2SO_4 concentration to 1.5 M did not increase water flux (6.9 ± 0.8 LMH). This may be attributed to a non-linear correlation between osmotic pressure (i.e., driven force) and solute concentration at a higher concentration, suggesting a biased estimation of *van't Hoff equation* for "non-ideal" solutions (e.g., 1.5 M Na_2SO_4, almost saturated) (Cath et al. 2006). Efficient water permeation can also be hindered by ICP resulted from limited mass transfer in the supportive layer (Wang et al. 2014a). The comparable volume of water extraction led to similar conductivity of the final feed solution (after dilution with extracted water), 536 ± 12 μS cm^{-1} and 524 ± 33 μS cm^{-1}, by using 1.0 M and 1.5 M draw solutions, respectively (Phillip et al. 2010). The electrolysis-assisted mitigation of RSF was more pronounced at relatively lower initial draw concentrations (0.5 and 1.0 M). With an applied voltage of 1.5 V, the RSF was reduced by 52.8 ± 1.7 % (0.5 M), 56.5 ± 2.3 % (1.0 M), and 39.4 ± 6.9 % (1.5 M), respectively, compared to that with 0 V (Fig. 4.8B embedded). This phenomenon could partially be attributed to a higher ion diffusion rate occurred at a larger concentration gradient. On the other hand, the dragging force provided by the electrode and electric field was rather similar among the three concentrations, indicated by comparable current generation over the 24-h operation: 0.034 ± 0.007 mA at 0.5 M, 0.037 ± 0.001 mA at 1.0 M, and 0.043 ± 0.001 mA at 1.5 M (Fig. 4.8B). The notable initial current fluctuation was observed with 0.5 M Na_2SO_4 as the draw, owing to a lower concentration and more significant concentration polarization near the electrode.

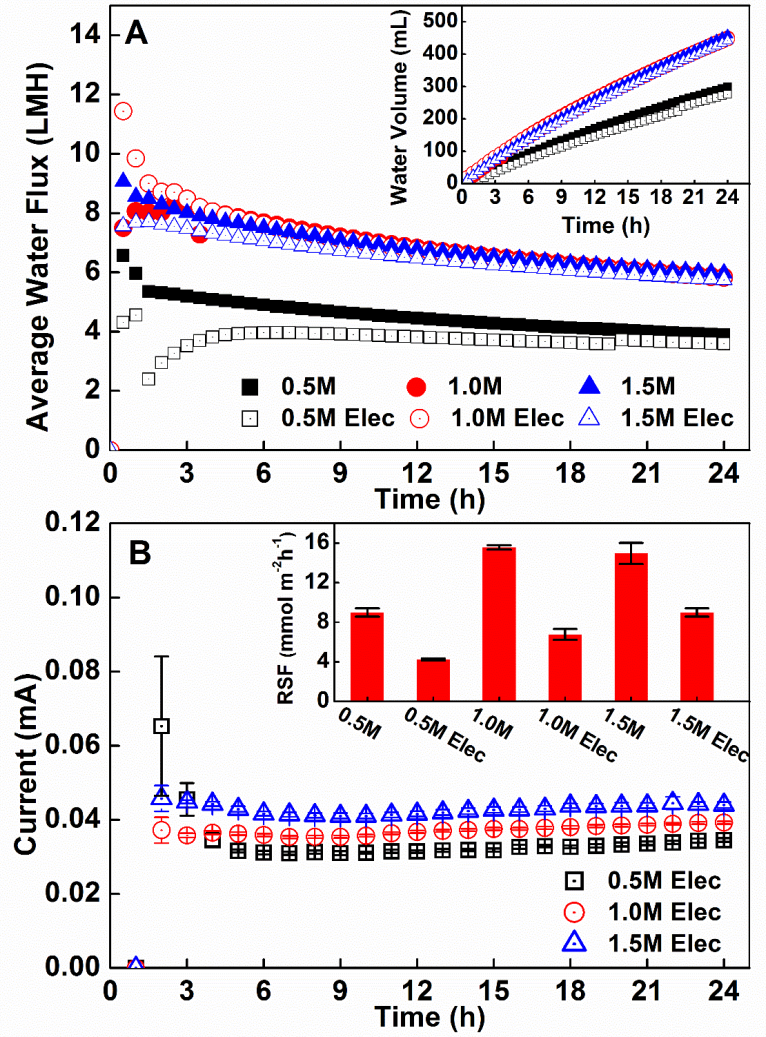

Figure 4.8 Effects of the initial draw concentration with an applied voltage of 0 V or 1.5 V: (A) water flux and the volume of the collected water; and (B) current generation together with RSF under different initial draw concentration (inset).

4.6.5 Energy consumption of the e-FO system

Although the FO process has been widely studied as an energy-efficient process, the information of energy consumption was rarely reported in the previous studies (Zou et al. 2016). In this e-FO system, energy was mainly consumed by the recirculation pumps of three chambers and the external power supply. At a constant recirculation rate of 60 mL min^{-1}, the highest energy consumption was estimated to be 1.03 ± 0.26 kWh m^{-3} with the applied voltage of 3 V, among which 33.1% was attributed to the power supply while the rest was used by the recirculation pump

(inset, Fig. 4.9A). When the external voltage was reduced to 2 V, the energy consumption was decreased to 0.72 ± 0.13 kWh m^{-3}. Further reduction of the applied voltage to 1.5 and 1 V rendered a comparable energy consumption (0.69-0.72 kWh m^{-3}) to that with 0 V (0.69 ± 0.13 kWh m^{-3}), resulted from the dominant consumption by the recirculation pump (> 96%) with 0-2 V (Fig. 4.9A inset). Thus, the effect of the recirculation rate was further investigated with an applied voltage of 1.5 V (Fig. 4.9B). Reducing the recirculation rate from 60 mL min^{-1} to 30 mL min^{-1} and finally 10 mL min^{-1} rendered similar FO performance (both water flux and final feed conductivity, Fig. 4.10), owning to negligible external concentration polarization (ECP) (Xie et al. 2015), but significantly reduced the energy consumption of the e-FO system. The highest recirculation rate of 60 mL min^{-1} resulted in overall energy consumption of 0.69 ± 0.13 kWh m^{-3}, which was reduced to 0.18 ± 0.03 kWh m^{-3} at 30 mL min^{-1}. Further reduction of the recirculation rate to 10 mL min^{-1} exhibited the lowest energy consumption of 0.022 ± 0.004 kWh m^{-3} (13% by the power supply and 86% by the recirculation pump, Fig. 4.9B inset), which was about 3.2 % of the energy consumption with 60 mL min^{-1}. The energy consumption of the e-FO system (with a recirculation rate of 10 mL min^{-1}) for water extraction was significantly lower than other (lab-scale) emerging water recovery approaches such as microbial desalination cell (MDC, as low as 1.3 kWh m^{-3}) (Ping et al. 2015), bench-scale ED (7.0 kWh m^{-3}) (Walker et al. 2014), air gap membrane distillation (AGMD, 2.5-3.0 kWh m^{-3}) (Alkhudhiri et al. 2013), and the FO system with thermolytic ammonium bicarbonate (0.1 kWh m^{-3}) (Qin and He 2014).

To better understand energy consumption interacted with reverse solute flux, the energy consumption of the power supply (E_s, kWh kg^{-1}) and the whole system ($E_{s,total}$, kWh kg^{-1}, including both power supply and the recirculation pump) was normalized by the mass of the reduced reverse-fluxed solutes. As shown in Fig. 4.9C, the lowest E_s was 0.015 ± 0.002 kWh kg^{-1} with 1.5 V, while the highest was 2.280 ± 0.140 kWh kg^{-1} with 3 V. The $E_{s,total}$ of different recirculation rates with 1.5 V was presented in the inset of Fig. 6C. As expected, a significant reduction of $E_{s,total}$ from 1.103 ± 0.059 kWh kg^{-1} to 0.044 ± 0.002 kWh kg^{-1} was obtained with decreasing the recirculation rate from 60 mL min^{-1} to 10 mL min^{-1}. Although the estimate of energy consumption in a bench-scale system cannot fully reflect that of a full-scale system for practical application (Xiang et al. 2017), it does provide implications that, to achieve mitigated RSF, electrolysis did not require significant energy input, and optimizing the operation of the e-FO system such as recirculation

could save energy and thus offset the energy input by electrolysis. In addition, the benefits brought by RSF mitigation may compensate the cost increase induced by exerting voltage.

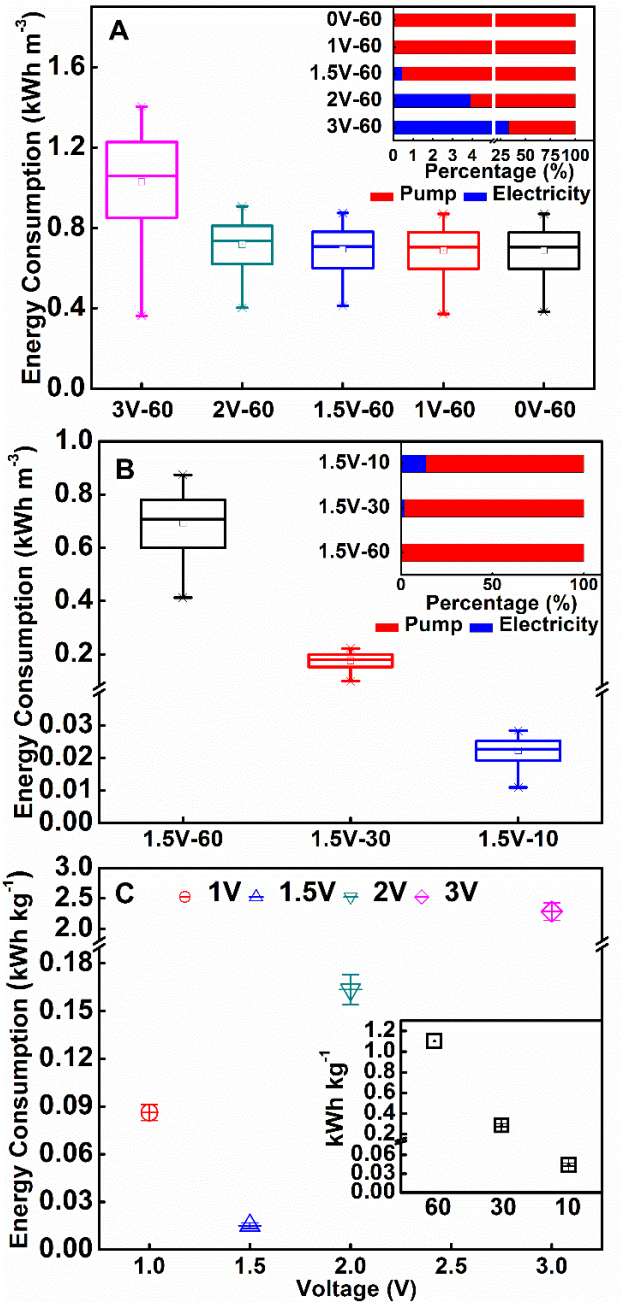

Figure 4.9 Energy consumption by the e-FO system: (A) E_w under different applied voltages and a recirculation rate of 60 mL min^{-1}; (B) E_w under different recirculation rates and an applied voltage of 1.5 V; and (C) E_s under different voltage (main figure) and $E_{s,total}$ under different recirculation (60, 30 and 10 mL min^{-1}) with applied voltage of 1.5V (inset). The "3V-60" stands for an applied voltage of 3 V and a recirculation rate of 60 mL min^{-1}.

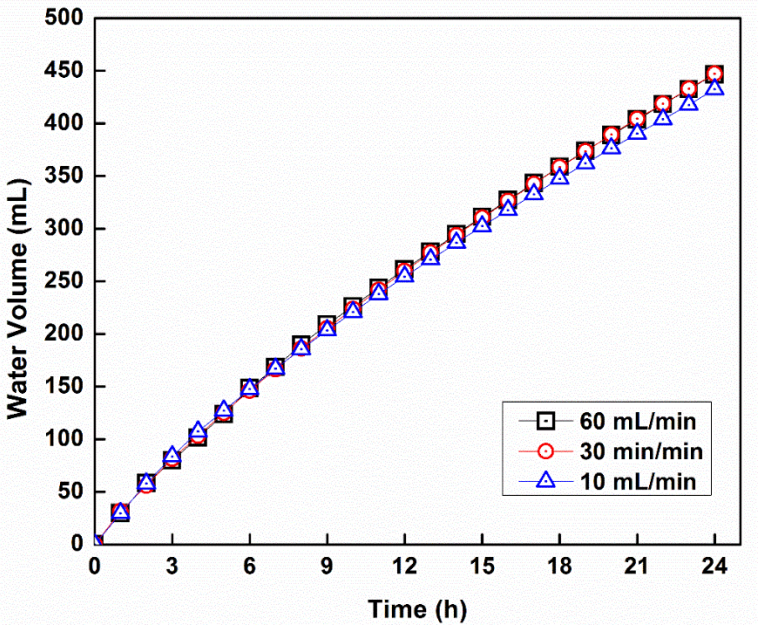

Figure 4.10 Comparison of recovered water by e-FO system under different recirculation rates.

4.7 Conclusions

This study has demonstrated the feasibility of in-situ mitigation of RSF in a three-chamber electrolysis-assisted FO system. The effects of several operation parameters, e.g., applied voltage, membrane orientation, and initial draw solute concentration, were systematically examined and optimized towards maximizing RSF reduction. The results have important implications to further development of the electrolysis-assisted RSF mitigation within the e-FO system with the following conclusions:

- Applying a voltage of 1.5 V achieved an RSF of 6.78 ± 0.55 mmol m^{-2} h^{-1} and a specific RSF of 0.138 ± 0.011 g L^{-1} in the FO mode and with 1 M Na_2SO_4 as the draw, rendering ~57% reduction of solute leakage compared to the control without the applied voltage.
- The reduced RSF should be attributed to constrained ion migration induced by the coactions of electric dragging force ($\geqslant$ 1.5 V) and high solute rejection of the FO membrane.
- Stable solution pH was achieved by continuous mixing of the anolyte and the catholyte towards prolonged lifespan of the FO membrane and electrodes in the e-FO system.

- Both membrane fouling and electrolysis-induced water loss (< 0.001 mL L^{-1} recovered water) were negligible during the experiment. Reversible membrane fouling was well-controlled by in-situ osmotic backwashing with a recovery rate of 98%.
- Reducing the intensity of the solution recirculation from 60 to 10 mL min-1 significantly reduced the specific energy consumption of the e-FO system from 0.693 ± 0.127 to 0.022 ± 0.004 kWh m^{-3} extracted water or from 1.103 ± 0.059 to 0.044 ± 0.002 kWh kg^{-1} reduced reversed solute. Such an energy-efficient e-FO system could serve as a promising technology for sustainable water recovery and reuse.
- This e-FO system with in-situ RSF mitigation warrants further investigation of selected draw solutes and long-term implementation of real wastewater as a feed solution.

References

Achilli, A., Cath, T.Y. and Childress, A.E. (2010) Selection of inorganic-based draw solutions for forward osmosis applications. Journal of Membrane Science 364(1), 233-241.

Achilli, A., Cath, T.Y., Marchand, E.A. and Childress, A.E. (2009) The forward osmosis membrane bioreactor: A low fouling alternative to MBR processes. Desalination 239(1-3), 10-21.

Alkhudhiri, A., Darwish, N. and Hilal, N. (2013) Produced water treatment: Application of Air Gap Membrane Distillation. Desalination 309, 46-51.

Bockris, J.O.M., Dandapani, B., Cocke, D. and Ghoroghchian, J. (1985) On the splitting of water. International Journal of Hydrogen Energy 10(3), 179-201.

Boo, C., Lee, S., Elimelech, M., Meng, Z. and Hong, S. (2012) Colloidal fouling in forward osmosis: Role of reverse salt diffusion. Journal of Membrane Science 390–391, 277-284.

Cath, T.Y., Childress, A.E. and Elimelech, M. (2006) Forward osmosis: principles, applications, and recent developments. Journal of Membrane Science 281(1), 70-87.

Cath, T.Y., Elimelech, M., McCutcheon, J.R., McGinnis, R.L., Achilli, A., Anastasio, D., Brady, A.R., Childress, A.E., Farr, I.V. and Hancock, N.T. (2013) Standard methodology for evaluating membrane performance in osmotically driven membrane processes. Desalination 312, 31-38.

Chung, T.-S., Li, X., Ong, R.C., Ge, Q., Wang, H. and Han, G. (2012a) Emerging forward osmosis (FO) technologies and challenges ahead for clean water and clean energy applications. Current Opinion in Chemical Engineering 1(3), 246-257.

Chung, T.-S., Zhang, S., Wang, K.Y., Su, J. and Ling, M.M. (2012b) Forward osmosis processes: yesterday, today and tomorrow. Desalination 287, 78-81.

Hancock, N.T. and Cath, T.Y. (2009) Solute coupled diffusion in osmotically driven membrane processes. Environmental Science & Technology 43(17), 6769-6775.

Holloway, R.W., Achilli, A. and Cath, T.Y. (2015) The osmotic membrane bioreactor: a critical review. Environmental Science: Water Research & Technology 1(5), 581-605.

Le-Clech, P., Fane, A., Leslie, G. and Childress, A. (2005) MBR focus: the operators' perspective. Filtration & separation 42(5), 20-23.

Li, X., Lu, Y. and He, Z. (2015) Removal of reverse-fluxed ammonium by anammox in a forward osmosis system using ammonium bicarbonate as a draw solute. Journal of Membrane Science 495, 424-430.

Liang, Y.Y., Fimbres Weihs, G.A. and Wiley, D.E. (2016) CFD modelling of electro-osmotic permeate flux enhancement in spacer-filled membrane channels. Journal of Membrane Science 507, 107-118.
Ling, M.M. and Chung, T.-S. (2011a) Desalination process using super hydrophilic nanoparticles via forward osmosis integrated with ultrafiltration regeneration. Desalination 278(1), 194-202.
Ling, M.M. and Chung, T.-S. (2011b) Novel dual-stage FO system for sustainable protein enrichment using nanoparticles as intermediate draw solutes. Journal of Membrane Science 372(1), 201-209.
Ling, M.M., Wang, K.Y. and Chung, T.-S. (2010) Highly water-soluble magnetic nanoparticles as novel draw solutes in forward osmosis for water reuse. Industrial & Engineering Chemistry Research 49(12), 5869-5876.
Liu, Z., Bai, H., Lee, J. and Sun, D.D. (2011) A low-energy forward osmosis process to produce drinking water. Energy & Environmental Science 4(7), 2582-2585.
Lu, Y. and He, Z. (2015) Mitigation of Salinity Buildup and Recovery of Wasted Salts in a Hybrid Osmotic Membrane Bioreactor–Electrodialysis System. Environmental Science & Technology 49(17), 10529-10535.
Luo, W., Hai, F.I., Kang, J., Price, W.E., Nghiem, L.D. and Elimelech, M. (2015) The role of forward osmosis and microfiltration in an integrated osmotic-microfiltration membrane bioreactor system. Chemosphere 136, 125-132.
McCutcheon, J.R., McGinnis, R.L. and Elimelech, M. (2006) Desalination by ammonia–carbon dioxide forward osmosis: influence of draw and feed solution concentrations on process performance. Journal of Membrane Science 278(1), 114-123.
Ng, H.Y., Tang, W. and Wong, W.S. (2006) Performance of forward (direct) osmosis process: membrane structure and transport phenomenon. Environmental Science & Technology 40(7), 2408-2413.
Nguyen, H.T., Nguyen, N.C., Chen, S.-S., Ngo, H.H., Guo, W. and Li, C.-W. (2015) A new class of draw solutions for minimizing reverse salt flux to improve forward osmosis desalination. Science of the Total Environment 538, 129-136.
Nightingale Jr, E. (1959) Phenomenological theory of ion solvation. Effective radii of hydrated ions. The Journal of Physical Chemistry 63(9), 1381-1387.
Phillip, W.A., Yong, J.S. and Elimelech, M. (2010) Reverse draw solute permeation in forward osmosis: modeling and experiments. Environmental Science & Technology 44(13), 5170-5176.
Phuntsho, S., Shon, H.K., Hong, S., Lee, S. and Vigneswaran, S. (2011) A novel low energy fertilizer driven forward osmosis desalination for direct fertigation: Evaluating the performance of fertilizer draw solutions. Journal of Membrane Science 375(1–2), 172-181.
Ping, Q., Huang, Z., Dosoretz, C. and He, Z. (2015) Integrated experimental investigation and mathematical modeling of brackish water desalination and wastewater treatment in microbial desalination cells. Water Research 77, 13-23.
Qin, M. and He, Z. (2014) Self-Supplied Ammonium Bicarbonate Draw Solute for Achieving Wastewater Treatment and Recovery in a Microbial Electrolysis Cell-Forward Osmosis-Coupled System. Environmental Science & Technology Letters 1(10), 437-441.
Qiu, C., Qi, S. and Tang, C.Y. (2011) Synthesis of high flux forward osmosis membranes by chemically crosslinked layer-by-layer polyelectrolytes. Journal of Membrane Science 381(1), 74-80.
Shaffer, D.L., Yip, N.Y., Gilron, J. and Elimelech, M. (2012) Seawater desalination for agriculture by integrated forward and reverse osmosis: Improved product water quality for potentially less energy. Journal of Membrane Science 415–416, 1-8.
Su, J., Zhang, S., Ling, M.M. and Chung, T.-S. (2012) Forward osmosis: an emerging technology for sustainable supply of clean water. Clean Technologies and Environmental Policy, 1-5.
Tuna, E., Kargi, F. and Argun, H. (2009) Hydrogen gas production by electrohydrolysis of volatile fatty acid (VFA) containing dark fermentation effluent. International Journal of Hydrogen Energy 34(1), 262-269.

Walker, W.S., Kim, Y. and Lawler, D.F. (2014) Treatment of model inland brackish groundwater reverse osmosis concentrate with electrodialysis — Part II: Sensitivity to voltage application and membranes. Desalination 345, 128-135.
Wang, H., Chung, T.S., Tong, Y.W., Jeyaseelan, K., Armugam, A., Chen, Z., Hong, M. and Meier, W. (2012) Highly Permeable and Selective Pore-Spanning Biomimetic Membrane Embedded with Aquaporin Z. Small 8(8), 1185-1190.
Wang, J., Dlamini, D.S., Mishra, A.K., Pendergast, M.T.M., Wong, M.C., Mamba, B.B., Freger, V., Verliefde, A.R. and Hoek, E.M. (2014a) A critical review of transport through osmotic membranes. Journal of Membrane Science 454, 516-537.
Wang, M., Wang, Z., Gong, X. and Guo, Z. (2014b) The intensification technologies to water electrolysis for hydrogen production–A review. Renewable and Sustainable Energy Reviews 29, 573-588.
Xiang, X., Zou, S. and He, Z. (2017) Energy consumption of water recovery from wastewater in a submerged forward osmosis system using commercial liquid fertilizer as a draw solute. Separation and Purification Technology 174, 432-438.
Xie, M., Zheng, M., Cooper, P., Price, W.E., Nghiem, L.D. and Elimelech, M. (2015) Osmotic dilution for sustainable greenwall irrigation by liquid fertilizer: Performance and implications. Journal of Membrane Science 494, 32-38.
Yuan, H., Abu-Reesh, I.M. and He, Z. (2016) Mathematical modeling assisted investigation of forward osmosis as pretreatment for microbial desalination cells to achieve continuous water desalination and wastewater treatment. Journal of Membrane Science 502, 116-123.
Zou, S. and He, Z. (2016) Enhancing wastewater reuse by forward osmosis with self-diluted commercial fertilizers as draw solutes. Water Research 99, 235-243.
Zou, S., Yuan, H., Childress, A. and He, Z. (2016) Energy Consumption by Recirculation: A Missing Parameter When Evaluating Forward Osmosis. Environmental Science & Technology 50(13), 6827-6829.

Table 4.1 Osmotic characteristics and specific cost of inorganic draw solutes under same osmotic pressure of 2.8 MPa (sorted by specific cost). Adapted from Achilli, et al.

	Osmotic pressure (MPa)	**Concentration (g L^{-1})**	**Specific cost ($ L^{-1})[a]**	**J_s/J_w (g L^{-1})[b]**
NaCl	2.8	35.2	0.53	0.74
NH_4Cl		32.6	0.85	0.73
$MgCl_2$		34.2	0.96	0.57
$NaHCO_3$		63.9	1.28	0.19
Na_2SO_4		84.7	1.28	0.36
$CaCl_2$		43.8	1.53	0.83
KCl		47.0	1.74	1.13
$KHCO_3$		65.5	2.1	0.17
NH_4HCO_3		52.8	2.38	2.48
$(NH_4)_2SO_4$		74.3	4.46	0.40
K_2SO_4		101.4	5.38	0.40
KBr		71.3	5.7	2.15
$Ca(NO_3)_2$		87.2	6.1	0.67
$MgSO_4$		141.3	7.35	0.21

a Specific cost means the cost of solutes to make 1L draw solution with 2.8 MPa of osmotic pressure.

b The unit of water flux (J_w) and reverse solute flux (J_s) are L $m^{-2}h^{-1}$ and g $m^{-2}h^{-1}$, respectively.

Table 4.2 Detailed experimental procedures for three-chamber e-FO system

Batch Test	Draw	Feed	Operation Mode	Voltage	Recirculation Rate	Fouling Control
Feasibility test						
Three-chamber e-FO	1M	DI water	FO mode	0 and 3V	60 mL min^{-1}	*In-situ* osmotic backwashing
System Optimization						
Applied voltage	1M	DI water	FO mode	0, 1, 1.5, 2, and 3V	60 mL min^{-1}	*In-situ* osmotic backwashing
Membrane orientation	1M	DI water	FO and PRO mode	1.5V	60 mL min^{-1}	*In-situ* osmotic backwashing
Draw concentration	0.5, 1, 1.5M	DI water	FO mode	1.5V	60 mL min^{-1}	*In-situ* osmotic backwashing
Fouling situation	1M	DI water	FO mode	3.0V	60 mL min^{-1}	No fouling control in first three batch tests, then *in-situ* osmotic backwashing
Energy consumption						
Different voltage	1M	DI water	FO mode	0, 1, 1.5, 2, and 3V	60 mL min^{-1}	*In-situ* osmotic backwashing
Different recirculation	1M	DI water	FO mode	1.5V	10, 30, 60 mL min^{-1}	*In-situ* osmotic backwashing

Table 4.3 Comparison of specific RSF (J_s/J_a) between three-chamber e-FO with different voltage and that of literature (~1M Na_2SO_4 as draw)

	Three-chamber e-FO system					Conventional FO (Achilli, et al.)
	0V	1V	1.5V	2V	3V	
J_s/J_a ($g\ L^{-1}$)	0.320±0.005	0.320±0.001	0.138±0.011	0.175±0.011	0.194±0.010	0.330

Table 4.4 Fe^{3+} concentration in the final draw solution

Applied Voltage (V)	**Fe^{3+} Concentration ($mg\ L^{-1}$)**
0	0.00
1	0.00
1.5	0.010 ± 0.008
2	0.10 ± 0.02
3	1.50 ± 0.08

5 Mitigation of Bidirectional Solute Flux in Forward Osmosis via Membrane Surface Coating of Zwitterion Functionalized Carbon Nanotubes

(This chapter has been published as "Zou, S., Smith, E., Martin, S., Lin, S., and Zhen, H. (2019) Mitigation of bidirectional solute flux in forward osmosis via membrane surface coating of zwitterion functionlized carbon Nanotubes. *under review*")

5.1 Abstract

Forward osmosis (FO) has emerged as a promising membrane technology to yield high-quality reusable water from various water sources. A key challenge remained to be solved is the bidirectional solute flux (BSF), including reverse solute flux (RSF) and forward solute flux (FSF). Herein, zwitterion functionalized carbon nanotubes (Z-CNTs) have been coated onto a commercial thin film composite (TFC) membrane resulting in BSF mitigation via both electrostatic repulsion force induced by zwitterionic functional groups and steric interaction with CNTs. At a coating density of 0.97 g m^{-2}, a significantly reduced specific RSF was observed for multiple draw solutes, including NaCl (0.281 g L^{-1}, 55.5% reduction), $NH_4H_2PO_4$ (0.110 g L^{-1}, 83.8%), $(NH_4)_2HPO_4$ (0.060 g L^{-1}, 74.5%), NH_4Cl (0.394 g L^{-1}, 70.8%), and NH_4HCO_3 (0.279 g L^{-1}, 61.9%). Meanwhile, FSF was notably reduced with fewer pollutants leaked to the draw solution, including NH_4^+-N (46.3% reduction), NO_2^--N (37.0%), NO_3^--N (30.3%), K^+ (56.1%), PO_4^{3-}-P (100%), and Mg^{2+} (100%). When fed with real wastewater, a consistent water flux was achieved during semi-continuous operation with enhanced fouling resistance. This study is among the earliest efforts to address BSF control via membrane modification, and the results will encourage further exploration of effective strategies for membrane coating to reduce BSF.

5.2 Graphical Abstract

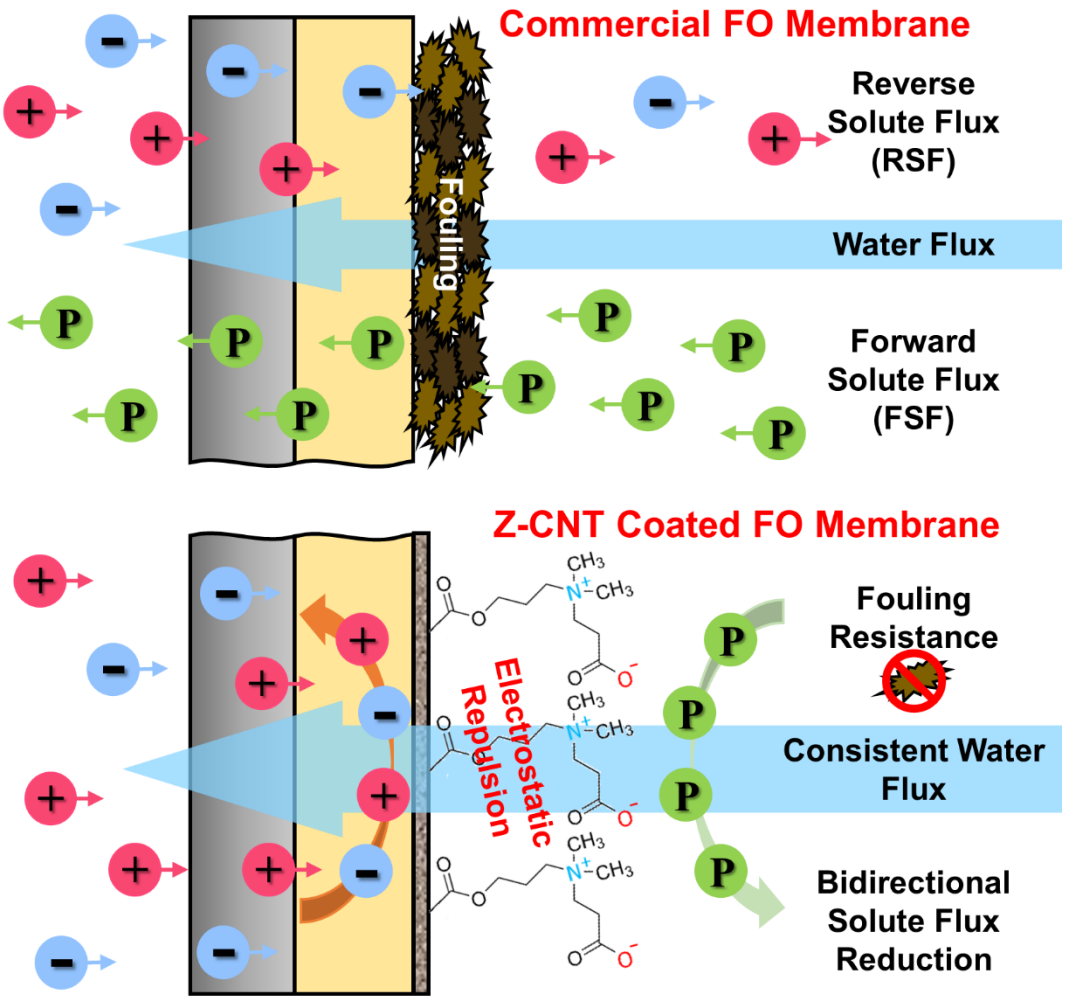

5.3 Keywords

Forward osmosis; Reverse solute flux; Forward solute flux; Zwitterion; Membrane modification

5.4 Introduction

Alternative water resources, e.g., via water reuse and desalination, are of significant interest for addressing mounting global water demand. Membrane-based treatment processes have been extensively developed to produce reusable water due to their reliable performance and compact footprint (Shannon et al. 2008). As an emerging membrane technology, forward osmosis (FO) is able to supply high-quality water by utilizing a natural osmotic pressure gradient, and can offer unique merits such as reduced pressure operation, low fouling propensity, excellent solute rejection, and relatively low energy consumption if proper regeneration/separation of draw solutes (DS) could be achieved (Zou et al. 2016). Advancement of FO-based technologies will need to address several technical bottlenecks, especially further enhancement of fouling resistance and reverse solute flux (RSF). RSF is defined as the cross-membrane DS diffusion to the feed (She et al. 2012), and has thus far received less attention than enhancing fouling resistance in the FO field. RSF has been studied via mathematical modeling (Lu et al. 2014), and can be affected by factors such as intrinsic membrane parameters (e.g., thickness, tortuosity, and porosity) (McCutcheon and Elimelech 2006) and solute characteristics (e.g., hydrated ion radius, aqueous diffusivity, solution viscosity, and ion charge) (Zhao and Zou 2011). Gradual DS leakage via RSF can lead to reduced osmotic driven force, salinity buildup on the feed side, potential feed contamination, aggravated membrane fouling, and elevated operating costs due to the need to continuously replenish DS (Lu and He 2015).

Increasing awareness of RSF's detrimental effects has led to the development of indirect and direct control strategies. Indirect RSF control focuses on addressing the consequence of RSF, i.e., salinity buildup on the feed side, and major approaches include solute removal by using microorganisms to eliminate/assimilate biodegradable DS (e.g., NH_4HCO_3) (Li et al. 2016) and integration of parallel desalination/separation process (e.g., microfiltration or electrodialysis) (Qiu et al. 2015, Zou and He 2017a). Nonetheless, alleviation of salinity accumulation in the feed solution does not mitigate RSF itself. The leaching of DS via RSF still leads to an economic loss in operation. Therefore, direct RSF control needs to be prioritized via smart DS selection, operational strategies, and advanced membrane development (Zou et al. 2019). Novel DS, such as stimuli-responsive polymers, can theoretically produce low RSF, due to their large hydrodynamic diameter (>100 nm), while achieving energy-efficient phase separation (Hartanto et al. 2015).

Operational strategies have also been investigated, including pressure- (Blandin et al. 2013), electrolysis- (Zou and He 2017b), and ultrasonic-assisted osmosis (Kowalski et al. 2015). However, additional energy is required to manipulate ion transport across the FO membrane, and inconsistent RSF reduction was reported due to potential membrane damage under some operating conditions (Lutchmiah et al. 2015).

Advanced membrane development aims at creating a better DS barrier via membrane fabrication or surface modification (Akther et al. 2015). New membrane fabrication techniques have yielded promising results in RSF reduction, including optimized substrate composition (Wang et al. 2015b), advanced substrate fabrication (Yasukawa et al. 2015), selection of novel supporting materials (Huang et al. 2013), and modified active layer composition (Kwon et al. 2015). Compared to membrane fabrication, surface modification via alterations of surface functional groups and hydrophilicity is a much simpler and easier method to enhance membrane performance through (Guo et al. 2018). Zwitterionic monomers have emerged as an attractive surface modifier to increase water flux and prevent adsorption of foulants in NF (Mi et al. 2017) and RO systems (Wang et al. 2015a), owing to their remarkable hydration capacity and electroneutrality (Zhou et al. 2014). Zwitterionic modification of FO membranes can lead to notable enhancement of fouling resistance (Wang et al. 2018), e.g., up to 30% less fouling with zwitterionic poly amino acid 3-(3,4-Dihydroxyphenyl)-$_{L}$-alanine ($_{L}$-DOPA) coated FO membrane compared to the uncoated membrane (Nguyen et al. 2013). However, to the best of our knowledge, no prior studies have used zwitterionic materials for simultaneous RSF and forward solute flux (FSF) reduction (i.e., bidirectional flux reduction, BSF) in FO systems.

Herein, zwitterion functionalized carbon nanotubes (Z-CNT) have been selected and coated onto a commercial Aquaporin Inside® FO membrane for performance enhancement, potentially facilitated water transport by CNTs (Holt et al. 2006), and BSF reduction. The specific objectives of this study are to (1) investigate the feasibility and consistency of RSF reduction by a Z-CNT coated FO membrane; (2) evaluate the effects of key operation parameters on RSF reduction, including Z-CNT coating density, DS concentration, and various DS species; (3) analyze membrane rejection (i.e., FSF) of the Z-CNT coated membrane; and (4) assess water flux consistency and membrane fouling resistance under semi-continuous operation.

5.5 Materials and Methods

5.5.1 Z-CNT preparation, membrane coating, and characterization

The functionalization process and detailed characterization were conducted according to a previous study (Chan et al. 2016). The final zwitterion functional group attached to CNTs (25.2 wt%, equal to ~2 zwitterion groups per 100 carbon atoms) had a positive charge at the tertiary amine group and a negative charge at the carboxylate group (Fig. 5.1). Before membrane coating, a Z-CNT stock solution (1.0 mg mL^{-1}) was prepared by adding 20 mg Z-CNTs into 20 mL of deionized (DI) water, followed by probe sonication for 5 min (Fisher EB705 Probe Sonicator). After being cooled to room temperature, 10 mL of the Z-CNT solution (unless otherwise stated) was uniformly distributed onto the surface of a commercial TFC FO membrane (Aquaporin A/S, Denmark), which was placed under a Teflon frame and clamped onto a glass plate with either its active layer (i.e., AL-coated) or supportive layer facing up (i.e., SL-coated). Multiple batches of commercial membranes were coated (0.97 g CNT m^{-2}, unless otherwise stated) using the same protocol. The Z-CNT coated membranes were then placed inside a fume hood overnight to allow water to evaporate (Fig. 5.2A), and van der Waals force was expected to be the primary binding force. The coated membrane was stored in DI water before use.

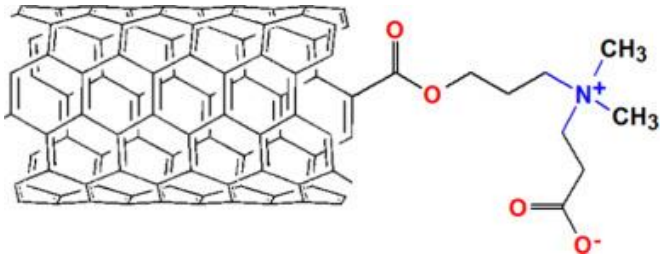

Figure 5.1 Schematic of the chemical structure of zwitterionic functional group attached on the SWNTs (Chan et al. 2016)

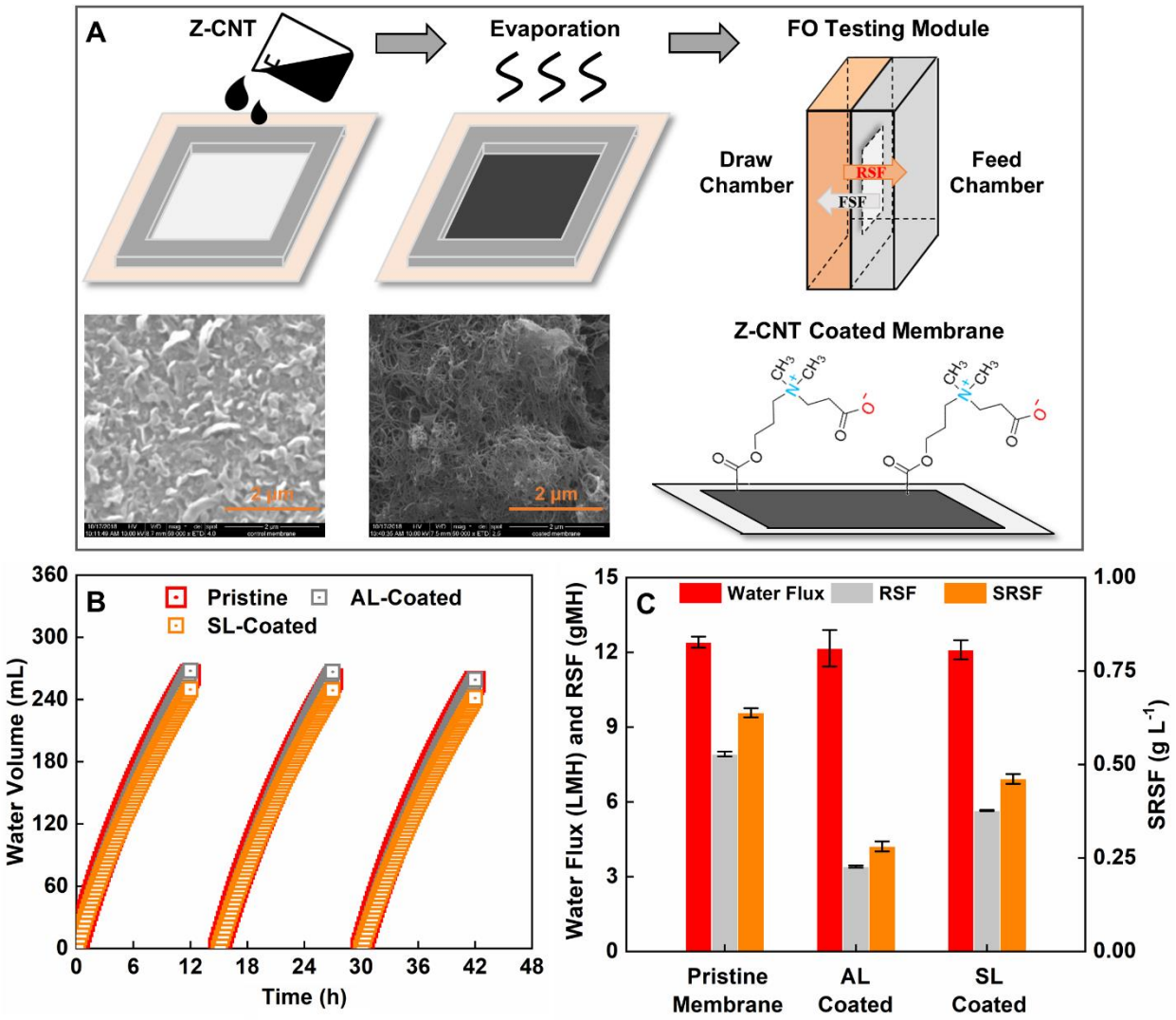

Figure 5.2 (A) Schematic of the membrane coating and testing process, (B) comparison of water recovery volume among the pristine, AL-coated, or SL-coated membranes over three successive batch tests, and (C) quantification of the corresponding water flux, RSF, and SRSF. In Fig. 5.2A, Z-CNT coating is confirmed by SEM image under 50,000 times magnification. In Fig. 5.2B and 5.2C, new pristine or coated membrane (0.97 g m^{-2}) was used for each batch test. In Fig. 1C, error bars represent triplicates with different membrane samples. Testing conditions: 100-mL 1-M NaCl as the draw and 500-mL DI water as the feed.

Both the pristine and coated FO membranes were characterized for zeta potential, membrane hydrophilicity, and surface morphology and composition. Membrane zeta potential was measured over a range of pH from 3.8 to 8.7 using a streaming potential analyzer (SurPASS, Anon

Paar) with an adjustable gap cell and 1-mM KCl as the electrolyte. Hydrochloric acid (HCl) and potassium hydroxide (KOH) were used for pH adjustment. The membrane hydrophilicity was determined by measuring the contact angle (CA) of a sessile drop (DI water, ~25 μL) using an optical goniometer (KSV Instruments CAM 200). For each sample, at least three CA measurements were performed using different spots of the membrane surface. Membrane surface morphology was examined using field emission scanning electron microscopy (FESEM) with a 7-nm Pt/Pd coating (80:20 wt%, Leica ACE600 Sputter), with composition analysis performed using elemental mapping via energy dispersive spectroscopy (EDS).

5.5.2 Setup of FO testing cells

Two identical cross-flow FO testing cells were constructed, with one equipped with a pristine membrane (control system) and the other equipped with a coated membrane (AL-coated or SL-coated experimental system). Each solution chamber (5×5×1 cm) connected to an external 600-mL reservoir. One piece of FO membrane (25 cm^2 effective area) was installed inside each testing module with its active layer facing the feed solution (i.e., AL-Feed, FO mode) to minimize potential membrane fouling. Upon membrane installation, the FO testing modules were rinsed with DI water at a flow rate of 120 mL min^{-1} for 3 hours to remove unattached Z-CNT or other residue chemicals from the membrane surface. Under a default setting, 100-mL of 1-M NaCl (conductivity 86.8-87.1 mS cm^{-1}) and 500-mL of DI water were recirculated at a flow rate of 60 mL min^{-1} as the draw and feed solutions, respectively. The FO testing systems were operated under either a batch or a semi-continuous mode. During the batch operation (triplicate runs), both FO testing modules were operated for 12 h with water sampled at the beginning and the end of the experiment. Sufficient physical crossflow flushing (3 h with DI water, 60 mL min^{-1}) was performed between batch tests for membrane cleaning. During the semi-continuous operation, samples were taken daily with no membrane cleaning performed. All experiments were conducted in a temperature-controlled lab (20 ± 2 °C).

5.5.3 Experimental procedure

The Feasibility of RSF Reduction via Z-CNT surface coating was first investigated in three successive batch tests (under default settings) by comparing the performance between the pristine and coated membranes (AL-coated or SL-coated, 0.97 g m^{-2}). *The Effects of Operating Parameters* on FO performance (i.e., water flux and RSF) were then evaluated by using the AL-coated

membranes with different Z-CNT coating densities (0, 0.10, 0.48, 0.97, or 1.45 g m^{-2}, Fig. 5.3), DS concentrations (0.25, 0.50, 0.75, or 1.00 mol L^{-1} NaCl), and DS compositions (0.25 mol L^{-1} NaCl, $(NH_4)_2HPO_4$, $NH_4H_2PO_4$, NH_4Cl, or NH_4HCO_3). Various coating densities were achieved by uniformly distributing 1, 5, 10, and 20 mL of the Z-CNT solution onto the FO membrane surface. *Coating-Enhanced FSF Reduction* was subsequently analyzed using two different synthetic contaminated solutions as the feed (500 mL). The ions of significant interest include NH_4^+-N (111.5 ± 3.5 mg L^{-1}), NO_3^--N (110.1 ± 0.2 mg L^{-1}), NO_2^--N (119.6 ± 1.5 mg L^{-1}), K^+ (107.1 ± 1.4 mg L^{-1}), Mg^{2+} (100.1 ± 0.9 mg L^{-1}), and Ca^{2+} (99.8 ± 0.3 mg L^{-1}) in synthetic solution 1, or SO_4^{2-}-S (130.4 ± 2.2 mg L^{-1}) and PO_4^{3-}-P (131.8 ± 3.9 mg L^{-1}) in synthetic solution 2. This experimental design was to prevent potential precipitation within synthetic solutions. Finally, *Water Flux Consistency* was explored with a focus on membrane fouling resistance via a 12-day semi-continuous operation, in which 100-mL 1-M NaCl (i.e., the draw) was replaced on a daily basis, whereas the secondary effluent (500 mL constant) from a local wastewater treatment plant (Christiansburg, VA) was supplied as the feed to achieve enhanced water reuse (Zou and He 2016).

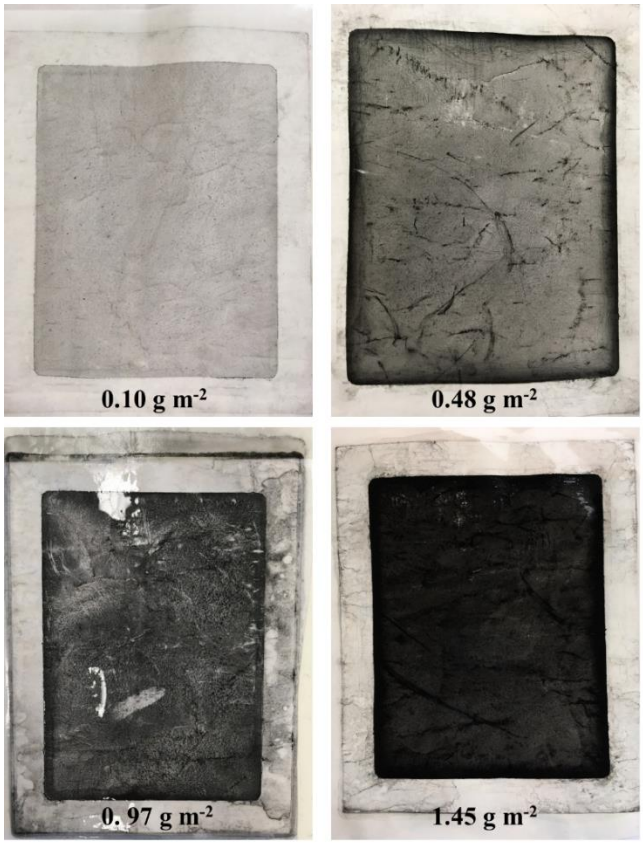

Figure 5.3 Membranes of various Z-CNT coating densities used in this study.

5.5.4 Measurement and analysis

Detailed water quality analysis is provided in Supplementary Data. Quantification of water flux and RSF (J_s, gMH) was based on previous studies (Zou and He 2017a, b). Both forward solute flux (FSF, J_f) and membrane rejection rate were parameters to indicate the magnitude of feed solutes (FS, usually pollutants) diffusion to the draw solution. FSF was via the following equation.

$$J_f = \frac{(n_{f,D} - n_{i,D}) \times Mw}{S \times t} = \frac{V_{f,D} \times C_{f,D}}{S \times t} \quad \text{(Eq. 5.1)}$$

where $C_{f,D}$ and $V_{f,D}$ are the final FS mass concentration in the draw and final draw volume, respectively. Considering no FS was presented in the initial draw solution, $n_{i,D}$ equals to 0. t stands for operating time. S is the effective surface area of the FO membrane. Mw stands for molecular weight. The membrane rejection rate of FS was calculated via Eq. 5.2.

$$\text{Membrane Rejection (\%)} = (1 - \frac{n_{f,D}}{n_{total}}) \times 100\% \quad \text{(Eq. 5.2)}$$

where $n_{f,D}$ is the FS amount in the final draw solution, and n_{total} is the total FS amount in the FO system (both the draw and the feed).

Specific RSF ($SRSF$, g L^{-1}) was calculated to rule out the influence of both membrane structural parameters and bulk draw solution concentration (Phillip et al. 2010). $SRSF$ quantifies the leakage of a DS or an ion that can leak across the FO membrane to the feed side per unit of recovered water.

$$SRSF = \frac{J_s}{J_w} \quad \text{(Eq. 5.3)}$$

RSF mitigation ratio (MR, %) was quantified by the ratio between the mitigated $SRSF$ with the coated membrane ($SRSF_m$) and that with the pristine membrane ($SRSF_o$).

$$MR = (1 - \frac{SRSF_m}{SRSF_o}) \times 100\% = (1 - \frac{J_{s,m} / J_{w,m}}{J_{s,o} / J_{w,o}}) \times 100\% \quad \text{(Eq. 5.4)}$$

where $J_{s,o}$ and $J_{w,o}$ are the original RSF and water flux of the pristine membrane, respectively; $J_{s,m}$ and $J_{w,m}$ are the mitigated RSF and water flux of the coated FO membrane, respectively.

5.6 Results and Discussion

5.6.1 RSF reduction via Z-CNT surface coating

The RSF reduction and water recovery capability of the Z-CNT coated membrane were investigated by comparing its performance to a pristine membrane. The FO system with the AL-coated membrane (0.97 g m^{-2}) could recover 264.5 ± 3.8 mL of water within 12 h, comparable to that of the pristine membrane (261.3 ± 2.2 mL, p>0.18) but higher than that of the SL-coated membrane (246.6 ± 3.7 mL, p<0.05, Fig. 5.1B). This result indicated that coating Z-CNTs on the dense and smooth active layer side had a negligible effect on water transport, whereas coating on the porous supportive layer resulted in a higher possibility of inner clogging, pore blockage, reduced structure parameter, and a more severe internal concentration polarization, leading to reduced water extraction. It should be noted that the SL-coated membrane did exhibit a comparable maximum water flux (11.96 ± 0.94 LMH, Fig. 5.1C) to that of the pristine or AL-coated membranes (~12 LMH, p>0.46), as the initial osmotic pressure gradient predominantly determined this parameter. In terms of RSF reduction, a notable decrease of both RSF and *SRSF* was observed with the coated membranes, compared to the pristine membrane (Fig. 5.1C), yielding an *MR* of 56.3% (AL-coated) and 28.1% (SL-coated), respectively.

The reduced RSF can be attributed primarily to the electrostatic repulsion force induced by the charged functional groups from the Z-CNTs on the membrane surface. For the pristine membrane, the diffusion of DS across the active layer (J_s^A) under the AL-Feed orientation (i.e., FO mode) can be described using Eq. 5.5 (Fig. 5.4A) (Phillip et al. 2010).

$$J_s^A = -D^A \frac{dC}{dt} = -\frac{D^A}{t_A}(C_a^i - C_f) = -\frac{D^A}{t_A}(C_a^i - 0) \tag{5.5}$$

where D^A is the diffusion coefficient of DS in the active layer, t_A is the thickness of the active layer, C_a^i is the concentration of DS on the active layer side of the supportive layer-active layer interface, and C_f is the concentration of draw solute in the feed (assuming $C_f^i \approx C_f$ in an FO system with negligible external concentration polarization) (Cath et al. 2006). Initially, C_f is equal to zero (DI water as the feed). Once the membrane surface is coated with Z-CNT, the negatively and positively charged functional groups provide an electrostatic repulsion against anions and cations attempting to diffuse across the coating layer, resulting in a decrease in RSF ($J_{s,1}^A < J_s^A$ and $J_{s,2}^A < J_s^A$, where

subscripts 1 and 2 represent the AL- and SL-coated orientations, respectively). To accurately measure the the extent of net electrostatic repulsion, the Debye length (κ^{-1}, nm) is introduced (Eq. 5.6, for a symmetric monovalent electrolyte) (Russel et al. 1991). With each Debye length, charges are increasingly electrically screened, providing reduced electrostatic repulsion force.

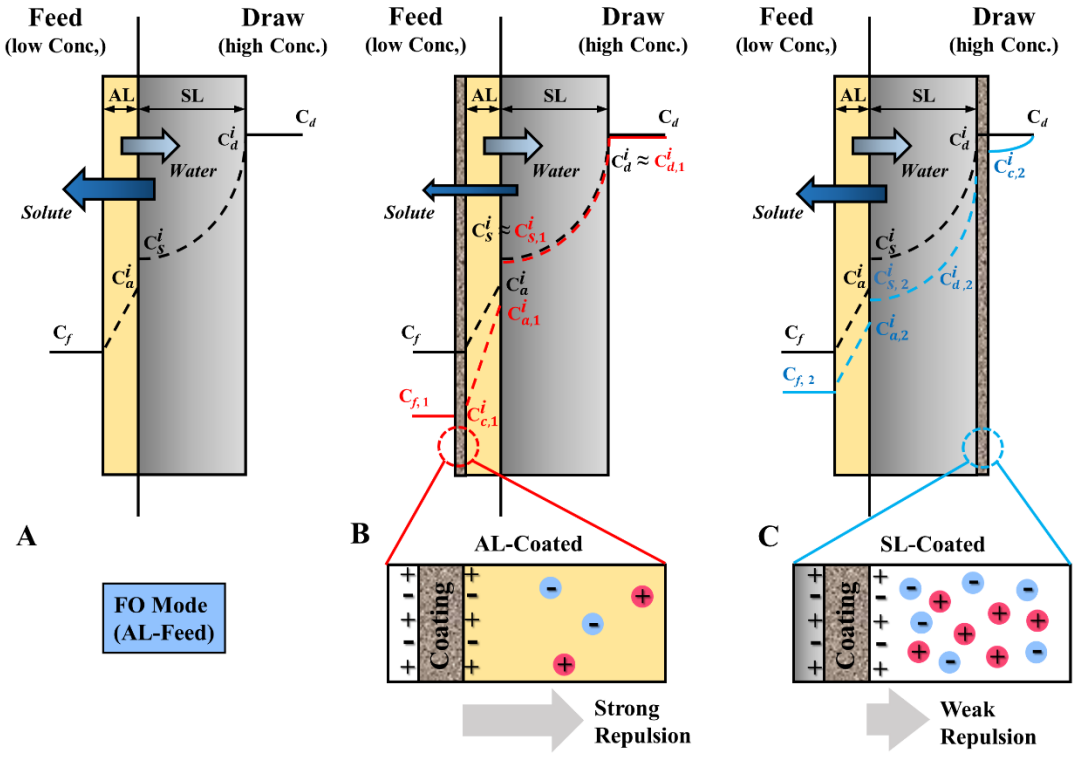

Figure 5.4 The proposed DS ion diffusion pattern within (A) the pristine FO membrane; (B) the AL-coated membrane; and (C) the SL-coated membrane. The black line in each figure represents the original DS ion diffusion pattern, while the red and blue lines represent the DS ion diffusion affected by electrostatic repulsion induced by Z-CNT coating materials. Subscript 1 and 2 indicate DS diffusion pattern in AL-coated and SL-coated membranes, respectively.

$$\kappa^{-1} = \sqrt{\frac{\varepsilon_r \varepsilon_0 RT}{2\times 10^3 F^2 C_0}} \tag{5.6}$$

where ε_0 is the permittivity of free space, ε_r is the dielectric constant, R is the gas constant, T is the temperature, F is the Faraday constant, and C_0 is the electrolyte concentration in molar units. Eq.

5.6 can be simplified as the following equation in the water solution at room temperature (~25 ℃) (Israelachvili 2011).

$$\kappa^{-1}(\text{nm}) = \frac{0.304}{\sqrt{I(\text{M})}} \tag{5.7}$$

where I is the ionic strength (molar unit) in the surrounding environment. This simplified Eq. 5.7 can further explain the *SRSF* reduction difference between the two coating orientations (i.e., $J_{s,1}^{A} < J_{s,2}^{A}$). Once coated on the active layer, Z-CNTs are exposed to a less concentrated environment with a relatively low ionic strength, due to the dilution effect of the clean water flux as well as rejection by the active layer ($C_{c,1}^{i} << C_d$, $C_{c,1}^{i}$ represents DS concentration at the interface of the coating layer for an AL-coated membrane). Thus, a relatively large Debye length and an extensive electrostatic repulsion lead to enhanced RSF reduction (Fig. 5.4B). Coating on the supportive layer, nonetheless, allows Z-CNTs to be directly exposed to the highly concentrated draw solution ($C_{c,2}^{i} \approx C_d$, $C_{c,2}^{i}$ represents the DS concentration at the interface of the coating layer in an SL-coated membrane), resulting in a smaller Debye length, a weakened electrostatic repulsion force due to the strong screening effect, and a smaller reduction in RSF (Fig. 5.4C). Considering the overall system performance, the AL-coated membrane was chosen for subsequent experiments.

5.6.2 Effect of Z-CNT coating density

Surface coating density (0, 0.10, 0.48, 0.97, and 1.45 g m^{-2}), as a key operating parameter, was investigated to assess its effects on zeta potential, membrane hydrophilicity, water flux, and RSF. In terms of zeta potential, the pristine FO membrane exhibited a negative charge due to abundant carboxylic groups (-COOH) on the TFC membrane (Fig. 5.5A) (Tiraferri and Elimelech 2012). A more negatively charged surface (from -39.1 to -67.4 mV) was observed with higher pH due to stronger deprotonation of the carboxylic groups (Jin et al. 2012). Surface charge neutralization was observed with Z-CNT coating, consistent with the results of a prior zwitterionic coating study (Wang et al. 2018). With an increase of coating density, the zeta potential became less negative. For example, at a pH of 5.7, the surface charge increased from -60.9 mV (pristine membrane) to -46.2 mV (1.45 g m^{-2}). Such a positive shift towards neutral surface charge could hinder Donnan-facilitated cation transport (Sarkar et al. 2010) while minimizing the diffusion of counter anions to maintain solution electroneutrality (Epsztein et al. 2018). For membrane hydrophilicity, the dominance of the hydrophobic CNT backbone (74.8 wt%) over the hydrophilic zwitterionic

functional groups (25.2 wt%) resulted in higher contact angles compared to that of the pristine membrane, even at a low coating density of 0.10 g m^{-2} (Fig. 5.5B) (Tijing et al. 2016, Wang et al. 2018). Increasing the coating density did not significantly affect membrane hydrophilicity, and the largest contact angle was observed under 1.45 g m^{-2} (an average of 28.5 ± 4.1°).

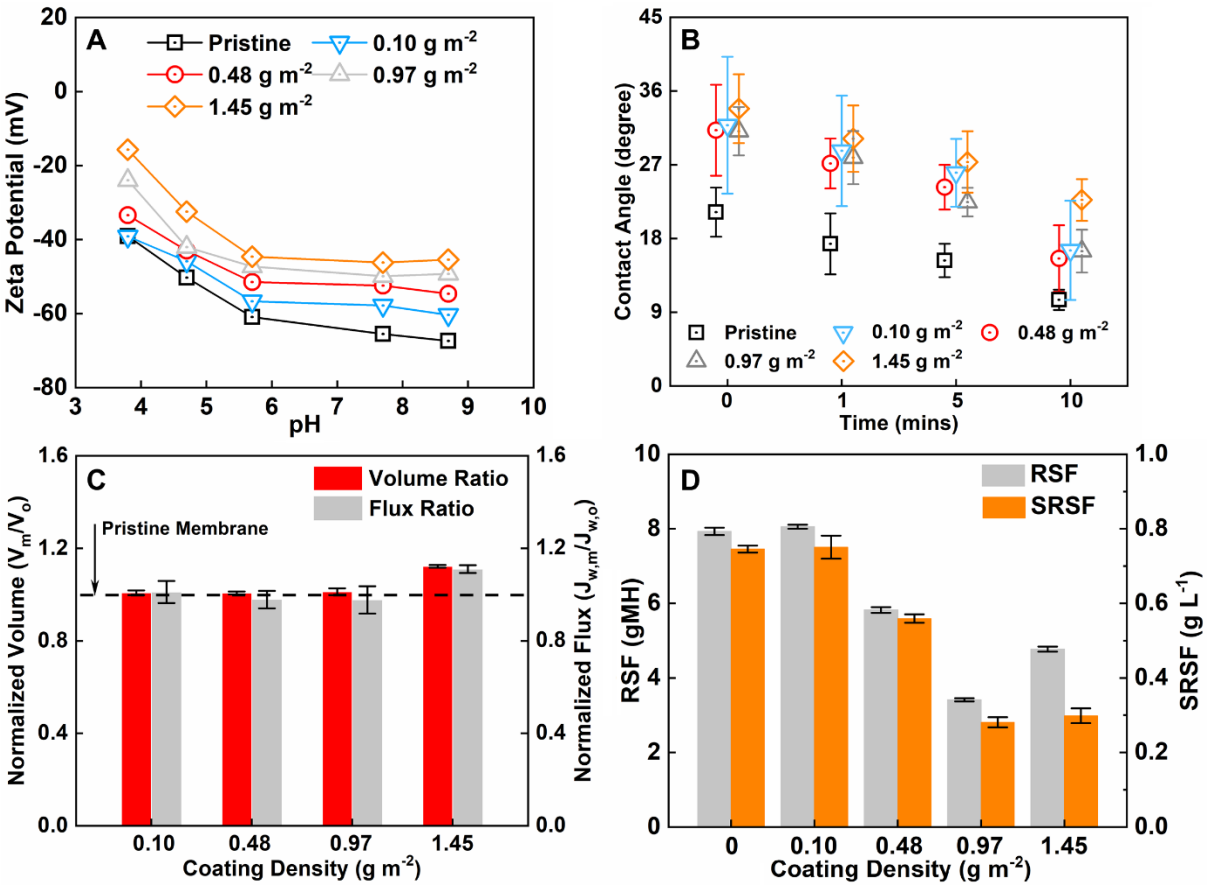

Figure 5.5 Comparison of FO performance and membrane characterization among various coating densities regarding (A) membrane zeta potential; (B) membrane contact angle; (C) normalized water recover volume and maximum water flux to that of the pristine membrane; and (D) RSF and SRSF values. Membrane coating densities include 0 (pristine membrane), 0.48, 0.97, and 1.45 g m^{-2}. In Fig. 5.5C and 5.5D, triplicate tests were performed for coated membrane at each coating density. Testing conditions: 100-mL 1-M NaCl as the draw and 500-mL DI water as the feed.

The effect of coating density on water recovery was subsequently investigated by using DI water as the feed (Fig. 5.5C). At lower coating densities (0.10-0.97 g m^{-2}), the volumes of recovered water (~247 mL) and water fluxes (10-13 LMH) were comparable to those of the pristine

membrane. This could result from a dynamic balance between a negligible mass transport resistance added owing to the Z-CNT coating and enhanced water permeation via zwitterionic groups. A further density increase to 1.45 g m^{-2} yielded in an increased recovered water volume (293.2 ± 1.5 mL, p<0.01) and water flux (13.8 ± 0.2 LMH, p<0.01), suggesting that a higher density of surface zwitterionic groups could facilitate water transport. The performance of RSF reduction was closely linked to coating densities (Fig. 5.5D) and effective surface electrostatic repulsion force. A lower coating density provided limited surface electrostatic repulsion, rendering a comparable RSF. With a higher coating density, a gradual decrease in both RSF and *SRSF* was observed. The lowest RSF and *SRSF* were 3.41 ± 0.04 gMH and 0.281 ± 0.013 g L^{-1}, respectively, with a coating density of 0.97 g m^{-2}, resulting in an *MR* of 55.5% compared to that of the pristine membrane ($SRSF_o$ of 0.631 ± 0.008 g L^{-1}). A further increase of density to 1.45 g m^{-2} led to an increase in RSF (4.77 ± 0.07 gMH) due to a higher water recovery volume (Fig. 5.5C) and potentially diminished electrostatic repulsion via surface charge neutralization (Fig. 5.5A). However, a similar *SRSF* (0.299 ± 0.019 g L^{-1}, p>0.45) was obtained to that of 0.97 g m^{-2} after normalizing RSF to water flux.

5.6.3 Effects of DS concentration and composition

To further investigate the relationship between ion concentration and the effectiveness of the electrostatic repulsion force (Eq. 5.7), a series of DS concentrations (0.25, 0.50, 0.75, and 1.00 M NaCl) were tested as a critical operating parameter. A gradual decrease in the draw concentration and osmotic driven force resulted in a reduced water flux for both the pristine ($J_{w,o}$) and the AL-coated membranes ($J_{w,m}$, Fig. 5.6A). Meanwhile, smaller amounts of NaCl leaked into the feed side with the lower draw concentration (0.25-M NaCl), leading to an RSF of 1.98 ± 0.10 gMH for the AL-coated ($J_{s,m}$) and 4.17 ± 0.16 gMH for the pristine membranes ($J_{s,o}$). A comparable *SRSF* was determined under 0.50-1.00 mol L^{-1} NaCl for the AL-coated membrane (0.301, 0.309, and 0.308 g L^{-1}, respectively), indicating a similar $C_{c,1}{}^{i}$ (DS level at the coating-active layer interface, Fig. 5.4B) and comparable Debye length (Eq. 5.7). However, *SRSF* decreased to 0.279 ± 0.001 g L^{-1} ($SRSF_m$) when 0.25-M NaCl was tested with an AL-coated membrane. Hence, the Z-CNT coated FO membranes are more effective to electrostatically repel ions at lower DS concentrations (Eq. 5.7). It is worth noting that a consistent *SRSF* was obtained for the pristine membrane under all DS concentrations (0.500 ± 0.011 g L^{-1}, $SRSF_o$), confirming that the *SRSF* of a certain DS in a

selected pristine membrane was only affected by membrane intrinsic parameters (Phillip et al. 2010).

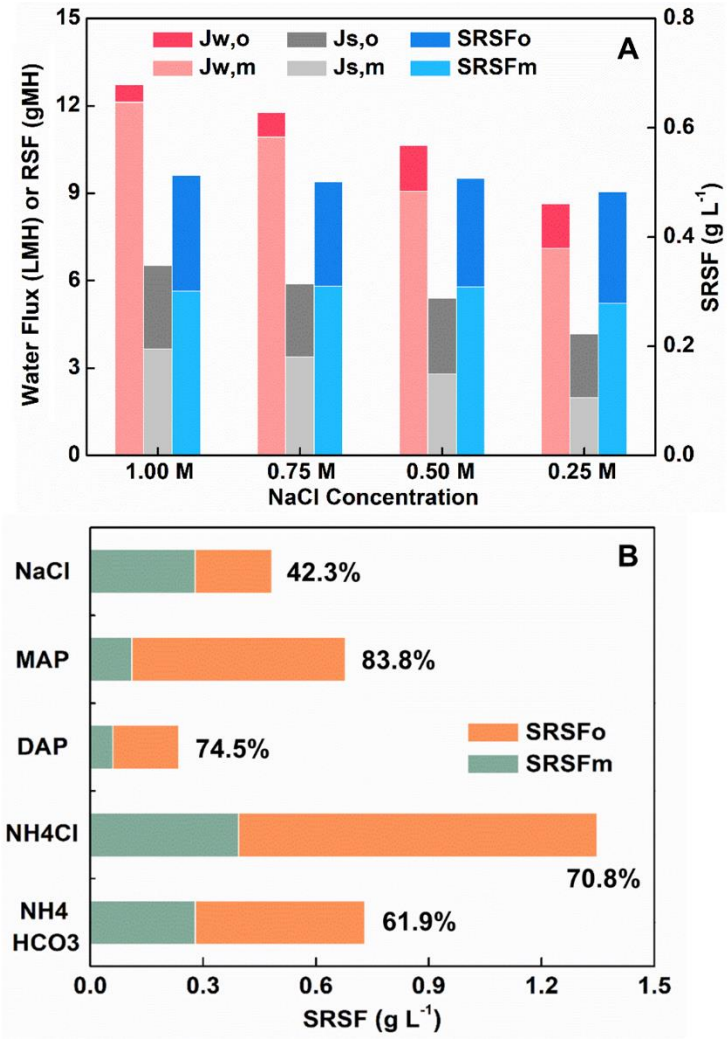

Figure 5.6 Comparison of FO performance between pristine and coating-AL membranes in terms of (A) various draw solution concentration (NaCl) and (B) various draw solutes. The subscripts o and m in Fig. 5.6A represent pristine membrane and AL-coated membrane (0.97 g m^{-2}), respectively. In Fig. 5.6B, the concentration for all the draw solutions is 0.25 M, and the MR of each DS is labeled beside the column (i.e., (1- $SRSF_m/SRSF_o$)×100%).

Various DSs were subsequently tested at 0.25 mol L^{-1} for *SRSF* reduction to evaluate the broad applicability of Z-CNTs. All the selected DSs were ammonium-based fertilizers and have been studied in fertilizer-driven FO (FDFO) to bypass energy-intensive DS

regeneration/separation, including $NH_4H_2PO_4$ (monoammonium phosphate, MAP), $(NH_4)_2HPO_4$ (diammonium phosphate, DAP), NH_4Cl, and thermolytic NH_4HCO_3. Ammonium-based DSs were found to exhibit relatively large *SRSF* in commercial FO membranes (Achilli et al. 2010), compared to that of the benchmark NaCl (Fig. 5.6B). DAP, however, exhibited a much lower *SRSF* due to the higher mole amount of phosphate ions and their larger hydrated radii (Zou and He 2017a). A significantly reduced *SRSF* was observed with the coated membrane (0.97g m^{-2}) for all the DSs ($SRSF_m$, Fig. 5.6B), including MAP (0.110 ± 0.004 g L^{-1}, 83.8% *MR*), DAP (0.060 ± 0.002 g L^{-1}, 74.5%), NH_4Cl (0.394 ± 0.013 g L^{-1}, 70.8% *MR*), and NH_4HCO_3 (0.279 ± 0.009 g L^{-1}, 61.9% *MR*). The high degree of repulsion for multiple DS ions, especially nutrient ions (e.g., N and P) could effectively prevent contamination of the feed solution (e.g., brine water, groundwater, or wastewater) and reduce subsequent polishing costs before final discharge.

5.6.4 Membrane rejection and forward solute flux

FO has been recognized for its superior rejection of a variety of contaminants (over 95%) in the feed stream, such as inorganic pollutants (nutrients and heavy metals) (Xie et al. 2016), trace organic compounds (pharmaceuticals and pesticides) (Madsen et al. 2015), and microorganisms (Liu et al. 2013). However, minor permeation of exotic contaminants via FSF could lead to enhanced system costs for downstream processes (e.g., fouling and/or scaling during pressure- or thermal-separation) and potential environmental concerns if being directly reused (e.g., agriculture irrigation in FDFO). To quantify the magnitude of contaminant permeation via FSF, a synthetic solution containing common pollutant ions (each with a concentration of 100-130 mg L^{-1}) was fed into an FO cell equipped with the pristine membrane. The results indicated that multivalent ions (e.g., Mg^{2+} and PO_4^{3-}-P) exhibited significantly less permeation than monovalent ions (NO_2^--N and K^+, Fig. 5.7A), due to their relatively larger hydrated ion radii and better size exclusion effect. It should be noted that Ca^{2+} was completed rejected (i.e., 100% rejection rate) by the pristine membrane. Among the monovalent ions, cations (NH_4^+-N and K^+) demonstrated a higher propensity to diffuse towards the draw side than anions (NO^{2-}-N and NO^{3-}-N), owing to the negative membrane charge and Donnan facilitated cation transport (similar to RSF). NH_4^+-N had the lowest rejection rate (12.2 ± 1.2%) and the highest FSF (1.68 ± 0.02 gMH). Hence, membrane rejection must be properly addressed to promote water reuse.

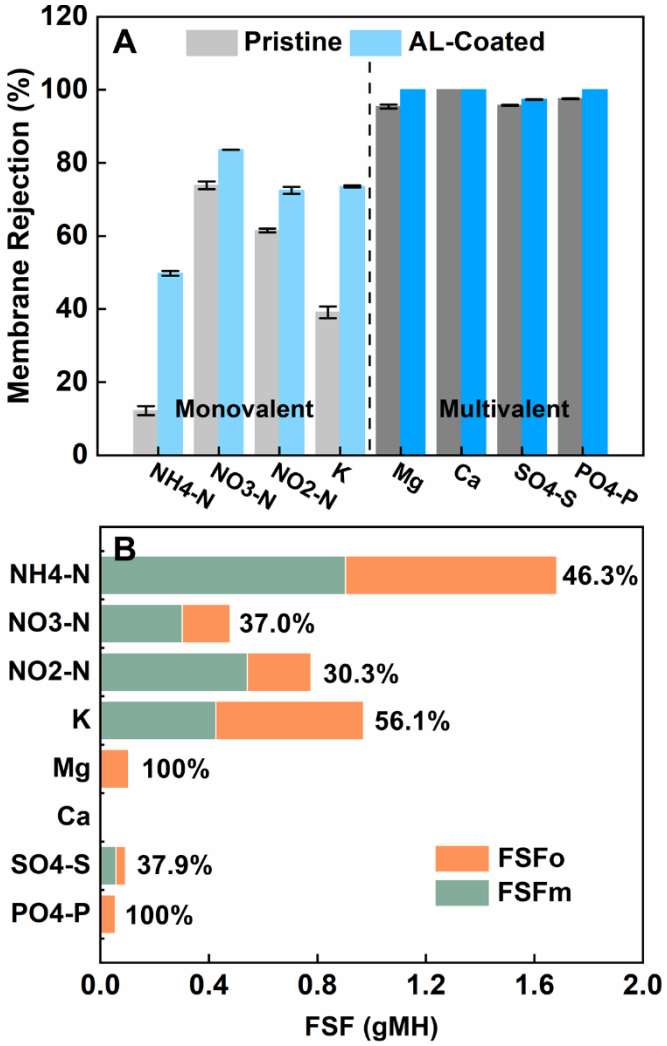

Figure 5.7 Comparison of FO performance between pristine and AL-coated membranes in terms of (A) membrane rejection and (B) FSF of various pollutant ions in the feed. A synthetic solution, instead of DI water, was selected as the feed solution. The subscripts o and m in Fig. 5.7A represent pristine membrane and AL-coated membrane (0.97 g m^{-2}), respectively. The percentage represents for FSF reduction efficiency (i.e., (1- FSF_m/FSF_o)×100%).

Enhanced membrane rejection was realized by using the Z-CNT coated FO membrane. The AL-coated membrane (0.97 g m^{-2}) exhibited zero or negligible permeation of multivalent ions, with an FSF of 0 gMH (i.e., 100% rejection, Fig. 5.7A) for Mg^{2+}, Ca^{2+}, and PO_4^{3-}-P, and an FSF< 0.06 gMH for SO_4^{2-}-S (95.7 ± 0.2% rejection). Significantly improved rejection was also obtained for monovalent ions (Fig. 5.7A and 5.7B), including NH_4^+-N (49.8% rejection, FSF of 0.90 gMH,

or 46.3% FSF reduction compared to pristine membrane), NO_2^--N (83.6% rejection, FSF of 0.30 gMH, or 37.0% FSF reduction), NO_3^--N (72.5% rejection, FSF of 0.54 gMH, or 30.3% FSF reduction), and K^+ (73.6% rejection, FSF of 0.43 gMH, or 56.1% FSF reduction). The enhanced rejection and reduced FSF could be attributed primarily to electrostatic repulsion as the Z-CNT was in direct contact with the feed. It should also be noted that domestic wastewater tends to have lower ion concentrations (<50 mg L^{-1}) than the synthetic solution used in this study (100-130 mg L^{-1}), resulting in elevated electrostatic repulsion forces based on Eq. 5.7. Together with a desirable RSF reduction, Z-CNT surface coatings have been proved to be effective in significantly decreasing BSF for multiple draw or feed solutes, allowing FO to potentially treat a variety of source waters (Lu et al. 2014).

5.6.5 Water flux consistency under semi-continuous operation

The lowest SRSF should be obtained by both minimizing DS penetration (i.e., low RSF) and more importantly, obtaining a consistent water flux under long-term operation. However, when fed with real wastewater, gradual fouling on the membrane surface could hinder efficient water transport through the FO membrane while accelerating DS leakage via fouling-intensified concentration polarization (She et al. 2012). Zwitterionic materials, either coated on membrane surface or embedded inside the membrane, have been utilized to maintain water flux consistency in previous studies (Lee et al. 2018, Zhao et al. 2016). In this study, the Z-CNT coated FO membranes were further examined under semi-continuous operation focusing on water flux consistency and membrane fouling resistance (Fig. 5.8A). On day 1, less water (184.4 mL and 3.76 LMH) was recovered in the FO equipped with the AL-coated membrane compared to that of the pristine membrane (230.7 mL and 4.92 LMH), likely due to additional water transport resistance. As the operation continued, relatively consistent daily water recovery volumes and water fluxes were obtained with the coated membrane, while the pristine membrane exhibited a dramatic decrease. By the end of day 12, the AL-coated membrane exhibited only a 25.2% and 14.9% decrease in water volume and flux, respectively, much lower than the pristine membrane (50.4% and 54.5%, respectively). This desirable enhancement of fouling resistance is attributed to several possible mechanisms (He et al. 2016): (1) formation of a hydration shell assisted by zwitterionic materials on the membrane surface as a barrier to prevent direct contact of foulants (Chen et al. 2005); (2) steric hindrance effects induced by the chain of zwitterionic functional groups (Chen et al. 2010);

and (3) potential antimicrobial properties of the CNT (Tiraferri et al. 2011), leading to an apparent visual difference of fouling coverage area on the membrane surface (Fig. 5.8B). Simple physical flushing appears to be very effective in removing most foulants on both membranes (day 13, Fig. 5.8B). On day 13 (after membrane cleaning), the recovery efficiency for the pristine membrane could reach 99.2%. However, flattened biofouling residues could still be observed under SEM (50K magnification). For the AL-coated membrane, a higher than 100% recovery was observed after membrane cleaning due to detachment of Z-CNTs (Fig. 5.8B, SEM image after membrane cleaning). The elemental mapping via EDS indicated that the remaining foulants on the AL-coated membrane were scattered inorganic scaling (e.g., Ca^{2+}, Fig. 5.8C), rather than biofouling.

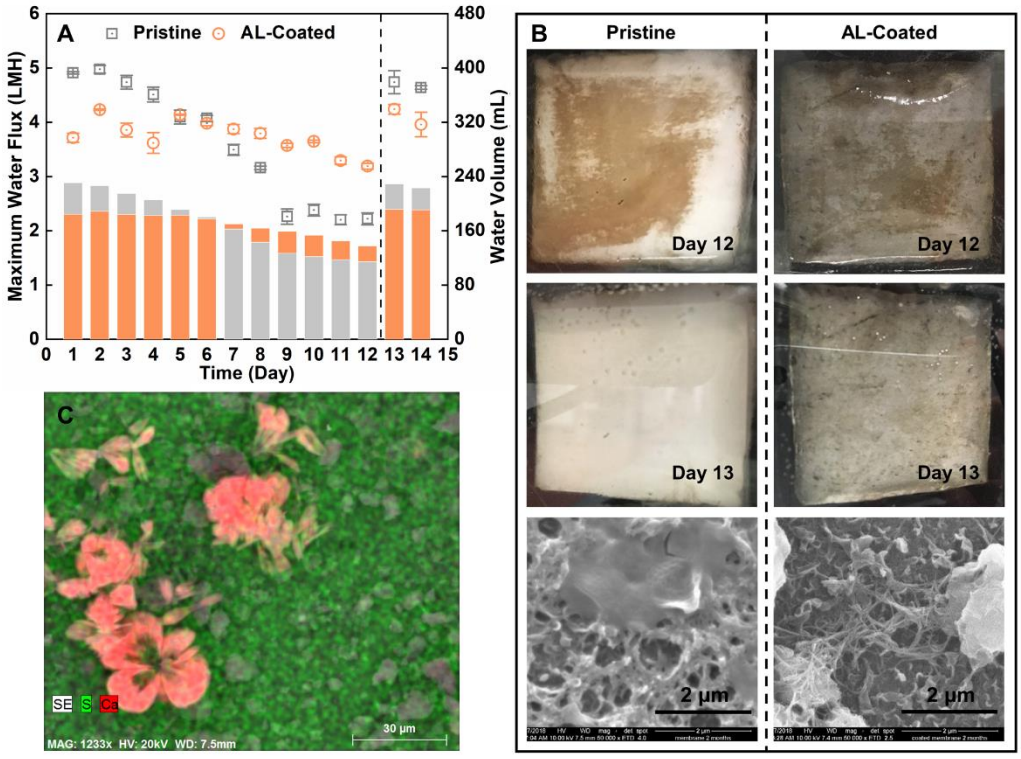

Figure 5.8 Comparison of FO performance between pristine and AL-coated membranes under a semi-continuous operation in terms of (A) daily maximum water flux and recovery volume; (B) visual images of membrane on day 12 (before membrane cleaning) and day 13 (after membrane cleaning with SEM characterization); and (C) elemental mapping of AL-coated membrane (day 13) under EDS. In Fig. 5.8C, the green and red color indicate sulfur from membrane framework and calcium from inorganic scaling. Raw secondary effluent from a local WWTP was collected as the feed solution.

5.6.6 Perspectives

Our results have collectively demonstrated effective control of bidirectional solute flux and consistent water flux by coating Z-CNTs on commercial FO membranes. To fully realize the potential of zwitterionic materials for the elimination of bidirectional solute flux, several key challenges need to be addressed. First, more robust approaches need to be employed to incorporate Z-CNTs onto the TFC membrane. Natural adhesion via physical adsorption in this study is one of the easiest, economically viable, and most scalable coating methods. However, Z-CNTs bond with FO active layer only through van der Waals force and may detach from the membrane during long-term operation (especially under higher hydraulic sheer force). The detached Z-CNTs can leave the membrane surface together with accumulated foulants, rendering temporarily enhanced fouling resistance. Other strategies have been exploited in previous studies to strengthen the bond between zwitterionic materials and membrane surface, including grafting zwitterionic polymers via polymerization, surface segregation, and biomimetic adhesion (He et al. 2016). However, most of these strategies were only assessed for their performance in anti-fouling resistance rather than BSF mitigation. Alternatively, embedding zwitterionic materials inside the TFC membrane can offer a more permanent solution for possible detachment (Chan et al. 2016). Nonetheless, such an approach requires high compatibility between the zwitterionic material and the intrinsic membrane framework to maintain membrane integrity. Second, other zwitterionic materials than Z-CNTs should be explored for potential control of bidirectional solute flux in FO. The current Z-CNTs do provide a good electrostatic repulsion force to repel feed and draw solutes, yet it decreases the membrane hydrophilicity with larger surface contact angles. A hydrophilic polymer-based backbone, instead of a hydrophobic CNT, could be selected to carry the zwitterionic functional groups. Finally, in the case when zwitterionic materials (e.g., Z-CNT) detach from the membrane surface, their presence in the feed stream could lead to potential environmental concerns. The toxicity and ecological effects of such substances need to be comprehensively studied with further research.

5.7 Conclusions

In this study, zwitterion functionalized carbon nanotubes (Z-CNTs) have been coated onto a commercial thin film composite (TFC) membrane to achieve BSF mitigation via electrostatic

repulsion force induced by zwitterionic functional groups and steric interaction with CNTs. The results have important implications for promoting high-quality water recovery via FO and will inspire further development of effective strategies for BSF and fouling control. The following conclusions are arrived:

- Better mitigation of RSF was achieved (under the AL-Feed mode) when coating Z-CNT on the active layer, rather than on the supportive layer, likely due to more extended electrostatic repulsion in the presence of lower ionic strength.
- With an optimal coating density of 0.97 g m^{-2}, a significantly reduced specific RSF was observed for multiple draw solutes, including NaCl (0.281 g L^{-1}, 55.5% reduction), $NH_4H_2PO_4$ (0.110 g L^{-1}, 83.8%), $(NH_4)_2HPO_4$ (0.060 g L^{-1}, 74.5%), NH_4Cl (0.394 g L^{-1}, 70.8%), and NH_4HCO_3 (0.279 g L^{-1}, 61.9%).
- FSF was notably reduced with fewer pollutants leaked to the draw solution, including NH_4^+-N (46.3% reduction), NO_2^--N (37.0%), NO_3^--N (30.3%), K^+ (56.1%), PO_4^{3-}-P (100%), and Mg^{2+} (100%). Successful BSF mitigation (both RSF and FSF) could allow FO to potentially treat a variety of source waters with a wide spectrum of DS.
- When fed with real wastewater, a much more stable water flux (only 14.9% decrease) was achieved with the Z-CNT coated membrane during a 12-day semi-continuous operation, compared to that of the pristine membrane (54.5% flux decline). Nearly all membrane foulants could be removed via simple physical flushing, rendering a more robust and cost-effective FO operation.
- This Z-CNT coating study is among the earliest efforts to address BSF control via membrane modification, and the results warrant future effort to explore alternative zwitterionic materials while strengthening the bond between coating materials and membrane surface.

References

Achilli, A., Cath, T.Y. and Childress, A.E. (2010) Selection of inorganic-based draw solutions for forward osmosis applications. Journal of Membrane Science 364(1), 233-241.

Akther, N., Sodiq, A., Giwa, A., Daer, S., Arafat, H.A. and Hasan, S.W. (2015) Recent advancements in forward osmosis desalination: A review. Chemical Engineering Journal 281, 502-522.

Blandin, G., Verliefde, A.R., Tang, C.Y., Childress, A.E. and Le-Clech, P. (2013) Validation of assisted forward osmosis (AFO) process: impact of hydraulic pressure. Journal of Membrane Science 447, 1-11.

Cath, T.Y., Childress, A.E. and Elimelech, M. (2006) Forward osmosis: principles, applications, and recent developments. Journal of Membrane Science 281(1), 70-87.

Chan, W.-F., Marand, E. and Martin, S.M. (2016) Novel zwitterion functionalized carbon nanotube nanocomposite membranes for improved RO performance and surface anti-biofouling resistance. Journal of Membrane Science 509, 125-137.

Epsztein, R., Shaulsky, E., Dizge, N., Warsinger, D.M., Elimelech, M. (2018) Role of ionic charge density in Donnan exclusion of monovalent anions by nanofiltration. Environmental Science & Technology 52(7), 4108-4116.

Guo, H., Yao, Z., Wang, J., Yang, Z., Ma, X. and Tang, C.Y. (2018) Polydopamine coating on a thin film composite forward osmosis membrane for enhanced mass transport and antifouling performance. Journal of Membrane Science 551, 234-242.

Hartanto, Y., Yun, S., Jin, B. and Dai, S. (2015) Functionalized thermo-responsive microgels for high performance forward osmosis desalination. Water Research 70, 385-393.

He, M., Gao, K., Zhou, L., Jiao, Z., Wu, M., Cao, J., You, X., Cai, Z., Su, Y. and Jiang, Z. (2016) Zwitterionic materials for antifouling membrane surface construction. Acta Biomaterialia 40, 142-152.

Holt, J.K., Park, H.G., Wang, Y., Stadermann, M., Artyukhin, A.B., Grigoropoulos, C.P., Noy, A. and Bakajin, O. (2006) Fast mass transport through sub-2-nanometer carbon nanotubes. Science 312(5776), 1034-1037.

Huang, L., Bui, N.-N., Meyering, M.T., Hamlin, T.J. and McCutcheon, J.R. (2013) Novel hydrophilic nylon 6, 6 microfiltration membrane supported thin film composite membranes for engineered osmosis. Journal of Membrane Science 437, 141-149.

Israelachvili, J.N. (2011) Intermolecular and surface forces, Academic press.

Jin, X., Shan, J., Wang, C., Wei, J. and Tang, C.Y. (2012) Rejection of pharmaceuticals by forward osmosis membranes. Journal of Hazardous Materials 227-228, 55-61.

Kowalski, S.J., Szadzińska, J. and Pawłowski, A. (2015) Ultrasonic-Assisted Osmotic Dehydration of Carrot Followed by Convective Drying with Continuous and Intermittent Heating. Drying Technology 33(13), 1570-1580.

Kwon, S.-B., Lee, J.S., Kwon, S.J., Yun, S.-T., Lee, S. and Lee, J.-H. (2015) Molecular layer-by-layer assembled forward osmosis membranes. Journal of Membrane Science 488, 111-120.

Li, X., Sun, S., Badgley, B.D. and He, Z. (2016) Long-term performance and microbial community characterization of an osmotic anammox system for removing reverse-fluxed ammonium. Bioresource Technology 211, 628-635.

Liu, X., Qi, S., Li, Y., Yang, L., Cao, B. and Tang, C.Y. (2013) Synthesis and characterization of novel antibacterial silver nanocomposite nanofiltration and forward osmosis membranes based on layer-by-layer assembly. Water Research 47(9), 3081-3092.

Lu, X., Boo, C., Ma, J. and Elimelech, M. (2014) Bidirectional Diffusion of Ammonium and Sodium Cations in Forward Osmosis: Role of Membrane Active Layer Surface Chemistry and Charge. Environmental Science & Technology 48(24), 14369-14376.

Lu, Y. and He, Z. (2015) Mitigation of Salinity Buildup and Recovery of Wasted Salts in a Hybrid Osmotic Membrane Bioreactor–Electrodialysis System. Environmental Science & Technology 49(17), 10529-10535.

Lutchmiah, K., Harmsen, D.J.H., Wols, B.A., Rietveld, L.C., Jianjun, Q. and Cornelissen, E.R. (2015) Continuous and discontinuous pressure assisted osmosis (PAO). Journal of Membrane Science 476, 182-193.

Madsen, H.T., Bajraktari, N., Helix-Nielsen, C., Van der Bruggen, B. and Søgaard, E.G. (2015) Use of biomimetic forward osmosis membrane for trace organics removal. Journal of Membrane Science 476, 469-474.

McCutcheon, J.R. and Elimelech, M. (2006) Influence of concentrative and dilutive internal concentration polarization on flux behavior in forward osmosis. Journal of Membrane Science 284(1), 237-247.
Mi, Y.-F., Zhao, F.-Y., Guo, Y.-S., Weng, X.-D., Ye, C.-C. and An, Q.-F. (2017) Constructing zwitterionic surface of nanofiltration membrane for high flux and antifouling performance. Journal of Membrane Science 541, 29-38.
Nguyen, A., Azari, S. and Zou, L. (2013) Coating zwitterionic amino acid l-DOPA to increase fouling resistance of forward osmosis membrane. Desalination 312, 82-87.
Phillip, W.A., Yong, J.S. and Elimelech, M. (2010) Reverse draw solute permeation in forward osmosis: modeling and experiments. Environmental Science & Technology 44(13), 5170-5176.
Qiu, G., Law, Y.-M., Das, S. and Ting, Y.-P. (2015) Direct and complete phosphorus recovery from municipal wastewater using a hybrid microfiltration-forward osmosis membrane bioreactor process with seawater brine as draw solution. Environmental Science & Technology 49(10), 6156-6163.
Russel, W.B., Russel, W., Saville, D.A. and Schowalter, W.R. (1991) Colloidal dispersions, Cambridge University Press.
Sarkar, S., SenGupta, A.K. and Prakash, P. (2010) The Donnan membrane principle: opportunities for sustainable engineered processes and materials. Environmental Science & Technology 44(4), 1161-1166.
Shannon, M.A., Bohn, P.W., Elimelech, M., Georgiadis, J.G., Marinas, B.J. and Mayes, A.M. (2008) Science and technology for water purification in the coming decades. Nature 452(7185), 301-311.
She, Q., Jin, X., Li, Q. and Tang, C.Y. (2012) Relating reverse and forward solute diffusion to membrane fouling in osmotically driven membrane processes. Water Research 46(7), 2478-2486.
Tijing, L.D., Woo, Y.C., Shim, W.-G., He, T., Choi, J.-S., Kim, S.-H. and Shon, H.K. (2016) Superhydrophobic nanofiber membrane containing carbon nanotubes for high-performance direct contact membrane distillation. Journal of Membrane Science 502, 158-170.
Tiraferri, A. and Elimelech, M. (2012) Direct quantification of negatively charged functional groups on membrane surfaces. Journal of Membrane Science 389, 499-508.
Wang, J., Wang, Z., Wang, J. and Wang, S. (2015a) Improving the water flux and bio-fouling resistance of reverse osmosis (RO) membrane through surface modification by zwitterionic polymer. Journal of Membrane Science 493, 188-199.
Wang, J., Xiao, T., Bao, R., Li, T., Wang, Y., Li, D., Li, X. and He, T. (2018) Zwitterionic surface modification of forward osmosis membranes using N-aminoethyl piperazine propane sulfonate for grey water treatment. Process Safety and Environmental Protection 116, 632-639.
Wang, Y., Ou, R., Wang, H. and Xu, T. (2015b) Graphene oxide modified graphitic carbon nitride as a modifier for thin film composite forward osmosis membrane. Journal of Membrane Science 475, 281-289.
Xie, M., Shon, H.K., Gray, S.R. and Elimelech, M. (2016) Membrane-based processes for wastewater nutrient recovery: Technology, challenges, and future direction. Water Research 89, 210-221.
Yasukawa, M., Mishima, S., Shibuya, M., Saeki, D., Takahashi, T., Miyoshi, T. and Matsuyama, H. (2015) Preparation of a forward osmosis membrane using a highly porous polyketone microfiltration membrane as a novel support. Journal of Membrane Science 487, 51-59.
Zhao, S. and Zou, L. (2011) Relating solution physicochemical properties to internal concentration polarization in forward osmosis. Journal of Membrane Science 379(1), 459-467.
Zhou, Q., Lei, X.-P., Li, J.-H., Yan, B.-F. and Zhang, Q.-Q. (2014) Antifouling, adsorption and reversible flux properties of zwitterionic grafted PVDF membrane prepared via physisorbed free radical polymerization. Desalination 337, 6-15.
Zou, S. and He, Z. (2016) Enhancing wastewater reuse by forward osmosis with self-diluted commercial fertilizers as draw solutes. Water Research 99, 235-243.
Zou, S. and He, Z. (2017a) Electrodialysis recovery of reverse-fluxed fertilizer draw solute during forward osmosis water treatment. Chemical Engineering Journal 330, 550-558.

Zou, S. and He, Z. (2017b) Electrolysis-assisted mitigation of reverse solute flux in a three-chamber forward osmosis system. Water Research 115, 111-119.
Zou, S., Qin, M. and He, Z. (2019) Tackle reverse solute flux in forward osmosis towards sustainable water recovery: reduction and perspectives. Water Research 149, 362-374.
Zou, S., Yuan, H., Childress, A. and He, Z. (2016) Energy Consumption by Recirculation: A Missing Parameter When Evaluating Forward Osmosis. Environmental Science & Technology 50(13), 6827-6829.

6 Tackle Reverse Solute Flux in Forward Osmosis towards Sustainable Water Recovery: Reduction and Perspectives

(This paper has been published as "Zou, S., Qin, M., and He, Z. (2019) Tackle reverse solute flux in forward osmosis towards sustainable water recovery: reduction and perspectives. *Water Research*, 149, 362-374")

6.1 Abstract

Forward osmosis (FO) has emerged as a potentially energy-efficient membrane treatment technology to yield high-quality reusable water from various wastewater/saline water sources. A key challenge remained to be solved for FO is reverse solute flux (RSF), which can cause issues like reduced concentration gradient and loss of draw solutes. Yet no universal parameters have been developed to compare RSF control performance among various studies, making it difficult to position us in this "battle" against RSF. In this paper, we have conducted a concise review of existing RSF reduction approaches, including operational strategies (e.g., pressure-, electricity-, and ultrasound-assisted osmosis) and advanced membrane development (e.g., new membrane fabrication and existing membrane modification). We have also analyzed the literature data to reveal the current status of RSF reduction. A new parameter, mitigation ratio (*MR*), was proposed and used together with specific RSF (*SRSF*) to evaluate RSF reduction performance. Potential research directions have been discussed to help with future RSF control. This review intends to shed more light on how to effectively tackle solute leakage towards a more cost-effective and environmental-friendly FO treatment process.

6.2 Graphical Abstract

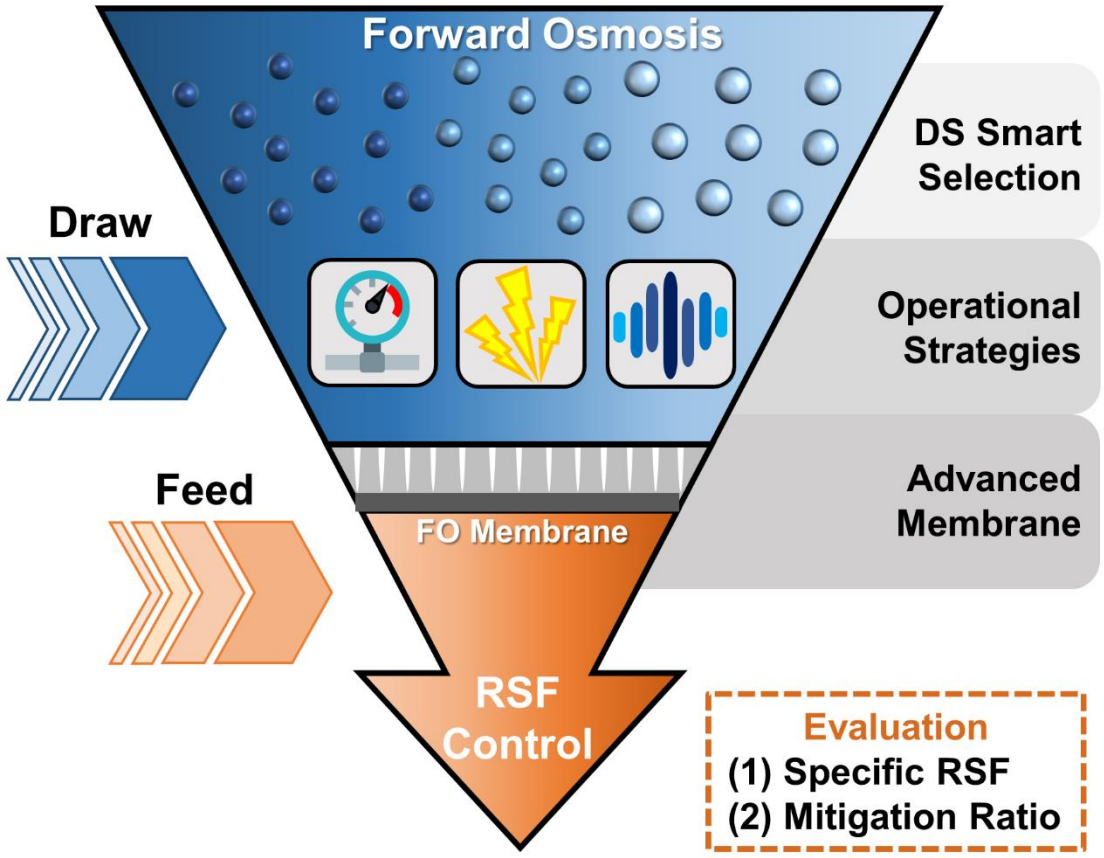

6.3 Keywords

Forward osmosis; Reverse solute flux; Water Recovery; Operational strategies; Membrane fabrication and modification

6.4 Introduction

Despite great promise and much progress of FO-based technologies, a major challenge and also an impediment remain to be solved is the salinity buildup on the feed side, resulted from both reverse solute flux (RSF, a significant contributor) and concentrating effect by FO membrane rejection (Hancock and Cath 2009). RSF is defined as the cross-membrane diffusion of DS to the feed side driven by solute concentration difference (Phillip et al. 2010) and has been utilized for process intensification, such as supplying substrate or buffer reagents in an osmotic microbial fuel cell (Bowden et al. 2012, Wu et al. 2018a), enhancement of anti-scaling resistance (Zhang et al. 2017), and facilitating struvite precipitation from sludge centrate/digestate (Wu et al. 2018b, Xie et al. 2014). Still, the detrimental effects of RSF include gradual loss of DS, reduced osmotic driving force (i.e., lower water flux), increased fouling propensity, and elevated operation cost due to periodical replenishment of DS (Akther et al. 2015). Accumulation of the reverse-fluxed DS, such as ammonium and phosphorus, will require further treatment of the feed stream (Phillip et al. 2010). To understand the solute permeation process, lab experiments integrated with mathematical modeling have been conducted to explore concentration polarization (both external and internal polarizations) (Phillip et al. 2010, Yaroshchuk 2010), solute-solvent interaction (Su and Chung 2011, Yong et al. 2012a), solute-solute interaction (Irvine et al. 2013, Lu et al. 2014), and chemical equilibrium (Yong et al. 2012b). The reverse permeation of solute ions is strongly linked to both intrinsic membrane parameters (affected by thickness, tortuosity, and porosity) (McCutcheon and Elimelech 2006) and solute characteristics (e.g., hydrated ion radius, aqueous diffusivity, solution viscosity, and ion charge) (Zhao and Zou 2011). For example, smaller hydrated ions have an elevated tendency to penetrate the FO active layer (Wang et al. 2010). Meanwhile, ion charge plays a pivotal role in the magnitude of RSF. Because most FO membranes, made of either cellulose triacetate (CTA) or polyamide thin film composite (TFC), are negatively charged, DS cations can migrate more easily than anions via Donnan dialysis (Sarkar et al. 2010). To maintain electroneutrality, DS anions either permeate FO membrane together with cations, or exchange with anions from the feed solution (Irvine et al. 2013). It is worth noting that some neutral DS, e.g., urea and ethylene glycol, have demonstrated significantly higher RSF compared to charged ions in FO process (Yong et al. 2012a, Zou and He 2016).

Control and reduction of RSF are critically important to a healthy FO operation. Reducing the RSF of a particular DS can be accomplished via operational strategies or advanced membrane development. Smart selection of novel and less permeable DS will help achieve less RSF in an FO system, thereby mitigating RSF. However, the lack of RSF data in many studies hinders our exploration and understanding of RSF and its mitigation. There also lack reliable judging criteria or universal parameters to compare RSF control performance among various reduction strategies. Herein, this paper aims to provide a concise review focusing on RSF quantification and control strategies, and to analyze and discuss the challenges and possible solutions for further investigation RSF mitigation. A new parameter, RSF mitigation ratio (*MR*), is proposed and used for comparison based on the data computed from available references. It should be noted that there have been a number of previous review papers on general FO development (Akther et al. 2015, Cath et al. 2006, Chekli et al. 2016, Chung et al. 2012a, Chung et al. 2012b, Coday et al. 2014a, Lutchmiah et al. 2014, Shaffer et al. 2015, Valladares Linares et al. 2014, Zhao et al. 2012), selection/regeneration of draw solutes (Cai and Hu 2016, Chekli et al. 2012, Ge et al. 2013, Luo et al. 2014a), and membrane rejection of pollutants (Coday et al. 2014b). The present review paper tends not to repeat what has been discussed before and aims to provide a unique perspective of elucidating and evaluating RSF control approaches and efficiency.

6.5 Quantification of Reverse Solute Flux

RSF (*Js*) can be quantified according to the following equation (Eq. 6.1) (Phillip et al. 2010):

$$J_s = \frac{J_w C_D}{1-(1+\frac{J_w}{B})\exp(\frac{J_w S}{D})} \quad \text{(Eq. 6.1)}$$

where J_w (L m^{-2} h^{-1}, LMH) is the water flux, C_D is the experimentally accessible bulk draw solution concentration, D is the draw solute diffusion coefficient in the bulk solution, S is the membrane structural parameter determined from FO and RO experiments (McCutcheon and Elimelech 2006, Yip et al. 2010), and B is the active layer draw solute permeability coefficient determined from RO or PRO experiments (Paul 2004, Phillip et al. 2010).

The above theoretical equation has its limitations (e.g., for strong electrolyte and single solute system) and is not convenient to directly quantify RSF. DS cations and anions may also

exhibit varied RSF due to charge difference, though most FO studies report RSF on the whole DS level. To quantify RSF in an FO system fed with a complicated feed stream (e.g., wastewater), solute buildup (*SBU*, in the feed solution) for a DS or a specific ion can be first calculated by using Eq. 6.2 (Zou and He 2016).

$$SBU = \frac{(n_{f,F} - n_{i,F}) \times Mw}{S \times t} = \frac{V_{f,F} \times C_{f,F} - V_{i,F} \times C_{i,F}}{S \times t} \quad \text{(Eq. 6.2)}$$

where $n_{i,F}$ and $n_{f,F}$ are the initial and final mole of a DS or a specific ion in the feed, respectively. $C_{i,F}$ and $C_{f,F}$ are the initial and final mass concentration in the feed, respectively. $V_{i,F}$ and $V_{f,F}$ are the initial and final feed volume. t stands for operating time. S is the effective surface area of the FO membrane. Mw stands for molecular weight. All these parameters can be directly measured or monitored during experiments.

SBU is typically resulted from both the concentrating effect in the feed (due to membrane rejection) and RSF from the draw side. The concentrating effect (*CE*) and RSF (J_s, g m^{-2} h^{-1}, gMH) of a DS or a specific ion are calculated according to Eq. 6.3 and 6.4, respectively.

$$CE = \frac{V_{recovered} \times C_{i,F}}{S \times t} = \frac{(V_{f,D} - V_{i,D}) \times C_{i,F}}{S \times t} \quad \text{(Eq. 6.3)}$$

$$J_s = SBU - CE \quad \text{(Eq. 6.4)}$$

where the recovered water volume ($V_{recovered}$) on the draw side can be determined by subtracting initial draw volume ($V_{i,D}$) from the final draw volume ($V_{f,D}$). When DI water is used as the feed, or no draw solute ion is presented in the feed stream, $C_{i,F}$ equals to 0 with no concentrating effect existed. In such a case, J_s=*SBU*.

To more accurately quantify RSF in an FO system, specific RSF (*SRSF*, g L^{-1}) can be calculated to rule out the influence of both membrane structural parameter (S) and bulk draw solution concentration (C_D) (Phillip et al. 2010). *SRSF* reveals the amount/mass of a DS or an ion that can leak across FO membrane to the feed side per unit water recovered (i.e., 1 liter), and is defined as the ratio of J_s (gMH) and J_w (LMH):

$$SRSF = \frac{J_s}{J_w} \quad \text{(Eq. 6.5)}$$

In this paper, a new parameter, RSF mitigation ratio (*MR*, %), is proposed and quantified based on *SRSF* to enable better comparison among various RSF control strategies. *MR* is determined by the ratio between the mitigated specific RSF ($SRSF_m$) and the original specific RSF ($SRSF_o$).

$$MR = (1 - \frac{SRSF_m}{SRSF_o}) \times 100\% = (1 - \frac{J_{s,m} / J_{w,m}}{J_{s,o} / J_{w,o}}) \times 100\% \quad \text{(Eq. 6.6)}$$

where $J_{s,o}$ and $J_{w,o}$ are the original RSF and water flux, respectively. $J_{s,m}$ and $J_{w,m}$ are the RSF and water flux under the RSF control operation, respectively. In the case where no change in water flux is observed ($J_{w,m}$=$J_{w,o}$), Eq. 6.6 can be simplified to:

$$MR = (1 - \frac{J_{s,m}}{J_{s,o}}) \times 100\% \quad \text{(Eq. 6.7)}$$

In some literature, system conductivity profiles are usually reported instead of RSF or *SRSF* values. Under such cases, total dissolved solids (*TDS*, mg L^{-1}), instead of the DS concentration in the feed solution, can be used to quantify SBU_{TDS}, CE_{TDS}, and J_{TDS}.

$$SBU_{TDS} = \frac{V_{f,F} \times TDS_{f,F} - V_{i,F} \times TDS_{i,F}}{S \times t} \quad \text{(Eq. 6.8)}$$

$$CE_{TDS} = \frac{V_{recovered} \times TDS_{i,F}}{S \times t} = \frac{(V_{f,D} - V_{i,D}) \times TDS_{i,F}}{S \times t} \quad \text{(Eq. 6.9)}$$

$$J_{TDS} = SBU_{TDS} - CE_{TDS} \quad \text{(Eq. 6.10)}$$

where $TDS_{i,F}$ and $TDS_{f,F}$ are initial and final *TDS* in the feed solution, respectively. *TDS* is measured via solution conductivity (σ, mS cm^{-1}) (Lu and He 2015):

$$TDS = 640\sigma \ (\sigma \leq 5) \ \text{ or } \ TDS = 800\sigma \ (5 < \sigma \leq 10) \quad \text{(Eq. 6.11)}$$

Then, MR_{TDS} is quantified via a revised equation from Eq. 6.6.

$$MR_{TDS} = (1 - \frac{J_{TDS,m} / J_{w,m}}{J_{TDS,o} / J_{w,o}}) \times 100\% \quad \text{(Eq. 6.12)}$$

6.6 Operational Strategies for RSF Reduction

Given an existing FO process with a predetermined DS and FO membrane, deploying operational strategies to reduce DS permeation is a straightforward approach. These strategies, including optimizing operation conditions and externally-assisted methods, have been investigated in previous studies to reduce RSF or SRSF potentially. In terms of optimizing operation conditions, the hydrodynamic condition of an FO system can affect RSF, and a higher cross-flow velocity decreases fouling propensity in a FO process, leading to diminished fouling-induced concentration polarization (She et al. 2012), higher water flux (Lee et al. 2010), and lower *SRSF*. Operating temperature of feed and draw solutions, however, is not very effective in *SRSF* reduction (Xie et al. 2013). Due to a lack of systematic RSF studies via optimizing operation conditions, only externally-assisted approaches, including pressure-, electrolysis-, and ultrasonic-assisted osmosis, are evaluated in this section.

6.6.1 Pressure-assisted Osmosis (PAO)

Unlike a natural FO process (ΔP=0, ΔP is the transmembrane pressure) (Chekli et al. 2016), Pressure-assisted osmosis (PAO) can realize energy-efficient (~2.0 kWh m^{-3}) enhancement of system performance (i.e. higher water flux and reduced solute transport) by exerting a relatively low hydraulic pressure on the feed side (<10 bar) (Banchik et al. 2016, Blandin et al. 2017), as compared to PRO (>10 bar) (Han et al. 2015, Straub et al. 2016) or RO (>59 bar, seawater as the feed, Fig. 6.1) (Davenport et al. 2018). One must not confuse PAO (ΔP<0) with the pressure-retarded osmosis (PRO, 0<ΔP<$\Delta\pi$) or RO (ΔP>$\Delta\pi$) (Lutchmiah et al. 2015). Comparing to conventional FO processes, an equivalent or elevated water flux could be obtained in these PAO systems (depending on the applied pressure, $J_{w,m} \geq J_{w,o}$, Fig. 6.2A). The water flux in a PAO process can consist of two portions (Shibuya et al. 2015):

$$J_{w,m} = J_{w,osmotic} + J_{w,hydraulic} \quad \text{(Eq. 6.13)}$$

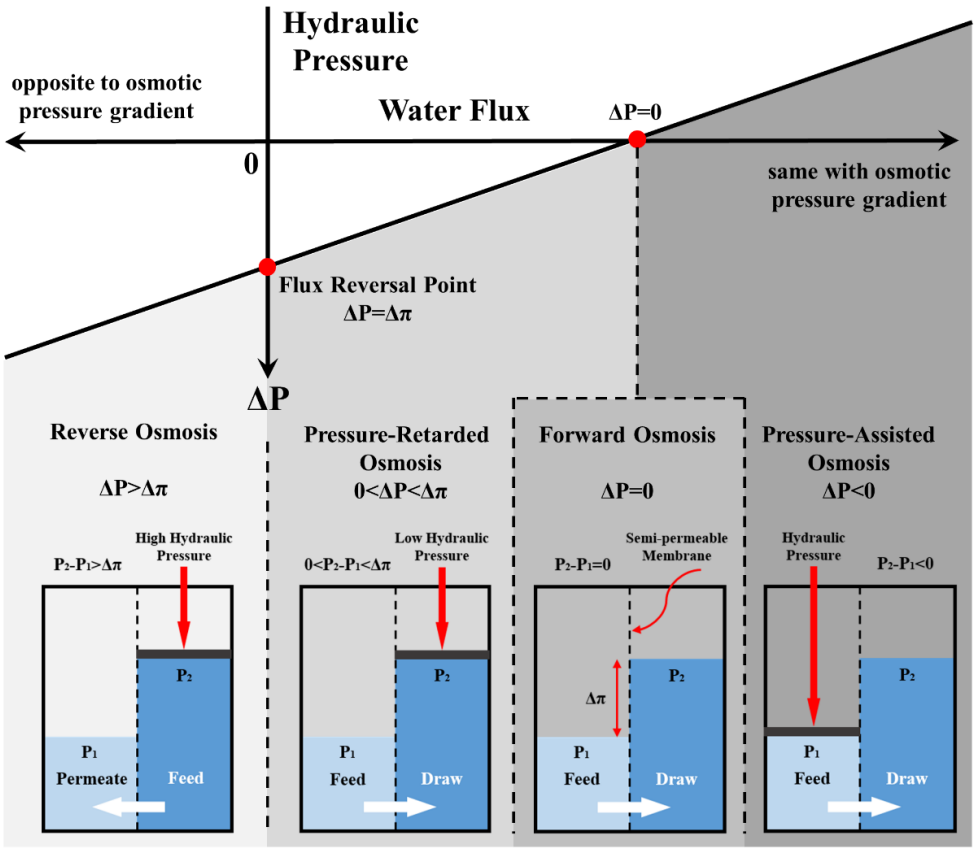

Figure 6.1 The conceptual relationship between external applied hydraulic pressure and water flux direction in reverse osmosis (RO), pressure-retarded osmosis (PRO), forward osmosis (FO), and pressure-assisted osmosis (PAO). ΔP and $\Delta\pi$ stand for external hydraulic pressure and the osmotic pressure difference between two solutions, respectively. This figure adapted from a previous study with permission (Lee et al. 1981).

When the active layer of FO membrane faces the feed side (AL-FS), the external hydraulic pressure exerted on the feed side can lead to an increased internal concentration polarization (Coday et al. 2013), especially under the operation with a relatively high salinity feed stream (Shibuya et al. 2015). As a result, a reduced effective cross-membrane osmotic pressure gradient will diminish water flux in the osmotic portion ($J_{w,osmotic}<J_{w,o}$) (Yun et al. 2014). Meanwhile, the compensation of water flux in the hydraulic portion ($J_{w,hydraulic}$) makes the overall water flux comparable to that in the original operation:

$$J_{w,m} = J_{w,osmotic} + J_{w,hydraulic} \approx J_{w,o} \quad \text{(low hydraulic pressure)} \qquad \text{(Eq. 6.14)}$$

With the increase of exerted hydraulic pressure, the increment of $J_{w,hydraulic}$ outcompetes the decrement of $J_{w,osmotic}$, rendering an elevated overall water flux, for example from 14.0 (0 bar, $J_{w,o}$) to 24.0 LMH (6 bar, $J_{w,m}$) in a PAO fed with red sea water as the draw and DI as the feed (Blandin et al. 2013):

$$J_{w,m} = J_{w,osmotic} + J_{w,hydraulic} > J_{w,o} \quad \text{(high hydraulic pressure)} \qquad \text{(Eq. 6.15)}$$

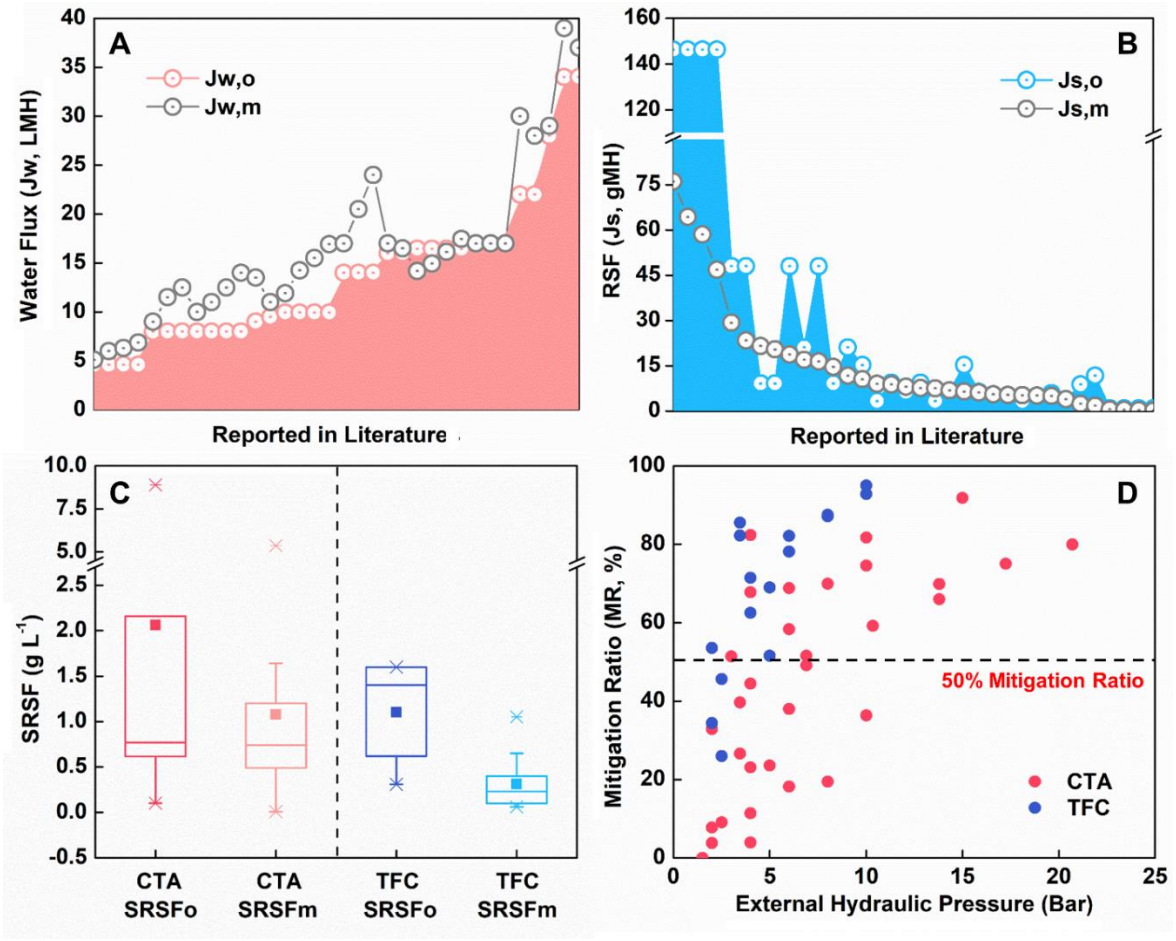

Figure 6.2 RSF reduction via pressure-assisted osmosis (PAO) in terms of (A) water flux, (B) reverse solute flux, (C) specific reverse solute flux, and (D) mitigation ratio. The subscript "o" and "m" stand for original and mitigated parameters, respectively. All data points are from previous PAO studies with NaCl as the draw solutes and DI water as the feed.

The reduced effective cross-membrane osmotic pressure gradient ($\Delta\pi_{eff}$) in PAO may lead to a reduced RSF (Fig. 6.2B), with the highest reduction of J_s from 0.857 to 0.102 gMH (85.7%)

by applying 15-bar hydraulic pressure (Shibuya et al. 2015). Both CTA and TFC membranes show significantly reduced *SRSF* under an applied hydraulic pressure (p<0.001, Fig. 6.2C). The *SRSF* of CTA membrane can be reduced from 2.02 ± 2.64 to 1.07 ± 1.12 g L^{-1}, rendering an average *MR* of 47.1%. For TFC membrane, SRSF is reduced from 1.10 ± 0.47 to 0.31 ± 0.25 g L^{-1}, with a much higher average *MR* of 71.6%. TFC membrane only requires a hydraulic pressure of ~5 bar to achieve a 50% *MR*, whereas a 10-bar hydraulic pressure must be exerted on CTA membrane to obtain the same performance (Fig. 6.2D). The highest *MR* is 95.0% by applying 10-bar pressure on a lab-prepared TFC membrane with compacted woven backing fabric inside (Sahebi et al. 2017).

Some limitations and challenges must be properly addressed for PAO development. PAO may obtain a negative *MR* under certain operating conditions. For example, negative *SRSF* and *MR* (-30.7% to -61.5%) were observed in a study with an AL-DS mode, despite an enhanced water flux ($J_{w,m}$) (Blandin et al. 2013). That is probably due to the potential cracking in the supportive layer as a consequence of local stretching under hydraulic pressure, accelerating the DS partitioning process. To minimize membrane deformation and obtain a positive *MR*, appropriate spacers can be developed and placed inside PAO (Blandin et al. 2016). The magnitude of exerted hydraulic pressure is vital to yield a desirable *MR*. For example, a low hydraulic pressure (≤1 bar) can result in elevated RSF ($J_{s,m}$) (Duan et al. 2014) and a negative *MR* (-8.1% to -84.6%) (Lutchmiah et al. 2015). On the other hand, a high hydraulic pressure that theoretically yields a more reduced RSF can cause membrane cracking. Pressure-enhanced membrane fouling has been observed in PAO (Jamil et al. 2016), and may lead to fouling-enhanced concentration polarization and larger RSF (She et al. 2012). To minimize fouling-enhanced RSF, periodic chemical cleaning (Lotfi et al. 2017) or osmotic backwashing (Blandin et al. 2015) must be performed to cleanse the foulants at the expense of deteriorated pollutant rejection and shortened membrane lifespan.

6.6.2 Electrolysis-assisted Osmosis (EAO)

Electrolysis-Assisted Osmosis (EAO), or e-FO process, utilizes the electrolysis and an electric field to manipulate cross-membrane ion migration towards reduced solute permeation. Electrolysis and applied electric field have long been deployed in electrodialysis (ED) processes to drive charged ions migration across the ion exchange membrane. It has been reported that effective RSF reduction (~57% decrease) could be obtained at an applied voltage ≥ 1.5V (water splitting detected) (Zou and He 2017b). To minimize the effect of pH on electrodes and FO membrane, a unique

design of three-chamber EAO with bilateral draw chambers (hydraulically connected) and the middle feed chamber was proposed (Fig. 6.3A). In a conventional FO process with AL-FS orientation, DS will diffuse first through the support layer ($J_{s,o}^{S}$), which is governed by the Fick's law of diffusion (Fig. 6.3B black line).(Phillip et al. 2010)

$$J_s^S = -D^S \frac{dC}{dt} = -\frac{D^S}{t_S}(C_d^i - C_s^i) = -\frac{D^S}{t_S}(C_d - 0) \quad \text{(Eq. 6.16)}$$

where D^S is the DS diffusion coefficient in the supportive layer, t_S is the thickness of the supportive layer, C_d^i is the DS concentration on the surface of the support layer, C_s^i is the DS concentration on the supportive layer side of the supportive layer-active layer interface (initially equals to 0), and C_d is the DS concentration in the bulk draw solution (assuming $C_d^i \approx C_d$ under a negligible external concentration polarization) (Cath et al. 2006).

When electrolysis (H^+ reduced to H_2 at the cathode and OH^- oxidized to O_2 at the anode) is sustained in EAO, the generated electric field manipulates ion movement inside the system, and such a movement across the supportive layer ($J_{s,e}^{S}$, '*e*' stands for electrolysis) is governed by Nernst-Plank equation (Fig. 6.3B red line, initially $C_{s,e}^{i}$ =0).

$$J_{s,e}^S = -\frac{D^S}{t_S}(C_{d,e}^i - C_{s,e}^i - \frac{FzC_d}{RT}E) = -\frac{D^S}{t_S}(C_{d,e}^i - 0 - \frac{FzC_d}{RT}E) \quad (17)$$

where F is Faraday constant, z is the valence of a specific ion, R is the gas constant, T is the temperature, and E is the applied voltage. In a cathode chamber, sodium ions in both the draw and the support layer will be dragged towards the cathode electrode (i.e., the dragging effect), leading to relatively lower DS concentration on the supportive layer ($C_{d,e}^i < C_d \approx C_d^i$) and hence reduced ion transport ($J_{s,e}^S < J_s^S$). This further renders slower ion transport in the active layer under effective electrolysis ($J_{a,e}^A < J_a^A$), leading to reduced sodium concentration in the feed compared to that of conventional FO ($C_f^e < C_f$, Fig. 6.3B red line). However, the electrolysis-assisted strategy can be a double-edged sword. When electrodes pose a dragging effect towards the opposite-charged ions favoring RSF reduction in EAO, the repelling effect of those electrodes on same-charged ions can accelerate their accumulation in the boundary layer and eventually create enhanced leakage of same-charged ions. As a result, the adverse effect of repelling effect can hinder or even exceed the mitigating effect caused by the dragging effect, especially at a high applied voltage. This was

confirmed by a study that showed an increased RSF from 0.96 gMH at 1.5V to 1.35 gMH at 3V, resulting in a deteriorated *MR* from 56.9% at 1.5V to 39.4% at 3V (Fig. 6.3C). Hence, weak electrolysis (V=1.5~2.0 V) should be exploited in EAO to render stable water flux, reduced RSF, and less energy consumption (Zou and He 2017b).

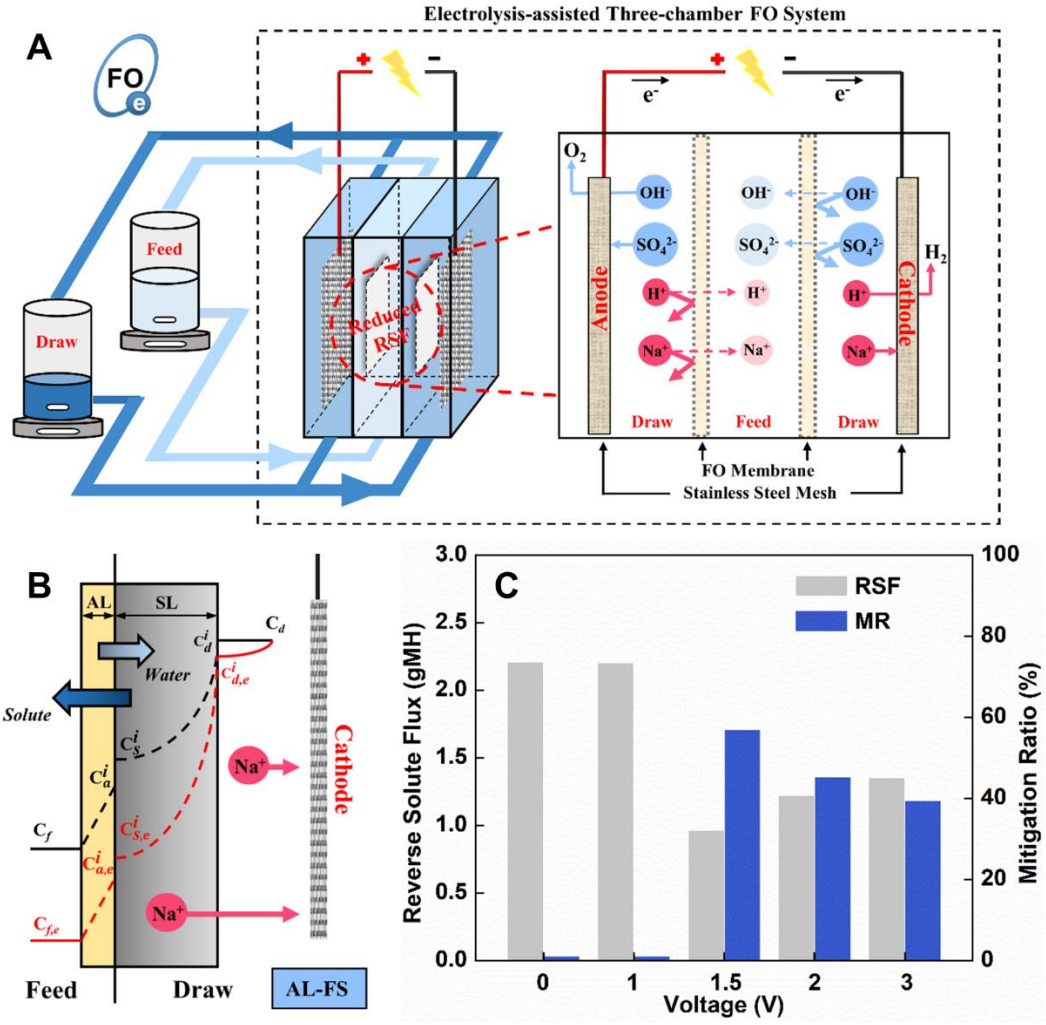

Figure 6.3 RSF reduction via electrolysis-assisted osmosis (EAO) in terms of (A) three-chamber system design, (B) conceptual illustration of ion diffusion pattern across the asymmetric FO membrane, and (C) RSF and MR under various applied voltages. Figures are adapted from a previous study with permission (Zou and He 2017b).

EAO may offer an energy-efficient solution (0.022 kWh m^{-3} recovered water, or 0.044 ± 0.002 kWh kg^{-1} reduced reversed solute) to secure an *MR* over 50%, and more research effort

should be invested to understand the underlying mechanism and to optimize system performance. Using alternative power sources to sustain an effective electric field, for example via bioelectrochemical systems, may further reduce the energy consumption of EAO while accomplishing RSF reduction (Qin et al. 2016). Selection of a suitable DS for EAO also warrants further investigation. The chemically-stable Na_2SO_4, which was used in the prior study, still requires downstream DS separation/regeneration process to produce high-quality water. As an electrochemical system, EAO needs optimized system design (e.g., chamber dimension and electrode distance) for more effective RSF control. In particular, conductive FO membrane serving as both the FO membrane and electrode will be of strong interest to achieve better electrochemical performance in EAO (Hou et al. 2018).

6.6.3 Ultrasonic-assisted Osmosis (UAO)

Ultrasonic-Assisted Osmosis (UAO) takes advantage of ultrasound to reduce ICP and has been used to concentrate fruit juice as well as the natural colorant (Chanukya and Rastogi 2017, Kowalski et al. 2015). With the aid of ultrasound, UAO gains enhanced water flux (up to 75%) at the expense of slightly increased RSF due to the combined effects of reduced ICP and localized heating (Heikkinen et al. 2017). Comparing to a conventional FO process, a reduced *SRSF* can be obtained in UAO based on Eq. 6.5 ($J_{s,m}>J_{s,o}$ while $J_{w,m}>>J_{w,o}$). For example, notably reduced *SRSF* (an MR_{TDS} of ~51.8%, Na_2SO_4 as the DS) was observed when 20-kHz ultrasound was applied in 1-min on-and-off mode, with comparable feed conductivity (mainly contributed by RSF) but an enhanced water flux from 13 LMH (FO) to 24 LMH (UAO) (Heikkinen et al. 2017). However, the effects of the operation mode on RSF reduction have yet to understand. The pulse operation (i.e., on-and-off mode) appears to be the most cost-effective mode to reduce RSF in UAO, and the optimal period for on and off operation remains to be explored. Applications of ultrasound may potentially damage membrane integrity and irreversibly alter the physicochemical features of the membrane (e.g. functional groups), leading to deteriorated RSF and even a negative *MR*. Long-term operation of UAO needs to be performed to understand system stability during RSF reduction better. In conclusion, UAO demands more investigation to demonstrate its RSF reduction performance.

6.7 Advancing Membrane development towards a Better Barrier

The existing commercial FO membranes, though progressed with increasing membrane performance and decreasing cost, still suffers from relatively high ICP and reverse solute leakage, leading to reduced $\Delta\pi_{eff}$ (lower water flux, Fig. 6.4A), gradual loss of DS, and elevated operational cost. Hence, developing the next generation FO membranes to achieve both low ICP (i.e., high $\Delta\pi_{eff}$ and more desirable water flux, Fig. 6.4B) and low solute permeation (i.e., high selectivity) is crucial towards a more environmental-friendly and cost-effective FO-based water reclamation process (Werber et al. 2016). A significant amount of research efforts have been invested in advancing material development and fabrication techniques at the lab scale (Li et al. 2016). RSF reduction can be potentially achieved in two ways, modification of existing membrane (either commercial or previously developed FO membranes) and fabrication of new membranes.

6.7.1 Membrane Modification

Membrane modification is usually realized via a surface coating on the active layer of an existing membrane (mostly TFC) to enhance antifouling and elevate surface hydrophilicity (Guo et al. 2016, Tiraferri et al. 2012), leading to reduced ICP and higher water flux (Arena et al. 2014). However, very few studies of membrane modification have focused on RSF reduction, and thus there is a limited amount of data about solute leakage (Table 6.1). An *MR* of 20.9% was estimated for a polydopamine (PDA) coated commercial TFC membrane (TFC-C0.5 in the original paper) (Guo et al. 2018). Such a reduction of RSF was likely due to that the coated PDA layer, although increasing physical water transport resistance, has enhanced membrane surface hydrophilicity while reducing the water contact angle, thereby leading to comparable water permeability coefficient and similar water flux; meanwhile, the solute permeability coefficient was reduced due to the coated PDA layer, rendering a higher salt rejection rate and resulting in a reduced *SRSF* (Eq. 6.5) and a desirable *MR* (comparing to pristine TFC). Silver nanoparticle-decorated graphene oxide nanosheets (AgNP-GO) have also been utilized as a surface modification material (Soroush et al. 2015), leading to an *MR* of up to 15.9% under the AL-DS orientation (Soroush et al. 2016) because of the enhanced water transport (~13%) sustained by improved membrane hydrophilicity (due to surface functional groups from GO and presence of cations from AgNPs) and a minor change in solute leakage (~3.5% increase in RSF). However, in some cases of membrane modification for anti-fouling enhancement, the coated layer would, unfortunately, hinder effective

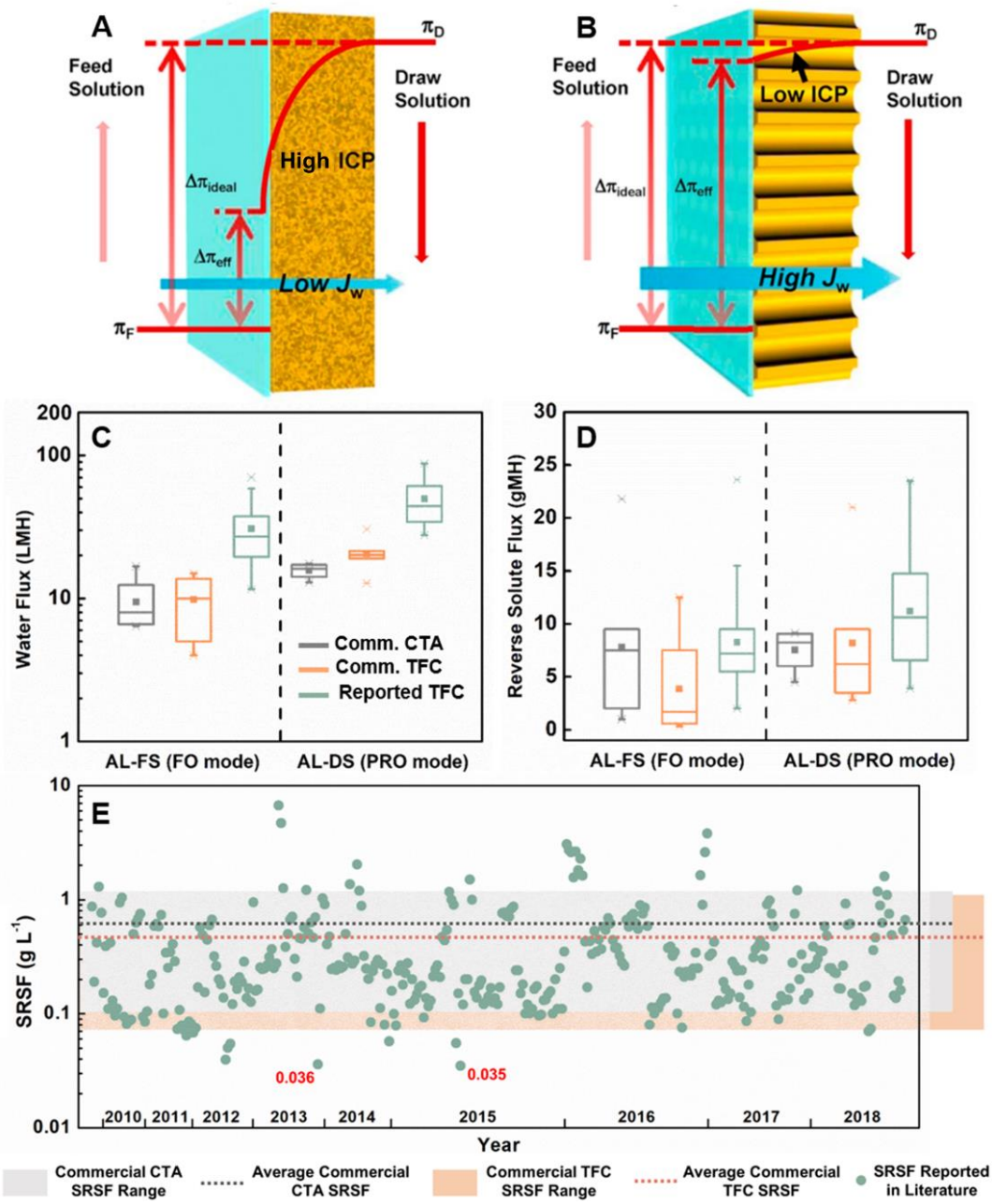

Figure 6.4 RSF reduction via new membrane fabrication in terms of (A) conventional FO membrane with a large ICP and lower water flux (AL-FS), (B) new FO membrane with a small ICP and higher water flux (AL-FS), (C) water flux and (D) RSF for commercial CTA, commercial TFC, and new TFC membrane reported in the literature with 1-M NaCl as the draw solution, and (E) SRSF reported in the literature (NaCl as the DS, sorted by year). Figure 6.4A and 6.4B are adapted from a previous study with permission (Liang et al. 2017).

water permeation ($J_{w,m}/J_{w,o}$<1) while facilitating salt permeation ($J_{s,m}/J_{s,o}$>1), rendering a negative *MR*. For example, an *MR* of -40.0 to -50.0% (Table 6.1) was obtained in TFC membranes coated with either AgNP-GO or Ag-polyethylene glycol PEGylated dendrimer nanocomposites (Soroush et al. 2015, Zhang et al. 2013). This was probably due to the introduction of biocidal surface functional groups (AgNPs) to the original ones (carboxyl groups), but the exact reasons remain unclear. Thus, more research efforts are required to fully understand the mass transport and ion interactions within the coated layer to yield both consistent antifouling performance and a positive *MR* via membrane modification.

6.7.2 Membrane Fabrication

New membrane fabrication has shown more promising results in terms of RSF reduction. We have analyzed more than 70 studies published in the past decade (2008-2018) to provide a comprehensive evaluation and comparison of solute flux, *SRSF*, and *MR* among various modified membranes (Table 6.2), including optimized substrate composition (e.g. addition of exotic polymers and nanomaterials into polyethersulfone (PES) (Wang et al. 2015, Widjojo et al. 2011), polysulfone (PSF) (Emadzadeh et al. 2014, Han et al. 2012), polyacrylonitrile (PAN) (Bui and McCutcheon 2016), or polyvinylidene fluoride (PVDF) (Obaid et al. 2016)), advanced substrate fabrication (e.g. double-blade casting and nonsolvent induced phase separation) (Liu and Ng 2014, Yasukawa et al. 2015), selection of novel supporting materials (e.g. commercially available nylon 6,6 microfiltration membrane) (Huang et al. 2013), and new development of active layer (e.g. addition of graphene oxide or molecular layer-by-layer assembly/deposition instead of conventional interfacial polymerization) (Kwon et al. 2015, Shen et al. 2016). A major research shift from CTA to TFC membrane was observed (especially in the past five years), with the latter being used in over 90% of the studies. The newly developed TFC FO membranes have exhibited an average water flux of 30.7 ± 14.4 LMH (AL-FS orientation, n=35 data points) or 49.9 ± 19.0 LMH (AL-DS orientation, n=32 data points) by using 1-M NaCl as the draw solution (Fig. 6.4C), much higher (p<0.05) than that of either commercial TFC membranes (9.8 ± 4.0 and 20.7± 4.4 LMH) or commercial CTA (9.5 ± 3.5 and 15.7 ± 1.8 LMH). The highest water flux of 70.3 and 84.2 LMH (AL-FS and AL-DS orientations, unless otherwise stated) was reported for a TFC membrane with vertically oriented porous substrates to significantly facilitate mass transport and reduce ICP (Liang et al. 2017).

Despite enhanced water flux, the newly developed TFC membranes have comparable RSF (1-M NaCl as the draw, 8.23 ± 4.66 gMH under AL-FS and 11.23 ± 5.23 gMH under AL-DS, p>0.05) to that of the commercial TFC (3.84 ± 4.24 under AL-FS and 8.20 ± 6.36 gMH under AL-DS) or commercial CTA (7.53 ± 1.86 gMH under AL-DS) (Fig. 6.4D). However, solute leakage propensity of an FO membrane needs to be analyzed by considering water flux, and the available *SRSF* from literature is provided in Fig. 6.4E (n=362 data points, sorted by year). When NaCl is selected as the DS, the commercial CTA membranes exhibit an average *SRSF* of 0.60 ± 0.32 g L^{-1} (0.10-1.29 g L^{-1}). The lowest *SRSF* (0.10 g L^{-1}) was reported with a CTA-NW flat sheet membrane manufactured by HTI (Wei et al. 2011). As for the commercial TFC membranes, an average *SRSF* value of 0.44 ± 0.32 g L^{-1} (0.07-1.17 g L^{-1}) has been reported. The lowest *SRSF* of a commercial TFC was obtained in a hollow fiber membrane (HF-B in the original study) manufactured by Toyobo Co., Ltd (Ren and McCutcheon 2018). By taking advantage of new membrane fabrication, *SRSF* could be significantly decreased, comparing to commercial membranes (*SRSF*<0.10 g L^{-1}, Table 6.2). For example, a novel hydrophilic nylon 6,6 microfiltration membrane supported TFC showed an *SRSF* of 0.036 g L^{-1} under the AL-DS orientation (Huang et al. 2013), owing to a notably higher water permeability coefficient (A=0.917 L m^{-2} h^{-1} bar^{-1}, twice that of HTI CTA), a much reduced solute permeability coefficient (B=0.300 L m^{-2} h^{-1}, 31.8% of HTI CTA), and a desirable membrane structure parameter (S=1940 μm, twice that of HTI CTA). The same research group reproduced a similar *SRSF* of 0.035 g L^{-1} via selecting nylon 6,6 microfiltration membrane as novel supporting material, rendering an *MR* of 92.4% and 92.0% compared to that of commercial CTA and TFC membrane) (Huang and McCutcheon 2015). In addition to the selection of novel supporting materials for TFC (Duong et al. 2015, Li et al. 2012), *SRSF* could also be reduced to less than 0.10 g L^{-1} via optimized substrate composition (Bui and McCutcheon 2013), advanced substrate fabrication (instead of conventional wet phase inversion) (Luo et al. 2014b, Shi et al. 2011, Xiao et al. 2015), and new development of active layer (Shen et al. 2016) (Table 6.2). Nonetheless, the majority of *SRSF* reported from new membrane fabrication falls inside the *SRSF* range of commercial ones, especially in the past three years (Fig. 6.4E). Based on the current analysis and results, neither membrane modification nor new membrane fabrication has achieved consistent results for notably reducing solute permeation. Several new membranes with significantly lower *SRSF* should be further examined for reliable

performance under varied conditions (e.g., feeding stream, operating conditions, etc.). Future efforts should consider RSF reduction in such design/development of FO membranes.

6.8 Future of RSF Control

To further advance RSF control for facilitating FO development, extensive efforts are still required in several aspects. RSF mitigation via smart selection of DS with low leakage propensity will be desired. These novel DS, especially stimuli-responsive polymers, can potentially achieve RSF mitigation due to their relatively large hydrodynamic diameter (>100 nm) (Hartanto et al. 2015) and membrane size exclusion effect. Stimuli-responsive substances have been studied as DS in recent years because they can be regenerated via reversible separation under a certain stimulus, such as temperature, pH, magnetic field, electric, or light (Fig. 6.5) (Razmjou et al. 2015). As a result, much less energy, compared to that of conventional inorganic DS, will be required in the DS separation/regeneration process. For example, polyacrylic acid sodium salts (PAA-Na) is a well-studied pH-responsive DS (Ge et al. 2012a, Gwak et al. 2015). Besides good water extraction capability (up to 25 LMH water flux) (Ge et al. 2012b), PAA-Na also exhibits extremely low RSF (0.004-0.08 gMH for CTA and 0.002-0.009 gMH for TFC), and very low *SRSF* (0.002-0.007 g L^{-1} for PAA-Na with a Mw of 2,000-5,000 and less than 0.001 g L^{-1} for PAA-Na with a Mw of 50,000) due to size exclusion (hydrodynamic diameter > 120 nm) (Yang et al. 2017). Nonetheless, little RSF data can be found for most thermal-, magnetic-, electric-, or light-responsive DS (to the best of our knowledge), making it extremely difficult to evaluate RSF decrease for these "smart" DS. Enhanced reporting of RSF data (*SRSF* and/or *MR*) should be encouraged in future research/development effort to render a comprehensive review.

Adding surfactant as an additive into conventional inorganic DS provides another promising solution for effective RSF reduction. Surfactants have been proposed as a DS since 2014 with low RSF due to their low level of high-micellar mass (14,000-29,000 g mol^{-1}) and membrane size exclusion effect (Gadelha et al. 2014). However, surfactants are subject to difficult regeneration process, requiring high energy investment and operation cost. Alternatively, surfactants have been added into conventional inorganic DS (e.g., $MgCl_2$) as an additive (at a minimal amount) (Nguyen et al. 2015), achieving desirable water flux (11.4 LMH) while providing sufficient electrostatic repulsion force to reduce RSF (RSF of 2.03 gMH and SRSF of 0.18 g L^{-1})

(Nguyen et al. 2016). Recently, one surfactant, Tergitol 15-S-9, was added as an additive in a fertilizer-driven FO using $(NH_4)_2SO_4$ as the DS (TFC membrane), resulting in an *MR* of over 50% achieved with a dosage of only 0.25 mM (*SRSF* reduced from 0.18 to 0.09 g L^{-1}) (Chekli et al. 2018). Those preliminary results have demonstrated that surfactant additives are worth further research effort for RSF reduction. However, the fate, transport, and potential health effects of surfactants, even at extremely low concentrations in the final draw solution, should be carefully evaluated in a regeneration-free FO process (e.g., direct fertigation in fertilizer-driven FO).

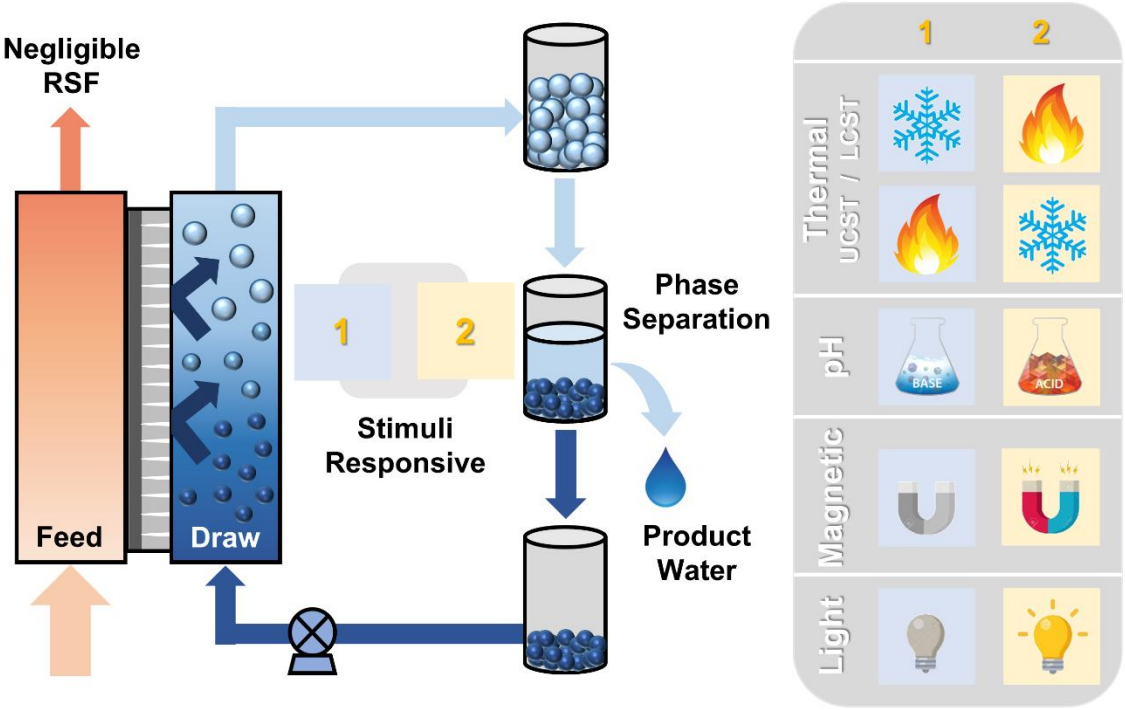

Figure 6.5 RSF mitigation via smart selection of stimuli-responsive draw solutes in FO. Reduced RSF should be expected due to size exclusion.

The relevant data for better understanding of RSF reduction and mitigation should be properly presented. Parameters such as *SRSF* and *MR* should be analyzed in parallel with conventional performance index (e.g., water flux and RSF) and membrane intrinsic constant (e.g., water permeation coefficient and solute diffusion coefficient). Report of *SRSF* and/or *MR*, especially for those stimuli-responsive polymers, can enable more accurate assessment for overall system performance. A threshold *SRSF* value (e.g., *SRSF*<0.1 g L^{-1}) should be proposed and used

for future RSF control studies to enable better comparison. Meanwhile, though mathematical modeling of solute transport has been conducted for pristine FO membranes to evaluate the effect of concentration polarization, solute-solvent interaction, solute-solute interaction, and chemical equilibrium (detailed studies listed in Introduction section), such research efforts have not been well utilized to better understand the RSF reduction performance and reveal the underlying mechanism of an RSF control strategy. For example, existing models should further extend to investigate ion transport (migration/diffusion) within the coating layer. Furthermore, RSF control has received much less attention compared to anti-fouling research in the FO field, though these two subjects are closely correlated in terms of operational strategies and advanced membrane development. A large RSF may increase biofouling and scaling, whereas the deposited cake layer can promote solute leakage as well. Hence, RSF control should be strongly related to membrane anti-fouling features. Last but not the least, complete elimination of RSF may not be possible, and thus effective backup strategies should be developed to neutralize salinity buildup (i.e., the consequence of RSF) on the feed side via solute removal or recovery. In terms of solute removal, physical separation of reverse-fluxed DS usually utilizes a parallel MF or UF system to create a "backdoor" for accumulated salts (Luo et al. 2015); Chemical separation takes advantage of reverse-fluxed DS to facilitate resource recovery via induced chemical precipitation (Xie et al. 2014); Biological removal depends on the degradation and assimilation of microorganisms to eliminate biodegradable DS (Li et al. 2015). Solute recovery, instead of removal, provides a better option to reuse and regenerate reverse-fluxed DS and can be realized with the help of electric field (e.g. bioelectrochemical system or electrodialysis) to separate charged DS ions from the feed stream (Qin and He 2014, Zou and He 2017a).

6.9 Conclusions

In this review, we have evaluated the potential strategies to decrease reverse permeation of draw solutes in FO processes with the following conclusions:

- RSF is a critical challenge in FO-based water treatment. To accurately quantify the leakage magnitude of DS and evaluate overall FO performance, *SRSF* and/or *MR* should be analyzed and reported together with conventional performance index (e.g., water flux and RSF) and membrane intrinsic constant (e.g., water permeation and solute diffusion coefficients).

- RSF reduction can be effectively achieved via operational strategies, including pressure-, electrolysis-, and ultrasonic-assisted osmosis. PAO is able to yield a reduced $\Delta\pi_{eff}$ via exerting a relatively low hydraulic pressure on the feed side (<10 bar) to achieve an *MR* as high as 95.0%. EAO takes advantage of the electric field to manipulate ion migration across the FO membrane, offering an energy-efficient solution (0.022 kWh m^{-3}, 1.5 V) to secure an over 50% *MR*. UAO harnesses the power of ultrasound to reduce ICP, rendering an MR_{TDS} of ~51.8% at the expense of high energy consumption. The research results encourage the further effort to optimize system design, develop a robust membrane, enhance system stability, and evaluate long-term reduction.
- RSF reduction can also be realized via advanced membrane development, including membrane modification and fabrication. Existing membrane modification via a surface coating on active layer can yield an *MR* over 20%, and more research efforts are required to understand better the mass transport and ion interactions within the coated layer to yield both consistent antifouling performance and a positive *MR*. New membrane fabrication has shown more promising results and can achieve significantly reduced *SRSF* (an *MR* over 92%).
- The future of RSF control lies in the further development of "smart" DS, particularly large-size stimuli-responsive polymers, enhanced reporting of RSF data (*SRSF* and/or *MR*), mathematical modeling to decipher underlying mechanism, comprehensive investigation of the relationship between RSF and fouling, and cost-effective strategies to neutralize salinity buildup.

References

Akther, N., Sodiq, A., Giwa, A., Daer, S., Arafat, H.A. and Hasan, S.W. (2015) Recent advancements in forward osmosis desalination: A review. Chemical Engineering Journal 281, 502-522.

Arena, J.T., Manickam, S.S., Reimund, K.K., Freeman, B.D. and McCutcheon, J.R. (2014) Solute and water transport in forward osmosis using polydopamine modified thin film composite membranes. Desalination 343, 8-16.

Banchik, L.D., Weiner, A.M., Al-Anzi, B. and Lienhard V, J.H. (2016) System scale analytical modeling of forward and assisted forward osmosis mass exchangers with a case study on fertigation. Journal of Membrane Science 510, 533-545.

Blandin, G., Myat, D.T., Verliefde, A.R.D. and Le-Clech, P. (2017) Pressure assisted osmosis using nanofiltration membranes (PAO-NF): Towards higher efficiency osmotic processes. Journal of Membrane Science 533, 250-260.

Blandin, G., Verliefde, A.R. and Le-Clech, P. (2015) Pressure enhanced fouling and adapted anti-fouling strategy in pressure assisted osmosis (PAO). Journal of Membrane Science 493, 557-567.

Blandin, G., Verliefde, A.R., Tang, C.Y., Childress, A.E. and Le-Clech, P. (2013) Validation of assisted forward osmosis (AFO) process: impact of hydraulic pressure. Journal of Membrane Science 447, 1-11.

Blandin, G., Vervoort, H., D'Haese, A., Schoutteten, K., Bussche, J.V., Vanhaecke, L., Myat, D.T., Le-Clech, P. and Verliefde, A.R.D. (2016) Impact of hydraulic pressure on membrane deformation and trace organic contaminants rejection in pressure assisted osmosis (PAO). Process Safety and Environmental Protection 102, 316-327.

Bowden, K.S., Achilli, A. and Childress, A.E. (2012) Organic ionic salt draw solutions for osmotic membrane bioreactors. Bioresource Technology 122, 207-216.

Bui, N.-N. and McCutcheon, J.R. (2013) Hydrophilic Nanofibers as New Supports for Thin Film Composite Membranes for Engineered Osmosis. Environmental Science & Technology 47(3), 1761-1769.

Bui, N.-N. and McCutcheon, J.R. (2016) Nanoparticle-embedded nanofibers in highly permselective thin-film nanocomposite membranes for forward osmosis. Journal of Membrane Science 518, 338-346.

Cai, Y. and Hu, X.M. (2016) A critical review on draw solutes development for forward osmosis. Desalination 391, 16-29.

Cath, T.Y., Childress, A.E. and Elimelech, M. (2006) Forward osmosis: principles, applications, and recent developments. Journal of Membrane Science 281(1), 70-87.

Chanukya, B.S. and Rastogi, N.K. (2017) Ultrasound assisted forward osmosis concentration of fruit juice and natural colorant. Ultrasonics Sonochemistry 34, 426-435.

Chekli, L., Pathak, N., Kim, Y., Phuntsho, S., Li, S., Ghaffour, N., Leiknes, T. and Shon, H.K. (2018) Combining high performance fertiliser with surfactants to reduce the reverse solute flux in the fertiliser drawn forward osmosis process. Journal of Environmental Management 226, 217-225.

Chekli, L., Phuntsho, S., Kim, J.E., Kim, J., Choi, J.Y., Choi, J.-S., Kim, S., Kim, J.H., Hong, S. and Sohn, J. (2016) A comprehensive review of hybrid forward osmosis systems: Performance, applications and future prospects. Journal of Membrane Science 497, 430-449.

Chekli, L., Phuntsho, S., Shon, H.K., Vigneswaran, S., Kandasamy, J. and Chanan, A. (2012) A review of draw solutes in forward osmosis process and their use in modern applications. Desalination and Water Treatment 43(1-3), 167-184.

Chung, T.-S., Li, X., Ong, R.C., Ge, Q., Wang, H. and Han, G. (2012a) Emerging forward osmosis (FO) technologies and challenges ahead for clean water and clean energy applications. Current Opinion in Chemical Engineering 1(3), 246-257.

Chung, T.-S., Zhang, S., Wang, K.Y., Su, J. and Ling, M.M. (2012b) Forward osmosis processes: yesterday, today and tomorrow. Desalination 287, 78-81.

Coday, B.D., Heil, D.M., Xu, P. and Cath, T.Y. (2013) Effects of transmembrane hydraulic pressure on performance of forward osmosis membranes. Environmental Science & Technology 47(5), 2386-2393.

Coday, B.D., Xu, P., Beaudry, E.G., Herron, J., Lampi, K., Hancock, N.T. and Cath, T.Y. (2014a) The sweet spot of forward osmosis: treatment of produced water, drilling wastewater, and other complex and difficult liquid streams. Desalination 333(1), 23-35.

Coday, B.D., Yaffe, B.G., Xu, P. and Cath, T.Y. (2014b) Rejection of trace organic compounds by forward osmosis membranes: a literature review. Environmental Science & Technology 48(7), 3612-3624.

Davenport, D.M., Deshmukh, A., Werber, J.R. and Elimelech, M. (2018) High-Pressure Reverse Osmosis for Energy-Efficient Hypersaline Brine Desalination: Current Status, Design Considerations, and Research Needs. Environmental Science & Technology Letters 5(8), 467-475.

Duan, J., Litwiller, E. and Pinnau, I. (2014) Solution-diffusion with defects model for pressure-assisted forward osmosis. Journal of Membrane Science 470, 323-333.

Duong, P.H., Chisca, S., Hong, P.-Y., Cheng, H., Nunes, S.P. and Chung, T.-S. (2015) Hydroxyl functionalized polytriazole-co-polyoxadiazole as substrates for forward osmosis membranes. ACS Applied Materials & Interfaces 7(7), 3960-3973.

Emadzadeh, D., Lau, W.J., Matsuura, T., Rahbari-Sisakht, M. and Ismail, A.F. (2014) A novel thin film composite forward osmosis membrane prepared from PSf–TiO2 nanocomposite substrate for water desalination. Chemical Engineering Journal 237, 70-80.

Gadelha, G., Nawaz, M.S., Hankins, N.P., Khan, S.J., Wang, R. and Tang, C.Y. (2014) Assessment of micellar solutions as draw solutions for forward osmosis. Desalination 354, 97-106.

Ge, Q., Ling, M. and Chung, T.-S. (2013) Draw solutions for forward osmosis processes: developments, challenges, and prospects for the future. Journal of Membrane Science 442, 225-237.

Ge, Q., Su, J., Amy, G.L. and Chung, T.-S. (2012a) Exploration of polyelectrolytes as draw solutes in forward osmosis processes. Water Research 46(4), 1318-1326.

Ge, Q., Wang, P., Wan, C. and Chung, T.-S. (2012b) Polyelectrolyte-promoted forward osmosis–membrane distillation (FO–MD) hybrid process for dye wastewater treatment. Environmental Science & Technology 46(11), 6236-6243.

Guo, H., Deng, Y., Tao, Z., Yao, Z., Wang, J., Lin, C., Zhang, T., Zhu, B. and Tang, C.Y. (2016) Does hydrophilic polydopamine coating enhance membrane rejection of hydrophobic endocrine-disrupting compounds? Environmental Science & Technology Letters 3(9), 332-338.

Guo, H., Yao, Z., Wang, J., Yang, Z., Ma, X. and Tang, C.Y. (2018) Polydopamine coating on a thin film composite forward osmosis membrane for enhanced mass transport and antifouling performance. Journal of Membrane Science 551, 234-242.

Gwak, G., Jung, B., Han, S. and Hong, S. (2015) Evaluation of poly (aspartic acid sodium salt) as a draw solute for forward osmosis. Water Research 80, 294-305.

Han, G., Zhang, S., Li, X. and Chung, T.-S. (2015) Progress in pressure retarded osmosis (PRO) membranes for osmotic power generation. Progress in Polymer Science 51, 1-27.

Han, G., Zhang, S., Li, X., Widjojo, N. and Chung, T.-S. (2012) Thin film composite forward osmosis membranes based on polydopamine modified polysulfone substrates with enhancements in both water flux and salt rejection. Chemical Engineering Science 80, 219-231.

Hancock, N.T. and Cath, T.Y. (2009) Solute coupled diffusion in osmotically driven membrane processes. Environmental Science & Technology 43(17), 6769-6775.

Hartanto, Y., Yun, S., Jin, B. and Dai, S. (2015) Functionalized thermo-responsive microgels for high performance forward osmosis desalination. Water Research 70, 385-393.

Heikkinen, J., Kyllönen, H., Järvelä, E., Grönroos, A. and Tang, C.Y. (2017) Ultrasound-assisted forward osmosis for mitigating internal concentration polarization. Journal of Membrane Science 528, 147-154.

Hou, D., Iddya, A., Chen, X., Wang, M., Zhang, W., Ding, Y., Jassby, D. and Ren, Z.J. (2018) Nickel-Based Membrane Electrodes Enable High-Rate Electrochemical Ammonia Recovery. Environmental Science & Technology 52(15), 8930-8938.

Huang, L., Bui, N.-N., Meyering, M.T., Hamlin, T.J. and McCutcheon, J.R. (2013) Novel hydrophilic nylon 6, 6 microfiltration membrane supported thin film composite membranes for engineered osmosis. Journal of Membrane Science 437, 141-149.

Huang, L. and McCutcheon, J.R. (2015) Impact of support layer pore size on performance of thin film composite membranes for forward osmosis. Journal of Membrane Science 483, 25-33.

Irvine, G.J., Rajesh, S., Georgiadis, M. and Phillip, W.A. (2013) Ion selective permeation through cellulose acetate membranes in forward osmosis. Environmental Science & Technology 47(23), 13745-13753.

Jamil, S., Jeong, S. and Vigneswaran, S. (2016) Application of pressure assisted forward osmosis for water purification and reuse of reverse osmosis concentrate from a water reclamation plant. Separation and Purification Technology 171, 182-190.

Kowalski, S.J., Szadzińska, J. and Pawłowski, A. (2015) Ultrasonic-Assisted Osmotic Dehydration of Carrot Followed by Convective Drying with Continuous and Intermittent Heating. Drying Technology 33(13), 1570-1580.
Kwon, S.-B., Lee, J.S., Kwon, S.J., Yun, S.-T., Lee, S. and Lee, J.-H. (2015) Molecular layer-by-layer assembled forward osmosis membranes. Journal of Membrane Science 488, 111-120.
Lee, K., Baker, R. and Lonsdale, H. (1981) Membranes for power generation by pressure-retarded osmosis. Journal of Membrane Science 8(2), 141-171.
Lee, S., Boo, C., Elimelech, M. and Hong, S. (2010) Comparison of fouling behavior in forward osmosis (FO) and reverse osmosis (RO). Journal of Membrane Science 365(1), 34-39.
Li, D., Yan, Y. and Wang, H. (2016) Recent advances in polymer and polymer composite membranes for reverse and forward osmosis processes. Progress in Polymer Science 61, 104-155.
Li, X., Lu, Y. and He, Z. (2015) Removal of reverse-fluxed ammonium by anammox in a forward osmosis system using ammonium bicarbonate as a draw solute. Journal of Membrane Science 495, 424-430.
Li, X., Wang, K.Y., Helmer, B. and Chung, T.-S. (2012) Thin-film composite membranes and formation mechanism of thin-film layers on hydrophilic cellulose acetate propionate substrates for forward osmosis processes. Industrial & Engineering Chemistry Research 51(30), 10039-10050.
Liang, H.-Q., Hung, W.-S., Yu, H.-H., Hu, C.-C., Lee, K.-R., Lai, J.-Y. and Xu, Z.-K. (2017) Forward osmosis membranes with unprecedented water flux. Journal of Membrane Science 529, 47-54.
Liu, X. and Ng, H.Y. (2014) Double-blade casting technique for optimizing substrate membrane in thin-film composite forward osmosis membrane fabrication. Journal of Membrane Science 469, 112-126.
Lotfi, F., Chekli, L., Phuntsho, S., Hong, S., Choi, J.Y. and Shon, H.K. (2017) Understanding the possible underlying mechanisms for low fouling tendency of the forward osmosis and pressure assisted osmosis processes. Desalination 421, 89-98.
Lu, X., Boo, C., Ma, J. and Elimelech, M. (2014) Bidirectional Diffusion of Ammonium and Sodium Cations in Forward Osmosis: Role of Membrane Active Layer Surface Chemistry and Charge. Environmental Science & Technology 48(24), 14369-14376.
Lu, Y. and He, Z. (2015) Mitigation of Salinity Buildup and Recovery of Wasted Salts in a Hybrid Osmotic Membrane Bioreactor–Electrodialysis System. Environmental Science & Technology 49(17), 10529-10535.
Luo, H., Wang, Q., Zhang, T.C., Tao, T., Zhou, A., Chen, L. and Bie, X. (2014a) A review on the recovery methods of draw solutes in forward osmosis. Journal of Water Process Engineering 4, 212-223.
Luo, L., Wang, P., Zhang, S., Han, G. and Chung, T.-S. (2014b) Novel thin-film composite tri-bore hollow fiber membrane fabrication for forward osmosis. Journal of Membrane Science 461, 28-38.
Luo, W., Hai, F.I., Kang, J., Price, W.E., Nghiem, L.D. and Elimelech, M. (2015) The role of forward osmosis and microfiltration in an integrated osmotic-microfiltration membrane bioreactor system. Chemosphere 136, 125-132.
Lutchmiah, K., Harmsen, D.J.H., Wols, B.A., Rietveld, L.C., Jianjun, Q. and Cornelissen, E.R. (2015) Continuous and discontinuous pressure assisted osmosis (PAO). Journal of Membrane Science 476, 182-193.
Lutchmiah, K., Verliefde, A., Roest, K., Rietveld, L.C. and Cornelissen, E.R. (2014) Forward osmosis for application in wastewater treatment: a review. Water Research 58, 179-197.
McCutcheon, J.R. and Elimelech, M. (2006) Influence of concentrative and dilutive internal concentration polarization on flux behavior in forward osmosis. Journal of Membrane Science 284(1), 237-247.
Nguyen, H.T., Chen, S.-S., Nguyen, N.C., Ngo, H.H., Guo, W. and Li, C.-W. (2015) Exploring an innovative surfactant and phosphate-based draw solution for forward osmosis desalination. Journal of Membrane Science 489, 212-219.

Nguyen, N.C., Chen, S.-S., Nguyen, H.T., Ray, S.S., Ngo, H.H., Guo, W. and Lin, P.-H. (2016) Innovative sponge-based moving bed–osmotic membrane bioreactor hybrid system using a new class of draw solution for municipal wastewater treatment. Water Research 91, 305-313.
Obaid, M., Ghouri, Z.K., Fadali, O.A., Khalil, K.A., Almajid, A.A. and Barakat, N.A. (2016) Amorphous SiO2 NP-incorporated poly (vinylidene fluoride) electrospun nanofiber membrane for high flux forward osmosis desalination. ACS Applied Materials & Interfaces 8(7), 4561-4574.
Paul, D.R. (2004) Reformulation of the solution-diffusion theory of reverse osmosis. Journal of Membrane Science 241(2), 371-386.
Phillip, W.A., Yong, J.S. and Elimelech, M. (2010) Reverse draw solute permeation in forward osmosis: modeling and experiments. Environmental Science & Technology 44(13), 5170-5176.
Qin, M., Abu-Reesh, I.M. and He, Z. (2016) Effects of current generation and electrolyte pH on reverse salt flux across thin film composite membrane in osmotic microbial fuel cells. Water Research 105, 583-590.
Qin, M. and He, Z. (2014) Self-Supplied Ammonium Bicarbonate Draw Solute for Achieving Wastewater Treatment and Recovery in a Microbial Electrolysis Cell-Forward Osmosis-Coupled System. Environmental Science & Technology Letters 1(10), 437-441.
Razmjou, A., Simon, G.P. and Wang, H. (2015) Forward Osmosis: Fundamentals and Applications, pp. 129-149.
Ren, J. and McCutcheon, J.R. (2018) A new commercial biomimetic hollow fiber membrane for forward osmosis. Desalination 442, 44-50.
Sahebi, S., Phuntsho, S., Tijing, L., Han, G., Han, D.S., Abdel-Wahab, A. and Shon, H.K. (2017) Thin-film composite membrane on a compacted woven backing fabric for pressure assisted osmosis. Desalination 406, 98-108.
Sarkar, S., SenGupta, A.K. and Prakash, P. (2010) The Donnan membrane principle: opportunities for sustainable engineered processes and materials. Environmental Science & Technology 44(4), 1161-1166.
Shaffer, D.L., Werber, J.R., Jaramillo, H., Lin, S. and Elimelech, M. (2015) Forward osmosis: Where are we now? Desalination 356, 271.
She, Q., Jin, X., Li, Q. and Tang, C.Y. (2012) Relating reverse and forward solute diffusion to membrane fouling in osmotically driven membrane processes. Water Research 46(7), 2478-2486.
Shen, L., Xiong, S. and Wang, Y. (2016) Graphene oxide incorporated thin-film composite membranes for forward osmosis applications. Chemical Engineering Science 143, 194-205.
Shi, L., Chou, S., Wang, R., Fang, W., Tang, C. and Fane, A. (2011) Effect of substrate structure on the performance of thin-film composite forward osmosis hollow fiber membranes. Journal of Membrane Science 382(1-2), 116-123.
Shibuya, M., Yasukawa, M., Takahashi, T., Miyoshi, T., Higa, M. and Matsuyama, H. (2015) Effects of operating conditions and membrane structures on the performance of hollow fiber forward osmosis membranes in pressure assisted osmosis. Desalination 365, 381-388.
Soroush, A., Ma, W., Cyr, M., Rahaman, M.S., Asadishad, B. and Tufenkji, N. (2016) In Situ Silver Decoration on Graphene Oxide-Treated Thin Film Composite Forward Osmosis Membranes: Biocidal Properties and Regeneration Potential. Environmental Science & Technology Letters 3(1), 13-18.
Soroush, A., Ma, W., Silvino, Y. and Rahaman, M.S. (2015) Surface modification of thin film composite forward osmosis membrane by silver-decorated graphene-oxide nanosheets. Environmental Science: Nano 2(4), 395-405.
Straub, A.P., Deshmukh, A. and Elimelech, M. (2016) Pressure-retarded osmosis for power generation from salinity gradients: is it viable? Energy & Environmental Science 9(1), 31-48.
Su, J. and Chung, T.-S. (2011) Sublayer structure and reflection coefficient and their effects on concentration polarization and membrane performance in FO processes. Journal of Membrane Science 376(1-2), 214-224.

Tiraferri, A., Kang, Y., Giannelis, E.P. and Elimelech, M. (2012) Superhydrophilic thin-film composite forward osmosis membranes for organic fouling control: fouling behavior and antifouling mechanisms. Environmental Science & Technology 46(20), 11135-11144.
Valladares Linares, R., Li, Z., Sarp, S., Bucs, S.S., Amy, G. and Vrouwenvelder, J.S. (2014) Forward osmosis niches in seawater desalination and wastewater reuse. Water Research 66, 122-139.
Wang, R., Shi, L., Tang, C.Y., Chou, S., Qiu, C. and Fane, A.G. (2010) Characterization of novel forward osmosis hollow fiber membranes. Journal of Membrane Science 355(1), 158-167.
Wang, Y., Ou, R., Wang, H. and Xu, T. (2015) Graphene oxide modified graphitic carbon nitride as a modifier for thin film composite forward osmosis membrane. Journal of Membrane Science 475, 281-289.
Wei, J., Qiu, C., Tang, C.Y., Wang, R. and Fane, A.G. (2011) Synthesis and characterization of flat-sheet thin film composite forward osmosis membranes. Journal of Membrane Science 372(1-2), 292-302.
Werber, J.R., Deshmukh, A. and Elimelech, M. (2016) The Critical Need for Increased Selectivity, Not Increased Water Permeability, for Desalination Membranes. Environmental Science & Technology Letters 3(4), 112-120.
Widjojo, N., Chung, T.-S., Weber, M., Maletzko, C. and Warzelhan, V. (2011) The role of sulphonated polymer and macrovoid-free structure in the support layer for thin-film composite (TFC) forward osmosis (FO) membranes. Journal of Membrane Science 383(1-2), 214-223.
Wu, S., Zou, S., Yang, Y., Qian, G. and He, Z. (2018a) Enhancing the performance of an osmotic microbial fuel cell through self-buffering with reverse-fluxed sodium bicarbonate. Chemical Engineering Journal 349, 241-248.
Wu, Z., Zou, S., Zhang, B., Wang, L. and He, Z. (2018b) Forward osmosis promoted in-situ formation of struvite with simultaneous water recovery from digested swine wastewater. Chemical Engineering Journal 342, 274-280.
Xiao, P., Nghiem, L.D., Yin, Y., Li, X.-M., Zhang, M., Chen, G., Song, J. and He, T. (2015) A sacrificial-layer approach to fabricate polysulfone support for forward osmosis thin-film composite membranes with reduced internal concentration polarisation. Journal of Membrane Science 481, 106-114.
Xie, M., Nghiem, L.D., Price, W.E. and Elimelech, M. (2014) Toward resource recovery from wastewater: extraction of phosphorus from digested sludge using a hybrid forward osmosis–membrane distillation process. Environmental Science & Technology Letters 1(2), 191-195.
Xie, M., Price, W.E., Nghiem, L.D. and Elimelech, M. (2013) Effects of feed and draw solution temperature and transmembrane temperature difference on the rejection of trace organic contaminants by forward osmosis. Journal of Membrane Science 438, 57-64.
Yang, Y., Chen, M., Zou, S., Yang, X., Long, T.E. and He, Z. (2017) Efficient recovery of polyelectrolyte draw solutes in forward osmosis towards sustainable water treatment. Desalination 422, 134-141.
Yaroshchuk, A. (2010) Influence of osmosis on the diffusion from concentrated solutions through composite/asymmetric membranes: Theoretical analysis. Journal of Membrane Science 355(1-2), 98-103.
Yasukawa, M., Mishima, S., Shibuya, M., Saeki, D., Takahashi, T., Miyoshi, T. and Matsuyama, H. (2015) Preparation of a forward osmosis membrane using a highly porous polyketone microfiltration membrane as a novel support. Journal of Membrane Science 487, 51-59.
Yip, N.Y., Tiraferri, A., Phillip, W.A., Schiffman, J.D. and Elimelech, M. (2010) High performance thin-film composite forward osmosis membrane. Environmental Science & Technology 44(10), 3812-3818.
Yong, J.S., Phillip, W.A. and Elimelech, M. (2012a) Coupled reverse draw solute permeation and water flux in forward osmosis with neutral draw solutes. Journal of Membrane Science 392–393, 9-17.
Yong, J.S., Phillip, W.A. and Elimelech, M. (2012b) Reverse permeation of weak electrolyte draw solutes in forward osmosis. Industrial & Engineering Chemistry Research 51(41), 13463-13472.

Yun, T., Kim, Y.-J., Lee, S., Hong, S. and Kim, G.I. (2014) Flux behavior and membrane fouling in pressure-assisted forward osmosis. Desalination and Water Treatment 52(4-6), 564-569.
Zhang, M., She, Q., Yan, X. and Tang, C.Y. (2017) Effect of reverse solute diffusion on scaling in forward osmosis: A new control strategy by tailoring draw solution chemistry. Desalination 401, 230-237.
Zhang, S., Qiu, G., Ting, Y.P. and Chung, T.-S. (2013) Silver–PEGylated dendrimer nanocomposite coating for anti-fouling thin film composite membranes for water treatment. Colloids and Surfaces A: Physicochemical and Engineering Aspects 436, 207-214.
Zhao, S. and Zou, L. (2011) Relating solution physicochemical properties to internal concentration polarization in forward osmosis. Journal of Membrane Science 379(1), 459-467.
Zhao, S., Zou, L., Tang, C.Y. and Mulcahy, D. (2012) Recent developments in forward osmosis: opportunities and challenges. Journal of Membrane Science 396, 1-21.
Zou, S. and He, Z. (2016) Enhancing wastewater reuse by forward osmosis with self-diluted commercial fertilizers as draw solutes. Water Research 99, 235-243.
Zou, S. and He, Z. (2017a) Electrodialysis Recovery of Reverse-fluxed Fertilizer Draw Solute during Forward Osmosis Water Treatment. Chemical Engineering Journal 330, 550-558.
Zou, S. and He, Z. (2017b) Electrolysis-assisted mitigation of reverse solute flux in a three-chamber forward osmosis system. Water Research 115, 111-119.

Table 6.1 RSF reduction via existing membrane modification in literature (NaCl as DS)

Membrane	Surface Coating	Modified Membrane	Mode	Conc. [a]	$J_{w,m}/J_{w,o}$	$J_{s,m}/J_{s,o}$	*MR* [a]
TFC/HTI (Guo et al. 2018)	Polydopamine	TFC-C0.5	AL-FS	0.5	1.11	0.98	12.2
			AL-DS	0.5	1.02	0.89	12.7
			AL-FS	1.0	1.09	0.94	13.8
			AL-DS	1.0	1.02	0.96	5.9
			AL-FS	2.0	1.12	0.92	18.3
			AL-DS	2.0	1.08	0.85	20.9
		TFC-C1	AL-FS	1.0	0.98	0.85	13.3
			AL-DS	1.0	0.99	0.90	9.1
		TFC-C4	AL-FS	1.0	0.92	0.85	7.6
			AL-DS	1.0	0.89	0.80	10.1
TFC/HTI (Soroush et al. 2015)	AgNPs-GO nanosheets	TFC-GO/Ag	AL-FS	1.0	0.98	1.40	-40.0
TFC/Lab Prepared (Zhang et al. 2013)	Ag-polyethylene glycol PEGylated dendrimer nanocomposite	M_Ag	AL-FS	1.0	0.83	1.25	-50.0
			AL-DS	1.0	0.89	1.33	-49.6
TFC/HTI (Soroush et al. 2016)	AgNPs-GO nanosheets	TFC-GO-Ag	AL-FS	1.0	1.02	1.04	-2.0
			AL-DS	1.0	1.13	0.95	15.9

a The units for draw concentration and *MR* are mol L^{-1} and %, respectively.

Table 6.2 Effective RSF reduction via new membrane fabrication in literature (SRSF<0.10 g L^{-1}, NaCl as DS)

TFC Membrane	Substrate Composition	Support Fabrication	Orientation	DS Conc. [a]	J_w [a]	J_s [a]	*SRSF* [a]
Optimized Substrate Composition							
Flat sheet (Han et al. 2012)	Polydopamine-Polysulfone	Wet phase inversion	AL-DS	2.0	24.0	1.8	0.075
Flat sheet (Widjojo et al. 2011)	Polyphenylsulfone-Polyethersulfone	Wet phase inversion	AL-DS	2.0	33.0	2.8	0.085
Flat sheet (Bui and McCutcheon 2013)	Cellulose Acetate-Polyacrylonitrile	Electrospinning	AL-DS	1.5	43.0	1.7	0.040
Flat sheet (Bui and McCutcheon 2016)	Si Nanoparticles-Polyacrylonitrile	Electrospinning	AL-FS	1.0	25.0	2.0	0.080
Advanced Substrate Fabrication							
Flat sheet (Shi et al. 2011)	(Polyetherimide)-Polysulfone	Polyetherimide as a sacrificial layer	AL-DS	0.5	33.1	2.6	0.079
Hollow fiber (Luo et al. 2014b)	Polyethersulfone	Dry-jet wet spinning	AL-DS	0.5	43.6	2.8	0.064
Hollow fiber (Luo et al. 2014b)	Matrimid® 5218 Polymer	Dry-jet wet spinning	AL-DS	1.0	26.3	1.5	0.057
Flat sheet (Liang et al. 2017)	Poly(vinylidene difluoride)	Vertically oriented porous substrates	AL-DS	1.0	52.3	3.9	0.075
Selection of Novel Supporting Materials							
Flat sheet (Yasukawa et al. 2015)	Polyketone	Nonsolvent induced phase separation	AL-DS	0.6	38.6	3.6	0.092
Flat sheet (Huang and McCutcheon 2015)	Nylon 6,6 MF membrane	Commercial support	AL-DS	1.5	22.5	0.8	0.035
Flat sheet (Li et al. 2012)	Cellulose acetate propionate	Wet phase inversion	AL-DS	2.0	31.8	1.6	0.050
Flat sheet (Duong et al. 2015)	Polytriazole-Polyoxadiazole	Wet phase inversion	AL-FS	1.0	30.3	2.9	0.096
New development of Active Layer							
Flat sheet (Shen et al. 2016)	Graphene oxide-polyamide [b] Polyacrylonitrile	Wet phase inversion	AL-FS	2.0	26.5	2.0	0.075

a The units for draw concentration, water flux (J_w), reverse solute flux (J_s), and *SRSF* are mol L^{-1}, LMH, gMH, and g L^{-1}, respectively.

b The active layer of this flat-sheet TFC is graphene oxide (GO) incorporated polyamide.

7 Nutrient-Energy-Water Recovery from Synthetic Sidestream Centrate Using a Microbial Electrolysis Cell - Forward Osmosis Hybrid System

(This chapter has been published as "Zou, S., Qin, M., Morean, Y. and He, Z. (2017) Nutrient-energy-water recovery from synthetic sidestream centrate using a microbial electrolysis cell - forward osmosis hybrid system. *Journal of Cleaner Production*, 154, 16-25.")

7.1 Abstract

Recovery of nutrients, water, and energy from high-strength sidestream centrate offers benefits such as reusable resource, minimized discharge and cost-savings in mainstream treatment. Herein, a microbial electrolysis cell - forward osmosis (MEC-FO) hybrid system has been investigated for integrated nutrient-energy-water (NEW) recovery with emphasis on quantified mass balance and energy evaluation. In a closed-loop mode, the hybrid system achieved recovery of 54.2 ± 1.9 % of water (70.4 ± 2.4 mL), 99.7 ± 13.0 % of net ammonium nitrogen (8.99 ± 0.75 mmol, with extended N_2 stripping), and 79.5 ± 0.5 % of phosphorus (as struvite, 0.16 ± 0.01 mmol). Ammonium loss primarily from reverse solute flux was fully compensated by the reclaimed ammonium under 6-h extended N_2 stripping to achieve self-sustained FO process. The generated hydrogen gas could potentially cover up to 28.7 ± 1.5 % of total energy input, rendering a specific energy consumption rate of 1.73 ± 0.08 kWh m^{-3} treated centrate, 0.57 ± 0.04 kWh kg^{-1} COD, 1.10 ± 0.05 kWh kg^{-1} removed NH_4^+-N, 1.17 ± 0.06 kWh kg^{-1} recovered NH_4^+-N, or 5.75 ± 0.54 kWh kg^{-1} struvite. Recycling of excess Mg^{2+} reduced its dosage to 0.08 kg Mg^{2+}/kg struvite. These results have demonstrated the successful synergy between MEC and FO to achieve multi-resource recovery, and encouraged further investigation to address the challenges such as enhanced hydrogen production, reducing nutrient loss, and optimizing MEC-FO coordination towards an energy-efficient NEW recovery process.

7.2 Graphical Abstract

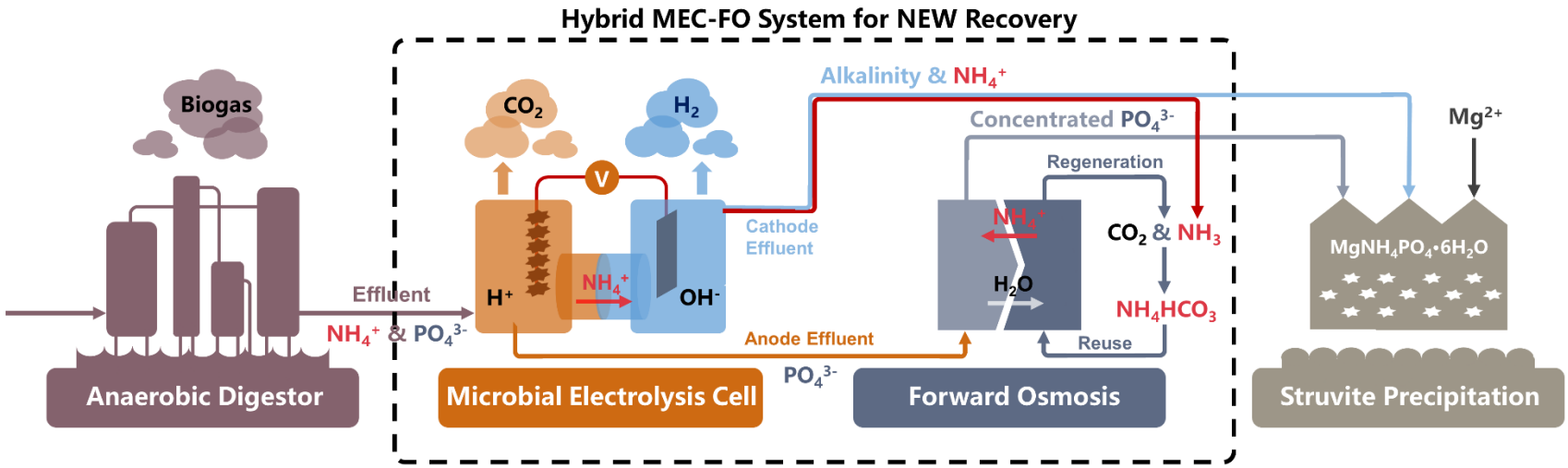

7.3 Keywords

Resource recovery; Forward osmosis; Microbial electrolysis cell; Nitrogen and phosphorus; Mass and energy balance

7.4 Introduction

Wastewater has been considered as a resource rather than waste in the 21st century to sustainably address some major challenges, i.e., water scarcity, nutrient depletion with increasing food demands, and energy shortage (McCarty et al. 2011). Conventional wastewater treatment generates a considerable amount of treated water while producing excess mixed liquor (high sludge content) as a sidestream. Subsequent sidestream treatment by anaerobic digestion (AD) enables degradation and stabilization of sludge featuring significant reduction of solid volume (up to 77%) (Kim et al. 2012). The concomitant resource recovery accredits to anaerobic conversion to biogas and nutrients reclamation (N and P) from digested sludge centrate (referred as "centrate" unless otherwise stated) as struvite ($MgNH_4PO_4 \cdot 6H_2O$) (De-Bashan and Bashan 2004, Qiu et al. 2015). However, the resource recovery capabilities of AD are greatly impaired by its incomplete organics removal (1000~2000 mg L^{-1} remaining COD) (Arango et al. 2016, Uggetti et al. 2014) and unsatisfying struvite crystallization under an imbalanced N/P ratio with a low P level (~ 56 mg L^{-1}) as a major limiting factor (Xie et al. 2016), rendering an abundant amount of NH_4^+-N (>1000 mg L^{-1}) that is not recovered. Recycling the nutrient-rich centrate back to the mainstream, though contributing less than 1% of total wastewater flow, leads to a notable increase of nutrient loading rate (up to 30%), additional energy investment, and elevated environmental footprint of mainstream treatment facilities (Lackner et al. 2008).

Insufficient resource recovery from sidestream centrate urges substantial process reformation with emphasis on comprehensive reclamation of nutrients (both N and P), bioenergy derived from remaining organics, and high-quality water towards zero-liquid discharge (Tong and Elimelech 2016). Physicochemical approaches deliver unique advantages for simultaneous nutrient concentration and centrate desalination. For example, clean water could be extracted from centrate in an electrodialysis-reverse osmosis (ED-RO) coupled system (Mondor et al. 2008), with ammonium being separated through air stripping (Ippersiel et al. 2012). The concentrate with an elevated P level (> 100 mg L^{-1}) could facilitate subsequent struvite precipitation (recovery rate > 95%) (Xie et al. 2016). RO could be replaced by microfiltration (MF) for the enrichment of volatile fatty acids (VFAs) towards biogas fermentation (Tao et al. 2016), or membrane distillation (MD) for generating contaminant-free fresh water (Kim et al. 2016). However, these electricity-,

pressure-, and thermal-driven membrane processes require substantial energy investment, weakening their potential for broader applications.

The path forward lies in energy-efficient innovations for integrated nutrient-energy-water (NEW) recovery from sidestream centrate, such as bioelectrochemical systems (BES) powered by bioenergy and osmotically-driven membrane processes (OMDPs). BES has been deemed as an attractive treatment method due to continuous nutrient enrichment and energy recovery as electricity (microbial fuel cell, MFC) (Logan et al. 2006) or value-added products such as hydrogen gas (microbial electrolysis cell, MEC) (Kelly and He 2014). OMDPs, especially forward osmosis (FO), take advantage of the osmotic pressure gradient across a semi-permeable membrane to spontaneously harvest high-quality product water (Lutchmiah et al. 2014). Integrating BES with OMDP may accomplish multiple tasks including nutrient recovery, bioenergy conversion, and wastewater treatment towards further reuse (Hou et al. 2016, Lu et al. 2014).

Our previous study has demonstrated the feasibility of a hybrid MEC-FO system using recovered ammonium as a draw solute for subsequent water recovery (Qin and He 2014). However, phosphorus recovery was not addressed, and this warranted synergistic coordination between MEC and FO towards multi-nutrient reclamation. Exact energy performance (i.e., energy output and recovery efficiency) was not quantified to enable better comparison with existing technologies aiming at similar targets. In addition, lacking a thorough mass/energy balance on a system level would jeopardize the scaling-up potential of this hybrid system. Herein, we have comprehensively evaluated the feasibility of the aforementioned NEW recovery from synthetic centrate by using this hybrid MEC-FO system (linked to a struvite precipitation process). The specific objectives of this study were to (1) enhance the effectiveness of phosphorus recovery via struvite from low-P synthetic centrate; (2) analyze NEW mass balance on a system level with emphasis on NH_4^+-N loss and self-compensation, closed-loop struvite precipitation yield, continuous water extraction capability, and bioenergy recovery as hydrogen gas; and (3) quantify specific energy consumption of the hybrid system to identify the challenges for future development.

7.5 Materials and Methods

7.5.1 MEC-FO hybrid system

The MEC-FO hybrid system was operated either in an open-loop mode for start-up or in a closed-loop mode to minimize liquid discharge (Fig. 7.1). In the open-loop mode, a synthetic centrate was continuously pumped into the MEC anode chamber, where exoelectrogens (electrochemically active microorganisms) converted the organics into electricity to power ammonium migration across the cation exchange membrane (CEM, 12 cm × 6 cm), rendering continuous enrichment of ammonium and energy recovery as hydrogen gas in the cathode. Upon utilization of biodegradable COD (indicated by diminished electricity), the anolyte was replaced by fresh synthetic centrate (for next batch cycle), and the discharged anolyte was transferred to the FO feed chamber for water recovery and phosphorus concentration. Finally, the concentrated feed solution was filtered, and the phosphorus was reclaimed from filtrate as struvite ($MgNH_4PO_4 \bullet 6H_2O$) via chemical precipitation. In a closed-loop mode, in addition to the above processes, the supernatant was then recycled back to the anode of the MEC mixing with fresh synthetic centrate as the influent. For example, the struvite precipitation supernatant from cycle 1 was mixed with fresh synthetic digestate to serve as the MEC anode influent in cycle 3 with a mixing ratio shown in Table 7.1. The whole system was operated in a temperature-controlled lab (20 ± 2 °C).

7.5.2 MEC setup and operation

A flat-plate MEC (20 cm × 10 cm) was constructed with two identical chambers (90 mL each). A 12-cm carbon brush was inserted into the anode chamber as an anode electrode. Two pieces of carbon cloth (12 cm × 4 cm) coated with Pt/C as catalyst (0.5 mg Pt cm^{-2}) were bound on two sides of a stainless-steel mesh (12 cm × 4 cm) and served as the cathode electrode. The synthetic centrate contained (per liter DI water): 2.60 g NaAc (2000 mg L^{-1} COD), 3.82 g NH_4Cl (1000 mg L^{-1} NH_4^+-N), 0.31 g KH_2PO_4 (70 mg L^{-1} PO_4^{3-}-P), 0.10 g $MgSO_4$, 0.05 g $CaCl_2$, and 1.0 mL trace elements, to mimic digestion centrate without any buffer agents (Münch and Barr 2001). Each of the anolyte and the catholyte (0.01 M NaCl) was connected with a 200-mL reservoir bottle (Table 7.1), and recirculated at 10 mL min^{-1} (0.85 cm s^{-1} for 0.5 cm pipe). The MEC was first operated in an MFC mode (detailed information in Supplementary Materials) for two weeks and then switched to the MEC mode with 0.8 V external voltage. The MEC was operated in a batch mode with its voltage monitored (2-min interval) over an external resistor of 10 Ω. The generated hydrogen gas in the cathode was collected and measured by using a water replacement method. One MEC operation cycle was terminated if the generated current was decreased to around 1.0 mA, and both reservoir

bottles were replenished with new anolyte/catholyte. Samples (5 mL) were taken directly from the reservoir bottles at the 0 h of each cycle with a 24-h interval thereafter for water quality analysis.

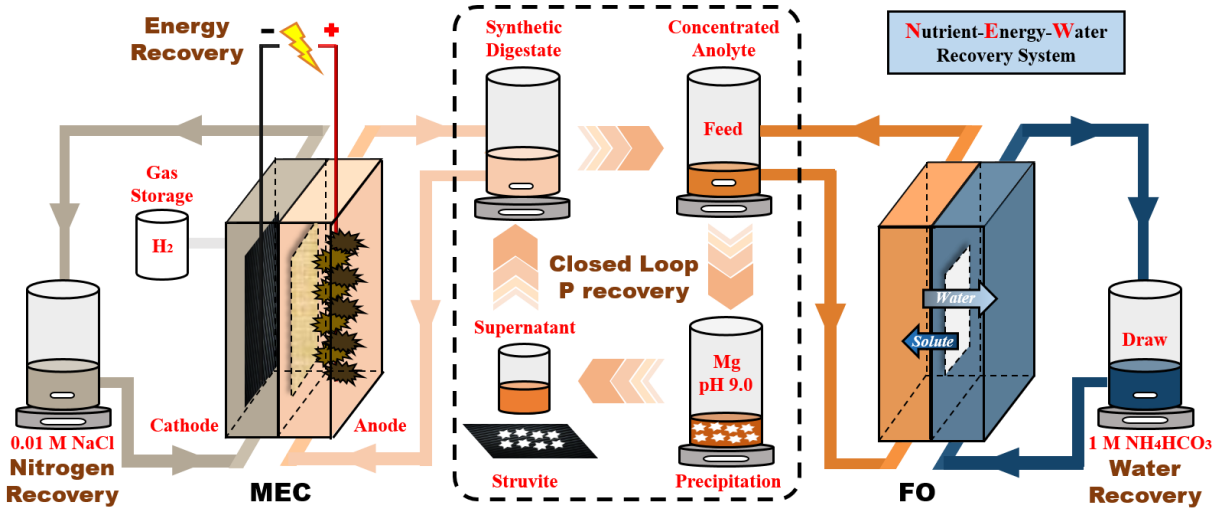

Figure 7.1 Schematic of the hybrid MEC-FO system for nutrient-energy-water (NEW) recovery.

7.5.3 FO setup and operation

In the cross-flow FO cell, one piece of Aquaporin Inside^{TM} membrane (Aquaporin A/S, Denmark) with an effective working area of 15 cm^2 was installed with its active layer facing the feed side (FO mode), creating an identical volume of 10 mL for each chamber. During operation, 100 mL 1-M NH_4HCO_3 (conductivity 64.9-65.4 mS cm^{-1}, pH 7.65-7.76) was used as the draw solution while the effluent of the MEC anolyte served as the feed. The recirculation flow rate for both draw and feed solution was 10 mL min^{-1} (0.85 cm s^{-1} for 0.5 cm pipe). The FO was operated in a batch mode with each cycle for 24 h. Membrane fouling was well-controlled by 6-h *in-situ* physical flushing with ~500 mL DI water (reused, 100-150 mL min^{-1}, or 8.49-12.74 cm s^{-1}) after each cycle. The FO cell was sealed without membrane replacement throughout the whole experiment. Samples were taken at the initial and the end of each cycle for analysis.

7.5.4 Struvite precipitation

The concentrated feed solution from the FO was filtered by 0.45 μm filter paper to remove biomass. The filtrate pH was adjusted by HCl (37%, ~33 μL) to around 2.0, followed by N_2 stripping (0.5 h) for removal of carbonate and bicarbonate. Stripping system was connected to an absorption

bottle filled with 1 mol L^{-1} sulfuric acid to collect ammonia. A certain amount of $MgCl_2 \cdot 6H_2O$ was then added (Mg:P=2:1) before pH adjustment to around 9.0 with 10-M NaOH (~40 μL) (Nelson et al. 2003). It should be noted that the volume of each chemical solution for pH adjustment was less than 0.1% of total concentrated feed volume, resulting in very small material expense in the operating cost of the proposed system. The mixed liquor was stirred at 30 rpm for 5 min to achieve complete struvite precipitation before the second filtration. The generated white crystals were washed twice with DI water, and the final products were air dried in the fume hood (RT) overnight. The remaining supernatant was sent back to the MEC anode and mixed with fresh synthetic centrate as the anolyte (closed-loop mode, starting from cycle 3).

7.5.5 Analytical methods

The concentrations of ammonium nitrogen (NH_4^+-N), total phosphorus and COD were determined by using a spectrophotometer according to the manufacturer instruction (DR 890, HACH Company, USA). Magnesium (Mg^{2+}) and calcium (Ca^{2+}) level were quantified by ion chromatography (Dionex LC20 ion chromatograph, Sunnnyvale, USA) together with an ED40 electrochemical detector. Conductivity was measured with a benchtop conductivity meter (Mettler-Toledo, Columbus, OH, USA). Water flux was determined by measuring the change of water weight on an electronic balance (Scort Pro, Ohous, Columbia, MD, USA) at a 30-s interval. In MEC module, Coulombic efficiency was described as the ratio of output charge (Q_{out}, as generated electricity) to the input charge (Q_{in}, originated from organics) (He et al. 2005):

$$CE = \frac{Q_{out}}{Q_{in}} = \frac{\sum It}{F \times \Delta COD \times V \times \frac{1\text{mol } O_2}{32\text{g } O_2} \times \frac{4\text{mol } e^-}{1\text{mol } O_2}} \times 100\%$$

where I (A) is the current over an extended period of time (t, s). F (96485 C mol e^{-1}) is the Faraday constant. ΔCOD (g L^{-1}) is the variation of COD in MEC anolyte, and V (L) is the anolyte volume.

Collected hydrogen gas was analyzed by gas chromatography coupled with thermal conductivity detector (GC-TCD, Shimadzu, Japan). The obtained solids from chemical

precipitation were coated with Au/Pd (6:4, wt%) and then characterized using scanning electron microscopy (SEM) coupled with energy dispersive spectroscopy (EDS). Powder X-ray diffraction (XRD) measurements were performed using a Rigaku MiniFlex 600. In the closed-loop mode (starting from cycle 3, Table 7.1), the initial nutrient concentration in the MEC anode influent (C_{inf}, mol L^{-1}) was calculated based on mass balance (Eq. 7.1).

$$C_{\inf} = \frac{m_{total}}{V} = \frac{C_{fresh}V_{fresh} + C_{recycled}V_{recycled}}{V} \quad \text{(Eq. 7.1)}$$

where m_{total} (g) is the total nutrient mass (e.g. N and P) of mixed digestate, and equals to the sum of fresh nutrient mass and recycled nutrient mass from the struvite precipitation supernatant. V (L) is the total anolyte volume.

In the FO, quantification of water flux (e.g., average water flux, J_a) and solute build-up (SBU) at the feed side were based on a previous study (Zou and He 2016). SBU is typically resulted from the concentrating effect in the feed (due to membrane rejection of the feed solute) and reverse solute flux (RSF, mmol m^{-2} h^{-1}) from the draw solution. Specific RSF (g L^{-1}, Eq. 7.2) was also calculated as the ratio of RSF and maximum water flux (J_w, L $m^{-2}h^{-1}$, LMH).

$$Specific\ RSF = \frac{RSF \times Mw}{J_w \times 1000} \quad \text{(Eq. 7.2)}$$

The yield (γ, %) for phosphorus recovery as struvite ($MgNH_4PO_4 \cdot 6H_2O$, MW = 245 g mol^{-1}) was defined as the ratio of recovered struvite mass to theoretical struvite amount (Eq. 7.3).

$$\gamma = \frac{m_{recovered}}{m_{theoretical}} = \frac{m_f - m_i}{V_{concentrate} \times \Delta C_p \times 245\ \text{g mol}^{-1}} \times 100\% \quad \text{(Eq. 7.3)}$$

where m_i (g) and m_f (g) are the initial and final mass of dried filter paper with/without struvite. $V_{concentrate}$ (L) is the volume of concentrated feed solution, whereas ΔC_p (mol L^{-1}) is the phosphorus concentration changes in bulk solution before and after struvite precipitation.

The substrate energy recovery efficiency (η_S) was described as the ratio of reclaimed energy (collected hydrogen gas) to intrinsic chemical energy originated from organic substrates (Call and Logan 2008).

$$\eta_S = \frac{W_{H_2}}{W_S} = \frac{n_{H_2} \times \Delta H_{H_2}}{n_S \times \Delta H_S} = \frac{V_{H_2} \times \frac{1\text{ mol}}{24\text{ L}} \times \Delta H_{H_2}}{m_S \times \frac{1\text{ mol}}{82\text{ g}} \times \Delta H_S} = \frac{V_{H_2} \times \frac{1\text{ mol}}{24\text{ L}} \times \Delta H_{H_2}}{\Delta COD \times \frac{1\text{g NaAc}}{0.78\text{g COD}} \times \frac{1\text{ mol}}{82\text{ g NaAc}} \times \Delta H_S} \quad \text{(Eq. 7.4)}$$

where W_{H2} (kJ) is the recovered energy based on heat combustion of H_2, ΔH_{H2}=285.83 kJ mol^{-1}. The mole amount of H_2 (n_{H2}) was estimated according to ideal gas law (1 mol H_2 equals to 24 L, 293 K). W_s (kJ) is the originated chemical energy from substrate (NaAc, ΔH_s=870.28 kJ mol^{-1}). The amount of consumed substrate was estimated from the degraded COD (ΔCOD, g) divided by a conversion factor (0.78 g COD g^{-1} NaAc).

The energy consumption was evaluated on the whole system level (MEC-FO), and the consumption rate was normalized by unit treated wastewater (kWh m^{-3}), unit reduced COD (kWh kg COD^{-1}), unit removed or recovered NH_4^+-N (kWh kg N^{-1}), or unit obtained struvite (kWh kg^{-1}). The energy consumption rate of the FO was normalized by unit extracted clean water (kWh m^{-3}) (Xiang et al. 2017). In MEC-FO system, the major energy consumers were external power supply and four recirculation pump heads (two for MEC and two for FO, operated in different time length). Hence, SEC for unit treated wastewater (E_{ww}, kWh m^{-3}), unit reduced COD (E_{COD}, kWh kg COD^{-1}), unit removed or recovered NH_4^+-N ($E_{removed,NH4\text{-}N}$, $E_{recovered,NH4\text{-}N}$, kWh kg N^{-1}), or unit obtained struvite ($E_{struvite}$, kWh kg^{-1} struvite) were estimated as Eqs. 7.5 to 7.9:

$$E_{ww} = \frac{W_{net}}{V} \approx \frac{W_{pump} + W_{electricity} - W_{H2}}{V} \quad \text{(Eq. 7.5)}$$

$$E_{COD} = \frac{W_{net} \times 1000}{\Delta COD \times V} \quad \text{(Eq. 7.6)}$$

$$E_{removed,NH4-N} = \frac{W_{net}}{\Delta m_{removed,NH4-N}} = \frac{W_{net}}{\Delta m_{MEC,anolyte}} \quad \text{(Eq. 7.7)}$$

$$E_{recovered,NH4-N} = \frac{W_{net}}{\Delta m_{MEC,catholyte} + \Delta m_{stripping} + \Delta m_{struvite}} \quad \text{(Eq. 7.8)}$$

$$E_{stuvite} = \frac{W_{net} \times 1000000}{m_{struvite}} \quad \text{(Eq. 7.9)}$$

where W_{pump} (kWh) and $W_{electricity}$ (kWh) are the energy consumption of the recirculation pump and external voltage supply, and V (m^3) is fresh centrate volume (treated wastewater), ΔCOD (mg L^{-1}) and $\Delta m_{removed,NH4\text{-}N}$ (kg L^{-1}) are COD concentration and NH_4^+-N mass changes in one cycle, respectively. $m_{struvite}$ (mg) is obtained struvite mass.

In FO process, energy consumption rate was normalized by unit extracted clean water (E_{water}, kWh m^{-3}):

$$E_{FO} = \frac{P_{system}}{Q} \approx \frac{2P_{pump} \times t}{V} \quad \text{(Eq. 7.10)}$$

7.6 Results and Discussion

7.6.1 Hydrogen Energy Recovery

Chemical energy in the remaining organics (expressed as COD) of centrate could partially be converted to hydrogen gas through microbial electrolysis, accompanying with current generation induced by an external voltage. When being operated in an open-loop mode (the MEC received only freshly prepared synthetic centrate), the MEC exhibited a typical batch profile of electricity production. With an applied voltage of 0.8 V, the MEC generated a maximum current of 5.52 ± 0.06 mA and a CE of 21.8 ± 1.5 % (Fig. 7.2A). The decrease in current generation was due to decreased organic concentration and anolyte pH (from 6.75 to 4.54, Fig. 7.2B) by oxidative H^+ generation, and concurrent increase of the catholyte pH (from 8.05 to 10.06) by reductive OH^- release, leading to elevated pH gradient over CEM and deteriorated potential loss (Rozendal et al. 2007). The MEC achieved a COD removal efficiency of 79.8 ± 0.6 % and COD removal rate of 0.322 ± 0.001 kg $m^{-3}d^{-1}$. In a closed-loop mode (the residue left from the struvite process was mixed with fresh anolyte, cycles 3-5), the MEC achieved a higher CE of 26.7 ± 1.8 % than that under the open-loop mode; this was likely benefited from a higher initial anolyte pH (8.58 vs. 6.75 in open-loop mode, Fig. 7.2B) with more alkalinity for buffering the pH during the following reaction. Increased current generation extended the operation length of each cycle to 6 days

(originally 5 days), rendering a more desired organic removal efficiency of 88.5 ± 2.7 % but a relatively lower COD removal rate of 0.266 ± 0.008 kg $m^{-3}d^{-1}$. Cross-CEM COD migration was low throughout the whole experiment (24.67 ± 4.19 mg L^{-1} in the catholyte), and no biofouling was with significant effects on ammonia recovery was observed in the cathode chamber.

Hydrogen gas production was observed under both modes, and because of a higher CE, the closed-loop mode produced 27.3 ± 1.2 mL of hydrogen gas per cycle, higher than 17.8 ± 0.9 mL per cycle in the open-loop mode. An average specific production rate of 18.2 ± 0.8 L H_2 $m^{-3}d^{-1}$ could be achieved for closed-loop operation, much higher than 11.8 ± 0.6 L H_2 $m^{-3}d^{-1}$ in the open-loop mode (Fig. 7.2C). The hydrogen production performance was comparable to stand-alone MECs treating domestic wastewater (15 L H_2 $m^{-3}d^{-1}$) (Heidrich et al. 2013) or winery wastewater (~25 L H_2 $m^{-3}d^{-1}$ average) (Cusick et al. 2011). The quantified substrate energy recovery (SER) efficiency in the closed-loop mode (6.4 ± 0.5 %) outcompeted that in the open-loop mode (4.1 ± 0.2 %, Fig. 7.2C inset), which was consistent with CE tendency. It should be noted that methane was not detected during gas collection, suggesting an absence of methanogens in the MEC cathode.

7.6.2 Water recovery

Recovering reusable water from the MEC anolyte effluent was successfully achieved by the FO process. In the open-loop mode, 73.3 ± 0.3 mL water was extracted with a maximum water flux of 6.25 ± 0.15 LMH (Fig. 7.3), rendering a 63.0 ± 1.6 % of volume reduction. The generated water flux using Aquaporin Inside^{TM} membrane was at least 2 times larger than that using cellulose triacetate (CTA) membrane (2.0~3.0 LMH) by using 1 mol L^{-1} NH_4HCO_3 as the draw (Chanukya et al. 2013, Qin and He 2014). In the closed-loop mode, a slightly lower amount of the reclaimed water (70.4 ± 2.4 mL, Fig. 7.3 inset) was collected due to the increased salinity of the feed solution (MEC anolyte effluent) (8.25 ± 0.13 mS cm^{-1} vs. 6.98 ± 0.28 mS cm^{-1} in the open-loop mode) and thus reduced osmotic gradient (i.e. driving force). No significant difference in the maximum water

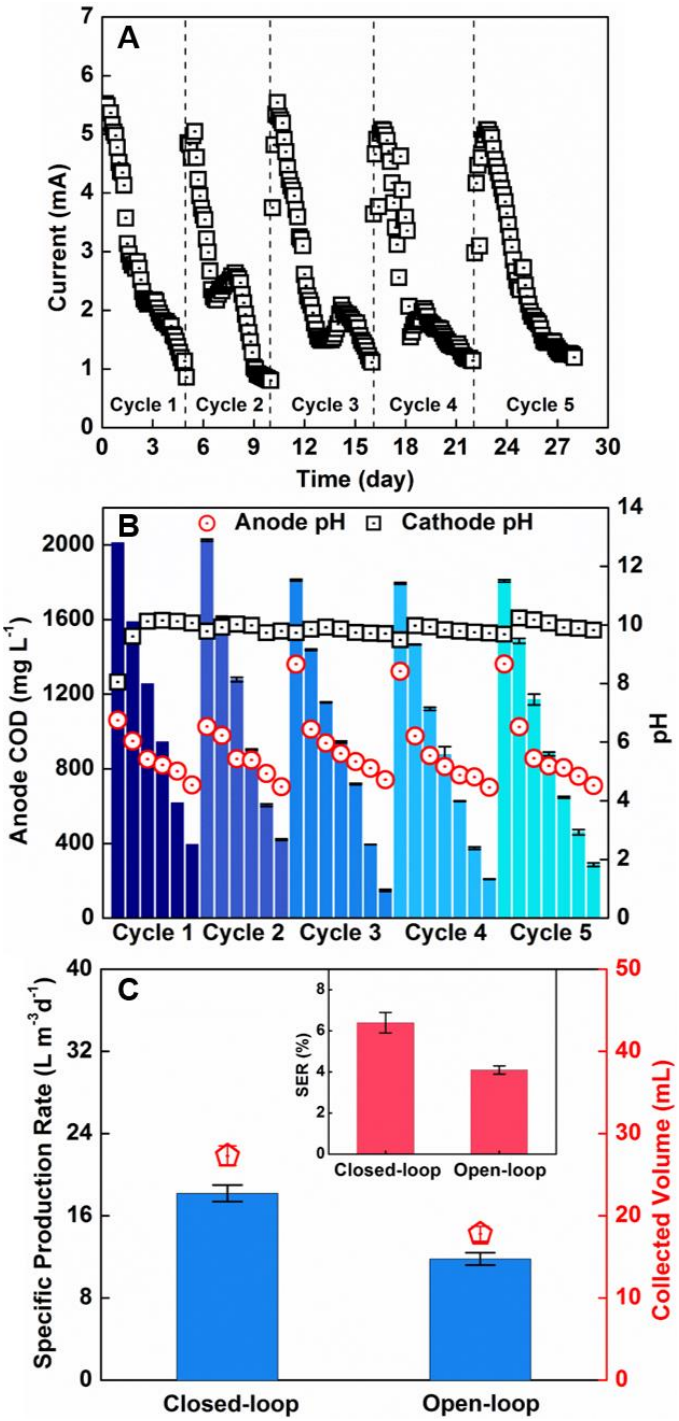

Figure 7.2 Energy recovery in the MEC: (A) current generation; (B) anolyte COD removal with anode/cathode pH variations; and (C) specific H_2 production rate and collected H_2 volume with substrate energy recovery (SER) efficiency (inset).

flux was observed between two operation modes (5.9 ± 1.2 LMH in closed-loop vs. 6.0 ± 0.3 LMH in open-loop, p>0.05, Fig. 7.3). Considering that 130 mL of fresh synthetic centrate was added in each closed-loop cycle, the hybrid system achieved a water recovery rate of 54.2 ± 1.9 %. The final diluted draw solution would then go through a heat-driven solute regeneration process (typically 60 °C, not investigated in the present study) (McGinnis and Elimelech 2007), where NH_4HCO_3 dissociates to NH_3 and CO_2 gas. Both NH_3 and CO_2 gas emit from the liquid phase and are absorbed in the condenser for regeneration (NH_4HCO_3), avoiding gradual organic, and nutrient build-up issues emerged in most RO regeneration processes (McGinnis et al. 2013a). The content of organics (49.00 ± 11.52 mg L^{-1}) and P (7.49 ± 0.63 mg L^{-1}) in the remaining product water (liquid phase) should not be a major concern for agricultural and industrial reuse (Agency 2012).

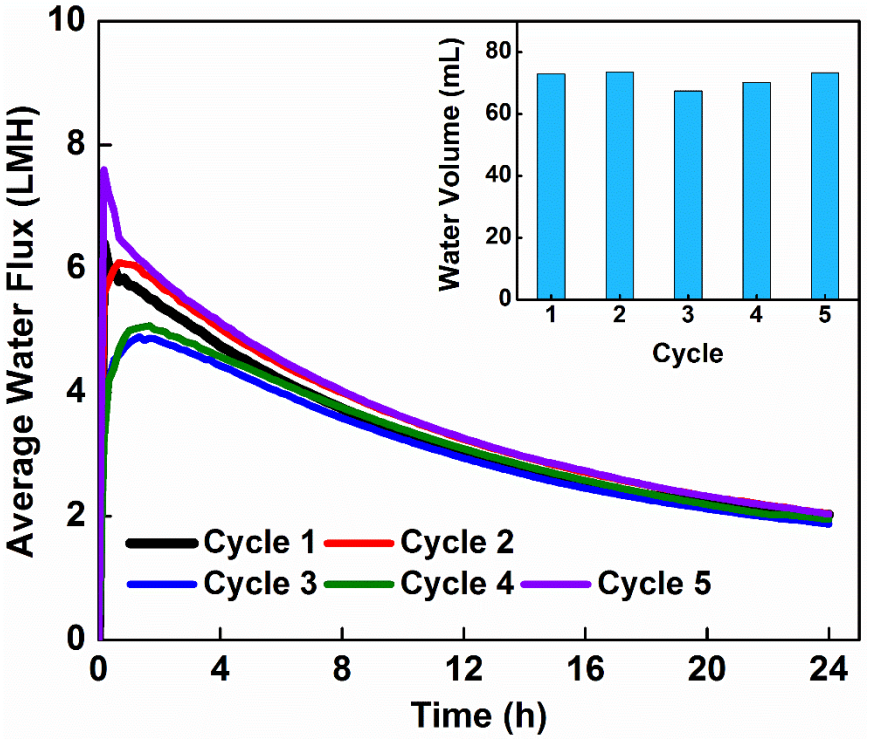

Figure 7.3 Water recovery in the FO in terms of average water flux and extracted water volume (inset).

7.6.3 Nitrogen recovery

Ammonium, as the dominant form of nitrogen in AD centrate, effectively migrated across the CEM with the aid of an electric field and was enriched in the MEC catholyte towards further

recovery. In the open-loop mode, the NH_4^+-N concentration of the MEC anolyte decreased from 699.3 ± 2.7 to 186.5 ± 14.2 mg L^{-1} (73.3 ± 1.9 % removal efficiency), resulting in a total removal amount of 9.66 ± 0.20 mmol (Fig. 7.4A). There was 8.96 ± 0.10 mmol of NH_4^+-N accumulated in the MEC catholyte. Though effectively decreased in the MEC module, the ammonium concentration in the centrate would inevitably increase when passing the following FO module, owing to the concentrating effect and reverse NH_4HCO_3 leakage. The NH_4^+-N amount at the FO feed side was increased from 1.56 ± 0.17 mmol (186.5 ± 14.2 mg L^{-1}) to 14.34 ± 1.58 mmol (4633.3 ± 166.7 mg L^{-1}) in an open-loop mode (Fig. 7.4B), indicating a specific RSF of 0.85 ± 0.16 g L^{-1} (Fig. 7.4C), which was 57.5% lower than that of CTA membrane (2.01 g L^{-1}) under similar operation conditions (Achilli et al. 2010). The NH_4^+-N concentration increment in the concentrated feed was mainly attributed to the concentrating effect (10.9%) induced by membrane rejection and RSF (89.1%, Fig. 7.4C).

In the closed-loop operation mode, additional NH_4^+-N was introduced to the MEC anolyte by the remaining supernatant from the struvite precipitation, leading to increased ammonium loading of 19.87 ± 0.92 mmol (nearly 60% higher than 12.48 ± 0.05 mmol in the open-loop mode) and doubled concentration (341.3 ± 47.3 mg L^{-1}) in the anode effluent. However, ammonium migration in MEC was greatly enhanced due to an elevated current generation in the closed-loop mode, rendering a superior ammonium recovery rate of 13.74 ± 0.28 mmol (vs. 8.96 ± 0.10 mmol in the open-loop mode, Fig. 7.4A). The ammonium recovery performance outcompeted lab-scale bipolar bioelectrodialysis in a previous study (~4 mmol for 5-day operation, 0.8 V) (Zhang and Angelidaki 2015b), and could be further enhanced if buffer solution was applied in MEC system (Zhang and Angelidaki 2015a). Reverse ammonium leakage in the subsequent FO process was comparable among cycles 3-5, but slightly higher than that in open-loop mode (15.56 ± 0.45 mmol, Fig. 7.4B). It should be noted that specific RSF of NH_4^+-N reached its maximum value of 1.22 g L^{-1} in cycle 3, owing to accumulated fouling and corresponding reduced water flux (Fig. 7.3). With the proper increase of post-cycle flushing rate from 100 mL min^{-1} to 150 mL min^{-1}, reversible fouling was well controlled with restored water recovery and reduced specific RSF in subsequent cycles. The average NH_4^+-N concentration in the concentrated feed was 5111.1 ± 175.0 mg L^{-1} with an increased contribution of the concentrating effect (16.4 ± 2.5 %, Fig. 7.4C).

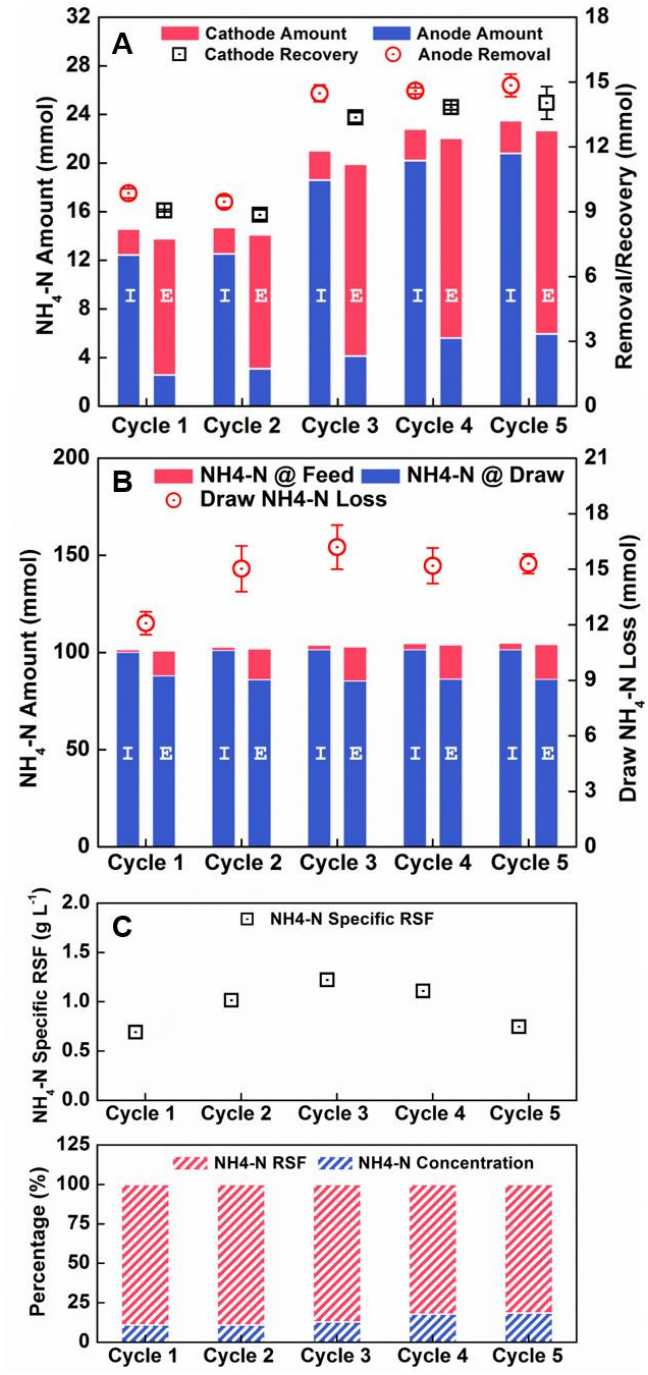

Figure 7.4 Nitrogen recovery: (A) anolyte/catholyte NH_4^+-N distribution (column) and corresponding removal/recovery amount; (B) NH_4^+-N distribution in draw/feed together with draw solute loss; and (C) RSF of NH_4^+-N with composition of NH_4^+-N build-up in final feed solution. The "I" and "E" in Fig. 7.4A and 7.4B stand for the initial and ending amount of NH_4^+-N in each cycle, and the total column height represents the overall amount on system level (either MEC or FO).

7.6.4 Phosphorus recovery

The hybrid MEC-FO system effectively concentrated the phosphorus in low-P centrate to achieve a more desirable recovery rate. In MEC process, phosphorus removal/recovery was rather limited due to negligible biological consumption and high rejection of CEM, leading to a consistent PO_4^{3-}-P concentration in the anode effluent at both modes (Fig. 7.5A). It should be noted that the lower PO_4^{3-}-P concentration in the closed-loop mode was attributed to a dilution effect from the recycled P-free struvite supernatant. In the FO process, the PO_4^{3-}-P level was elevated from 71.5 ± 0.5 to 153.5 ± 4.5 mg L^{-1} in the open-loop mode, or from 57.0 ± 0.7 to 116.8 ± 5.3 mg L^{-1} in the closed-loop mode (Fig. 7.5B). During this concentration process, part of P would inevitably diffuse through FO membrane to the draw side, i.e., forward solute flux (FSF) due to its same direction with water flux. Hence, the total PO_4^{3-}-P amount was decreased from 0.268 ± 0.010 to 0.213 ± 0.009 mmol in the open-loop mode (20.5 ± 0.5 % loss rate, Fig. 7.5B), indicating a specific FSF of 0.008 ± 0.001 g L^{-1}. The PO_4^{3-}-P loss was alleviated (down to 0.042 ± 0.004 mmol, Fig. 7.5B) in the following closed-loop cycles because of the reduced concentration gradient (i.e., lower initial P level) and lower FSF (0.006 ± 0.001 g L^{-1}). The struvite precipitation efficiency was 100% (no P detected in the supernatant), rendering an overall phosphorus recovery efficiency of 79.5 ± 0.5 % due to FSF PO_4^3-P loss in the FO process. Owing to recycling of excess Mg^{2+} in the supernatant, Mg^{2+} dosage was significantly reduced from 0.17 g Mg^{2+} g^{-1} struvite (open-loop) to 0.08 g Mg^{2+} g^{-1} struvite (closed-loop), though slightly higher than that of a previous study (0.06 g Mg^{2+} g^{-1} struvite) (Xie et al. 2014).

The obtained struvite crystals were examined by using SEM-EDS and powder XRD. The SEM image of standard struvite sample (Fig. 7.6A) presented an orthorhombic structure with an average size of ~60 μm, whereas the recovered struvite (Fig. 7.6B and 7.6C) showed amorphous structure owing to filtration/grinding treatment. The coupled EDS analysis confirmed three major elements (Mg, P, and O) composing struvite in the recovered powders (Fig. 7.5C). The absence of N peak was due to its lightweight, and hence could not be detected in EDS (Xie et al. 2014). The mass percentage of Mg (12.65 ± 0.61 %) and P (15.17 ± 0.61 %) in recovered struvite were close to that of the standard struvite (9.79 ± 0.17 % for Mg and 13.41 ± 1.66 % for P, Table 7.2). Further XRD analysis indicated that the obtained solids had identical peak positions to that of standard struvite samples (Fig. 7.5D). All these results confirmed that phosphorus recovery from the low-P

synthetic centrate was desirably enhanced by the MEC-FO hybrid system, compared to that of direct precipitation (Fig. 7.7).

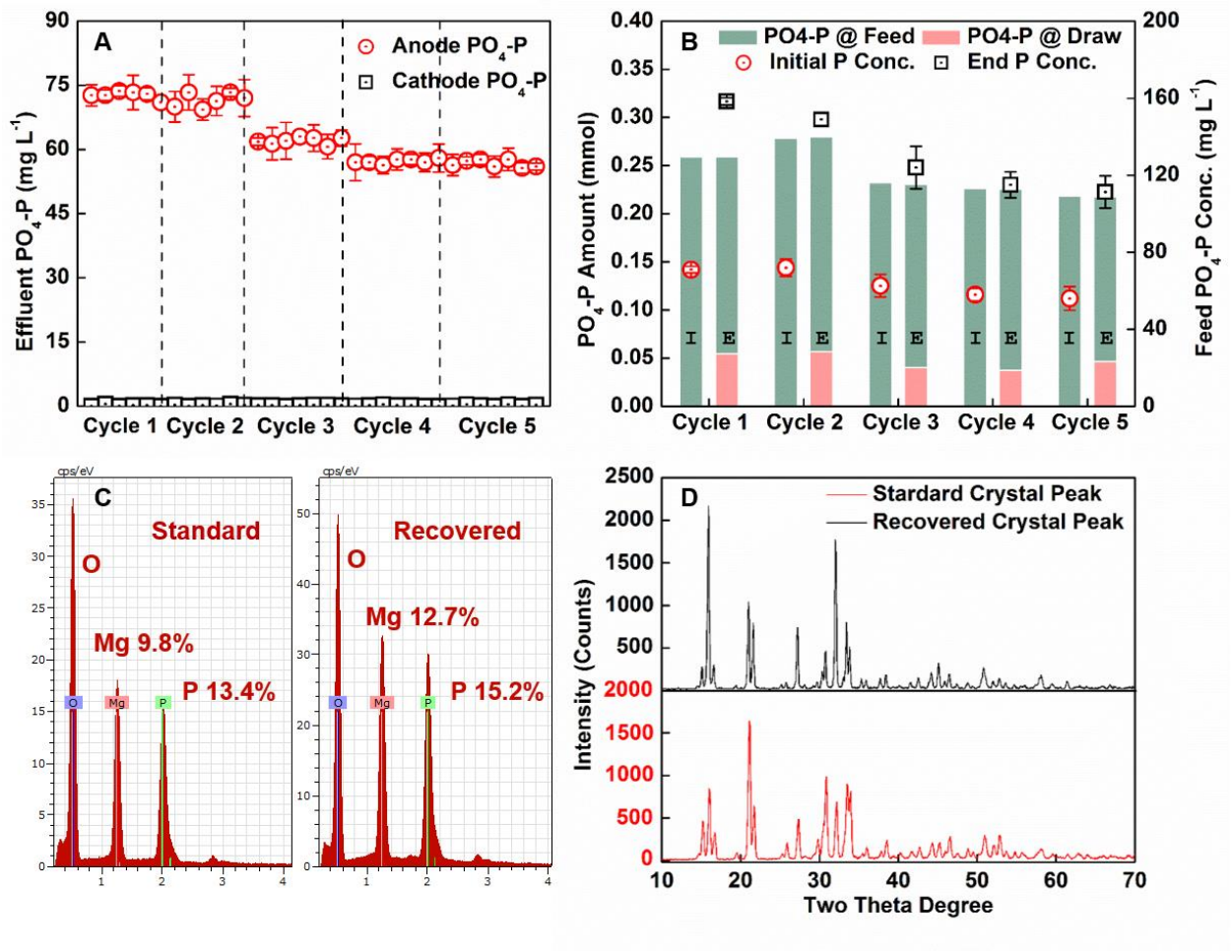

Figure 7.5 Phosphorus recovery: (A) PO_4^{3-}-P concentration in anode/cathode effluent; (B) PO_4^{3-}-P distribution in draw/feed together with initial/end concentration in feed solution; (C) EDS peaks of standard/recovered struvite; and (D) XRD spectrum of standard/recovered struvite. The "I" and "E" in Fig. 7.5B stand for the initial and ending amount of PO_4^{3-}-P in each cycle, and the total column height represents the sum of feed and draw amount.

7.6.5 Mass Balance

The mass balance for both N and P (in the closed-loop mode) is presented in Fig. 7.8. Within one cycle (on average), a total of 16.91 ± 0.43 mmol NH_4^+-N could be reclaimed, including 13.74 ±

0.28 mmol in the MEC (81.3%), 3.01 ± 0.30 mmol by N_2 stripping (17.8%), and 0.16 ± 0.01 mmol by struvite recovery (0.9%) (the latter two were presented together in struvite precipitation process, Fig. 7.8A). Thus, the MEC acted as a major process for ammonium recovery with a negligible loss (0.01 ± 0.00 mmol).

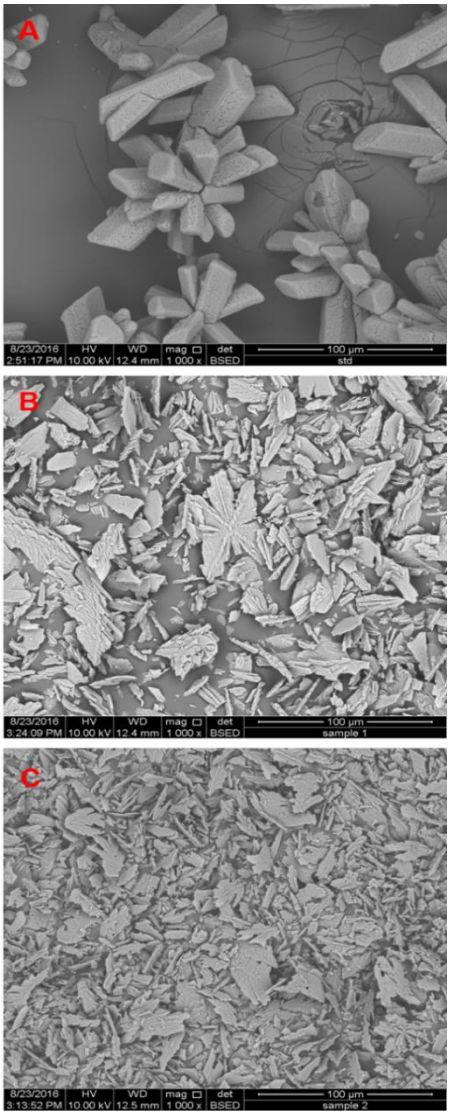

Figure 7.6 SEM images of (A) standard struvite, (B) recovered struvite sample 1, and (C) recovered struvite sample 2. Images were taken under 1000× magnification.

In the FO, RSF (15.56 ± 0.45 mmol) and evaporation (0.75 ± 0.05 mmol) were demonstrated to be the primary source of ammonium loss (Fig. 7.8A), resulting from undesired

cross-membrane diffusion and NH_4HCO_3 decomposition into NH_3/CO_2 at a relatively higher concentration (1.0 mol L^{-1} in draw solution). It should be noted that ammonium loss by RSF (15.56 ± 0.45 mmol, Fig. 7.8A) and system operation (0.76 ± 0.05 mmol) could be fully compensated because of supernatant recycling and MEC ammonium recovery (detailed approach illustrated in our previous study (Qin and He 2014)) in the subsequent cycle, leading to self-supplied and continuous-replenished FO draw solutes that will notably reduce operational cost. Other processes, such as regeneration of thermolytic NH_4HCO_3 and NH_4^+-N isolation from the MEC catholyte, could cause additional ammonium loss and will warrant further assessment. Nonetheless, based on current data, the MEC-FO could achieve self-compensated ammonium recovery. To further enhance net ammonium recovery in current MEC-FO system, an extended N_2 stripping (25 mL min^{-1}) could be performed followed by filtered feed concentrate (Fig. 7.9). As a result, 53.8% of ammonium (~8.4 mmol) in the FO concentrate (15.57 ± 0.17 mmol, Fig. 7.8A) could be stripped out and recovered as $(NH_4)_2SO_4$ in the absorption tank, rendering a net ammonium recovery amount (operation loss and ammonium self-compensation excluded) and efficiency of 8.99 ± 0.75 mmol and 99.7 ± 13.0 %, respectively.

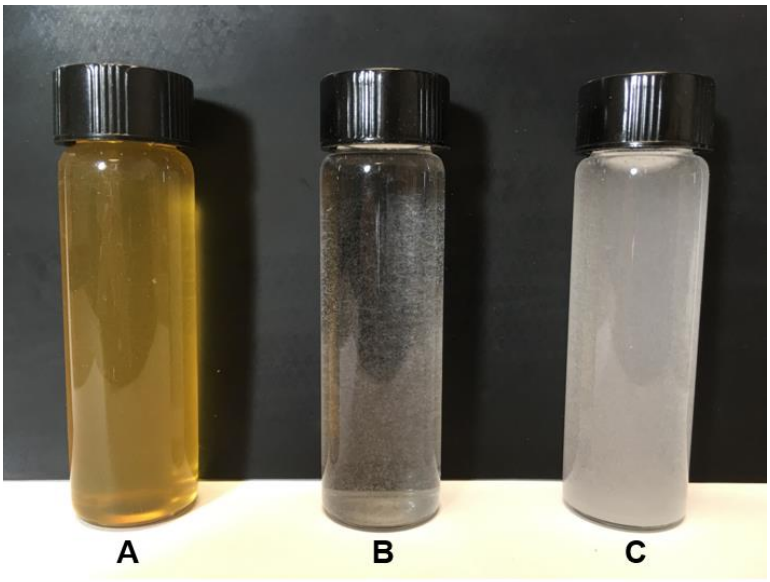

Figure 7.7 Struvite precipitation from (A) unfiltered MEC anolyte, (B) filtered MEC anolyte, and (C) concentrated anolyte after FO.

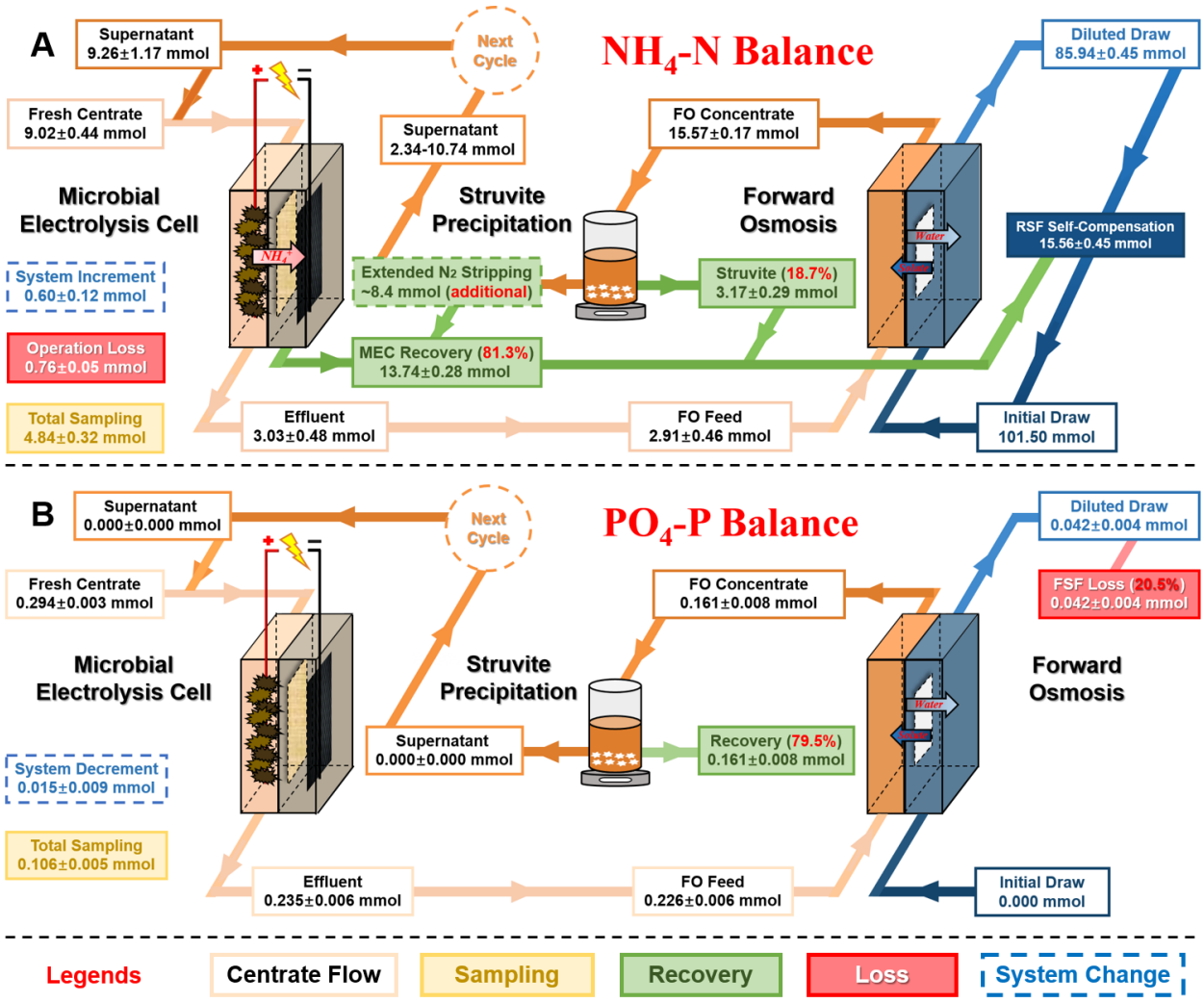

Figure 7.8 Mass balance of nutrients in the proposed system: (A) NH_4^+-N; and (B) PO_4^{3-}-P. The ammonium reclamation amount in struvite recovery of Fig. 7.8A is the sum of regular N_2 stripping (to remove HCO_3^-/CO_2) and struvite precipitation. Ammonium percentage in Fig. 7.8A is based on total recovery amount per cycle (16.91 mmol, extended N_2 stripping excluded). The yellow-orange line, green line and blue line stand for centrate flow, nutrient recovery, and draw solution (with ammonium regeneration).

Phosphorus was efficiently precipitated from the centrate in the form of struvite. Though phosphorus recovery was negligible in the MEC (rejected by CEM), the centrate was desirably enriched in phosphorus by the FO to secure a phosphorus recovery of 0.16 ± 0.01 mol via struvite, rendering 100% struvite precipitation yield and 80% overall phosphorus recovery efficiency. The

only loss was through FSF in the FO (0.042 ± 0.004 mmol, Fig. 7.8B), which could be reduced with further advancement of membrane fabrication and alleviated fouling-induced concentration polarization (She et al. 2012). Complete removal of carbonate and bicarbonate through stripping was a key to ensure struvite purity. With less sampling points and corresponding loss, higher phosphorus recovery efficiency (0.267 mmol total recovery with 0.042 mmol loss in FO, up to 86%, Fig. 7.8B) can be expected. It was observed that gradual ammonium increment (0.60 ± 0.12 mmol per cycle) and phosphorus decrement (0.015 ± 0.009 mmol per cycle) occurred in the MEC anode, owing to recycling of ammonium-rich and phosphorus-free supernatant. Our calculation indicated that the initial phosphorus input could reach a stable amount of 0.452 mmol in long-term operation, leading to a fixed initial anolyte concentration of 55 mg L^{-1}. However, ammonium input would continuously increase, and to maintain balanced system performance, enhanced ammonium recovery via extended N_2 stripping time should be encouraged.

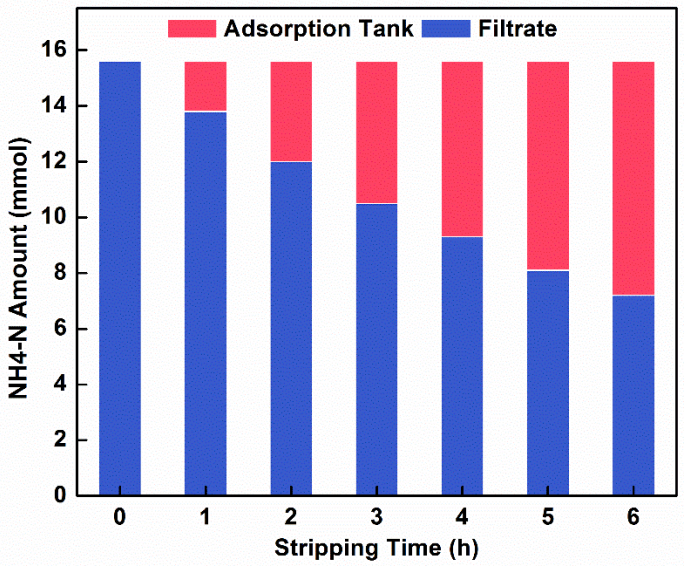

Figure 7.9 Ammonium amount distribution during extended N_2 stripping process. To enhance the capability of ammonium recovery of hybrid MEC-FO system, an extended N_2 stripping was conducted before struvite precipitation. Once the concentrated feed solution was filtered by 0.45 μm filter paper to remove biomass, the filtrate (42 mL, no pH adjustment, pH=8) was flushed with N_2 gas (25 mL min^{-1} flow rate) for 6 hours. The stripping system was connected to an absorption bottle filled with 1 mol L^{-1} sulfuric acid to collect ammonia. Samples were taken at a 1-h interval in both filtrate and adsorption bottle to monitor ammonium concentration changes. Initially, a total of 15.6 mmol ammonium (~52 mg L^{-1}) was presented in FO feed solution (filtrate). N_2 stripping

successfully recovered more than 50% of ammonium in filtrate after 6 hours, recovering 8.4 mmol ammonium in adsorption bottle. Hence, on system level, a total 25.3 mmol ammonium (13.7 mmol MEC recovery, 8.4 mmol extended N_2 stripping, and 3.2 mmol struvite recovery with N_2 stripping pretreatment) would be recovered, surpassing the ammonium input of 24.7 mmol (9.0 mmol centrate influent and 15.7 mmol RSF) in every cycle to achieve net ammonium recovery. The remaining ammonium (~7.1 mmol) in filtrate was sufficient for 100% struvite precipitation. It should be noted that ammonium recovery through stripping process should subject to flow rate and stripping time, and the final recovery amount may vary.

7.6.6 Energy consumption

The information of energy input is often missing in many prior studies of resource recovery (Zou et al., 2016). Although an estimate of energy consumption from a bench-scale system would not reflect actual conditions of the pilot- or full-scale applications, it will give us a rough picture of energy consumption with guiding next-step optimization. In the closed-loop mode, 27.3 ± 1.2 mL hydrogen gas (per cycle) could provide a maximum of 0.33 ± 0.01 kJ through combustion, accounting for up to 28.9 ± 1.6 % of total energy input in the MEC (1.13 ± 0.04 kJ, 5.3% pump and 94.7% power supply) and 28.7 ± 1.5 % of total energy input in MEC-FO system (1.14 ± 0.04 kJ, 99.1% from the MEC and 0.9% from the FO, Fig. 7.10A). It should be noted that an energy consumption rate of 0.73 kWh m^{-3} would be expected for draw solute regeneration (0.50 ± 0.01 mol L^{-1} initial diluted draw concentration, low-pressure single distillation column) (McGinnis and Elimelech 2007). Recent research confirmed that this part of energy consumption could be compensated by waste heat, and hence it was not counted in the evaluation in this study (Zhou et al. 2015).

Specific energy consumption was subsequently quantified on a system level (MEC-FO). Net energy consumption, with recovered hydrogen energy deducted, was normalized by unit treated water, unit degraded COD, unit removed or recovered NH_4^+-N (Fig. 7.10B, detailed calculation in Supplementary Materials). The MEC-FO system consumed 1.73 ± 0.08 kWh m^{-3} treated centrate, 0.57 ± 0.04 kWh kg^{-1} eliminated COD, 1.10 ± 0.05 kWh kg^{-1} removed NH_4^+-N, 1.17 ± 0.06 kWh kg^{-1} recovered NH_4^+-N, or 5.75 ± 0.54 kWh kg^{-1} struvite. The proposed hybrid

system could be more energy-efficient than other lab-scale nutrient recovery processes, such as a single chamber MEC for struvite production (1.8 ± 0.2 kWh kg^{-1} COD) (Cusick and Logan 2012)

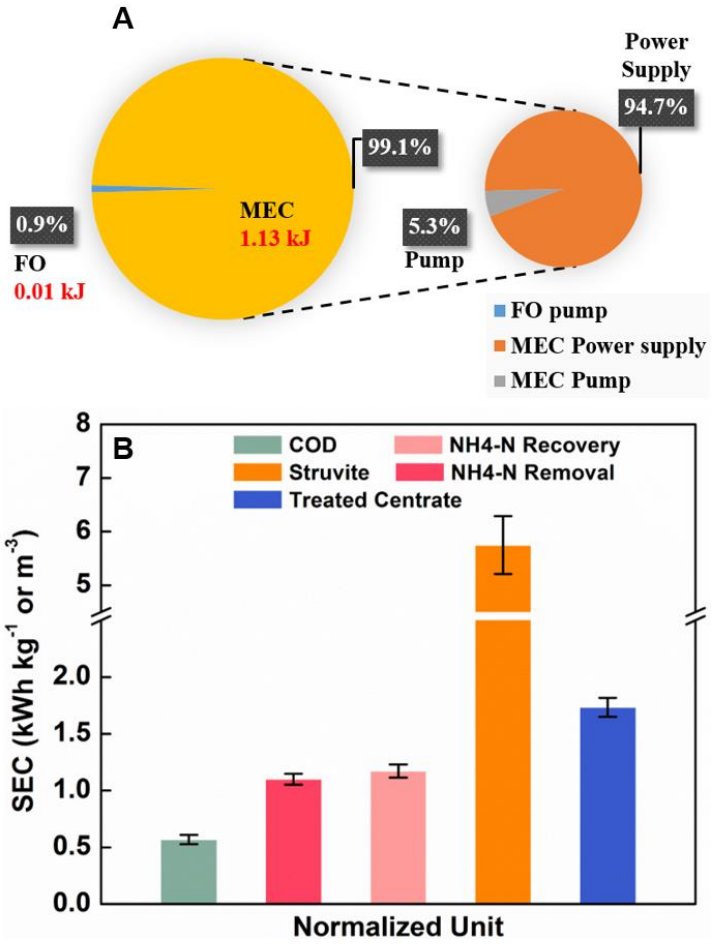

Figure 7.10 Profiles of energy consumption in MEC-FO hybrid system: (A) total energy input on system level; and (B) specific energy consumption (SEC) normalized by unit treated wastewater (kWh m^{-3}), unit reduced COD (kWh kg COD^{-1}), unit removed or recovered NH_4^+-N (kWh kg N^{-1}), or unit obtained struvite (kWh kg^{-1}).

and electrochemical ammonium recovery from digestate (down to 5.0 kWh kg N^{-1} recovered) (Desloover et al. 2012). Although struvite precipitation from separated urine had a much lower energy requirement of 0.76 kWh kg^{-1} struvite (Maurer et al. 2003), the hybrid system could accomplish multiple goals (i.e., integrated NEW recovery). It should be noted that ammonium regeneration from the MEC catholyte and FO diluted draw solution was not studied here but would

require an additional amount of energy input (Desloover et al. 2012). The energy consumption could be offset by reduced electricity consumption from mainstream treatment due to minimized nutrient and hydraulic loading rate (i.e., minimized sidestream discharging). The FO process alone consumed merely 0.14 ± 0.01 kWh m^{-3} recovered fresh water, outcompeting other lab-scaling emerging water recovery technologies such as microbial desalination cell (MDC, as low as 1.3 kWh m^{-3}) (Ping et al. 2015), bench-scale ED (7.0 kWh m^{-3}) (Walker et al. 2014), air gap membrane distillation (AGMD, 2.5-3.0 kWh m^{-3}) (Alkhudhiri et al. 2013).

7.6.7 Perspectives

The MEC-FO hybrid system has offered attractive merits of simultaneous multi-nutrient recovery, water extraction, and hydrogen production. The quantified mass balance and energy consumption enable a better understanding of competing challenges within this system and warrant further investigations for process optimization in the aspects of draw solute, system coordination, and system scaling up. First, the present system adopted thermolytic NH_4HCO_3 as a draw solute, which can relatively easier to regenerate and has been applied in the pilot test of desalination (McGinnis et al. 2013b). However, NH_4HCO_3 exhibits relatively larger specific RSF compared to other inorganic salts with the same osmotic pressure, such as Na_2SO_4, NaCl, and $MgCl_2$ (Achilli et al. 2010). Though the lost ammonium is fully recovered and reused in the closed-loop operation, it gradually elevates the influent ammonium concentration in the subsequent cycle. Extended N_2 stripping followed by FO offers a promising solution to mitigate ammonium build-up with enhanced ammonium recovery. However, to truly reduce RSF and strengthen long-term performance, membrane advancements, for example emerging fabrication materials with specialized salt rejection, and operation strategies (e.g., electrolysis-assisted solute capture) (Zou and He 2017) should be encouraged. Second, the MEC and FO exhibits different treatment capacity and should be well-coordinated for maximized resource recovery output (Lu et al. 2014). For example, one cycle of MEC lasts for 6 days while FO only takes 1 day in the present hybrid system. To solve this, the volume ratio of MEC to FO can be designed as 6:1. Alternatively, six parallel MECs can be linked to one FO module with stagger discharging. As a result, increased membrane fouling propensity should be expected while more phosphorus may be lost by FSF resulting from intensified fouling-induced concentration polarization. Third, further scaling-up of the proposed system will be necessary with long-term operation of treating actual centrate. Given

the fact that struvite process has been commercialized (Prasad et al. 2007), the challenge of scaling up the proposed hybrid system will lie in FO and MECs. FO has been successfully scaled up to a pilot scale for treating different waters and examining draw solutes and membrane fouling (Hancock et al. 2011, Hancock et al. 2013, Phuntsho et al. 2016). Because of a relatively simple structure, an FO system could be scaled up without much difficulty. Once the key problems such as draw solute regeneration and membrane cost/durability are solved, we believe that FO systems could be quickly developed to a full scale. MECs or relevant bioelectrochemical systems such as MFCs and MDCs have also been scaled up to the scale of pilot systems or significantly beyond a bench scale (e.g., a few hundred liters) (Cusick et al. 2011, Ge and He 2016, Heidrich et al. 2014, Zhang et al. 2013), and those prior efforts will provide valuable experiences to scaling up the proposed system. The critical issues for MEC scaling up include the optimization of reactor design for maximal hydrogen production and reduction of electrode/membrane cost.

7.7 Conclusions

In this study, an innovative MEC-FO hybrid system has been investigated for integrated NEW recovery from synthetic sidestream centrate. Detailed energy performance (i.e. energy output and recovery efficiency) was analyzed to enable better comparison with existing technologies. Mass balance was evaluated on the system level for performance optimization towards maximized resource output. The results of this study have demonstrated the effectiveness and high-efficiency of this MEC-FO hybrid system with the following conclusions:

- In a closed-loop mode, the hybrid MEC-FO system recovered 54.2 ± 1.9 % of water (70.4 ± 2.4 mL), 99.7 ± 13.0 % of net ammonium nitrogen (8.99 ± 0.75 mmol, with extended N_2 stripping), and 79.5 ± 0.5 % of phosphorus (as struvite, 0.16 ± 0.01 mmol).
- Ammonium loss primarily from RSF in the FO system was fully compensated by the reclaimed ammonium under 6-h extended N_2 stripping to achieve self-sustained osmotic water recovery.
- The generated hydrogen gas could potentially support up to 28.7 ± 1.5 % of total energy input, rendering a specific energy consumption rate of 1.73 ± 0.08 kWh m^{-3} treated centrate, 0.57 ±

0.04 kWh kg^{-1} COD, 1.10 ± 0.05 kWh kg^{-1} removed NH_4^+-N, 0.95 ± 0.03 kWh kg^{-1} recovered NH_4^+-N, or 5.75 ± 0.54 kWh kg^{-1} struvite.

- Continuous recycling of the supernatant after struvite recovery achieved reduced Mg^{2+} dosage (0.08 kg Mg^{2+}/kg struvite), buffered anolyte with better MEC performance, and most importantly minimized liquid discharge for further treatment.
- Further investigation should focus on solute leakage reduction via RSF mitigation, long-term performance evaluation with actual sidestream centrate, and system scaling up and coordination between modules.

References

Achilli, A., Cath, T.Y. and Childress, A.E. (2010) Selection of inorganic-based draw solutions for forward osmosis applications. Journal of Membrane Science 364(1), 233-241.

Alkhudhiri, A., Darwish, N. and Hilal, N. (2013) Produced water treatment: Application of Air Gap Membrane Distillation. Desalination 309, 46-51.

Arango, L., Cuervo, F.M., González-Sánchez, A. and Buitrón, G. (2016) Effect of microalgae inoculation on the start-up of microalgae–bacteria systems treating municipal, piggery and digestate wastewaters. Water Science and Technology 73(3), 687-696.

Call, D. and Logan, B.E. (2008) Hydrogen production in a single chamber microbial electrolysis cell lacking a membrane. Environmental Science & Technology 42(9), 3401-3406.

Chanukya, B.S., Patil, S. and Rastogi, N.K. (2013) Influence of concentration polarization on flux behavior in forward osmosis during desalination using ammonium bicarbonate. Desalination 312, 39-44.

Cusick, R.D., Bryan, B., Parker, D.S., Merrill, M.D., Mehanna, M., Kiely, P.D., Liu, G. and Logan, B.E. (2011) Performance of a pilot-scale continuous flow microbial electrolysis cell fed winery wastewater. Applied Microbiology and Biotechnology 89(6), 2053-2063.

Cusick, R.D. and Logan, B.E. (2012) Phosphate recovery as struvite within a single chamber microbial electrolysis cell. Bioresource Technology 107, 110-115.

De-Bashan, L.E. and Bashan, Y. (2004) Recent advances in removing phosphorus from wastewater and its future use as fertilizer (1997–2003). Water Research 38(19), 4222-4246.

Desloover, J., Abate Woldeyohannis, A., Verstraete, W., Boon, N. and Rabaey, K. (2012) Electrochemical resource recovery from digestate to prevent ammonia toxicity during anaerobic digestion. Environmental Science & Technology 46(21), 12209-12216.

EPA, U.S.(2012) Guidelines for Water Reuse. Washington, D.C.

Ge, Z. and He, Z. (2016) Long-term performance of a 200 liter modularized microbial fuel cell system treating municipal wastewater: treatment, energy, and cost. Environmental Science: Water Research & Technology 2(2), 274-281.

Hancock, N.T., Xu, P., Heil, D.M., Bellona, C. and Cath, T.Y. (2011) Comprehensive bench-and pilot-scale investigation of trace organic compounds rejection by forward osmosis. Environmental Science & Technology 45(19), 8483-8490.

Hancock, N.T., Xu, P., Roby, M.J., Gomez, J.D. and Cath, T.Y. (2013) Towards direct potable reuse with forward osmosis: Technical assessment of long-term process performance at the pilot scale. Journal of Membrane Science 445, 34-46.

He, Z., Minteer, S.D. and Angenent, L.T. (2005) Electricity generation from artificial wastewater using an upflow microbial fuel cell. Environmental Science & Technology 39(14), 5262-5267.

Heidrich, E.S., Dolfing, J., Scott, K., Edwards, S.R., Jones, C. and Curtis, T.P. (2013) Production of hydrogen from domestic wastewater in a pilot-scale microbial electrolysis cell. Applied Microbiology and Biotechnology 97(15), 6979-6989.
Heidrich, E.S., Edwards, S.R., Dolfing, J., Cotterill, S.E. and Curtis, T.P. (2014) Performance of a pilot scale microbial electrolysis cell fed on domestic wastewater at ambient temperatures for a 12 month period. Bioresource Technology 173, 87-95.
Hou, D., Lu, L. and Ren, Z.J. (2016) Microbial fuel cells and osmotic membrane bioreactors have mutual benefits for wastewater treatment and energy production. Water Research 98, 183-189.
Ippersiel, D., Mondor, M., Lamarche, F., Tremblay, F., Dubreuil, J. and Masse, L. (2012) Nitrogen potential recovery and concentration of ammonia from swine manure using electrodialysis coupled with air stripping. Journal of Environmental Management 95, S165-S169.
Kelly, P.T. and He, Z. (2014) Nutrients removal and recovery in bioelectrochemical systems: A review. Bioresource Technology 153, 351-360.
Kim, S., Lee, D.W. and Cho, J. (2016) Application of direct contact membrane distillation process to treat anaerobic digestate. Journal of Membrane Science 511, 20-28.
Kim, Y.M., Chon, D.-H., Kim, H.-S. and Park, C. (2012) Investigation of bacterial community in activated sludge with an anaerobic side-stream reactor (ASSR) to decrease the generation of excess sludge. Water Research 46(13), 4292-4300.
Lackner, S., Terada, A. and Smets, B.F. (2008) Heterotrophic activity compromises autotrophic nitrogen removal in membrane-aerated biofilms: results of a modeling study. Water Research 42(4), 1102-1112.
Logan, B.E., Hamelers, B., Rozendal, R., Schröder, U., Keller, J., Freguia, S., Aelterman, P., Verstraete, W. and Rabaey, K. (2006) Microbial fuel cells: methodology and technology. Environmental Science & Technology 40(17), 5181-5192.
Lu, Y., Qin, M., Yuan, H., Abu-Reesh, I.M. and He, Z. (2014) When bioelectrochemical systems meet forward osmosis: accomplishing wastewater treatment and reuse through synergy. Water 7(1), 38-50.
Lutchmiah, K., Verliefde, A.R.D., Roest, K., Rietveld, L.C. and Cornelissen, E.R. (2014) Forward osmosis for application in wastewater treatment: A review. Water Research 58, 179-197.
Maurer, M., Schwegler, P. and Larsen, T. (2003) Nutrients in urine: energetic aspects of removal and recovery. Water Science and Technology 48(1), 37-46.
McCarty, P.L., Bae, J. and Kim, J. (2011) Domestic wastewater treatment as a net energy producer–can this be achieved? Environmental Science & Technology 45(17), 7100-7106.
McGinnis, R.L. and Elimelech, M. (2007) Energy requirements of ammonia–carbon dioxide forward osmosis desalination. Desalination 207(1), 370-382.
McGinnis, R.L., Hancock, N.T., Nowosielski-Slepowron, M.S. and McGurgan, G.D. (2013a) Pilot demonstration of the NH3/CO2 forward osmosis desalination process on high salinity brines. Desalination 312, 67-74.
McGinnis, R.L., Hancock, N.T., Nowosielski-Slepowron, M.S. and McGurgan, G.D. (2013b) Pilot demonstration of the NH 3/CO 2 forward osmosis desalination process on high salinity brines. Desalination 312, 67-74.
Mondor, M., Masse, L., Ippersiel, D., Lamarche, F. and Masse, D. (2008) Use of electrodialysis and reverse osmosis for the recovery and concentration of ammonia from swine manure. Bioresource Technology 99(15), 7363-7368.
Münch, E.V. and Barr, K. (2001) Controlled struvite crystallisation for removing phosphorus from anaerobic digester sidestreams. Water Research 35(1), 151-159.
Nelson, N.O., Mikkelsen, R.L. and Hesterberg, D.L. (2003) Struvite precipitation in anaerobic swine lagoon liquid: effect of pH and Mg:P ratio and determination of rate constant. Bioresource Technology 89(3), 229-236.

Phuntsho, S., Kim, J.E., Johir, M.A.H., Hong, S., Li, Z., Ghaffour, N., Leiknes, T. and Shon, H.K. (2016) Fertiliser drawn forward osmosis process: Pilot-scale desalination of mine impaired water for fertigation. Journal of Membrane Science 508, 22-31.

Ping, Q., Huang, Z., Dosoretz, C. and He, Z. (2015) Integrated experimental investigation and mathematical modeling of brackish water desalination and wastewater treatment in microbial desalination cells. Water Research 77, 13-23.

Prasad, R., Britton, A., Balzer, B. and Schafran, G. (2007) Nutrient recovery by struvite crystallization process: virginia experience. Proceedings of the Water Environment Federation 2007(19), 344-358.

Qin, M. and He, Z. (2014) Self-Supplied Ammonium Bicarbonate Draw Solute for Achieving Wastewater Treatment and Recovery in a Microbial Electrolysis Cell-Forward Osmosis-Coupled System. Environmental Science & Technology Letters 1(10), 437-441.

Qiu, G., Law, Y.-M., Das, S. and Ting, Y.-P. (2015) Direct and complete phosphorus recovery from municipal wastewater using a hybrid microfiltration-forward osmosis membrane bioreactor process with seawater brine as draw solution. Environmental Science & Technology 49(10), 6156-6163.

Rozendal, R.A., Hamelers, H.V., Molenkamp, R.J. and Buisman, C.J. (2007) Performance of single chamber biocatalyzed electrolysis with different types of ion exchange membranes. Water Research 41(9), 1984-1994.

She, Q., Jin, X., Li, Q. and Tang, C.Y. (2012) Relating reverse and forward solute diffusion to membrane fouling in osmotically driven membrane processes. Water Research 46(7), 2478-2486.

Tao, B., Passanha, P., Kumi, P., Wilson, V., Jones, D. and Esteves, S. (2016) Recovery and concentration of thermally hydrolysed waste activated sludge derived volatile fatty acids and nutrients by microfiltration, electrodialysis and struvite precipitation for polyhydroxyalkanoates production. Chemical Engineering Journal 295, 11-19.

Tong, T. and Elimelech, M. (2016) The Global Rise of Zero Liquid Discharge for Wastewater Management: Drivers, Technologies, and Future Directions. Environmental Science & Technology 50(13), 6846-6855.

Uggetti, E., Sialve, B., Latrille, E. and Steyer, J.-P. (2014) Anaerobic digestate as substrate for microalgae culture: The role of ammonium concentration on the microalgae productivity. Bioresource Technology 152, 437-443.

Walker, W.S., Kim, Y. and Lawler, D.F. (2014) Treatment of model inland brackish groundwater reverse osmosis concentrate with electrodialysis — Part II: Sensitivity to voltage application and membranes. Desalination 345, 128-135.

Xiang, X., Zou, S. and He, Z. (2017) Energy consumption of water recovery from wastewater in a submerged forward osmosis system using commercial liquid fertilizer as a draw solute. Separation and Purification Technology 174, 432-438.

Xie, M., Nghiem, L.D., Price, W.E. and Elimelech, M. (2014) Toward resource recovery from wastewater: extraction of phosphorus from digested sludge using a hybrid forward osmosis–membrane distillation process. Environmental Science & Technology Letters 1(2), 191-195.

Xie, M., Shon, H.K., Gray, S.R. and Elimelech, M. (2016) Membrane-based processes for wastewater nutrient recovery: Technology, challenges, and future direction. Water Research 89, 210-221.

Zhang, F., Ge, Z., Grimaud, J., Hurst, J. and He, Z. (2013) Long-Term Performance of Liter-Scale Microbial Fuel Cells Treating Primary Effluent Installed in a Municipal Wastewater Treatment Facility. Environmental Science & Technology 47(9), 4941-4948.

Zhang, Y. and Angelidaki, I. (2015a) Counteracting ammonia inhibition during anaerobic digestion by recovery using submersible microbial desalination cell. Biotechnology and Bioengineering 112(7), 1478-1482.

Zhang, Y. and Angelidaki, I. (2015b) Recovery of ammonia and sulfate from waste streams and bioenergy production via bipolar bioelectrodialysis. Water Research 85, 177-184.

Zhou, X., Gingerich, D.B. and Mauter, M.S. (2015) Water Treatment Capacity of Forward-Osmosis Systems Utilizing Power-Plant Waste Heat. Industrial & Engineering Chemistry Research 54(24), 6378-6389.
Zou, S. and He, Z. (2016) Enhancing wastewater reuse by forward osmosis with self-diluted commercial fertilizers as draw solutes. Water Research 99, 235-243.
Zou, S. and He, Z. (2017) Electrolysis-assisted mitigation of reverse solute flux in a three-chamber forward osmosis system. Water Research 115, 111-119.

Table 7.1 Detailed experimental procedures for NEW recovery in closed-loop MEC-FO hybrid system

Cycle	Length (days)	MEC Anolyte Volume (mL)				FO Feed Volume (mL)			Struvite Precipitation (mL)		
		Influent	Sampling	Loss/ Vapor.	Effluent	Initial	End	Sampling	Concentrate	Sampling/Filter loss	Supernatant
1	5	160 fresh	6*5 mL	10	120	113	40.0	5.0	35	5.0	30 (MEC C3)
2	5	160 fresh	6*5 mL	5	125	120	46.4	5.4	41	5.0	36 (MEC C4)
3	6	130 fresh + 30 supernatant	7*5 mL	5	120	115	47.5	6.2	41.3	5.3	36 (MEC C5)
4	6	130 fresh + 36 supernatant	7*5 mL	5	126	121	50.7	5.7	45	5.0	40
5	6	130 fresh + 36 supernatant	7*5 mL	5	126	121	47.6	5.8	41.8	6.8	35

Table 7.2 Mass percentage of Mg and P in standard and recovered struvite

	Mg (wt %)	P (wt %)
Theoretical $MgNH_4PO_4$	17.52	22.62
Theoretical $MgNH_4PO_4 \cdot 6H_2O$	9.80	12.65
Standard struvite	9.79 ± 0.17	13.41 ± 1.66
Recovered struvite 1	12.95 ± 0.64	15.31 ± 0.84
Recovered struvite 2	12.34 ± 0.39	15.04 ± 0.10

8 Perspectives

Forward osmosis has received lots of attention in the past two decades to advance it towards a truly energy-efficient water reclamation technology. Comparing to the "benchmark" RO process, FO still has a long way to go and need to enhance its competitiveness in multiple ways. Scientists and engineers (for example, this study) have made tremendous effort in developing/modifying a more perfect "barrier" (i.e., the FO membrane) or utilizing operational strategies to enhanced either the system performance and/or the energy efficiency of the FO process. Some key challenges (such as membrane fouling and bidirectional solute flux) and technical barriers (e.g., advanced fabrication methods and robust membrane structure) has been or will be addressed properly in the near future (related perspectives can be found in Chapter 6 Section 6.8 "Future of the RSF Control"). It is equally important to find a desirable application niche to implement FO process considering most of the current studies were conducted in the lab or pilot scale. If FO operates as a standalone process, fertilizer-driven FO (FDFO) appears to be one of the most promising research direction to recover freshwater from all kinds of sources towards direct non-potable water reuse, and has been successfully tested at pilot scale for over 6 months in Australia. Full-scale FDFO should be encouraged with systematic evaluation (such as life cycle assessment and techno-economic analysis). Besides utilization of fertilizer as the draw solute, other cost-effective non-toxic draw solute that can bypass separation or achieve self-separation should be proposed and thoroughly investigated. Reclamation of freshwater in space station and for emergency-relief are other promising research directions for standalone FO process, but potential health concerns must be comprehensive investigated and be understood over the long term. If FO operates as an integrated part of a hybrid system (e.g., integration of bioelectrochemical systems), it can achieve the multiple resource recovery and minimized wastewater discharge. A hybrid system consisting of two or more processes will bring complex operation and will potential increase operation cost on the system level, and hence we must have a convincing justification (such as a significant boost in performance or product value) for such synergistic integration of two processes. The future of FO relies not only on the advancement of material science to fine tune the membrane structure tailored to specific feed solution (e.g. various types of wastewaters) and to enhance its selectivity to reject certain ions (either in the draw or the feed), chemical/environmental engineering to optimize the system setup, and mathematical modelling to understand the underlying ion/water transport

mechanism, but also on process engineers and operators of the water/wastewater plants to embrace modularized FO process (e.g., hollow fiber FO module) and test this technology on site to provide more pilot-scale or full-scale data on system performance, capital cost, and operational cost. All these efforts on FO process will help sustainably tackle urgent resource needs and enhance food-energy-water security on a global scale.